Exploring the Chemistry of Silyl-Substituted Metallylenes



Lewis L. Wales

The Queen's College

A Thesis Submitted for the Degree of Doctor of Philosophy

April 2024

Firstly, I would like to thank Simon Aldridge for all his help and support throughout my DPhil (and Part II). In so many sub-group meetings, the enthusiasm that Simon had for chemistry reinvigorated me and made me eager to resume hand-to-hand combat with my own research. This is a truly special skill and one that I hope I can possess one day.

I'm very grateful to the OxICFM CDT for the opportunity to carry out my research. I really enjoyed being a member of the first cohort and part of a larger community of students as the CDT grew. I'm also grateful to the CDT, and Professor Dr Udo Radius, for giving me the opportunity to spend three months at the University of Würzburg in AK Radius. I had an incredible time out there which was in large part due to all the members of the Radius group making me feel so welcome.

I have been lucky during my stint in the Aldridge group to work with so many brilliant people who made the lab an enjoyable place to work. The list is very long but Drs Matt Roy, Alexa Caise, Anna Booth, Malte Fischer, Mathias Elwanger and Marcel Schropp deserve a particular mention. Additionally, thanks to my former Part II student Aidan Murray, it was a pleasure to supervise him, and I wish him luck with the rest of his DPhil and beyond.

Aisling Roper, Agamemnon Crumpton, Caitilín McManus, Josef Boronski and Liam Griffin have all provided me with so much joy over the past four years, both in and out of the lab, for which I'm very grateful. They made the CRHell into probably the most enjoyable working environment I will ever experience in my life and have given me some incredibly cherished memories.

Thanks also to Amelia Brasnett for three wonderful years living together. Despite two lockdowns, the general stress of DPhils, and all the issues with working in the CRL, we managed to stay sane and I couldn't have asked for a better flatmate.

I'd also like to express my gratitude to my family for all their encouragement throughout my DPhil. From celebrating even the smallest of synthetic successes, to offering encouragement when things hadn't been working, I feel incredibly fortunate to have such a supportive family.

Finally, I will always be grateful to Myfanwy both for proofreading this thesis and for creating the most reassuring and comforting atmosphere whilst I was writing it. Our past six months in Norwich have been incredible and I wouldn't have wanted to be anywhere else.

Summary

In this thesis, the synthesis and reactivity of silyl-substituted metallylenes will be explored.

In Chapter 1, literature relevant to this thesis will be presented. Metallylene structure and bonding will be introduced along with a description of the ligand classes employed throughout this thesis. Some small molecule reactivity of metallylenes will also be discussed.

In Chapter 2, the experimental methods employed throughout this thesis will be documented. In addition, the modified syntheses of some starting materials used in this work will be described.

In Chapter 3, some small molecule reactivity of an aryl(silyl)germylene will be discussed. The ability of both alkenes and alkynes to insert into the Ge–Si bond of the germylene will be shown.

In Chapter 4, the syntheses of novel metallylenes are reported using aryl, silyl, and amido ligands. The synthesis of the second acyclic bis(silyl)stannylene will be disclosed, along with the first crystallographically characterised amido(silyl)stannylene.

In Chapter 5, the reactivities of an aryl(silyl)stannylene and a bis(silyl)stannylene are described. The ambiphilicities of both stannylenes are demonstrated and the migratory capacity of silyl-substituents evidenced by the reactivity of both stannylenes with azides.

In Chapter 6, the alkyne insertion chemistries of a range of silyl-substituted stannylenes are detailed. The first examples of reversible alkyne insertion into the E–X bonds of metallylenes will be reported, along with a calculated mechanism for the reaction.

In Chapter 7, conclusions from this thesis will be given and some suggestions for future research made.

Abbreviations

In this thesis, literature and novel compounds are numbered X.Y, where X is the chapter they first appear in and Y is the position that compound appears in the chapter. The list below details some common abbreviations used in this work. Some additional compound abbreviations may be used, but the name will always be defined in the text.

Ar – aryl

br. – broad

calc. – calculated

C_6D_6 – deuterated benzene

C_7D_8 – deuterated toluene

Cp – cyclopentadienyl

Cp* – pentamethylcyclopentadienyl

d – doublet

Dipp – diisopropylphenyl

$DippN_3$ – diisopropylphenyl azide

DMAP – dimethyl aminopyridine

Et – ethyl

Et_2O – diethyl ether

h – hour

HMDS – hexamethyldisilylamide

HMDSO – hexamethyldisilyloxane

HOMO – highest occupied molecular orbital

i - ipso

^{i}Pr – iso-propyl

J – coupling constant

LUMO – lowest occupied molecular orbital

m/m – meta/multiplet

Mes – 2,4,6-trimethyl-phenyl

min – minute

MIPK – methylisopropenyl ketone

MSK – methylstyryl ketone

mol – moles

o – ortho

^{n}Bu – normal butyl

NH_3 – ammonia

Np – neopentyl

p – para

PhCCH – phenylacetylene

PhCCPh – diphenylacetytlene

ppm – parts per million

q – quartet

sept – septet

$^{s}BuNH_2$ – *sec*-butylamine

t – triplet

^{t}BuNC – *tert*-butyl isonitrile

$^{t}BuNH_2$ – *tert*-butylamine

TDP – *tert*-butyldiphenylsilyl

THF – tetrahydrofuran

THF-d_8 – deuterated tetrahydrofuran

THT – tetrahydrothiophene

TMS – trimethylsilyl

TMSCCH – trimethylsilylacetylene

$TMSN_3$ – trimethylsilyazide

Tripp – triisopropylphenyl

δ – NMR chemical shift

Table of Contents

Summary iii

Abbreviations iv

1 Introduction 1

1.1 Metallylenes 1

1.1.1 Carbenes 1

1.1.2 Electronic Structure of Carbenes 2

1.1.3 Heavier Carbene Analogues 6

1.2 The Importance of Substituent Choice 6

1.2.1 Terphenyl Ligands 7

1.2.2 Silyl Ligands 9

1.2.3 Amide Ligands 11

1.3 Reactivity of Metallylenes 12

1.3.1 Ambiphilic Metallylenes 13

1.3.2 Reactivity of Metallylenes with Hydrogen 15

1.3.3 Reactivity of Metallylenes with Ammonia 18

1.3.4 Reactivity of Metallylenes with C=E Multiple Bonds 21

1.4 Research Proposal 31

1.5 References 32

2 Experimental Methods 36

2.1 Handling of Air- and Moisture- Sensitive Compounds 36

2.2 Spectroscopic and Analytical Techniques 36

2.2.1 NMR Spectroscopy 36

2.2.2 Variable Temperature Experiments for Alkyne Uptake 37

2.2.3 X-ray Diffraction 37
2.2.4 UV/Vis Spectroscopy 38
2.2.5 Elemental Analysis 38
2.2.6 Quantum Chemical Calculations 38
2.3 Known Compounds 39
2.3.1 $Ar^{Mes}I$, **2.1** (Scheme 2-1) 39
2.3.2 $Ar^{Mes}Li$, **2.2** (Scheme 2-2) 40
2.3.3 $Ge(Ar^{Mes})_2$, **1.3** (Scheme 2-3) 41
2.3.4 $[Ge(Ar^{Mes})Cl]_2$, **2.3** (Scheme 2-4) 41
2.3.5 $K(THF)_2Si(TMS)_3$, **2.5** (Scheme 2-5) 42
2.3.6 $Sn(HMDS)_2$, **1.13** (Scheme 2-6) 43
2.3.7 $Si(TMS)_3(Si^tBuPh_2)$, **2.6** (Scheme 2-7) 43
2.4 References 44
3 Reactivity of an Aryl(silyl)germylene 46
3.1 Introduction 46
3.2 Results and Discussion 48
3.2.1 Synthesis of $GeAr^{Mes}Si(TMS)_3$ 48
3.2.2 Reactivity of an Aryl(silyl)germylene with N–H Bonds 51
3.2.3 Small Molecule Reactivity of $GeAr^{Mes}Si(TMS)_3$ 60
3.3 Conclusions 82
3.4 Characterisation of Novel Materials 84
3.4.1 Reaction of $GeAr^{Mes}Si(TMS)_3$ with $MeNH_2$ (Scheme 3-9) 84
3.4.2 Reaction of $GeAr^{Mes}Si(TMS)_3$ with $^sBuNH_2$ (Scheme 3-10) 84
3.4.3 Reaction of $GeAr^{Mes}Si(TMS)_3$ with $^tBuNH_2$ (Scheme 3-11) 85
3.4.4 Reaction of $GeAr^{Mes}Si(TMS)_3$ with Et_2NH (Scheme 3-12) 85
3.4.5 Reaction of $GeAr^{Mes}Si(TMS)_3$ with *p*-Toluidine (Scheme 3-13) 86

3.4.6 Synthesis of $GeAr^{Mes}Si(TMS)_3(H)(CN)$, **3.11** (Scheme 3-16) 86
3.4.7 Synthesis of $GeAr^{Mes}Si(TMS)_3{\cdot}W(CO)_5$, **3.14** (Scheme 3-18) 87
3.4.8 Reaction of $GeAr^{Mes}Si(TMS)_3$ with Ethene (Scheme 3-19) 87
3.4.9 Reaction of $GeAr^{Mes}Si(TMS)_3$ with Norbornene (Scheme 3-20) 88
3.4.10 Reaction of $GeAr^{Mes}Si(TMS)_3$ with Excess PhCCH (Scheme 3-21) 88
3.4.11 Reaction of $GeAr^{Mes}Si(TMS)_3$ with 1 Equiv. of PhCCH (Scheme 3-22) 89
3.5 References 89
4 Synthesis of Novel Metallylenes 91
4.1 Introduction 91
4.2 Results and Discussion 93
4.2.1 Synthesis of Aryl(silyl)stannylenes 93
4.2.2 Synthesis of Bis(silyl)metallylenes 101
4.2.3 Synthesis of Amido(silyl)stannylenes 111
4.3 Conclusions 116
4.4 Characterisation of Novel Materials 117
4.4.1 Synthesis of $SnAr^{Mes}HMDS$, **4.8** (Scheme 4-3) 117
4.4.2 Synthesis of $SnAr^{Dipp}HMDS$, **4.9** (Scheme 4-3) 117
4.4.3 Synthesis of $SnAr^{Mes}Si(TMS)_3$, **4.10** (Scheme 4-4) 118
4.4.4 Synthesis of $SnAr^{Dipp}Si(TMS)_3$, **4.11** (Scheme 4-4) 119
4.4.5 Synthesis of $Sn(Si(TMS)_2(Si^tBuPh_2))_2$, **4.13** (Scheme 4-7) 119
4.4.6 Synthesis of $Pb(Si(TMS)_2(Si^tBuPh_2))_2$, **4.15** (Scheme 4-9) 120
4.4.7 Synthesis of $Sn(N(Dipp)(TMS))Si(TMS)_3$, **4.19** (Scheme 4-11) 120
4.4.8 Reaction of $[Sn(N(Dipp)(TMS))Cl]_2$ with $KSi(TMS)_2(Si^tBuPh_2)$ (Scheme 4-12) 121
4.5 References 121
5 Small Molecule Reactivity of Novel Stannylenes 123

5.1 Introduction 123

5.2 Results and Discussion 126

5.2.1 Reactivity with N–H Bonds 126

5.2.2 Reactivity with Lewis Acids 134

5.2.3 Reactivity with Lewis Bases 140

5.2.4 Reactivity with Dienes and Heterodienes 146

5.2.5 Reactivity with Azides 158

5.2.6 Attempted Formation of a Stannanone 168

5.2.7 Reactivity with Alkenes 170

5.3 Conclusions 173

5.4 Characterisation of Novel Materials 174

5.4.1 Reaction of $SnAr^{Mes}Si(TMS)_3$ with Methylamine (Scheme 5-6) 174

5.4.2 Synthesis of $SnAr^{Mes}Si(TMS)_3{\cdot}NH_2{}^sBu$, **5.14** (Scheme 5-7) 174

5.4.3 Synthesis of $SnAr^{Mes}Si(TMS)_3{\cdot}W(CO)_5$, **5.16** (Scheme 5-9) 175

5.4.4 Reaction of $Sn(Si(TMS)_2(Si^tBuPh_2))_2$ with $AuPPh_3Cl$ (Scheme 5-11) 175

5.4.5 Synthesis of $SnAr^{Mes}Si(TMS)_3(C(H_2)C(Me)C(Me)O)$, **5.23** (Scheme 5-15) 176

5.4.6 Synthesis of $SnAr^{Mes}Si(TMS)_3(C(H)(Ph)C(H)C(Me)O)$, **5.24** (Scheme 5-16) 176

5.4.7 Reaction of $Sn(Si(TMS)_2(Si^tBuPh_2))_2$ with PhC(H)C(H)COMe (Scheme 5-17) 177

5.4.8 Synthesis of $SnAr^{Mes}Si(TMS)_3(C(H_2)C_2Me_2C(H_2))$, **5.26** (Scheme 5-19) 177

5.4.9 Synthesis of $Sn(Ar^{Mes})(Si(TMS)_3)(OC_2Me_2O)$, **5.27** (Scheme 5-20) 178

5.4.10 Reaction of $Sn(Si(TMS)_2(Si^tBuPh_2))_2$ with MeC(O)C(O)Me (Scheme 5-21) 178

5.4.11 Synthesis of $Sn(Ar^{Mes})(N(TMS)(Si(TMS)_3))$, **5.29** (Scheme 5-23) 179

5.4.12 Synthesis of $SnSi(TMS)_3(NH(TMS)(Ar^{Mes}\text{-}CH_2)$, **5.30** (Scheme 5-23) 179

5.4.13 Synthesis of $SnAr^{Mes}N(Dipp)(Si(TMS)_3)$, **5.32** (Scheme 5-25) 180

5.4.14 Reaction of $Sn(Si(TMS)_2(Si^tBuPh_2))_2$ with $DippN_3$ (Scheme 5-26) 180

5.4.15 Reaction of $SnAr^{Mes}Si(TMS)_3$ with Ethene (Scheme 5-28) 181

5.5 References 181

6 The Alkyne Insertion Chemistry of Silylstannylenes 183

6.1 Introduction 183

6.2 Results and Discussion 186

6.2.1 Irreversible Alkyne Insertion 186

6.2.2 Reversible Alkyne Insertion 203

6.2.3 Mechanism of Insertion 210

6.3 Conclusions 217

6.4 Characterisation of Novel Materials 219

6.4.1 Synthesis of *Z*-Sn(Ar^{Mes})(C(H)=C(H)($Si(TMS)_3$), **6.6** (Scheme 6-4) 219

6.4.2 Reaction of $SnAr^{Mes}Si(TMS)_3$ with But-2-yne (Scheme 6-6) 219

6.4.3 Reaction of $SnAr^{Dipp}Si(TMS)_3$ with But-2-yne (Scheme 6-7) 220

6.4.4 Synthesis of *Z*-Sn(Ar^{Mes})(C(Ph)=C(H)($Si(TMS)_3$), **6.10** (Scheme 6-9) 220

6.4.5 Reaction of $SnAr^{Mes}Si(TMS)_3$ with PhCCMe (Scheme 6-14) 221

6.4.6 Reaction of $SnAr^{Mes}Si(TMS)_3$ with $CF_3(C_6H_4)CCMe$ (Scheme 6-15) 221

6.4.7 Reaction of $SnAr^{Mes}Si(TMS)_3$ with TMSCCH (Scheme 6-20) 222

6.5 References 222

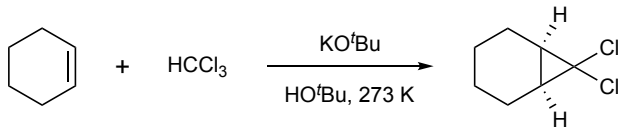
7 Conclusions and Future Work 223

1 Introduction

1.1 Metallylenes

1.1.1 Carbenes

Carbenes are neutral species which contain a divalent carbon atom in the formal +2 oxidation state with only six electrons in its valence shell.[1] In their 1954 work, Doering *et al.* succeeded in trapping, for the first time, a transient carbene by the use of cyclohexene.[2] This success initiated more research into carbenes to better understand their chemistry.



Scheme 1-1: The cheletropic addition of dichlorocarbene to cyclohexene.[2]

In 1988 Bertrand *et al.* reported the first synthesis of a λ^3-phosphino-carbene, which possesses strong C–P multiple-bond character between the pendant phosphorus substituent and the carbenic centre (Figure 1-1).[3] Nevertheless, this species was thought to be capable of reacting as a carbenic species, such as with chlorotrimethylsilane.[3] Alongside this work, the discovery by Arduengo *et al.* three years later of the first "bottle-able carbene" (meaning crystalline), which is stabilised kinetically and thermodynamically by the bulky N-heterocyclic framework employed, led to a dramatic expansion of research into carbenes and their chemistry.[4]

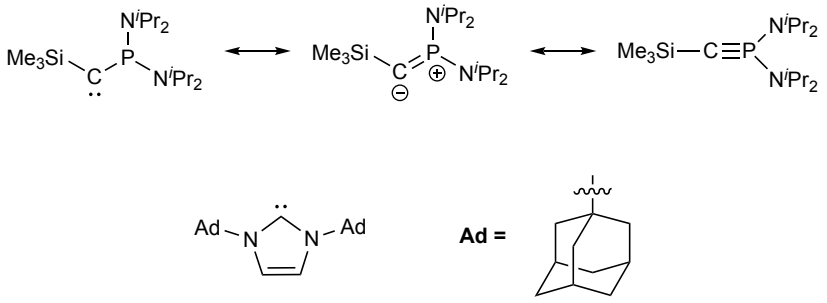


Figure 1-1: Top – The first isolable carbene and the resonance forms which stabilise the carbon centre.[3] Bottom – The N-heterocyclic carbene synthesised by Arduengo *et al*.[4]

Due to the ease with which carbenes can be tailored both electronically and sterically, they are now ubiquitous in both academic and industrial chemistry, finding applications in homogeneous and heterogeneous catalysis as well as being capable of acting as organo-catalysts themselves.[5–7]

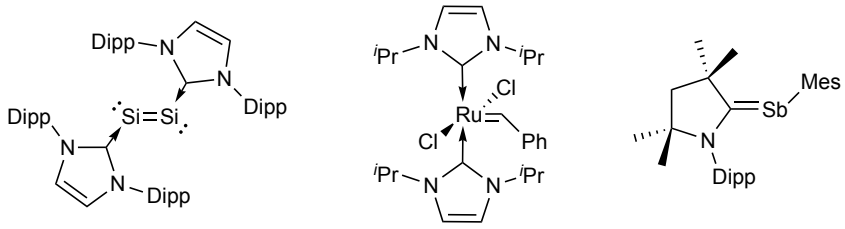


Figure 1-2: Assorted examples of carbenes being used in molecular chemistry.[8–10]

1.1.2 Electronic Structure of Carbenes

As mentioned above, a carbene is a divalent species with six electrons in its valence shell.[1] This divalency means that a carbene can adopt a linear or bent structure. When linear, it will possess a formally sp-hybridised carbon centre with two degenerate non-bonding p-orbitals.[1] Upon bending, the degeneracy of these two orbitals is broken and the carbene will form sp^2 like hybrid bonds with its substituents.[1] One of the p-orbitals will be stabilised as it acquires more s-character (now labelled σ) and the other (p_π) maintains the same energy (Figure 1-3).[1]

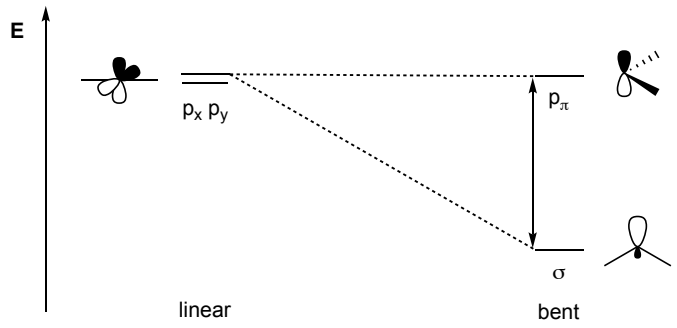


Figure 1-3: Effect on the electronic structure of carbenes from bending at the central carbon atom. Adapted from Bertrand *et al*.[1]

A natural result of this orbital description is that bent carbenes will be either triplets or singlets depending on their σ–p_π energy gap. When the gap is small, calculated by Hoffman to be less than 2 eV, the carbene will possess a triplet ground state.[11] Any larger and the carbene will have a singlet ground state. For singlet carbenes, the p_π-orbital will be the lowest unoccupied molecular orbital (LUMO) and the σ-orbital will be the highest occupied molecular orbital (HOMO). This has important ramifications for the reactivity of carbenes because singlet carbenes should behave as ambiphiles, whereas triplet carbenes should behave as diradicals.

1.1.2.1 Electronic Effects

Given that the magnitude of the σ–p_π energy gap influences the reactivity of a carbene, tuning this gap is very important when designing carbenes (and by implication heavier group 14 metallylenes). One factor which affects the energy gap is the electronegativity of the two carbene substituents. The σ-orbital (lone pair) possesses C–X anti-bonding character (where X is a carbene substituent). This means that as the electronegativity of the substituents increases, the σ-orbital is stabilised (Figure 1-4).[1] This lowering of the σ-orbital energy serves to widen the HOMO–LUMO gap, as the empty p-orbitals remain unchanged.[1]

Similarly, as more electropositive substituents are used, the σ-orbital energy increases, and therefore the HOMO–LUMO gap decreases.[1]

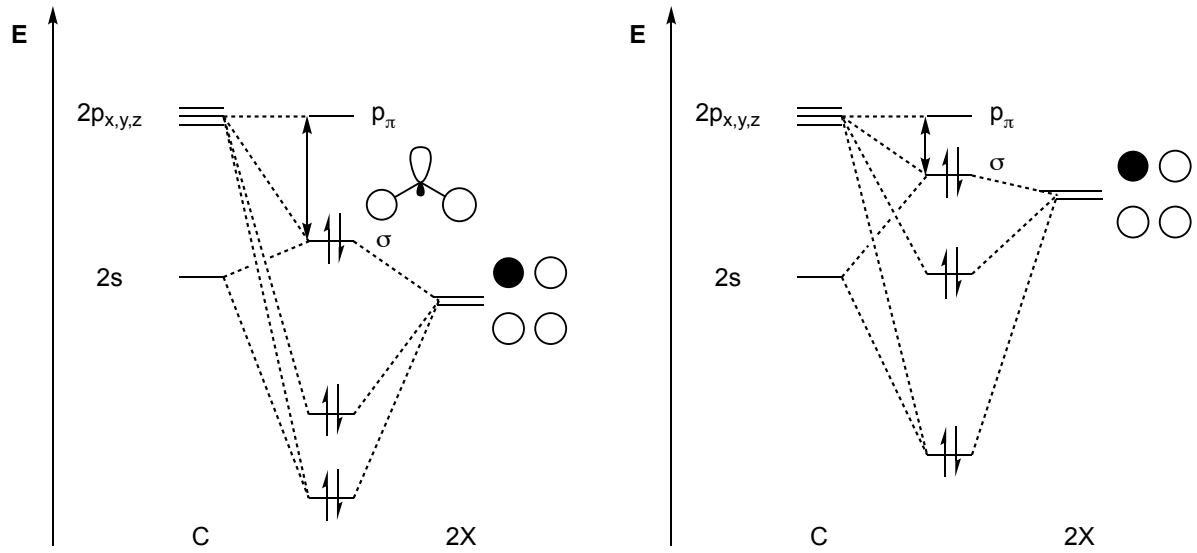


Figure 1-4: Diagrams to show the effect of electronegative substituents (left) and electropositive substituents (right) on the HOMO–LUMO gap of carbenes. Adapted from Bertrand *et al*.[1]

Another electronic factor which affects the HOMO–LUMO gap of a carbene is the extent to which its substituents are π-electron donating or π-electron withdrawing. When π-electron donating groups are bonded to the central carbon, there is overlap between the formally empty p-orbital on the carbon and the filled π-orbitals of the adjacent groups.[1] This yields a bonding and anti-bonding orbital, and the increased energy of this anti-bonding orbital increases the HOMO–LUMO gap.[1]

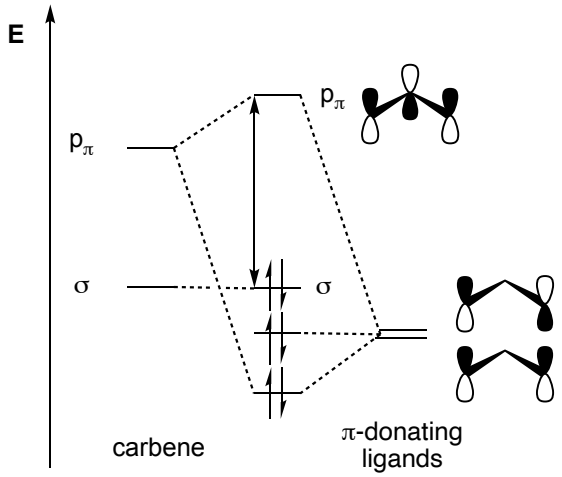
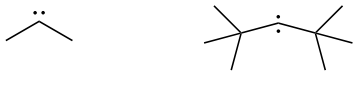


Figure 1-5: Diagram to show the effect of π-electron donating groups on the HOMO–LUMO gap of metallylenes. Adapted from Bertrand *et al*.[1]

1.1.2.2 Steric Effects

In addition to electronic effects, steric effects can play a role in changing the HOMO–LUMO gap of carbenes. As seen above (Figure 1-3), as a carbene approaches linearity, the HOMO and LUMO become degenerate. Therefore, the wider the angle between the substituents at the carbon centre, the narrower the HOMO–LUMO gap will become.[1] An example for this can be seen when comparing the angles at the central carbon centre of dimethylcarbene, **1.1**, and ditertbutylcarbene, **1.2**, and their electronic ground states. While **1.1** is calculated to have an angle of 111° at the carbon centre and to be a singlet, **1.2** is predicted to have a corresponding angle of 143° at the carbenic centre and to be a triplet, reflecting a smaller σ–p_π energy gap gap.[12,13]



1.1 **1.2**

Figure 1-6: Diagram of dimethyl carbene, **1.1**, and ditertbutylcarbene, **1.2**. Angle at the central carbon: **1.1**, 111°; **1.2**, 143°. [12,13]

1.1.3 Heavier Carbene Analogues

Metallylenes are the heavier group 14 analogues of carbenes. An important difference between carbenes and their heavier analogues is that as group 14 is descended, the stability of the +2 oxidation state increases.[14] This is a result of the diminished ability of the heavier elements to form strong covalent bonds in the +4 oxidation state and the increasing electron promotion energies ($M(s^2p^2)$–$M(sp^3)$) as group 14 is descended.[15] The weaker covalent bonds formed by the heavier elements are due to the valence electrons residing in more diffuse orbitals which then have poorer overlap, as well as the increased Coulombic repulsion between the greater number of inner shell electrons of the group 14 elements and the element to which it bonds.[16] In addition to their weaker covalency, heavier metallylenes also have a reduced tendency to form mixed ns/np hybrid orbitals, meaning that their lone pairs tend to have significantly more s-character than carbenes.[14] Therefore, heavier metallylenes are significantly more likely to exist in a singlet ground state, since this orbital is significantly lower in energy than the vacant p-orbital.[14] The larger HOMO–LUMO gap of metallylenes can nevertheless be modulated using the same principles as discussed above. As with carbenes, the narrower the HOMO–LUMO gap, the better able heavier metallylenes will be to perform "transition metal like" chemistry towards synergistic substrates. Much research has been carried out aimed at tailoring this gap to promote small molecule activation.[17–19]

1.2 The Importance of Substituent Choice

The effects of substituent choice on electronic structure result in profound implications for the reactivity of metallylenes. Substituent choice is therefore important when designing metallylenes capable of small molecule activation. In this section, key substituent types which are used throughout this thesis will be introduced.

1.2.1 Terphenyl Ligands

Since their first synthesis in 1942, terphenyl ligands have been used to stabilise a wide variety of reactive main group species.[20–24] Terphenyl ligands have the general form $–C_6H_3$-2,6-$Aryl_2$, however in some cases the backbone carbons (at positions 3, 4 and 5) of the central aryl ring can also be substituted.[25,26] The flanking aryl rings are typically also substituted in their ortho and para positions, further increasing steric bulk. One effect of this steric loading is that the flanking rings typically adopt a geometry almost perpendicular to the central ring. This also shields the ligating carbon and protects nearby reactive sites, making terphenyl ligands very adept at stabilising low coordinate species.[27–30]

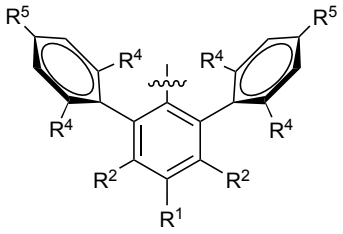
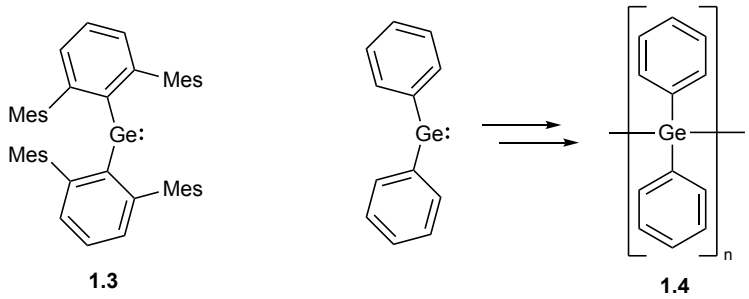


Figure 1-7: A diagram of a terphenyl ligand where all R groups can be substituted, typically for small alkyl groups such as methyl or isopropyl.

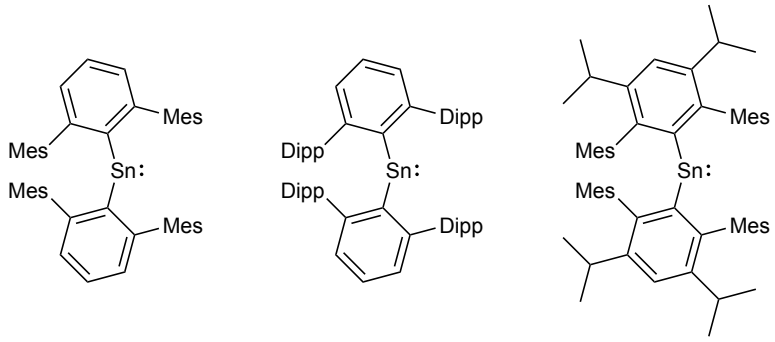
An illustration of the stabilisation that terphenyl ligands can provide to adjacent reactive sites is demonstrated by the relative stabilities of the two bis(aryl)germylenes, **1.3** and **1.4** shown in Figure 1-8. Whilst **1.3** is an isolable compound, albeit in the absence of air and moisture, **1.4** is not isolable and forms a polygermane instead.[31,32] This difference in stabilities is due to the steric bulk of the terphenyl substituents, which shield the germanium centre, making the polymerisation of **1.3** impossible under ambient conditions.



1.3 **1.4**

Figure 1-8: Diagram of the bis(terphenyl)germylene, **1.3**, and the polygermane **1.4**.[31,32]

As mentioned above, the smaller the HOMO–LUMO gap, the more reactive heavier group 14 metallylenes will be. Terphenyl ligands, due to their steric bulk, typically enforce a wide angle at the metal centre and as a result can be used to narrow the σ–p_π energy gap. One way to increase the bulk of terphenyl ligands is to change the nature of the flanking rings. When the mesityl groups of **1.5** (Figure 1-9 below) are changed to the 2,6-(diisopropyl)phenyl groups of **1.6**, a widening of the angle at the metal centre is seen from 114.7(2)° to 117.56(8)°.[31,33] Substituents can also be added to the central ring to widen the angle at the metal centre even further. The terphenyl ligands of **1.7** feature isopropyl groups in the meta-positions of the central phenyl ring, which serve to widen the angle at the tin centre to 123.4(2)° *via* steric "buttressing".[34] The effect of these angle changes on the HOMO–LUMO gap can be probed by analysis of the UV-Vis spectra of these species. Key electronic transitions observed in these spectra are due to n–p transitions, which are directly correlated to the HOMO–LUMO gap.[34] The widening at the metal centre from **1.5** to **1.6** and **1.7** is accompanied by a bathochromic shift from 553 nm to 600 nm and 591 nm respectively, consistent with a smaller HOMO–LUMO gap caused by a larger angle at the metal centre.[34]



1.5 **1.6** **1.7**

Figure 1-9: Diagrams of three bis(terphenyl)stannylenes. Angle at Sn centre: **1.5**, 114.7(2)°; **1.6**, 117.56(8)°; **1.7**, 123.4(2)°. UV-transitions: **1.5**, 553 nm; **1.6**, 600 nm; **1.7**, 591 nm. [31,33,34]

1.2.2 Silyl Ligands

The use of silyl ligands in complexes of elements across the Periodic Table is a well-researched area. The lower electronegativity of silicon compared to carbon, and the greater ease with which bulky groups can be substituted onto a silicon centre, make silyl ligands an effective means of stabilising species in unusual oxidation states and geometries.[35–40]

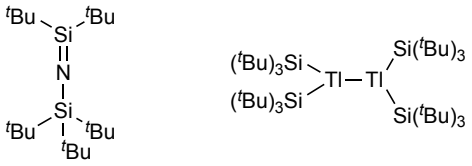


Figure 1-10: Two examples of silyl groups as ligands in main group chemistry.[41,42]

Pioneering work in the use of silyl ligands in group 14 chemistry was carried out by Klinkhammer *et al.* in 1995, when they attempted to synthesise the homoleptic hypersilyl-ligated (-$Si(SiMe_3)_3$) stannylene and plumbylene (Figure 1-11).[43] Whilst only the plumbylene, **1.10**, could be isolated as a monomer in the solid state, this work demonstrated the potential of silyl ligands in the isolation of reactive metallylenes.[43] The corresponding stannylene, **1.8**, exists as a dimer in the solid state, **1.9**, but in solution is thought to exist as a monomer.[43]

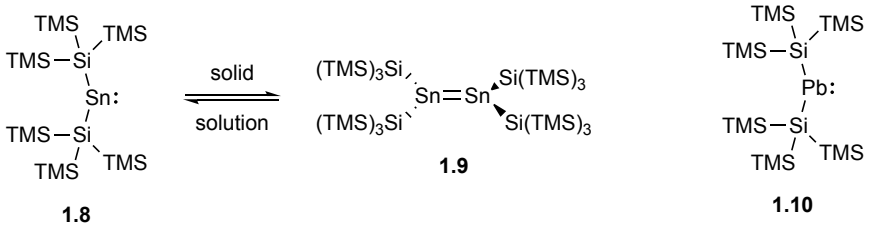
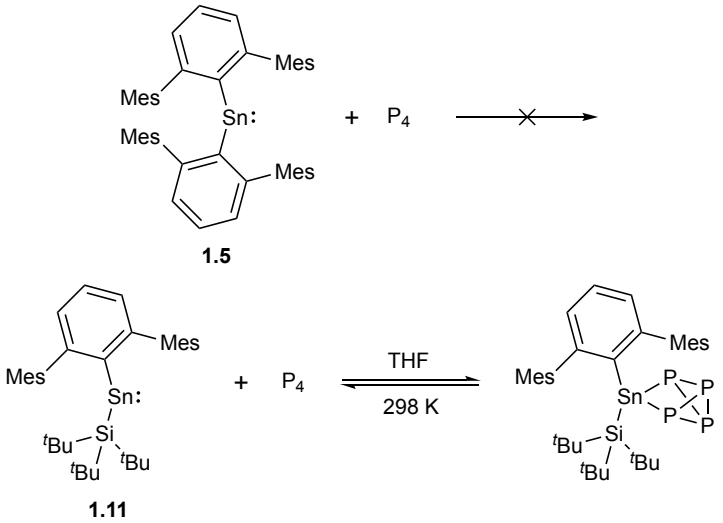


Figure 1-11: Tetrakis(hypersilyl)distannene and bis(hypersilyl)plumbylene as synthesised by Klinkhammer *et al*.[43]

Silicon is relatively electropositive (Pauling electronegativity: 1.90) and therefore silyl ligands are strongly σ-donating.[44] The strength of their σ-donating abilities was the subject of quantum chemical analysis carried out by Marder *et al.* in 2005.[45] They investigated the *trans*-influence of an array of ligands within square planar platinum (II) complexes, using the Pt–Cl bond *trans* to the ligand as a probe metric. The *trans*-influence of the -$SiMe_3$ ligand was found to be very strong, causing a significant lengthening of the Pt–Cl bond (2.594 Å) due to its high σ-donating ability.[45] Only the -BMe_2 substituent was calculated to cause a more pronounced lengthening in the Pt–Cl bond (2.608 Å).[45] As a result of this electronic effect, it is expected that the incorporation of a silyl ligand in a metallylene would lead to a narrowing of the HOMO–LUMO gap as shown in Figure 1-4.

An experimental demonstration of the increased reactivity of silyl-substituted metallylenes can be seen by comparing the behaviour of a bis(terphenyl)stannylene, **1.5**, and silyl(terphenyl)stannylene, **1.11**, with P_4 (Scheme 1-2). In 2020, Sarkar *et al.* demonstrated the reversible activation of P_4 by **1.11**.[46] By contrast, despite **1.5** being known since 1997, and widely investigated in the literature, no reactivity has ever been reported with P_4.[31] Sarkar *et al.* attribute the divergent reactivity to the smaller HOMO–LUMO gap of **1.11** (**1.10**, 3.08 eV; **1.5**, 3.41 eV), due to its electropositive silyl ligand which destabilises the HOMO of **1.10**.



Scheme 1-2: Top – No reaction has been reported between the bis(terphenyl)stannylene and P_4. Bottom – The reversible activation of P_4 as reported by Sarkar *et al.*[46]

1.2.3 Amide Ligands

The use of amide ligands has been an active field of research for almost a century.[47–50] Although they were known as ligands long before, it was only in 1973 that Lappert *et al.* demonstrated the first structurally characterised group 14 metal amide, $Sn(N(SiMe_3)_2)_2$, synthesised through the reaction of $SnCl_2$ with $LiN(SiMe_3)_2$.[51] Since this discovery, a wealth of other metallylenes incorporating a variety of amide ligands has been reported.[52–57]

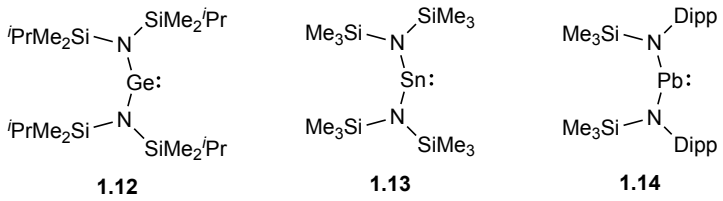
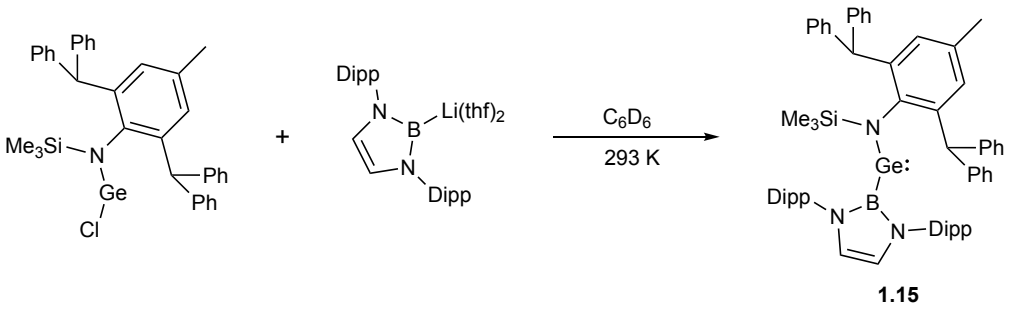


Figure 1-12: Examples of metallylenes with amide ligands.[51,58,59]

Due to nitrogen being more electronegative than silicon, amide ligands are not as σ-donating as silyl ligands. Therefore, metallylenes featuring amide ligands tend to have a more stabilised HOMO and thus a larger HOMO–LUMO gap than silylated metallylenes. Additionally, the presence of a lone pair at nitrogen means that amide ligands are π-electron donating, further

increasing the HOMO–LUMO gap. While these electronic effects mean that amide-substituted heavier metallylenes may not be suitable for small molecule activation, they are capable of stabilising otherwise highly reactive tetrylenes. This was demonstrated in 2012, when Aldridge *et al.* reported the synthesis of a boryl(amido)germylene, **1.15**, which calculations predicted should be isolable due to its singlet-triplet gap (123.0 kJ mol^{-1}).[60] In contrast, calculations suggested that the corresponding bis(boryl)germylene would have a very small singlet-triplet gap (17.9 kJ mol^{-1}), suggesting that isolation of the germylene would not be possible.[60]



Scheme 1-3: Synthesis of a boryl(amido)germylene, **1.15**.[60]

1.3 Reactivity of Metallylenes

As mentioned above, the nature of the metallylene substituents strongly influences what chemistry it can perform, implying that it is possible to design metallylenes capable of reacting with small molecules. In this section, the reactivity of metallylenes with a range of small molecules will be explored to demonstrate how their behaviour varies down group 14 and how chemists have tuned the HOMO–LUMO gap of metallylenes to facilitate reactivity with synergistic substrates such as hydrogen.

1.3.1 Ambiphilic Metallylenes

A key aspect of singlet carbene chemistry is their ambiphilicity. This arises from their HOMO and LUMO both being energetically accessible. However, as group 14 is descended, the HOMO obtains more s-character and is energetically stabilised. As a consequence, heavier metallylenes are expected to exhibit more electrophilic and less nucleophilic chemistry than their lighter congeners.

1.3.1.1 Behaviour as Lewis Bases

Despite the greater s-orbital character of the HOMO on descending group 14, the lone pair is still readily available and, as a result, there are a wealth of examples of the coordination chemistry of the heavier group 14 metallylenes in the literature.[61–65]

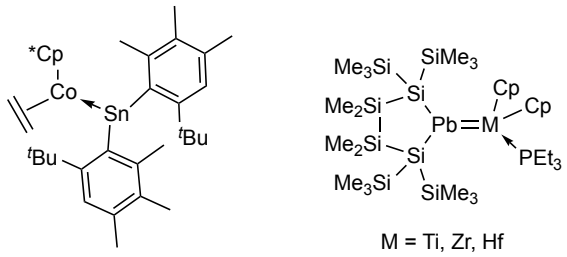
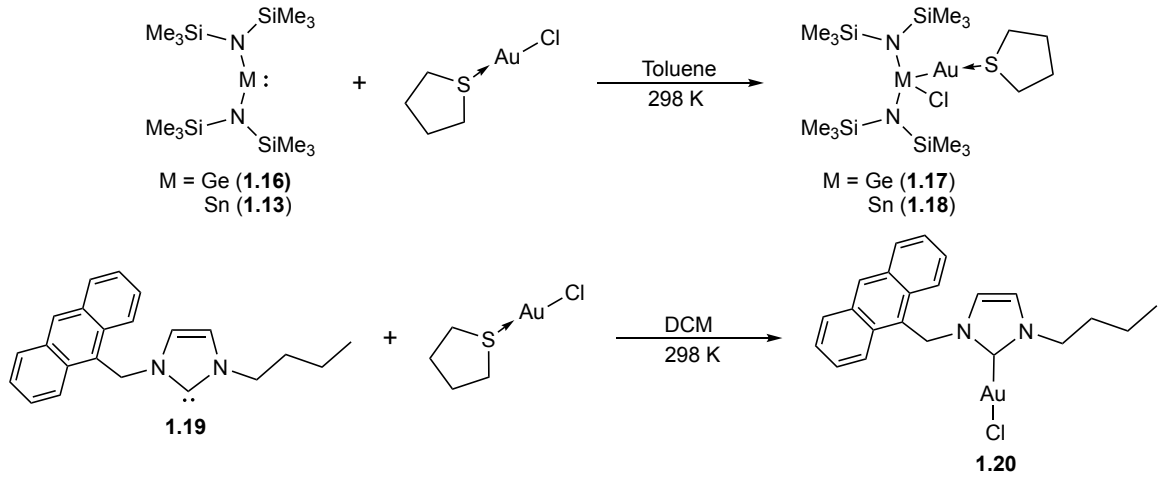


Figure 1-13: Examples of the coordination chemistry of stannylenes and plumbylenes.[66,67]

An example of the increased nucleophilicity of carbenes compared to germylenes and stannylenes can be seen in their reactions with a gold(I) chloride complex. Polo *et al.* demonstrated the oxidative addition of a Au(I)–Cl bond at both germanium and tin bis(bis(trimethylsilyl)amide) derivatives, **1.16** and **1.13** (Scheme 1-4).[68] This is not an unknown reaction, and is a common method of making systems with Au–Ge bonds.[69] However, when a carbene is reacted with the same gold(I) reagent, substitution of the THT ligand by the

carbene is observed instead, consistent with the greater nucleophilicity of the carbene lone pair (Scheme 1-4).[70]



Scheme 1-4: Top – Oxidative addition of an Au–Cl bond by $E(HMDS)_2$ (E= Ge, Sn). Bottom – Substitution of a tetrahydrothiophene ligand with an N-heterocyclic carbene.[68,70]

1.3.1.2 Behaviour as Lewis Acids

As a result of their energetically accessible formally vacant p_π orbital, the heavier group 14 metallylenes can also behave as Lewis acids and are capable of coordinating a wide range of Lewis bases.[71–73]

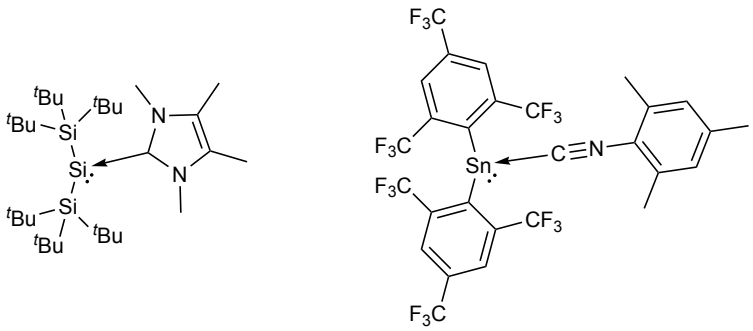
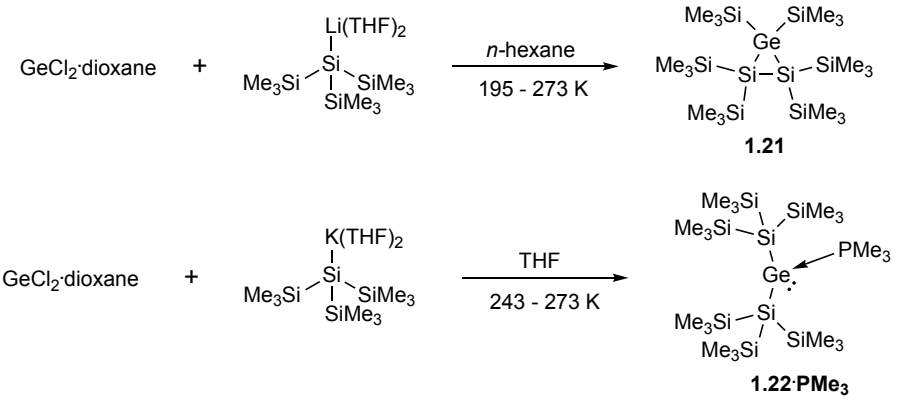


Figure 1-14: Two examples of Lewis bases coordinating to metallylenes.[74,75]

In some instances, the coordination of strong sigma donors, such as N-heterocyclic carbenes and phosphines, can help stabilise reactive metallylenes. In their 1994 work, Stalke *et al.*

synthesised the first disilagermirane, **1.21**, through the reaction of germanium dichloride and tris(trimethylsilyl)silyl lithium (Scheme 1-5).[76] The authors proposed that this reaction proceeds *via* a bis(silyl)germylene, before subsequent rearrangement to give **1.21**.[76] This pathway is consistent with the 2014 work of Marschner *et al.,* in which the same reaction was carried out (albeit with the potassium salt) in the presence of trimethyl phosphine, yielding the bis(silyl)germylene base adduct, **1.22·PMe$_3$**, rather than germirane **1.21**.[77] As a demonstration of the importance of the base in this reaction, when the bulkier triethyl phosphine is used instead of trimethyl phosphine, adduct formation is unfeasible and **1.21** is therefore produced as **1.22** cannot be stabilised.[77]

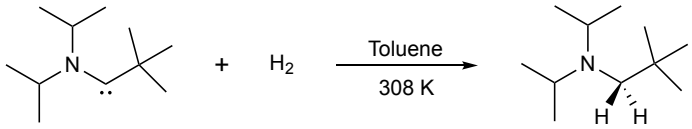


Scheme 1-5: Top – Synthesis of a disilagermirane. Bottom – Synthesis of a base stabilised bis(silyl)germylene.[76,77]

1.3.2 Reactivity of Metallylenes with Hydrogen

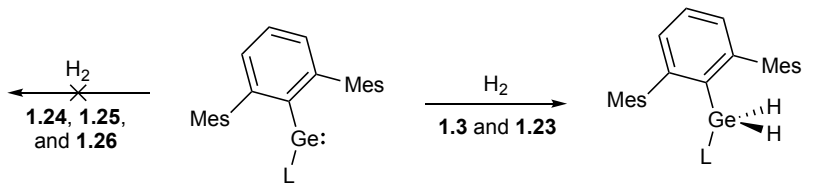
For a large part of the last century reactivity towards hydrogen was thought to be the exclusive preserve of transition metals. Research in the last 20 years has challenged this notion.[78] Metallylenes, due to their potentially narrow HOMO–LUMO gaps, are ideal candidates for activating non-polar bonds like that in H_2.[60,79–82] In 2007, Bertrand *et al.* demonstrated the first example of the oxidative addition of hydrogen at a carbene centre,

and this subsequently led to a great deal of interest in the ability of the heavier metallylene analogues to do the same.[79]



Scheme 1-6: Oxidative addition of hydrogen to a carbene.[79]

Power *et al.* reported the first example of oxidative addition of hydrogen at a germylene centre (bis(aryl)germylene, **1.3**) in their 2009 work (Scheme 1-7).[82] While this represented a fascinating example of how main group compounds could affect "transition metal like" reactivity, the importance of the HOMO–LUMO gap was not explicitly discussed. In their 2016 paper, Aldridge *et al.* demonstrated this through an investigation of the reactivity of a series of arylgermylenes with hydrogen.[80] By varying the X-substituent within a X–Ge(Ar^{Mes}) framework, the effects of ligand choice on structure, HOMO–LUMO gap, and reactivity could be determined.[80] For aryl(amido)germylene, **1.24**, aryl(alkyl)germylene **1.25**, and aryl(phosphide)germylene, **1.26**, (Scheme 1-7) the HOMO–LUMO gaps were calculated to be 275 kJ mol^{-1}, 177 kJ mol^{-1}, and 203 kJ mol^{-1} respectively. The narrower calculated HOMO–LUMO gap for aryl(silyl)germylene, **1.23** (134 kJ mol^{-1}) is caused by the more σ-donating nature of the silyl ligand and suggests that **1.23** is more likely to be capable of reacting with hydrogen than **1.24**, **1.25**, and **1.26**.[80] This hypothesis is borne out experimentally, as **1.23** (Scheme 1-7), is capable of the oxidative addition of hydrogen, forming **1.28**, whereas **1.24**, **1.25**, and **1.26** are inert towards H_2.

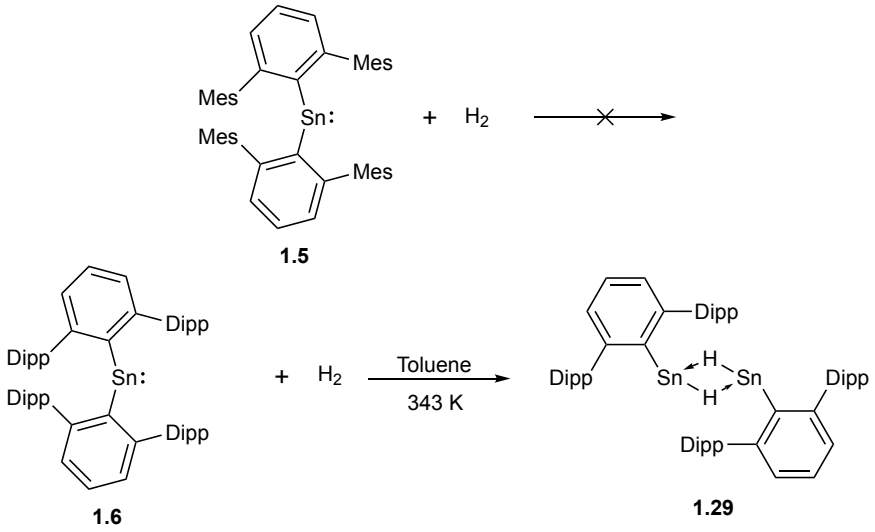


1.3, L = - Ar^{Mes}
1.23, L = -$Si(TMS)_3$
1.24, L = -NHDipp
1.25, L = -$CH(TMS)_2$
1.26, L= -$P(TMS)_2$

1.27, L = - Ar^{Mes}
1.28, L = -$Si(TMS)_3$

Scheme 1-7: The reaction and lack of reaction of a series of arylgermylenes with hydrogen.[80,82]

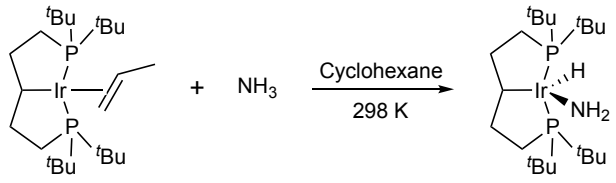
When bis(aryl)stannylene, **1.5**, is exposed to hydrogen, no reaction is observed (Scheme 1-8).[82] However, the isostructural bis(aryl)germylene, **1.3**, does react with H_2 to yield the Ge(IV) dihydride, **1.27**.[82] As the two metallylenes possess the same steric and electronic ligand profile, this difference in reactivity can be understood thermodynamically by the increased stability of the +2 oxidation state as group 14 is descended, and kinetically by the stabilisation of the metallylene lone pair and consequent widening of the HOMO–LUMO gap. Nevertheless, stannylenes can still be designed to bring about reactivity with H_2. Bulkier ligands widen the angle at the metal centre and therefore narrow the HOMO–LUMO gap. When the flanking rings of the terphenyl ligand are changed from mesityl groups (as in **1.5**) to 2,6-diisopropylphenyl groups (as in **1.6**) reactivity towards hydrogen is "switched on".[82,83] While the difference in angles at the metal centres between **1.5** and **1.6** is modest (114.7(2)° *vs.* 117.56(8)°), it is demonstrably sufficient to make the metallylene more reactive and result in a narrower calculated HOMO–LUMO gap for **1.6** (**1.5**: 270.1 kJ mol^{-1}, **1.6**: 257.6 kJ mol^{-1}).[31,33,82] Although a reaction is observed, it is not oxidative addition. Instead, a Sn(II) hydride dimer is formed, **1.29**, with the concomitant elimination of two equivalents of protonated ligand. For stannylenes to oxidatively add hydrogen at the metal centre, sufficiently sigma donating ligands (such as boryl ligands) must be used not only to raise the HOMO in energy, but also to stabilise the resultant Sn(IV) product.[84]



Scheme 1-8: Top – No reaction is observed between bis(mesitylterphenyl)stannylene, **1.5**, and hydrogen. Bottom – The reaction between hydrogen and a bis(2-6(diisopropyl)phenylterphenyl)stannylene, **1.6**, and hydrogen.[82]

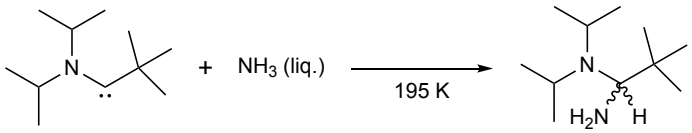
1.3.3 Reactivity of Metallylenes with Ammonia

The synthesis of a catalyst capable of the hydroamination of a diverse scope of olefins with ammonia has been referred to as one of the greatest challenges facing the catalysis research community.[85] The challenge of this catalytic process stems from the chemistry of ammonia itself. The lone pair of ammonia coordinates to typical transition metal catalysts, forming Werner ammine complexes, which tend to be catalytically inactive.[86,87] Additionally, the strength of the N–H bond (*circa.* 445 kJ mol^{-1}) makes formal oxidative addition at the metal centre difficult.[88,89] Finally, the poor capacity of ammonia as a base and its very low acidity (pKa = 9.25 at 298 K) results in proton exchanges to/from ammonia being disfavoured.[90,91] These issues explain why, to date, there has only been one example of formal oxidative addition of ammonia at a transition metal centre (Scheme 1-9).[90]



Scheme 1-9: The first example of single site oxidative addition of ammonia at a transition metal centre.[90]

In 2007, Bertrand *et al.* reported the activation of ammonia at a singlet carbene. The advantage of alkyl(amino)carbenes is that, unlike transition metals, they are nucleophilic, so Werner type adducts should not form irreversibly.[79] Instead, the lone pair of the carbene is donated into the N–H σ* orbital, and the N–H σ orbital donates into the vacant orbital of the carbene. It is therefore apparent that controlling the HOMO–LUMO gap of nucleophilic carbenes determines whether they will activate ammonia.[79]

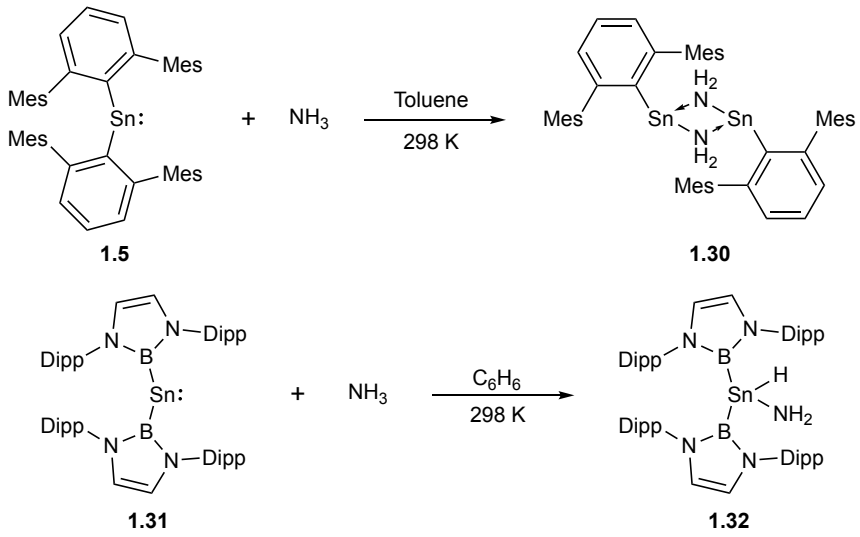


Scheme 1-10: Oxidative addition of ammonia at a carbene.[79]

Whilst Roesky and Power have reported systems using silylenes and germylenes respectively, the 2016 paper from Aldridge *et al.* on a stannylene capable of ammonia activation demonstrates the key issues which need to be considered when designing a metallylene system for ammonia activation.

As previously discussed, the bis(aryl)stannylene, **1.6**, does not yield the formal oxidative addition product upon exposure to hydrogen, nor upon exposure to an atmosphere of ammonia.[83] Instead, ligand elimination accompanied by the formation of an amido bridged Sn(II) complex, **1.30**, occurs. To modulate the Sn^{II}/Sn^{IV} redox couple, Aldridge *et al.* synthesised a stannylene with two strongly σ-donating boryl ligands, **1.31**, hoping to promote

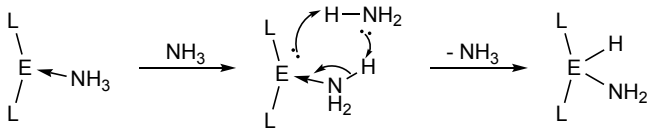
oxidative addition by stabilizing the Sn^{IV} state.[84] The σ-donating capacity of these ligands also raises the energy of the HOMO, reducing the HOMO–LUMO gap.[45] This is an important kinetic consideration because the smaller this energy gap, the more reactive the metallylene will be. Bis(boryl)stannylene, **1.31**, was found to be capable of the single-site oxidative addition of both hydrogen and ammonia, proving their hypotheses about the use of boryl ligands to promote oxidative addition both thermodynamically and kinetically.[84]



Scheme 1-11: Top – Reaction of bis(aryl)stannylene, **1.5**, with ammonia to form a Sn(II) dimer. Bottom – Oxidative addition of ammonia at bis(boryl)stannylene, **1.31**.[27,84]

The heavier group 14 metallylenes are thought to activate ammonia *via* a different mechanism than that proposed by Bertrand *et al.* for carbenes.[79,92] The first step is postulated to be the formation of a Werner-like complex, followed by interaction with a second equivalent of ammonia, which acts as a proton shuttle – transferring H^+ from the coordinated ammonia to the metal centre – to yield the formal oxidative addition product.[82,84,92] The intermediate Werner-like complex could be isolated in the reaction between **1.31** and ammonia, suggesting that it is at least the first step in the mechanism.[84] A similar mechanism

for N–H bond addition has been reported for a bis(aryl)germylene with hydrazines both experimentally and computationally by Power *et al*.[93]



Scheme 1-12: Proposed reaction mechanism of the activation of the N–H bond of ammonia by the heavier group 14 metallylenes.[92]

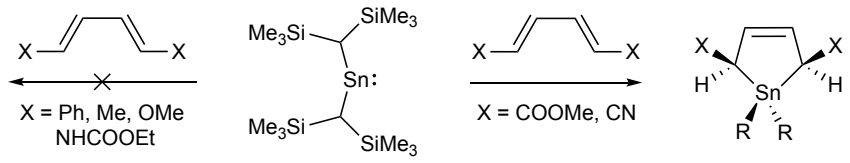
1.3.4 Reactivity of Metallylenes with C=E Multiple Bonds

The reactivity of the heavier group 14 metallylenes with carbon-carbon multiple bonds (alkenes and alkynes) has been the subject of research for decades.[94–97] The study of these reactions allows for the discovery of potential new modes of alkene/alkyne functionalisation facilitated by heavier metallylenes, such as alkene hydroamination.

1.3.4.1 Conjugated Systems

As detailed above, heavier group 14 metallylenes, in almost all cases, have singlet electronic ground states.[1,14] This suggests that metallylenes should be able to react in a concerted fashion with conjugated systems, analogous to their lighter singlet carbene analogues.[98]

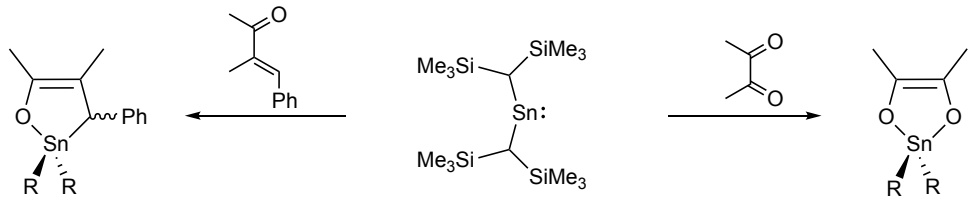
In 1983 and 1984, Hillner and Neumann demonstrated the 1,4-cycloaddition of germylenes and stannylenes with a variety of dienes.[96,99] The authors demonstrated that the HOMO of the metallylene interacts with the LUMO of the diene because the metallylenes were only able to react with the most electron deficient dienes.[99] The products of these reactions were exclusively the syn-isomers, supporting the idea that these are pericyclic [2+4]-cycloaddition reactions.[96,99]



1.33

Scheme 1-13: Reactions of bis(alkyl)stannylene, **1.33**, with an array of dienes (R = -CH($SiMe_3$)$_2$).[99]

In 1986, Hillner and Neumann demonstrated that stannylenes could also react with vinyl carbonyl compounds and diketones.[100] The concerted nature of these reactions could not be confirmed due to the lack of stereospecificity expected (or observed) in the products.[100] However, the dependence of the reaction on the concentration of the s-*cis* conformer suggests that the reactions do not proceed *via* a 1,2-addition across the carbonyl or vinyl group followed by a subsequent rearrangement. Instead, they also proceed *via* a concerted pericyclic [2+4]-cycloaddition.



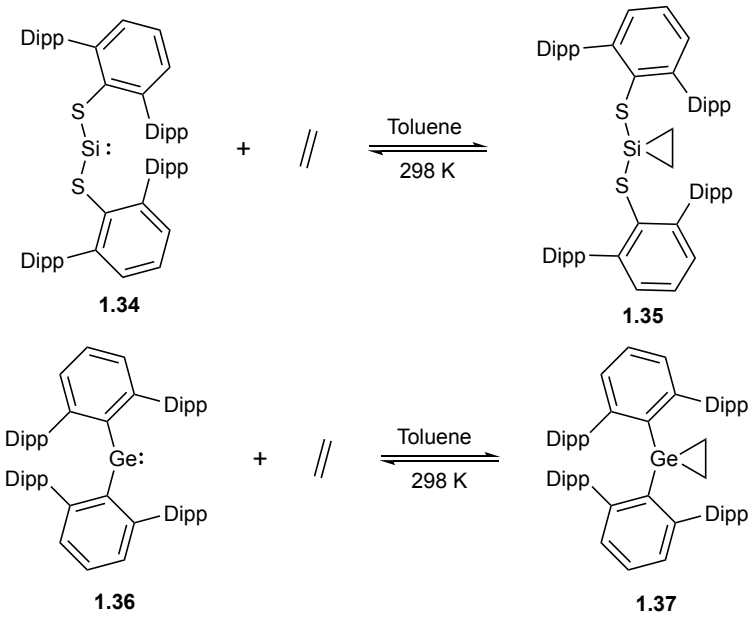
1.33

Scheme 1-14: Cycloaddition reactions of a bis(alkyl)stannylene, **1.33**, with a vinylcarbonyl compound and a diketone (R is -CH($SiMe_3$)$_2$).[100]

1.3.4.2 Alkenes

The cheletropic addition of dichlorocarbene to an alkene yielding a cyclopropane ring is a familiar reaction to undergraduate chemists.[101,102] Due to their singlet ground states, heavier metallylenes may be expected to behave similarly. However, the high ring strain inherent in the resulting metallocyclopropanes, coupled with the weaker E–C bonds, means that further rearrangement of these reactive species might be expected.[103]

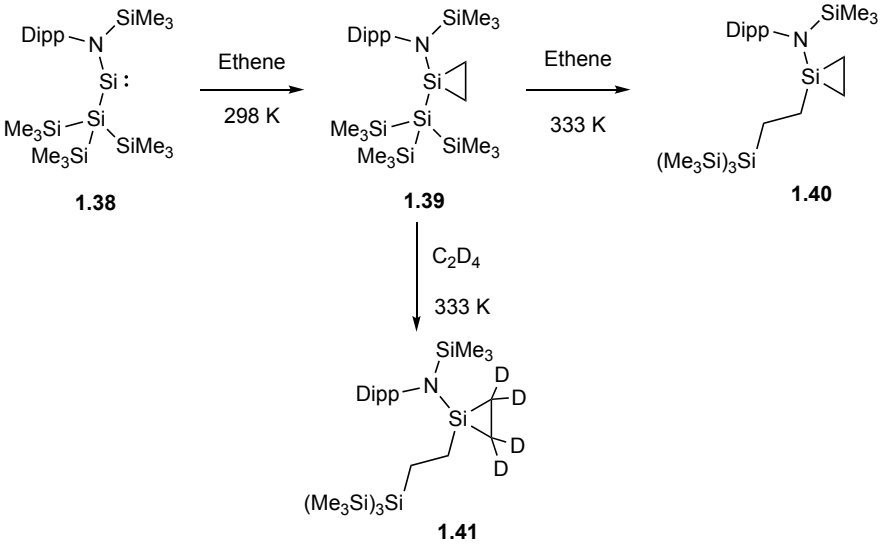
The reversible formation of both siliranes and germiranes from their corresponding metallylenes and ethylene has been demonstrated by Power *et al.*[104,105] In their 2014 work, they described the reversible reaction of a silylene, **1.34**, with an unspecified pressure of ethene at room temperature.[106] Mechanistically, they propose the reaction to result from a synergic donor-acceptor interaction between the two species, resulting in overall cycloaddition.[105] A similar mechanism was proposed for the reaction between a bis(aryl)germylene, **1.36**, and ethene.[104] Comparing the equilibrium data for **1.34** and **1.36** ($\Delta G(300\ K) = -24.9\ kJ\ mol^{-1}$ and $\Delta G(300\ K) = -7.3\ kJ\ mol^{-1}$ respectively) gives an indication of how much more stable the silirane is compared to the germirane, consistent with the differing E^{II}/E^{IV} redox potentials.[104,106]



Scheme 1-15: Top – Reversible activation of ethene by silylene, **1.34**. Bottom – Reversible activation of ethene by bis(aryl)germylene, **1.36**.[104,105]

In 2016, Rieger *et al.* synthesised a more stable system: silirane, **1.39**, is formed irreversibly from the parent silylene, **1.38**, and 0.5 bar of ethene.[107] Interestingly, when exposed to further ethene and heated to 333 K, a migratory insertion reaction of the pendant hypersilyl

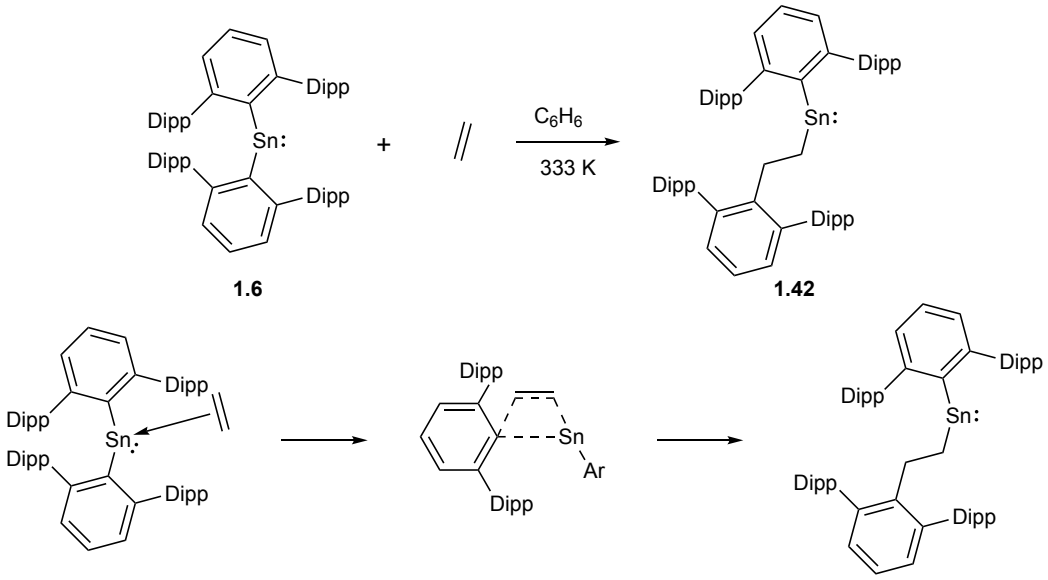
ligand occurs, followed by the cycloaddition of another equivalent of ethene to form **1.40**.[107] The authors confirmed this order of mechanistic steps by exposing **1.39** to per-deuterated ethene and heating to 333 K to form **1.41**. Uptake of the labelled ethene was limited to the new silirane unit and not the ethylene unit formed by insertion into the Si–Si bond.[107]



Scheme 1-16: Reaction of silylene, **1.38**, with ethene and the subsequent rearrangements when heated under an ethene and ethene-d^4 atmosphere at 333 K.[107]

Unlike their silicon and germanium analogues there have been no reported examples of a stannylene undergoing cycloaddition with ethene or other olefins to date. However, in 2019, Power *et al.* demonstrated that ethylene could insert into the Sn–C bond of bis(aryl)stannylene, **1.6**, reminiscent of the work by Rieger *et al.* (Scheme 1-17).[107,108] The insertion occurs at 333 K in the presence of excess ethylene (no pressure given) to yield an alkyl(aryl)stannylene, **1.41**, with a significantly narrower angle at the metal centre than the parent stannylene (**1.6**: 117.56(8)° *cf.* **1.41**: 94.7(5)°).[33,108] The mechanism is proposed to proceed *via* the formation of a weak ethylene complex utilising the empty Sn 5p-orbital, followed by the displacement of the ethylene to sit over one of the Sn–C bonds.[108] From this intermediate, the concerted formation of Sn–C and C–C bonds occurs to yield the insertion

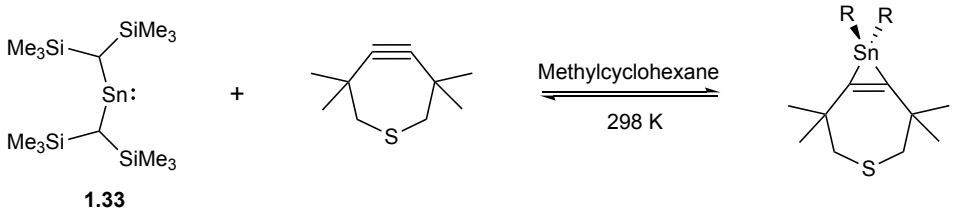
product.[108] The difference in olefin reactivity with stannylenes as compared to silylenes and germylenes is most likely due to larger HOMO–LUMO gaps for the stannylenes and the poorer stability of the E(IV) state for tin, akin to the ammonia reactivity discussed above.



Scheme 1-17: Top – Insertion of ethene into the Sn–C bond of bis(aryl)stannylene, **1.6**. Bottom – Proposed mechanism for the insertion of ethene in the Sn–C bond of a bis(aryl)stannylene.[108]

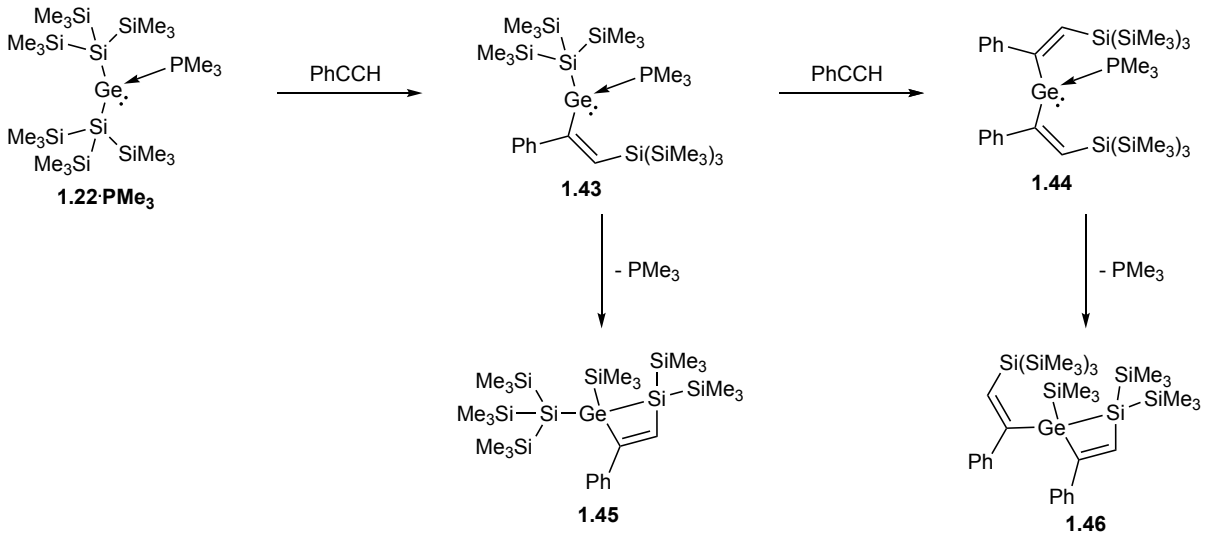
1.3.4.3 Alkynes

In contrast to alkenes, cheletropic addition of metallylenes to alkynes has been achieved with silylenes, germylenes, and stannylenes.[109–111] Of particular importance is the work of Sita *et al.* in which a stannylene was shown to reversibly form a stannacyclopropene with a strained alkyne.[111,112]



Scheme 1-18: Reaction of bis(alkyl)stannylene, **1.33**, with a strained alkyne to form a stannacyclopropene (R is $CH(SiMe_3)_2$).[112]

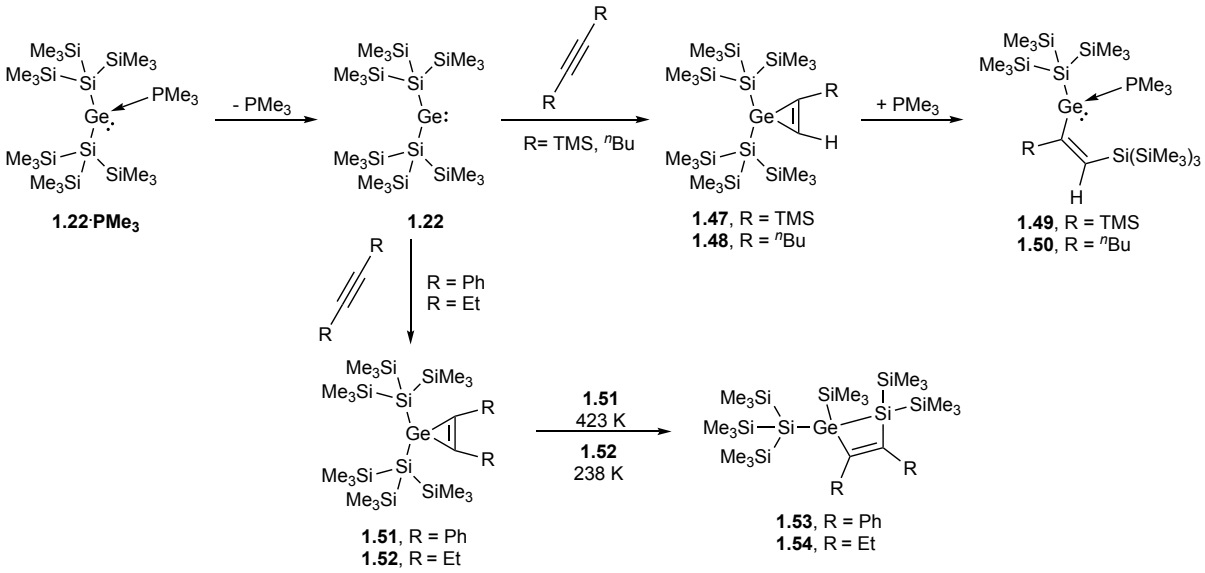
Insertion into the E–X bond, as observed with alkenes above, is another prominent mode of reactivity which metallylenes can display towards alkynes.[77,113–117] This pathway was first observed in 2014 by Marschner *et al.*, in which phenylacetylene was found to insert regio- and stereoselectively into the Ge–Si bonds of base-stabilised bis(silyl)germylene, **1.22·PMe$_3$**.[77] In contrast to the insertion chemistry observed with ethene (above), two equivalents of the alkyne could be inserted, potentially reflecting the greater sigma donor abilities of silyl ligands as compared to aryl ligands.[77] The phosphine plays an important role in stabilising the insertion products.[77] Upon its removal, subsequent rearrangement of both **1.43** and **1.44** is seen, brought about by the insertion of the germylene into one of the Si–SiMe$_3$ bonds.[77]



Scheme 1-19: Reactivity of base stabilised bis(silyl)germylene, **1.22·PMe$_3$**, with phenyl acetylene.[77]

In 2016, Müller *et al.* expanded on this work to try to elucidate the mechanism of the reaction (Scheme 1-20).[118] Insertions of trimethylsilylacetylene (TMSCCH) and hex-1-yne into the Ge–Si bond of **1.22·PMe$_3$** were also regio- and stereoselective, with the syn-addition product, **1.49** and **1.50** respectively, formed in both cases. The reactions proceed *via* initial decomplexation of the phosphine to yield the free germylene (**1.22**) followed by alkyne cycloaddition to yield the germacyclopropene intermediates, **1.47** (TMSCCH) and **1.48**

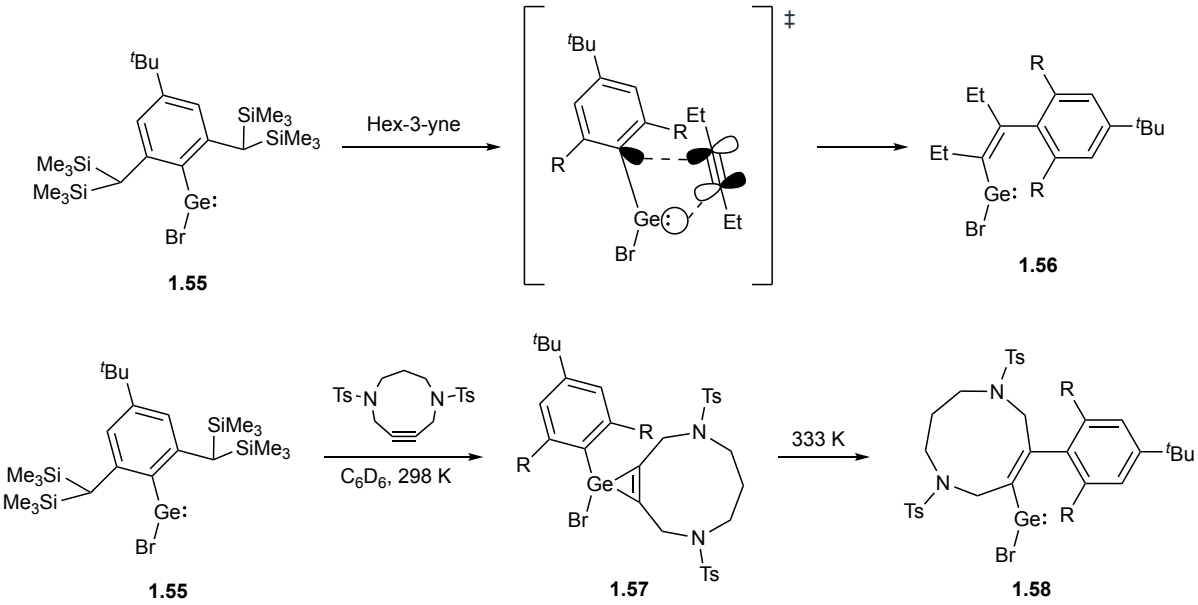
(hex-1-yne). Attack at the least hindered position of **1.47** and **1.48** by the silyl group then occurs to yield vinylgermylenes, **1.49** and **1.50** respectively.[118] The driving force for the reaction is the subsequent re-complexation of the phosphine to the vinylgermylene which significantly stabilises the product compared to the germacyclopropene (44 kJ mol^{-1}), which cannot be stabilised by the base.[113] Disubstituted alkynes behave differently, with the reactions of diphenylacetylene (PhCCPh) and hex-3-yne terminating at the cycloaddition products (**1.51** and **1.52** respectively), with no onward insertion (Scheme 1-20).[113] The divergent reactivity is attributed to the greater steric repulsion from the disubstituted alkynes, making the barrier to the insertion reaction much higher than with the monosubstituted alkynes.[113] Indeed, when **1.51** is heated to 423 K, it undergoes insertion into one of the Si–Si bonds, to form silagermacyclobutene, **1.53**, analogous to the decay product of the insertion compound formed with phenylacetylene (**1.45** and **1.46** Scheme 1-19).[113] Similarly, when **1.52** is left to stand for one week at 238 K, the formation of silagermacyclobutene, **1.54**, is observed.[113] The less forcing conditions required for the formation of **1.54** versus **1.53** are proposed to be due to the reduced steric bulk of **1.52** compared to **1.51**.[113]



Scheme 1-20: Reaction of a base stabilised bis(silyl)germylene with a variety of mono- and disubstituted alkynes.[113]

Further mechanistic work was carried out by Tokitoh *et al.* who investigated the insertion reactions of alkynes into the Ge–C bond of aryl(bromo)germylene, **1.55** (Scheme 1-21).[117] When **1.55** is reacted with hex-3-yne, the vinyl(bromo)germylene, **1.56**, is obtained, but only after heating at 333 K for 2 d, which the authors attribute to the low electrophilicity of the bromogermylene.[117] When a strained diazacyclononyne was employed (Scheme 1-21), the cheletropic addition product, **1.57**, was initially observed, but this isomerises to the final vinylgermylene product, **1.58**, after 8 h.[117] Mechanistically, for the reaction with hex-3-yne, the authors maintain that a concerted insertion of the alkyne into the Ge–C bond occurs through the interaction of the LUMO of the alkyne and the HOMO of **1.55** (a combination of a tilted p-type atomic orbital at the carbon and a sp-type atomic orbital at the germanium) to yield **1.56**.[117] This is a markedly different mechanism than that proposed by Marschner *et al.*, which could potentially be attributed to the very different electronic structures of **1.22** and **1.55**.[113] There is no mention of how isomerisation of the kinetic product, **1.57**, to the

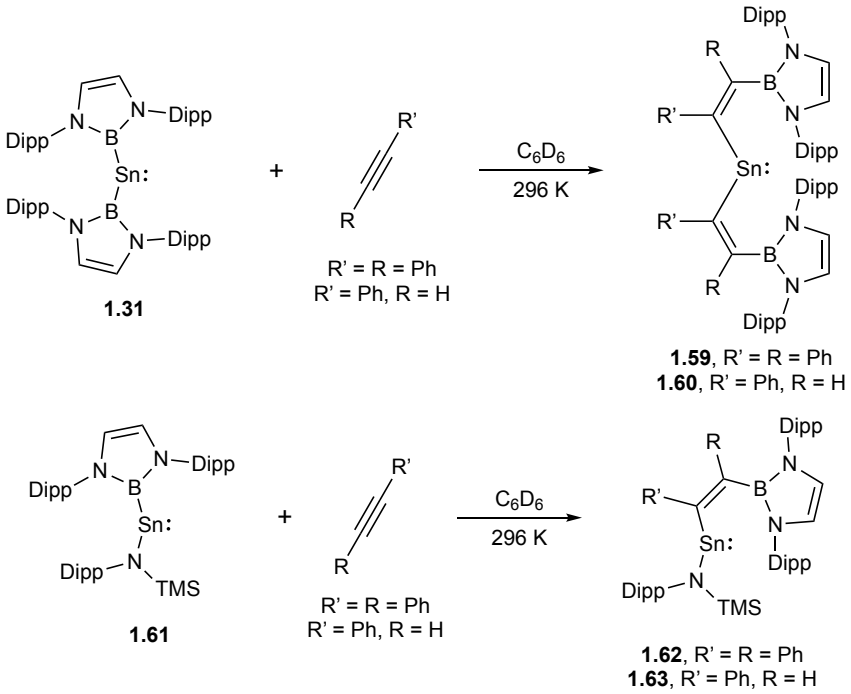
thermodynamic product, **1.58**, occurs, but it is likely that this step proceeds similarly to the processes reported by Marschner *et al.* above.[117,118]



Scheme 1-21: Top – Reaction of hex-3-yne with aryl(bromo)germylene, **1.55**. Bottom – Reaction of a strained cycloalkyne with aryl(bromo)germylene, **1.55** (R is $CH(SiMe_3)_2$).[117]

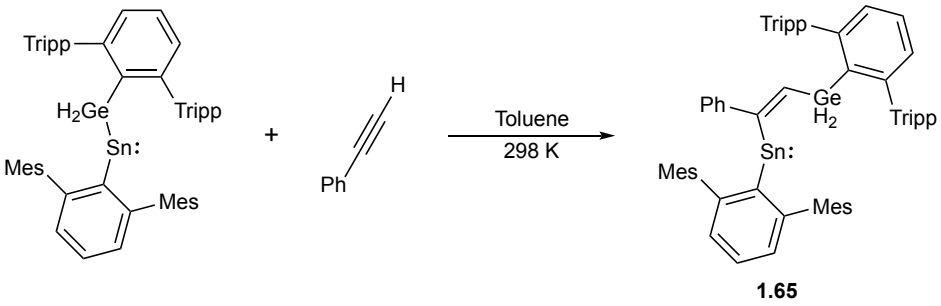
Similar insertion chemistry has also been observed with stannylenes. In 2015, Aldridge *et al.* synthesised two borylstannylenes, **1.31** and **1.61**, capable of inserting both phenyl- and diphenylacetylene into the Sn–B bonds at room temperature.[114] The same regio- and stereoselectivity is observed as with the germylene examples previously discussed, suggesting that the same mechanism might be at work.[114] The dramatic difference in the electronic structure of **1.31** and **1.61**, coupled with the fact that **1.31** undergoes a double insertion, suggests that a very narrow HOMO–LUMO gap may not be essential to ensure reactivity with alkynes. These observations would be more consistent with the concerted addition of the alkyne into the Sn–B bond, akin to the work of Tokitoh *et al*.[114,117] However, in the reaction of **1.61** with diphenylacetylene, a decolourisation is seen before the development of the deep green colour of the product.[117] This suggests that an intermediate is formed in the reaction

and, while it could not be trapped or identified, the authors postulate that it could be a stannacyclopropene, which can then undergo boryl group migration to yield the product, as seen in the work of Marschner *et al*.[117]



Scheme 1-22: Top – Reactions of bis(boryl)stannylene, **1.31**, with alkynes to form bis(vinyl)stannylenes, **1.59** and **1.60**. Bottom – Reaction of amido(boryl)stannylene, **1.61**, with alkynes to form amido(vinyl)stannylenes, **1.62** and **1.63**.[114]

In a separate study by Wesemann *et al.*, it was found that an aryl(germyl)stannylene, **1.64**, reacts with phenylacetylene to form the corresponding aryl(vinyl)stannylene, with the same syn-conformation product as observed with borylstannylenes **1.31** and **1.61**.[115] Unlike in the work from Aldridge *et al.*, no intermediate colour change was observed, potentially reflecting the more labile nature of the Sn–Ge bond which might be expected to migrate quicker than the corresponding Sn–B bond.[114,115] However, this lack of an observable intermediate could also suggest that this reaction undergoes insertion *via* concerted addition of the alkyne across the Sn–Ge bond, in a similar fashion to the work of Tokitoh *et al.*[115,117]



Scheme 1-23: Insertion of phenyl acetylene into the Sn–Ge bond of aryl(germyl)stannylene, **1.64**.[115]

1.4 Research Proposal

This thesis will investigate the chemistry of silyl-substituted metallylenes. As detailed above, the strong σ-donating ability of silyl ligands serves to narrow the HOMO–LUMO gaps of metallylenes and makes them ideal candidates for small molecule activation. In light of the reactivity already displayed by the aryl(silyl)germylene, **1.23**, synthesised by Aldridge *et al.*, initial studies will focus on using **1.23** to provide experimental evidence for the coordination/proton shuttling mechanism of N–H activation proposed by Peng *et al*. (Scheme 1-12).[82] Additionally, studies into the reactivity of **1.23** with alkenes and alkynes will be performed to ascertain whether the Ge–Si bond of **1.23** is as prone to migration as the Ge–Si bonds of the bis(silyl)germylene reported by Walewska *et al.* (Schemes 1-19 and 1-20).[118,119]

To date there are only three examples of crystallographically characterised acyclic silyl-substituted stannylenes.[46,120,121]The report of reversible P_4 activation at an aryl(silyl)stannylene from Sarkar *et al.* (Scheme 1-2) illustrates the potential of these systems to demonstrate interesting chemistry.[46] Therefore, the synthesis of a host of new silyl-substituted stannylenes will be attempted, and where appropriate their onward reactivity explored. Initial research will focus on trying to achieve the oxidative addition of

N–H bonds by a silylstannylene, as the similar σ-donating abilities of silyl and boryl-substituents is theorised to make replicating the oxidative addition of ammonia by bis(boryl)stannylene, **1.31**, (Scheme 1-11) possible.[84] Research will also investigate the reactivity of silyl-substituted stannylenes with alkenes and alkynes to determine whether the same insertion chemistry as seen with Sn–B (Scheme 1-22) and Sn–Ge (Scheme 1-23) bonds is seen and to elucidate what mechanism underpins this process.[114,115]

1.5 References

1 D. Bourissou, O. Guerret, F. P. Gabbaï and G. Bertrand, *Chem Rev*, 1999, **100**, 39–92.
2 W. von E. Doering and A. K. Hoffmann, *J Am Chem Soc*, 1954, **76**, 6162–6165.
3 A. Igau, H. Grutzmacher, A. Baceiredo and G. Bertrand, *J Am Chem Soc*, 1988, **110**, 6463–6466.
4 A. J. Arduengo, R. L. Harlow and M. Kline, *J Am Chem Soc*, 1991, **113**, 361–363.
5 M. Koy, P. Bellotti, M. Das and F. Glorius, *Nat Catal*, 2021, **4**, 352–363.
6 S. Díez-González, N. Marion and S. P. Nolan, *Chem Rev*, 2009, **109**, 3612–3676.
7 M. N. Hopkinson, C. Richter, M. Schedler and F. Glorius, *Nature*, 2014, **510**, 485–496.
8 Y. Wang, Y. Xie, P. Wei, R. B. King, H. F. Schaefer, P. von R. Schleyer and G. H. Robinson, *Science (1979)*, 2008, **321**, 1069–1071.
9 C. Samojłowicz, M. Bieniek and K. Grela, *Chem Rev*, 2009, **109**, 3708–3742.
10 M. S. M. Philipp and U. Radius, *Z Anorg Allg Chem*, 2022, **648**, e202200085.
11 R. Hoffmann, *J Am Chem Soc*, 1968, **87**, 1475–1485.
12 C. A. Richards, S.-J. Kim, Y. Yamaguchi and H. F. Schaefer III, *J. Am. Chem. Soc*, 1995, **117**, 10104–10107.
13 D. R. Myers, V. P. Senthilnathan, M. S. Platz and M. Jones, *J Am Chem Soc*, 1986, **108**, 4232–4233.
14 Y. Mizuhata, T. Sasamori and N. Tokitoh, *Chem Rev*, 2009, **109**, 3479–3511.
15 R. S. Drago, *Journal of Physical Chemistry*, 1958, **62**, 353–357.
16 R. S. Drago, *Journal of Inorganic and Nuclear Chemistry*, 1960, **15**, 237–241.
17 T. J. Hadlington, J. A. B. Abdalla, Rémi Tirfoin, Simon Aldridge and Cameron Jones, *Chemical Communications*, 2016, **52**, 1717–1720.
18 R. Guthardt, C. Bruhn, C. Färber and U. Siemeling, *Organometallics*, 2020, **39**, 4174–4177.
19 A. Jana, C. Schulzke and H. W. Roesky, *J Am Chem Soc*, 2009, **131**, 4600–4601.
20 C. Cui, M. M. Olmstead and P. P. Power, *J Am Chem Soc*, 2004, **126**, 5062–5063.
21 T. Y. Lai, J. C. Fettinger and P. P. Power, *Organometallics*, 2022, **41**, 1590–1594.
22 B. Twamley, C. S. Hwang, N. J. Hardman and P. P. Power, *J Organomet Chem*, 2000, **609**, 152–160.
23 C. Cui, M. M. Olmstead, J. C. Fettinger, G. H. Spikes and P. P. Power, *J Am Chem Soc*, 2005, **127**, 17530–17541.
24 J. W. Dube, Z. D. Brown, C. A. Caputo, P. P. Power and P. J. Ragogna, *Chem. Commun.*, 2014, **50**, 1944–1946.
25 C. Stanciu, A. F. Richards, J. C. Fettinger, M. Brynda and P. P. Power, *J Organomet Chem*, 2006, **691**, 2540–2545.
26 A. J. Valentine, A. M. Geer, L. J. Taylor, A. M. Teale, K. E. Wood, H. E. L. Williams, W. Lewis, S. P. Argent, J. McMaster and D. L. Kays, *Dalton Transactions*, 2021, **50**, 722–728.
27 Z. Zhu, X. Wang, Y. Peng, H. Lei, J. C. Fettinger, E. Rivard and P. P. Power, *Angewandte Chemie - International Edition*, 2009, **48**, 2031–2034.
28 J. D. Queen, A. Lehmann, J. C. Fettinger, H. M. Tuononen and P. P. Power, *J Am Chem Soc*, 2020, **142**, 20554–20559.
29 P. P. Power, *J Organomet Chem*, 2004, **689**, 3904–3919.
30 E. Rivard and P. P. Power, *Inorg Chem*, 2007, **46**, 10047–10064.

31 R. S. Simons, L. Pu, M. M. Olmstead and P. P. Power, *Organometallics*, 1997, **16**, 1920–1925.
32 S. Kobayashi and S. Cao, *Chem Lett*, 1993, **22**, 1385–1388.
33 G. H. Spikes, Y. Peng, J. C. Fettinger and P. P. Power, *Z Anorg Allg Chem*, 2006, **632**, 1005–1010.
34 P. Wilfling, K. Schittelkopf, M. Flock, R. H. Herber, P. P. Power and R. C. Fischer, *Organometallics*, 2015, **34**, 2222–2232.
35 K. W. Klinkhammer, J. Klett, Y. Xiong and S. Yao, *Eur J Inorg Chem*, 2003, **2003**, 3417–3424.
36 P. D. Lickiss and C. M. Smith, *Coord Chem Rev*, 1995, **145**, 75–124.
37 A. Sekiguchi, T. Tanaka, M. Ichinohe, K. Akiyama and S. Tero-Kubota, *J Am Chem Soc*, 2003, **125**, 4962–4963.
38 D. M. Roddick, T. D. Tilley, A. L. Rheingold and S. J. Geib, *J Am Chem Soc*, 1987, **109**, 945–946.
39 P. Braunstein and N. M. Boag, *Angewandte Chemie International Edition*, 2001, **40**, 2427–2433.
40 C. Marschner, *Eur J Inorg Chem*, 2015, **2015**, 3805–3820.
41 N. Wiberg, K. Amelunxen, H. Nöth, M. Schmidt and H. Schwenk, *Angewandte Chemie International Edition in English*, 1996, **35**, 65–67.
42 N. Wiberg, K. Schurz, G. Reber and G. Müller, *J Chem Soc Chem Commun*, 1986, 591–592.
43 K. W. Klinkhammer and W. Schwarz, *Angewandte Chemie International Edition in English*, 1995, **34**, 1334–1336.
44 L. Pauling, *The nature of the chemical bond and the structure of molecules and crystals : an introduction to modern structural chemistry*, Cornell University Press, Ithaca, 3rd ed., 1960.
45 J. Zhu, Z. Lin and T. B. Marder, *Inorg Chem*, 2005, **44**, 9384–9390.
46 D. Sarkar, C. Weetman, D. Munz and S. Inoue, *Angewandte Chemie International Edition*, 2021, **60**, 3519–3523.
47 B. E. C Alyea, J. S. Basi, D. C. Bradley, M. H. Chisholm, D. H. Brown, J. Chem SOC, D. J. Machin, D. F. C Morris and A. H. Westlake, *Chemical Communications (London)*, 1968, **95**, 495–495.
48 R. G. Jones, G. Karmas, G. A. Martin and H. Gilman, *J Am Chem Soc*, 1956, **78**, 4285–4286.
49 E. D. Brady, D. L. Clark, J. C. Gordon, P. J. Hay, D. W. Keogh, R. Poli, B. L. Scott and J. G. Watkin, *Inorg Chem*, 2003, **42**, 6682–6690.
50 P. G. Eller, D. C. Bradley, M. B. Hursthouse and D. W. Meek, *Coord Chem Rev*, 1977, **24**, 1–95.
51 D. E. Goldberg, D. H. Harris, M. F. Lappert and K. M. Thomas, *J Chem Soc Chem Commun*, 1976, 261–262.
52 R. J. Schwamm, C. A. von Randow, A. Mouchfiq, M. J. Evans, M. P. Coles and J. Robin Fulton, *Eur J Inorg Chem*, 2021, **2021**, 3466–3473.
53 T. J. Hadlington, C. E. Kefalidis, L. Maron and C. Jones, *ACS Catal*, 2017, **7**, 1853–1859.
54 S. Wang, L. Tao, T. A. Stich, M. M. Olmstead, R. D. Britt and P. P. Power, *Inorg Chem*, 2017, **56**, 14596–14604.
55 E. W. Y. Wong, T. J. Hadlington and C. Jones, *Main Group Metal Chemistry*, 2013, **36**, 133–136.
56 T. Řezníček, L. Dostál, A. Růžička and R. Jambor, *Eur J Inorg Chem*, 2012, **2012**, 2983–2987.
57 A. Hinz, *Chemistry – A European Journal*, 2019, **25**, 7843–7846.
58 A. Schnepf, *Z Anorg Allg Chem*, 2006, **632**, 935–938.
59 J. BareŠ, V. Šourek, Z. Padělková, P. Meunier, N. Pirio, I. Císařová, A. Růžička and J. Holeček, *Collect Czechoslov Chem Commun*, 2010, **75**, 121–131.
60 A. V. Protchenko, K. H. Birjkumar, D. Dange, A. D. Schwarz, D. Vidovic, C. Jones, N. Kaltsoyannis, P. Mountford and S. Aldridge, *J Am Chem Soc*, 2012, **134**, 6500–6503.
61 K. Osakada, Y. Tsuchido and M. Tanabe, *Coord Chem Rev*, 2020, **412**, 213195.
62 J. Baumgartner and C. Marschner, *Reviews in Inorganic Chemistry*, 2014, **34**, 119–152.
63 B. Blom, M. Stoelzel and M. Driess, *Chemistry – A European Journal*, 2013, **19**, 40–62.
64 G. G. Kazakov, N. O. Druzhkov, E. V. Baranov, A. V. Piskunov and V. K. Cherkasov, *J Organomet Chem*, 2021, **946–947**, 121887.
65 H. Arp, C. Marschner, J. Baumgartner, P. Zark and T. Müller, *J Am Chem Soc*, 2013, **135**, 7949–7959.
66 J. J. Schneider, N. Czap, D. Bläser and R. Boese, *J Organomet Chem*, 1999, **584**, 338–343.
67 H. Arp, J. Baumgartner, C. Marschner, P. Zark and T. Müller, *J Am Chem Soc*, 2012, **134**, 10864–10875.
68 J. A. Cabeza, J. M. Fernández-Colinas, P. García-Álvarez and D. Polo, *Inorg Chem*, 2012, **51**, 3896–3903.
69 U. Anandhi and P. R. Sharp, *Inorganica Chim Acta*, 2006, **359**, 3521–3526.
70 A. L. F. Chow, M. H. So, W. Lu, N. Zhu and C. M. Che, *Chem Asian J*, 2011, **6**, 544–553.
71 H. Arp, J. Baumgartner, C. Marschner and T. Müller, *J Am Chem Soc*, 2011, **133**, 5632–5635.
72 A. Mansikkamäki, P. P. Power and H. M. Tuononen, *Organometallics*, 2013, **32**, 6690–6700.
73 K. Klinkhammer, *Polyhedron*, 2002, **21**, 587–598.

74 H. Grützmacher, S. Freitag, R. Herbst-Irmer and G. S. Sheldrick, *Angewandte Chemie International Edition in English*, 1992, **31**, 437–438.
75 H. Tanaka, M. Ichinohe and A. Sekiguchi, *J Am Chem Soc*, 2012, **134**, 5540–5543.
76 A. Heine and D. Stalke, *Angewandte Chemie International Edition in English*, 1994, **33**, 113–115.
77 M. Walewska, J. Baumgartner and C. Marschner, *Chemical Communications*, 2014, **51**, 276–278.
78 G. H. Spikes, J. C. Fettinger and P. P. Power, *J Am Chem Soc*, 2005, **127**, 12232–12233.
79 G. D. Frey, V. Lavallo, B. Donnadieu, W. W. Schoeller and G. Bertrand, *Science (1979)*, 2007, **316**, 439–441.
80 M. Usher, A. V. Protchenko, A. Rit, J. Campos, E. L. Kolychev, R. Tirfoin and S. Aldridge, *Chemistry – A European Journal*, 2016, **22**, 11685–11698.
81 A. V. Protchenko, D. Dange, M. P. Blake, A. D. Schwarz, C. Jones, P. Mountford and S. Aldridge, *J Am Chem Soc*, 2014, **136**, 10902–10905.
82 Y. Peng, J.-D. Guo, B. D. Ellis, Z. Zhu, J. C. Fettinger, S. Nagase and P. P. Power, *J Am Chem Soc*, 2009, **131**, 16272–16282.
83 Y. Peng, B. D. Ellis, X. Wang and P. P. Power, *J Am Chem Soc*, 2008, **130**, 12268–12269.
84 A. V. Protchenko, J. I. Bates, L. M. A. Saleh, M. P. Blake, A. D. Schwarz, E. L. Kolychev, A. L. Thompson, C. Jones, P. Mountford and S. Aldridge, *J Am Chem Soc*, 2016, **138**, 4555–4564.
85 J. Haggin, *Chemical and Engineering News*, 1993, 71, 23–27.
86 A. Werner, *Z Anorg Allg Chem*, 1893, **3**, 267.
87 J. L. Klinkenberg and J. F. Hartwig, *Angewandte Chemie - International Edition*, 2011, 50, 86–95.
88 M. R. A. Blomberg, P. E. M. Siegbahn and M. Svensson, *Inorg Chem*, 1993, **32**, 4218–4225.
89 S. A. Macgregor, *Organometallics*, 2001, **20**, 1860–1874.
90 J. Zhao, A. S. Goldman and J. F. Hartwig, *Science (1979)*, 2005, **307**, 1080–1082.
91 W. M. Haynes, *CRC Handbook of Chemistry and Physics*, 95th edn., 2015.
92 M. E. Alberto, N. Russo and E. Sicilia, *Chemistry - A European Journal*, 2013, **19**, 7835–7846.
93 Z. D. Brown, J. D. Guo, S. Nagase and P. P. Power, *Organometallics*, 2012, **31**, 3768–3772.
94 T. Kusukawa, Y. Kabe and W. Ando, *Advances in Strain in Org. Chem.*, 1993, **3**, 985–988.
95 R. L. Lambert and D. Seyferth, *J Am Chem Soc*, 1972, **94**, 9246–9248.
96 M. Schriewer and W. P. Neumann, *J Am Chem Soc*, 1983, **105**, 897–901.
97 F. T. Edelmann and M. Belay, *J Fluor Chem*, 1997, **84**, 29–33.
98 P. S. Skell and R. C. Woodworth, *J Am Chem Soc*, 1956, **78**, 4496–4497.
99 R. Marx, W. P. Neumann and K. Hillner, *Tetrahedron Lett*, 1984, **25**, 625–628.
100 K. Hillner and W. P. Neumann, *Tetrahedron Lett*, 1986, **27**, 5347–5350.
101 I. Fleming, *Pericyclic reactions*, Oxford University Press, Oxford, Second edition., 2015.
102 B. Dinda, *Essentials of Pericyclic and Photochemical Reactions*, Springer Nature, Cham, 1st edn., 2016, vol. 93.
103 H. Ohgaki, Y. Kabe and W. Ando, *Organometallics*, 1995, **14**, 2139–2141.
104 K. L. Gullett, T. Y. Lai, C. Y. Chen, J. C. Fettinger and P. P. Power, *Organometallics*, 2019, **38**, 1425–1428.
105 F. Lips, J. C. Fettinger, A. Mansikkamäki, H. M. Tuononen and P. P. Power, *J Am Chem Soc*, 2014, **136**, 634–637.
106 F. Lips, A. Mansikkamäki, J. C. Fettinger, H. M. Tuononen and P. P. Power, *Organometallics*, 2014, **33**, 6253–6258.
107 D. Wendel, W. Eisenreich, C. Jandl, A. Pöthig and B. Rieger, *Organometallics*, 2016, **35**, 1–4.
108 T. Y. Lai, J. D. Guo, J. C. Fettinger, S. Nagase and P. P. Power, *Chemical Communications*, 2019, **55**, 405–407.
109 R. T. Conlin and P. P. Gaspar, *J Am Chem Soc*, 1976, **98**, 3715–3716.
110 T. Y. Lai, K. L. Gullett, C. Y. Chen, J. C. Fettinger and P. P. Power, *Organometallics*, 2019, **38**, 1421–1424.
111 J. R. Babcock, L. Liable-Sands, A. L. Rheingold and L. R. Sita, *Organometallics*, 1999, **18**, 4437–4441.
112 L. R. Sita and R. D. Bickerstaff, *J Am Chem Soc*, 1988, **110**, 5208–5209.
113 M. Walewska, J. Baumgartner, C. Marschner, L. Albers and T. Müller, *Chemistry – A European Journal*, 2016, **22**, 18512–18521.
114 A. V. Protchenko, M. P. Blake, A. D. Schwarz, C. Jones, P. Mountford and S. Aldridge, *Organometallics*, 2015, **34**, 2126–2129.
115 J. J. Maudrich, F. Diab, S. Weiß, M. Zweigart, K. Eichele, H. Schubert, R. Müller, M. Kaupp and L. Wesemann, *Chemistry – A European Journal*, 2021, **27**, 4691–4699.
116 M. L. McCrea-Hendrick, S. Wang, K. L. Gullett, J. C. Fettinger and P. P. Power, *Organometallics*, 2017, **36**, 3799–3805.

117 T. Sugahara, A. Espinosa Ferao, A. Rey Planells, J. D. Guo, S. Aoyama, K. Igawa, K. Tomooka, T. Sasamori, D. Hashizume, S. Nagase and N. Tokitoh, *Dalton Transactions*, 2020, **49**, 7189–7196.
118 M. Walewska, J. Baumgartner, C. Marschner, L. Albers and T. Müller, *Chemistry – A European Journal*, 2016, **22**, 18512–18521.
119 M. Walewska, J. Baumgartner and C. Marschner, *Chemical Communications*, 2014, **51**, 276–278.
120 C. Drost, B. Gehrhus, P. B. Hitchcock and M. F. Lappert, *Chemical Communications*, 1997, 1845–1846.
121 B. Gehrhus, P. B. Hitchcock and M. F. Lappert, *Angewandte Chemie International Edition in English*, 1997, **36**, 2514–2516.

2 Experimental Methods

2.1 Handling of Air- and Moisture- Sensitive Compounds

The manipulations described in this thesis were performed using standard Schlenk line techniques under an argon atmosphere. Dry-box techniques were also employed under a nitrogen atmosphere. Diethyl ether and THF were distilled over sodium and benzophenone, and then stored over activated molecular sieves in Teflon valve ampoules. All other solvents were degassed by sparging with argon and dried by passing through a column of the appropriate drying agent, then stored over potassium mirrors in Teflon valve ampoules.

2.2 Spectroscopic and Analytical Techniques

2.2.1 NMR Spectroscopy

NMR spectra were measured on a Bruker Avance III HD nanobay 400 MHz NMR spectrometer, a Bruker Avance III 500 MHz NMR spectrometer, or a Bruker NEO 600 MHz NMR spectrometer equipped with a broadband helium cryoprobe. All ^{13}C NMR measurements were performed with proton decoupling. ^{1}H NMR spectra were referenced internally to residual protio-solvent. ^{13}C NMR spectra were referenced internally to the deuterated solvent employed. ^{19}F, ^{29}Si, and ^{119}Sn were referenced externally with respect to $CFCl_3$, $SiMe_4$, and $SnMe_4$ respectively. 2D NMR techniques (COSY, HSQC, and HMBC) were used to aid in assignment of NMR spectra.

2.2.2 Variable Temperature Experiments for Alkyne Uptake

Reaction mixtures were made up inside a nitrogen glove box, in NMR tubes fitted with J-Young valves. The reaction mixtures were then allowed to equilibrate by being left overnight at ambient conditions. The NMR samples were maintained at the desired temperature in the NMR spectrometer and monitored by *in situ* ^{1}H NMR spectroscopy until no change was seen in the ratio of intensities between the product and reactant resonances. From the measured ratio of intensities of the resonances corresponding to the reactants and the product, the equilibrium constant at a particular temperature could be obtained (Equation 1).

$$\text{Equation 1: } K_{eq} = \frac{[product]}{[stannylene][alkyne]}$$

With the values of K_{eq} obtained at six different temperatures, the van't Hoff equation (Equation 2) was used to determine graphically the thermodynamic parameters of the reaction.

$$\text{Equation 2: } lnK_{eq} = -\frac{\Delta H}{RT} + \frac{\Delta S}{R}$$

2.2.3 X-ray Diffraction

Single-crystal X-ray diffraction data were collected on an Oxford Diffraction/Agilent SuperNova diffractometer equipped with a 135 mm Atlas CCD area detector. Crystals were picked under Pantone-N oil and mounted on MiTeGen Micromount loops whilst being quench cooled using an Oxford Cryosystems open flow N_2 cooling device.[1] All data were collected at 150 K using mirror monochromated Cu Kα radiation (λ = 1.54184 Å) or Mo Kα radiation (λ = 0.71073 Å). Once collected, the data were processed using the CrysAlisPro package.[2]

Structures were solved *ab initio* from the integrated intensities using SHELXT and refined on F2 using SHELXL with the graphical interface OLEX2.[3–5] Once solved, the depictions of the crystal structures used in this thesis were generated using POV-Ray.[6] The single-crystal X-ray diffraction data presented in this thesis were collected by myself, Ms Aisling F. Roper, Mr Agamemnon E. Crumpton, Dr Caitilín McManus, Dr Andreas Heilmann, and Dr Mathias A. Ellwanger.

2.2.4 UV/Vis Spectroscopy

All UV/Vis spectra were measured in hexane solution in quartz cuvettes of 1 cm path length using a JASCO V-770 UV-Visible/NIR Spectrophotometer.[7]

2.2.5 Elemental Analysis

Elemental analyses were carried out by London Metropolitan University.[8]

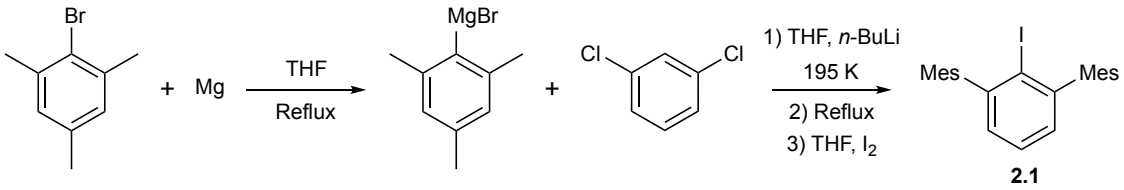
2.2.6 Quantum Chemical Calculations

Calculations were carried out by Mr Agamemnon E. Crumpton (Aldridge Group, University of Oxford). All calculations were performed with the ORCA (Revision 5.0.4) programme.[9–11] All structures were first optimised using the meta-generalized-gradient approximation (mGGA) functional R2-SCAN in conjunction with the Def2-TZVPPm basis set with the D4 dispersion correction, and employing the geometrical counterpoise correction gCP (together known as the R2SCAN-3c method).[12–15] Frequency calculations were performed to confirm the nature of minima by the lack of imaginary frequencies.

2.3 Known Compounds

The synthesis of some known compounds was required in the course of this work: $Ge(Ar^{Mes})(Si(TMS)_3)$[16], $W(CO)_5(NMe_3)$[17], $KSi(TMS)_2(Si^tBuPh_2)$[18], HN(Dipp)(TMS)[19], LiN(Dipp)(TMS)[20], $Ar^{Dipp}I$ [21], Ar^{Dipp2}[22], and $[Sn(N(Dipp)(TMS))Cl]_2$[23] were synthesised according to literature procedures. Other compounds were synthesised *via* new methods; and their syntheses are detailed below. All other reagents were purchased from chemical suppliers and used without further purification.

2.3.1 $Ar^{Mes}I$, **2.1** (Scheme 2-1)

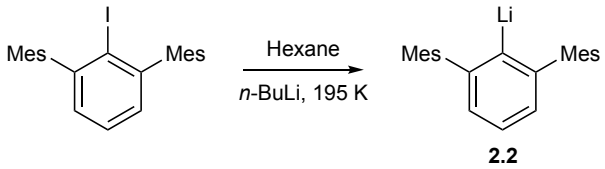


Scheme 2-1: Synthesis of 2,6-dimesityl-iodobenzene, **2.1**.

(Adapted from the procedure by Du *et al.*)[24] To a suspension of magnesium shavings (6.4 g, 26 mmol) in THF (60 mL) in a three-necked round-bottom flask fitted with a reflux condenser was added dropwise a solution of mesitylbromide (34 mL, 22 mmol) in THF (100 mL). After the addition was finished, the reaction was heated to reflux and maintained at this temperature for 4 h before being cooled to ambient temperature. A solution of dichlorobenzene (10 mL, 88 mmol) in THF (100 mL) was cooled to 195 K and *n*-butyllithium (58 mL, 92 mmol) added slowly with rapid stirring. After the addition was complete, the reaction mixture was stirred at 195 K for 2 h before dropwise addition of the filtered Grignard solution at 195 K. The solution was then allowed to warm to ambient temperature and stirred for 12 h. The reaction mixture was then heated to reflux for 2 h before being cooled to 273 K.

Once at 273 K, a solution of iodine (33 g, 131 mmol) in THF (150 mL) was added slowly to the reaction mixture. After warming to room temperature and stirring for 12 h, any excess iodine was quenched with an aqueous sodium sulphite solution, with the organic and aqueous layers separated, and the aqueous layer was extracted with diethyl ether (3 x 20 mL). The combined organic fractions were then dried over magnesium sulphate, and volatiles removed *in vacuo*, to yield the crude product. The spectroscopically pure product was isolated by washing the crude product with hot ethanol to yield $Ar^{Mes}I$ as a white fluffy solid. Yield 16 g, 41%. NMR spectra matched those reported by Du *et al.*[24]

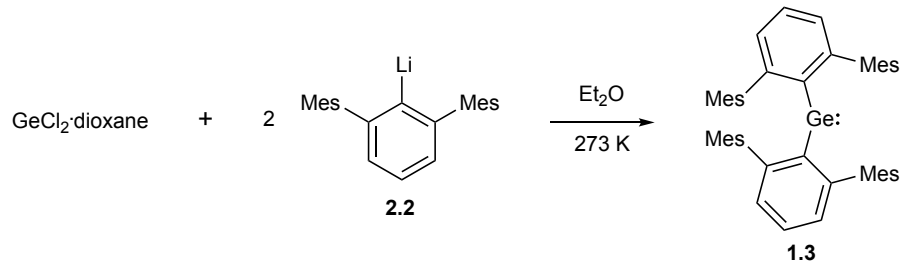
2.3.2 $Ar^{Mes}Li$, **2.2** (Scheme 2-2)



Scheme 2-2: Synthesis of 2,6-dimesityl-phenyllithium, **2.2**.

To a suspension of **2.1** (7.0 g, 16 mmol) in hexane (100 mL) at 195 K was added dropwise *n*-butyllithium (1.6 M, 11 mL, 17 mmol) with rapid stirring. The reaction mixture was then allowed to warm to room temperature and stirred for 12 h. After filtration, the residue was washed with pentane at room temperature (2 x 15 mL) to yield the spectroscopically pure product as a white solid. An additional crop of product could be obtained by removing the volatiles from the filtrate *in vacuo* and washing the residue with pentane (3 x 20 mL) at room temperature. Overall yield: 3.7 g, 73%. NMR data matched those reported by Schulz *et al.*[25]

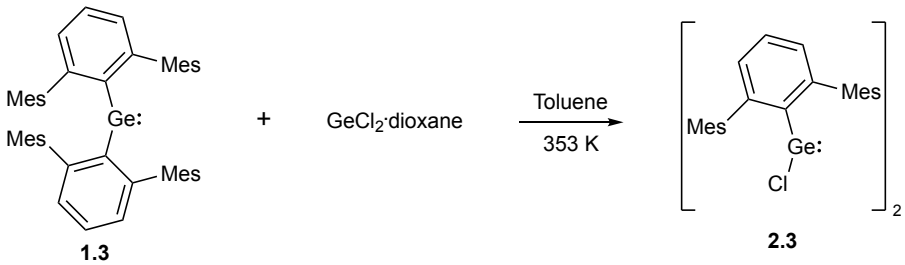
2.3.3 $Ge(Ar^{Mes})_2$, **1.3** (Scheme 2-3)



Scheme 2-3: Synthesis of bis(aryl)germylene, **1.3**, from germanium(II) dichloride dioxane adduct.

To a suspension of germanium dichloride dioxane (1.1 g, 4.7 mmol) in diethyl ether (50 mL) at 273 K was added a solution of **2.2** (3.0 g, 9.4 mmol) also in diethyl ether (75 mL). The reaction mixture was stirred at 273 K for 30 min and then warmed to room temperature and stirred for 12 h. Volatiles were removed *in vacuo*, and the residue extracted into toluene (100 mL) before hexane (10 mL) was added to precipitate any dissolved lithium chloride. The suspension was filtered, and the filtrate concentrated to incipient crystallisation before being stored at 243 K to afford the product as purple crystals (1.9 g). A second crop of crystals was obtained by concentrating the mother liquor to incipient crystallisation and storing at 243 K (0.50 g). Overall yield: 2.4 g, 72%. NMR data matched those reported by Simons *et al.*[26]

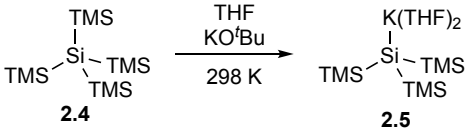
2.3.4 $[Ge(Ar^{Mes})Cl]_2$, **2.3** (Scheme 2-4)



Scheme 2-4: Synthesis of an aryl(chloro)germylene dimer, **2.3**, from bis(aryl)germylene, **1.3**.

Germanium dichloride dioxane (1.0 g, 4.4 mmol) and **1.3** (3.1 g, 4.4 mmol) were combined as solids in a Schlenk flask, and toluene was added (50 mL). The reaction mixture was heated to 353 K and maintained at this temperature for 15 min before being cooled to ambient temperature. The reaction mixture was then concentrated *in vacuo* until incipient crystallisation, with pentane (5 mL) being added. After storage at 243 K and filtration, the product was obtained as a red crystalline material which was washed with pentane and dried *in vacuo*. Yield: 1.9 g, 50%. NMR data matched those reported by Simons *et al.*[26]

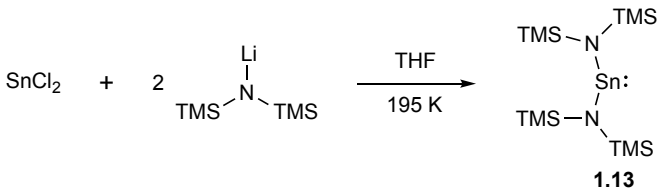
2.3.5 $K(THF)_2Si(TMS)_3$, **2.5** (Scheme 2-5)



Scheme 2-5: Synthesis of the potassium hypersilyl THF solvate, **2.5**, from tetrakistrimethylsilylsilane.

(Adapted from the procedure reported by Marschner *et al.*)[27] A Schlenk flask was charged with tetrakis(trimethylsilyl)silane, **2.4**, (5.5 g, 17 mmol) and potassium *tert*-butoxide (2.0 g, 18 mmol). THF (100 mL) was added with rapid stirring at ambient temperature, and the reaction mixture stirred for 12 h. Volatiles were removed *in vacuo* and the residue extracted into minimal toluene (40 mL). Removal of the volatiles *in vacuo* afforded the product as a yellow-green solid. Yield: 4.6 g, 95%. NMR data matched those reported by Marschner *et al.*[27]

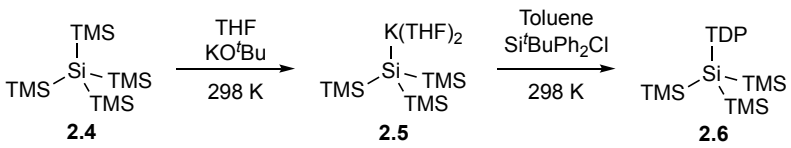
2.3.6 $Sn(HMDS)_2$, **1.13** (Scheme 2-6)



Scheme 2-6: Synthesis of tin(bis(bis(trimethylsilyl)amide)), **1.13**, from tin(II) chloride.

$SnCl_2$ (2.3 g, 12 mmol) and Li(HMDS) (4.0 g, 24 mmol) were combined in a Schlenk flask as solids and the mixture cooled to 195 K. THF (50 mL) was added with rapid stirring and the reaction mixture was warmed to room temperature and stirred for 12 h. Volatiles were removed *in vacuo* and the residue was extracted with toluene (100 mL). After filtration, volatiles were again removed *in vacuo* to yield spectroscopically pure $Sn(HMDS)_2$ as an orange solid. Yield: 4.5 g, 84%. NMR data matched those reported by Davidson *et al.*[28]

2.3.7 $Si(TMS)_3(Si^tBuPh_2)$, **2.6** (Scheme 2-7)



Scheme 2-7: Synthesis of $Si(SiMe_3)_3(Si^tBuPh_2)$, **2.6**, from tetrakis(silyl)silane (TDP is $-Si(^tBu)(Ph)_2$).

(Adapted from the synthesis of Baumgartner *et al.*)[29] **2.4** (11 g, 33 mmol) and KO^tBu (3.9 g, 35 mmol) were combined in a Schlenk flask and THF (100 mL) added at room temperature with stirring. The reaction was stirred for 12 h and volatiles then removed *in vacuo*, and the residue extracted into toluene (150 mL). To this solution was added dropwise a solution of Si^tBuPh_2Cl (9.5 g, 35 mmol) also in toluene (50 mL) at 195 K. The reaction mixture was then warmed to room temperature and stirred for 12 h. At this point it was added to a mixture of ice, de-ionised water, sulphuric acid (0.50 M), and diethyl ether.

The aqueous and organic layers were separated, and the aqueous layer extracted with diethyl ether (3 x 20 mL). The combined organic layers were then dried over magnesium sulphate, and volatiles removed *in vacuo.* Recrystallisation of the residue from acetone afforded the spectroscopically pure product as colourless blocks. Yield: 11 g, 67%. NMR data matched those reported by Baumgartner *et al.*[29]

2.4 References

1 J. Cosier and A. M. Glazer, *J Appl Crystallogr*, 1986, **19**, 105–107.
2 Agilent Technologies, 2022.
3 G. M. Sheldrick, *Acta Crystallogr A Found Adv*, 2015, **71**, 3–8.
4 G. M. Sheldrick, *Acta Crystallogr C Struct Chem*, 2015, **71**, 3–8.
5 O. V. Dolomanov, L. J. Bourhis, R. J. Gildea, J. A. K. Howard and H. Puschmann, *J Appl Crystallogr*, 2009, **42**, 339–341.
6 POV-Ray - The Persistence of Vision Raytracer, https://www.povray.org/, (accessed 5 February 2024).
7 V-770 UV-visible/NIR spectrophotometer | JASCO, https://jascoinc.com/products/spectroscopy/uv-visible-nir-spectrophotometers/models/v-770-uv-visible-nir-spectrophotometer/, (accessed 11 March 2024).
8 Elemental analysis service - London Metropolitan University, https://www.londonmet.ac.uk/services-and-facilities/elemental-analysis-service/, (accessed 6 February 2024).
9 F. Neese, *Wiley Interdiscip Rev Comput Mol Sci*, 2012, **2**, 73–78.
10 F. Neese, *WIREs Computational Molecular Science*, 2018, **8**, e1327.
11 F. Neese, F. Wennmohs, U. Becker and C. Riplinger, *Journal of Chemical Physics*, 2020, **152**, 224108.
12 J. W. Furness, A. D. Kaplan, J. Ning, J. P. Perdew and J. Sun, *Journal of Physical Chemistry Letters*, 2020, **11**, 8208–8215.
13 S. Grimme, A. Hansen, S. Ehlert and J.-M. Mewes, *J Chem Phys*, 2021, **154**, 064103.
14 E. Caldeweyher, S. Ehlert, A. Hansen, H. Neugebauer, S. Spicher, C. Bannwarth and S. Grimme, *J Chem Phys*, 2019, **150**, 154122.
15 H. Kruse and S. Grimme, *J Chem Phys*, 2012, **136**, 154101.
16 M. Usher, A. V. Protchenko, A. Rit, J. Campos, E. L. Kolychev, R. Tirfoin and S. Aldridge, *Chemistry – A European Journal*, 2016, **22**, 11685–11698.
17 S. L. Matthews and D. M. Heinekey, *J Am Chem Soc*, 2006, **128**, 2615–2620.
18 T. Kunz, O. Şahin and A. Schnepf, *Z Anorg Allg Chem*, 2022, **648**, e202200081.
19 A. Schulz, A. Villinger and A. Westenkirchner, *Inorg Chem*, 2013, **52**, 11457–11468.
20 M. Á. Fuentes, A. Zabala, A. R. Kennedy and R. E. Mulvey, *Chemistry – A European Journal*, 2016, **22**, 14968–14978.
21 B. R. Barnett, C. C. Mokhtarzadeh, J. S. Figueroa, P. Lummis, S. Wang, J. D. Queen, J. Gavenonis, N. Schüwer, T. D. Tilley, J. N. Boynton, P. P. Power, T. B. Ditri, N. Weidemann, D. W. Agnew, P. W. Smith, T. B. Ditri, A. E. Carpenter, J. K. Pratt and N. D. Mendelson, John Wiley & Sons, Ltd, 2018, pp. 85–122.
22 M. Fischer, S. Nees, T. Kupfer, J. T. Goettel, H. Braunschweig and C. Hering-Junghans, *J Am Chem Soc*, 2021, **143**, 4106–4111.
23 M. Brynda, R. Herber, P. B. Hitchcock, M. F. Lappert, I. Nowik, P. P. Power, A. V. Protchenko, A. Růžička and J. Steiner, *Angewandte Chemie International Edition*, 2006, **45**, 4333–4337.
24 C. J. F. Du, H. Hart and K. K. D. Ng, *Journal of Organic Chemistry*, 1986, **51**, 3162–3165.
25 A. Schulz, M. Thomas and A. Villinger, *Dalton Transactions*, 2019, **48**, 125–132.
26 R. S. Simons, L. Pu, M. M. Olmstead and P. P. Power, *Organometallics*, 1997, **16**, 1920–1925.
27 C. Marschner, *Eur J Inorg Chem*, 1998, **1998**, 221–226.

28 P. J. Davidson, D. H. Harris and M. F. Lappert, *Journal of the Chemical Society, Dalton Transactions*, 1976, 2268–2274.
29 J. Hlina, F. Stella, M. A. Meshgi, C. Marschner and J. Baumgartner, *Molecules 2016, Vol. 21, Page 1079*, 2016, **21**, 1079.

3 Reactivity of an Aryl(silyl)germylene

3.1 Introduction

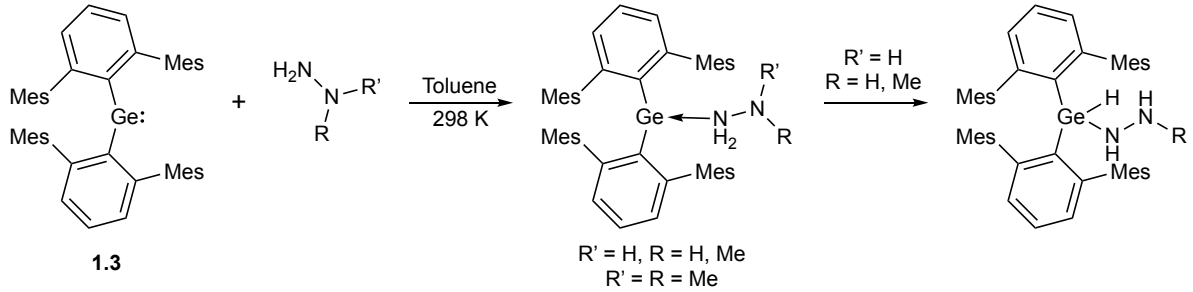
The σ-donating strength of boryl and silyl ligands is well known, and when incorporated in metallylenes these substituents serve to narrow the HOMO–LUMO gap.[1–3] The smaller this HOMO–LUMO gap, the more likely it is that the metallylene will display reactivity reminiscent of transition metals towards substrates, such as H_2, which act as both σ-donors and π-acceptors.[4–7] However, despite these useful potential patterns of reactivity, only a handful of boryl or silyl germylenes have been synthesised.[8,9] One such example is the aryl(silyl)germylene synthesised by Usher *et al.* (**1.23**), which was found to be capable of the oxidative addition of ammonia and hydrogen (see Schemes 3-1 and 1-7).[9]



Scheme 3-1: Oxidative addition of ammonia by aryl(silyl)germylene, **1.23**.[9]

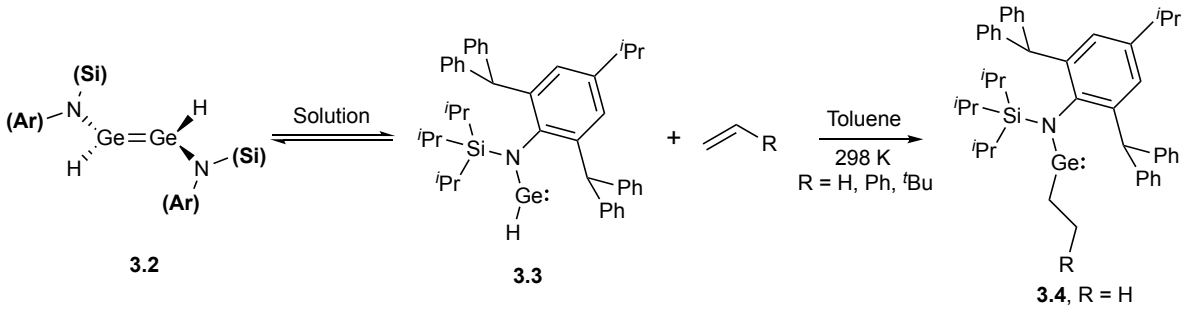
Despite a mechanism for the oxidative addition of N–H bonds being proposed by Power *et al.* in which a second equivalent of ammonia can act as a proton shuttle (Scheme 1-12), no experimental evidence to support this mechanism for germylenes has been reported.[7] A similar proton shuttling mechanism was proposed for the separate but related reactions of a bis(aryl)germylene, **1.3**, with hydrazines by Nagase *et al.* (Scheme 3-2).[10] When **1.3** is reacted with hydrazine or methylhydrazine, the oxidative addition of one N–H bond occurs.[10] However, when N,N-dimethylhydrazine is reacted with **1.3**, only coordination is observed,

which the authors postulate is due to the greater bulk preventing a second equivalent from acting as a proton shuttle.[10] Nevertheless, the formation of the adduct serves as important experimental evidence for the first step in the mechanism proposed by the authors.[10]



Scheme 3-2: Reactivity of hydrazines with bis(aryl)germylene, **1.3**. Oxidative addition of the N–H bond is not observed for N,N-dimethylhydrazine.[10]

Another interesting feature of boryl and silyl germylenes is insertion of the C=C bonds of alkenes and alkynes into the E–B/Si bonds (see Introduction).[11–13] This chemistry resembles that of the hydridogermylene, **3.3**, reported by Jones *et al.*[14] In this study, an array of alkenes and alkynes were found to be hydrometallated by the Ge–H bond (Scheme 3-3).[14] The authors proposed that the reaction occurs between **3.3** and the alkene, rather than its dimer, **3.2**, as the interaction between the alkene and the vacant p-orbital of the germylene is necessary for hydrometallation to occur.[14] The insertion of ethene into the Ge–H bond of **3.3** to form alkyl(amido)germylene, **3.4**, increases the steric bulk of the germylene. While **3.3** exists in equilibrium in solution with its dimer, **3.2**, no dimerisation is observed for **3.4**, or any of the other hydrometallated products.[14] Indeed, it is likely that after the hydrometallation of the alkene, the increased steric bulk of the resultant germylene prohibits subsequent dimerisation.



Scheme 3-3: Hydrometallation of an array of alkenes with hydridogermylene, **3.3** (**(Ar)** is $-C_6H_2$-2,6-$(CH(Ph)_2)_2$-4-(^{i}Pr) and **(Si)** is $-Si(^iPr)_3$).[14]

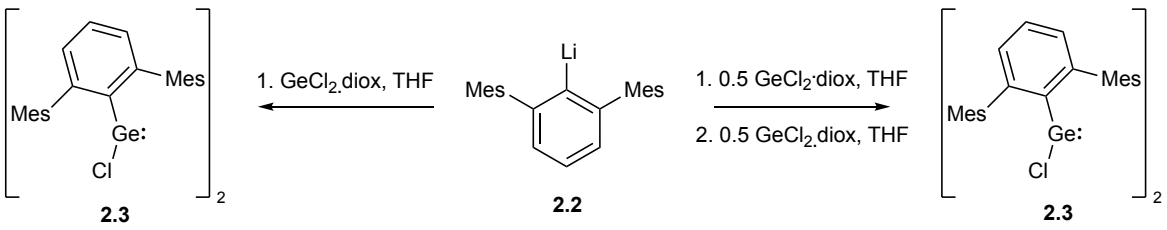
Encouraged by the reactivity of the aryl(silyl)germylene, **1.23**, towards hydrogen and ammonia, it was decided that its reactivity with other small molecules should be explored. This chapter documents efforts to obtain experimental evidence confirming the postulated mechanism of oxidative addition of N–H bonds. More broadly, the ability of **1.23** to exhibit both Lewis acidic and basic reactivity will be described. Finally, the capability of **1.23** to silylmetallate alkenes and alkynes will be investigated to see whether the narrow HOMO–LUMO gap of **1.23** coupled with the labile Ge–Si bond enable novel reactivity.

3.2 Results and Discussion

3.2.1 Synthesis of $GeAr^{Mes}Si(TMS)_3$

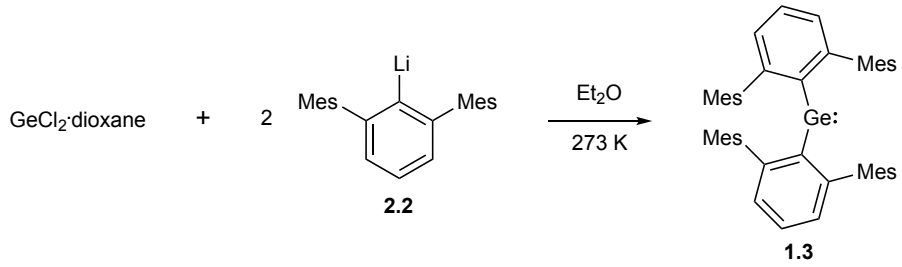
Whilst the synthesis of **1.23** had previously been reported by Usher *et al.* in 2016, significant difficulty was encountered in the current study when attempting to synthesise its chlorogermylene precursor ($[Ge(Ar^{Mes})Cl]_2$), **2.3**.[9] Two syntheses for this species were initially disclosed in 1997 by Power *et al.* and both were reported to produce **2.3** in similar yields (between 35% and 40%).[15] One method involves adding one equivalent of aryllithium, **2.2**, to $GeCl_2$·dioxane, while the other synthesis involves forming the bis(aryl)germylene, **1.3**, *in situ* before an additional equivalent of $GeCl_2$·dioxane is added to yield **2.3** in two steps

(Scheme 3-4). Both syntheses were followed in the current study, and the obtained yields were significantly lower (under 10%) than in the literature reports. More significant purification processes were also found to be required than reported in the original syntheses to access the product cleanly. Analysis of the crude reaction products of both methods by ^{1}H NMR spectroscopy showed a variety of impurities containing a terphenyl ligand, one of which is the protonated mesityl terphenyl hydrocarbon. Despite repeated attempts with different $GeCl_2$·dioxane precursors and freshly distilled and degassed THF, accessing **2.3** cleanly and reproducibly was not possible *via* these methods.



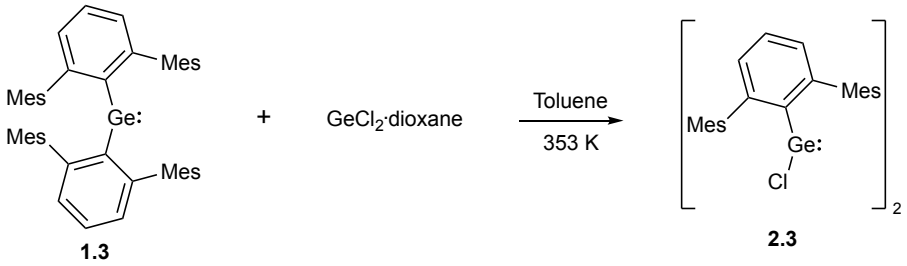
Scheme 3-4: Two routes reported by Power *et al.* to synthesise an aryl(chloro)germylene, **2.3**.[15]

In trying to improve these syntheses, two main issues became clear: THF and dioxane are very good donors so could be affecting the synthesis and the solubility of **2.3** is too great in the reaction mixture to afford easy isolation. To circumvent these issues, an alternative synthesis was developed in which diethyl ether was used as the solvent and bis(aryl)germylene, **1.3**, was isolated and purified before onward reaction, as it was thought this compound could have markedly differing solubility from **2.3**, and hence reduce the need for long purification processes. Combination of aryllithium **2.2** with $GeCl_2$·dioxane at 273 K in diethyl ether affords the characteristic purple colour of **1.3** (Scheme 3-5). From the reaction mixture, **1.3** could be isolated in yields of over 70%, with the NMR signals of the isolated product matching those previously reported by Power *et al.*[15]



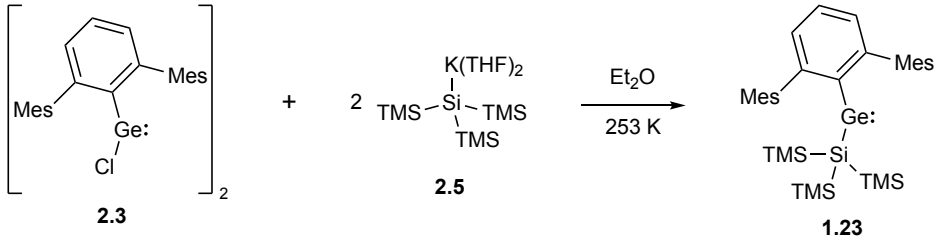
Scheme 3-5: Synthesis of bis(aryl)germylene, **1.3**, via a salt metathesis reaction.

From isolated **1.3**, **2.3** can be accessed in better yields by employing toluene as the reaction medium. Combining the solids in toluene and heating the reaction mixture to 353 K leads to a colour change from purple to red. Once cooled, the reaction mixture can be concentrated *in vacuo* and the product precipitated through the addition of pentane. This method allowed the isolation of **2.3** in yields of around 50%. Whilst this resulted in a combined yield of 35%, slightly lower than both procedures reported by Power *et al.* (39% and 36%), this method proved to be repeatedly reproducible.[15]



Scheme 3-6: Synthesis of aryl(chloro)germylene, **2.3**, via ligand exchange between germanium dichloride dioxane and bis(aryl)germylene, **1.3**.

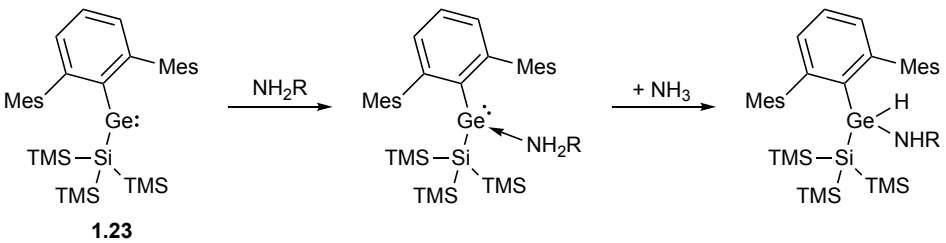
From **2.3**, the synthesis of the aryl(silyl)germylene proceeds as described by Usher *et al.* and allowed the clean and repeatable synthesis of **1.23** in overall yields of 19-28%.[9]



Scheme 3-7: Synthesis of aryl(silyl)germylene, **1.23**, as reported by Usher *et al*.[9]

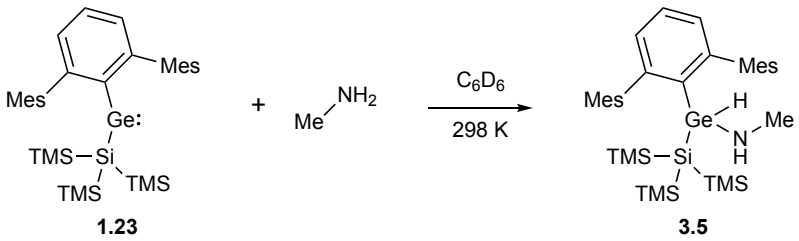
3.2.2 Reactivity of an Aryl(silyl)germylene with N–H Bonds

As it was previously shown that aryl(silyl)germylene, **1.23**, can activate the N–H bond of ammonia, investigations were carried out to attempt to understand the mechanism of this reaction.[9] Quantum chemical calculations by two groups suggest that the reaction proceeds *via* a mechanism in which an adduct forms between the amine and the metallylene and a second equivalent of amine acts then as a proton shuttle (Scheme 1-13).[7,16] In an effort to isolate the amine adduct, and to serve as evidence of the proposed mechanism, the steric bulk of the amine was varied, as this had proved successful in the work of Nagase *et al*. with hydrazine substrates (Scheme 3-2).[10] It was thought that if a persistent adduct between **1.23** and an amine could be isolated, it could then be reacted with ammonia to yield the formal N–H oxidative addition product because ammonia, unlike the bulkier amine, would be sufficiently small enough to act as a proton shuttle (Scheme 3-8).



Scheme 3-8: Putative scheme for proving the proton shuttling mechanism of amine oxidative addition by germylene, **1.23**.

When methylamine is added to a solution of **1.23**, an immediate colour change from teal to yellow is observed, which is then followed within 1 min by the decolourisation of the solution (Scheme 3-9). This is reminiscent of the reaction of **1.23** with ammonia as reported by Usher *et al.* in 2016, in which immediate decolourisation of the teal germylene solution is observed, to yield the colourless oxidative addition product.[9] The intermediate yellow species in this reaction is thought to be the methylamine-germylene adduct. However, due to the rapidity with which the reaction proceeds, it has been impossible to prove this spectroscopically. Analysis of the final colourless product of this reaction by ^{1}H NMR spectroscopy confirms its identity as the Ge(IV) oxidative addition product, **3.5**, due to the diagnostic germanium hydride resonance in the ^{1}H NMR spectrum at 4.92 ppm. Crystals of the product suitable for analysis by X-ray crystallography could also be grown to confirm the connectivity of the product.



Scheme 3-9: Oxidative addition of methylamine by aryl(silyl)germylene, **1.23**.

The crystal structure of **3.5** is shown below (Figure 3-1). When solving the structure, it was found that the amine was disordered over two positions, suggesting that both enantiomers are present in the crystal, as a result of the presence of four different functional groups at the tetrahedral germanium centre. This created difficulty in locating the Ge–H bond in the difference Fourier map. Nevertheless, there are other features in the crystal structure which suggest the formation of a Ge(IV) species. A slight shortening of the Ge–Si bond is seen for **3.5** when compared to **1.23** (2.404(1) Å *vs.* 2.439(1) Å and 2.440(1) Å respectively), a

phenomenon which is also observed with the oxidative addition of ammonia (Scheme 3-1) to form **3.1** (2.400(1) Å).[9] In addition, significant widening of the angle at the germanium centre is observed (**1.23**: 112.5(1)° and 112.7(1)°, **3.5**: 127.8(1)°), which is consistent with the formation of a Ge(IV) species (as seen in the oxidative addition of ammonia **3.1**: 125.8(2)°). This is thought to result from the reduced size of the Ge(IV) centre, meaning that the bulky ligands must move further apart in angular terms.

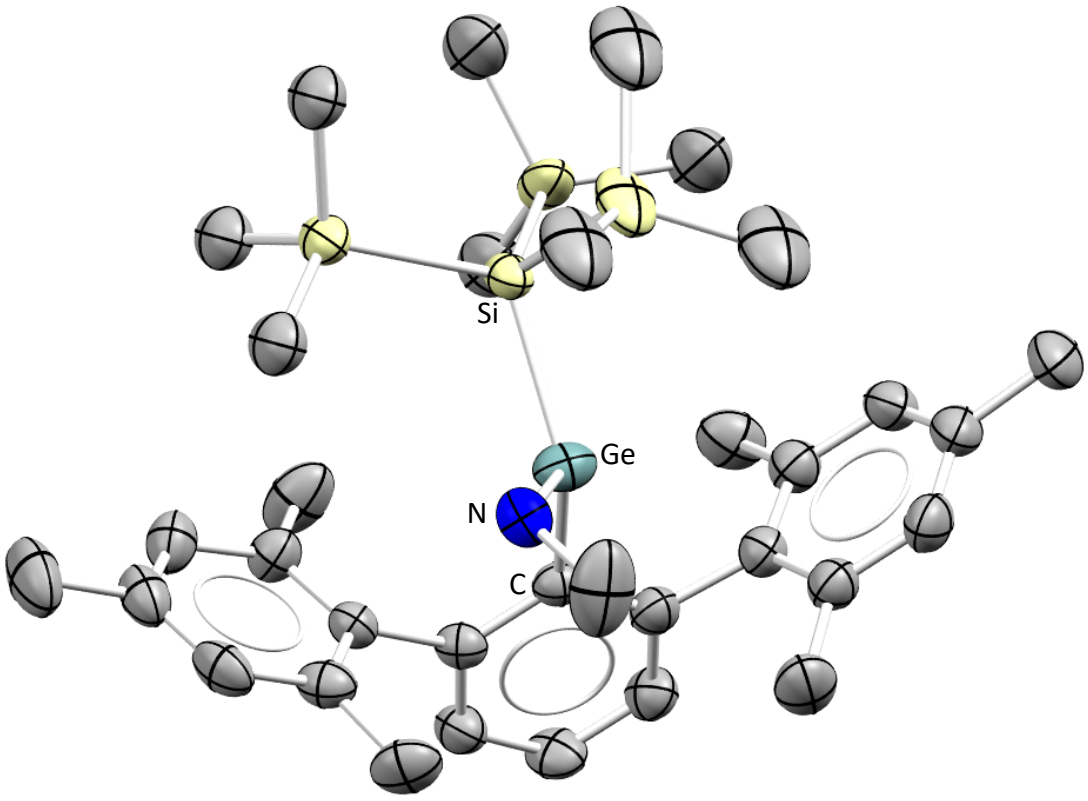
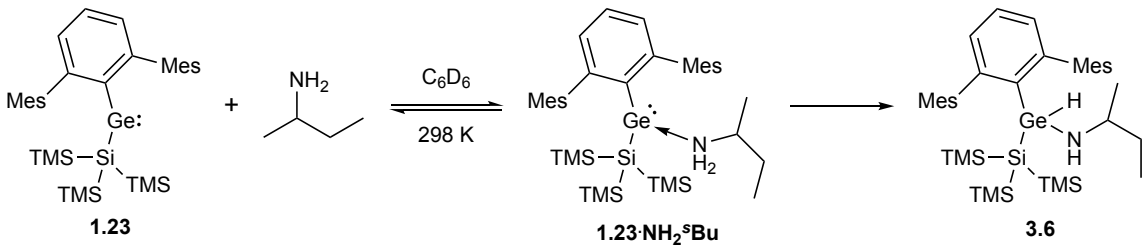


Figure 3-1: Molecular structure of **3.5** as determined by X-ray crystallography. The thermal ellipsoids are set to the 50% probability level. Hydrogen atoms are omitted for clarity. Key bond lengths (Å) and angles (°): Ge–Si: 2.404(1), Ge–C: 1.996(4), Ge–N: 1.835(6), Si–Ge–C: 127.8(1).

When the steric bulk of the amine is increased further and *sec*-butylamine is reacted with a solution of **1.23**, a similar colour change from teal to yellow is observed (Scheme 3-10). When the reaction mixture is left overnight, the decolourisation of the yellow reaction mixture is

observed. As with methylamine, the oxidative addition of the N–H bond of *sec*-butylamine is thought to occur, forming the germanium(IV) hydride, **3.6**. Analysis of the reaction mixture by ^{1}H NMR spectroscopy confirms this assignment due to the presence of the diagnostic Ge–H resonance at 3.62 ppm along with the N–H resonance of the amine fragment at -0.23 ppm. As the intermediate is longer lived, it can be studied by *in situ* NMR spectroscopy. It is found that the distribution of ^{1}H NMR resonances of the intermediate, **1.23·NH$_2$^{s}Bu**, are similar to those of **1.23** but shifted (*e.g. p*-H of central terphenyl ring: **1.23·NH$_2$^{s}Bu** = 7.21 ppm, **1.23** = 7.30 ppm). When the reaction is tracked by ^{1}H NMR spectroscopy (Figure 3-2), the resonances corresponding to the intermediate decrease in intensity while those corresponding to the oxidative addition product grow. These data suggest that the yellow intermediate is the *sec*-butylamine adduct of **1.23**; however, given that the adduct reacts on quickly, the NMR data of **1.23·NH$_2$^{s}Bu** are always contaminated with resonances belonging to **3.6**. Furthermore, attempts to crystallise out **1.23·NH$_2$^{s}Bu** were also unsuccessful because even at 243 K, the formation of **3.6** occurs before **1.23·NH$_2$^{s}Bu** can crystallise.



Scheme 3-10: Oxidative addition of the N–H bond of sec-butylamine by aryl(silyl)germylene, **1.23**.

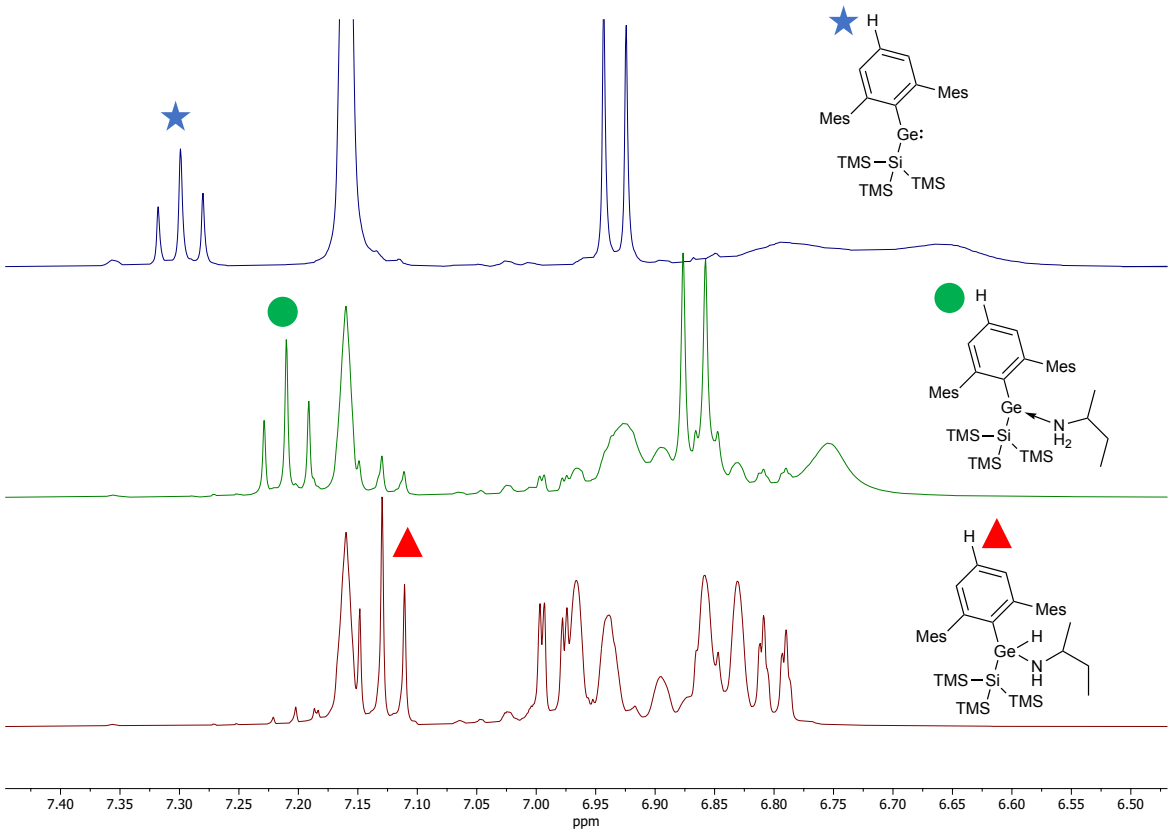
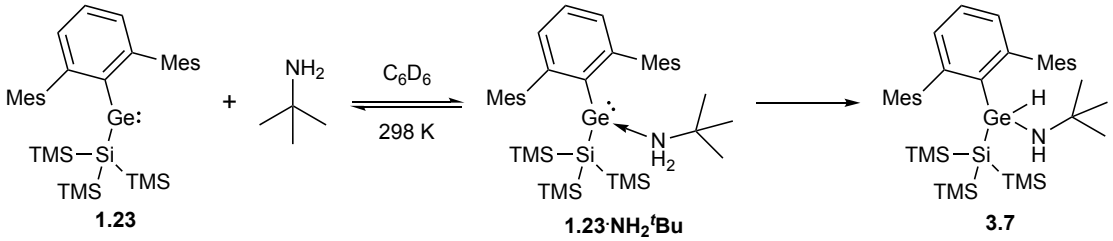


Figure 3-2: Aryl C–H signals in the ^{1}H NMR spectra of species present in the activation of sec-butylamine: Top – ^{1}H NMR spectrum of **1.23**. Middle – ^{1}H NMR spectrum of the reaction mixture immediately after the addition of sec-butylamine to **1.23**. Bottom – ^{1}H NMR spectrum of the reaction mixture 12 h after the addition of sec-butylamine to **1.23**.

The reaction of **1.23** with *tert*-butylamine proceeds analogously (Scheme 3-11). Similar colour changes occur and, like *sec*-butylamine, the yellow intermediate is sufficiently long-lasting that it can be investigated by ^{1}H NMR spectroscopy. The results of these investigations suggest that the intermediate is the amine-germylene adduct, **1.23·NH$_2$^{t}Bu**. As seen with *sec*-butylamine, the distribution of the ^{1}H NMR resonances of the adduct, **1.23·NH$_2$^{t}Bu**, are similar to those of **1.23**, but shifted (*e.g.* *p*-H of central terphenyl ring: **1.23·NH$_2$^{t}Bu** = 7.20 ppm, **1.23** = 7.30 ppm). When this intermediate is tracked *via* ^{1}H NMR spectroscopy in the presence of excess *tert*-butylamine, the resonances of the oxidative addition product, **3.7**, can be seen growing in, as evidenced by the formation of a germanium

hydride peak at 3.50 ppm. Importantly, throughout this process no free germylene is seen in the ^{1}H NMR spectra (Figure 3-3), as indicated by the absence of the characteristic triplet resonance (7.30 ppm), corresponding to the *para*-C*H* of the central ring of the mesityl terphenyl ligand. This is consistent with the idea that the oxidative addition product is formed directly from the coordination complex intermediate, as proposed by Sicilia *et al.*[16]



Scheme 3-11: Oxidative addition of the N–H bond of tert-butylamine by aryl(silyl)germylene, **1.23**.

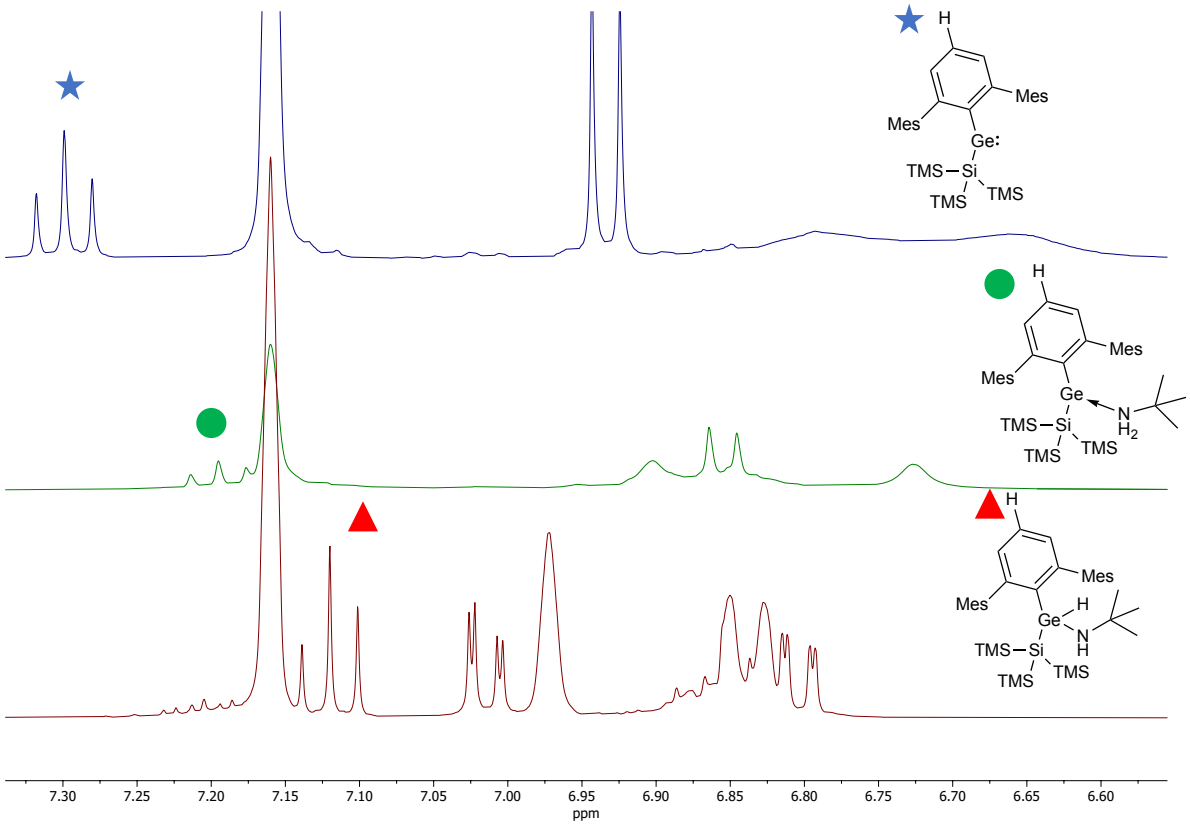
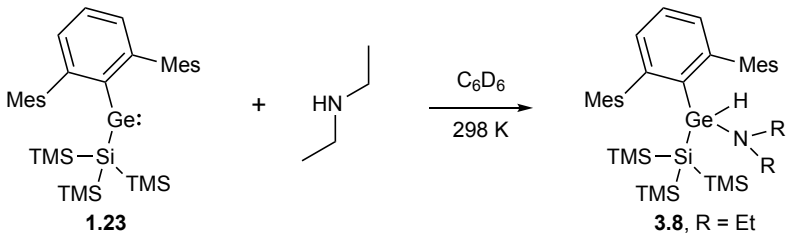


Figure 3-3: Aryl C–H signals in the ^{1}H NMR spectra of species present in the activation of tert-butylamine: Top – ^{1}H NMR spectrum of **1.23**. Middle – ^{1}H NMR spectrum of the reaction mixture immediately after the

addition of tert-butylamine to **1.23**. Bottom – ^{1}H NMR spectrum of the reaction mixture 12 h after the addition of tert-butylamine to **1.23**.

As monoalkylamines do not prove to be bulky enough to afford a persistent amine-germylene adduct, the reactivity of **1.23** with dialkylamines was investigated. When diethylamine, Et_2NH, is reacted with **1.23**, no immediate colour change is observed, but after leaving overnight the reaction mixture decolourises and yields the oxidative addition product **3.8** (Scheme 3-12). This pattern of reactivity was determined by analysis of the product by ^{1}H NMR spectroscopy, which revealed a diagnostic germanium hydride resonance at 3.75 ppm. The intermediate coordination product was not observed experimentally, as evidenced by *in situ* ^{1}H NMR spectroscopy tracking of the reaction mixture, which shows that the only species present in the spectra are **1.23** and **3.8** (Figure 3-4). However, this need not mean it does not form, simply that its concentration is never very high. Indeed, as diethylamine is a stronger base than the monoalkylamines previously discussed ($pK_{aH}(H_2O)$: Et_2NH = 11.02, $MeNH_2$ = 10.65), the deprotonation of the coordinated amine intermediate might be expected to be quicker, and hence the intermediate coordination product shorter lived.[17] On the other hand, these observations could indicate that the bulkier dialkylamines oxidatively add to the germylene centre *via* a mechanism which does not involve coordination at the metal centre. More research is required to ascertain which of these mechanistic pathways the dialkylamines adopt.



Scheme 3-12: Oxidative addition of the N–H bond of diethylamine by aryl(silyl)germylene, **1.23**.

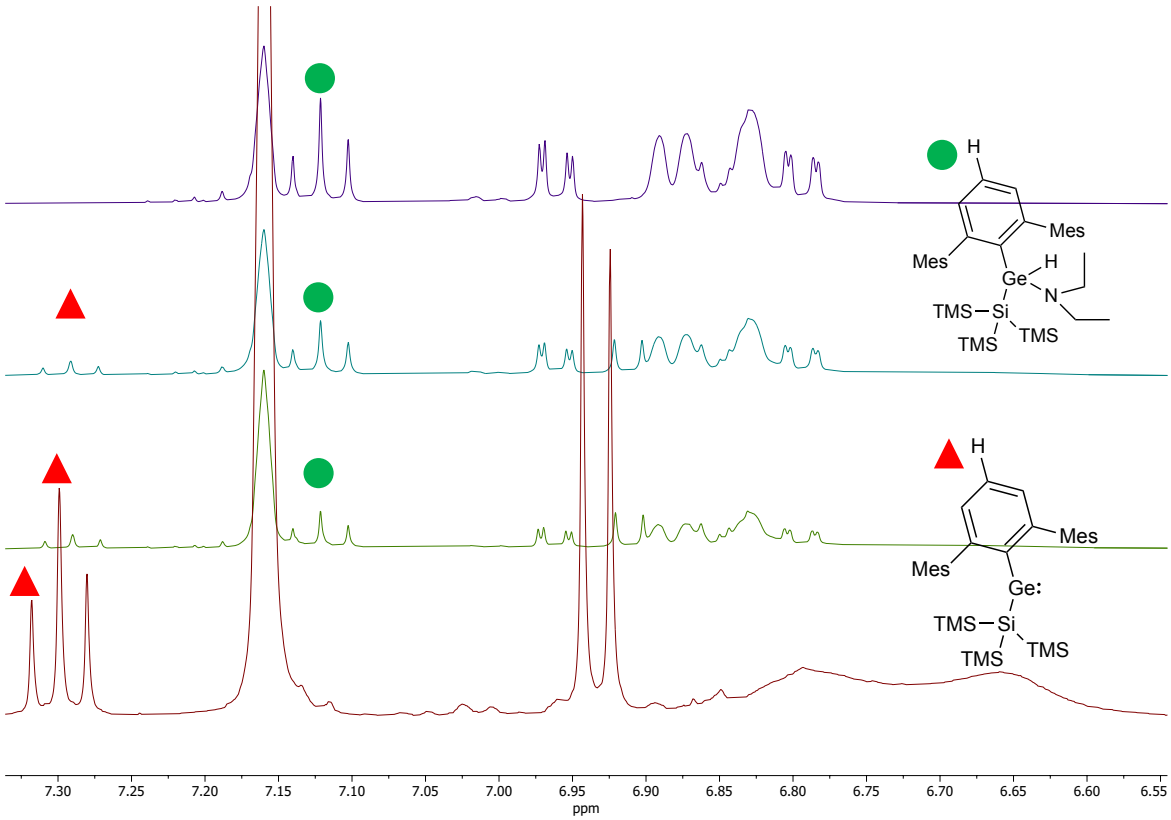
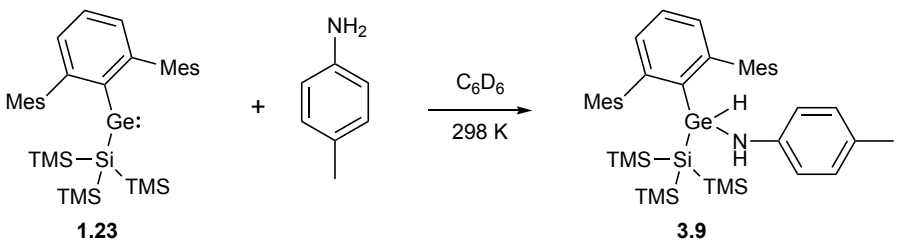


Figure 3-4: Aryl C–H signals in the ^{1}H NMR spectra of species present in the activation of diethylamine: Top – ^{1}H NMR spectrum of the reaction mixture of **1.23** with diethylamine after 6 h. Second top – ^{1}H NMR spectrum of the reaction mixture of **1.23** with diethylamine after 4 h. Second bottom – ^{1}H NMR spectrum of the reaction mixture of **1.23** with diethylamine after 2 h. Bottom – ^{1}H NMR spectrum of **1.23**.

When the bulk of the amine is increased further and diisopropylamine is added to a solution of **1.23**, no reaction is observed at room temperature. When the reaction mixture is heated to 353 K, a change is observed in the ^{1}H NMR spectrum accompanied by the decolourisation of the solution. The lack of an identifiable germanium hydride resonance implies that formal oxidative addition has not occurred, and the identity of the product could not be determined unequivocally. It was found that **1.23** was also unable to oxidatively add the N–H bond of carbazole, with no reactivity observed between the two reagents even after prolonged heating at 353 K. This is no doubt in part due to the steric bulk of the carbazole reagent.

To further assess the role which coordination played in the oxidative addition of N–H bonds by germylenes, **1.23** was reacted with *p*-toluidine. An aniline was chosen because they are significantly less basic than alkylamines and therefore are less likely to form an adduct. As predicted, no intermediate colour change was observed when the solids were dissolved. Instead, the reaction mixture slowly decolourised overnight (Scheme 3-13). The oxidative addition product, **3.9** (featuring a characteristic germanium hydride resonance at 3.73 ppm), *p*-toluidine, and the free germylene ,**1.23**, are the only species visible in the spectra when analysing the reaction by *in situ* ^{1}H NMR spectroscopy (Figure 3-5). As noted above, the absence of resonances belonging to a coordinative intermediate in the ^{1}H NMR data is not necessarily sufficient to prove it does not form during the reaction. In fact, the ability of germylenes to form coordinative *equilibria* with Lewis bases could explain the lack of detectable resonances due to the coordination product in the ^{1}H NMR spectra.[18,19] As *p*-toluidine is less basic than the monoalkylamines discussed above ($pK_{aH}(H_2O)$: *p*-toluidine = 5.08), the position of the coordination equilibrium will lie further in favour of the reagents. Therefore, the concentration of the germylene-toluidine complex will be reduced rendering it less detectable by *in situ* ^{1}H NMR spectroscopy. Nevertheless, these results warrant further study into whether the coordination product is an intermediate in this reaction or whether a different mechanism of N–H bond activation occurs between **1.23** and *p*-toluidine.



Scheme 3-13: Oxidative addition of the N–H bond of p-toluidine by aryl(silyl)germylene, **1.23**.

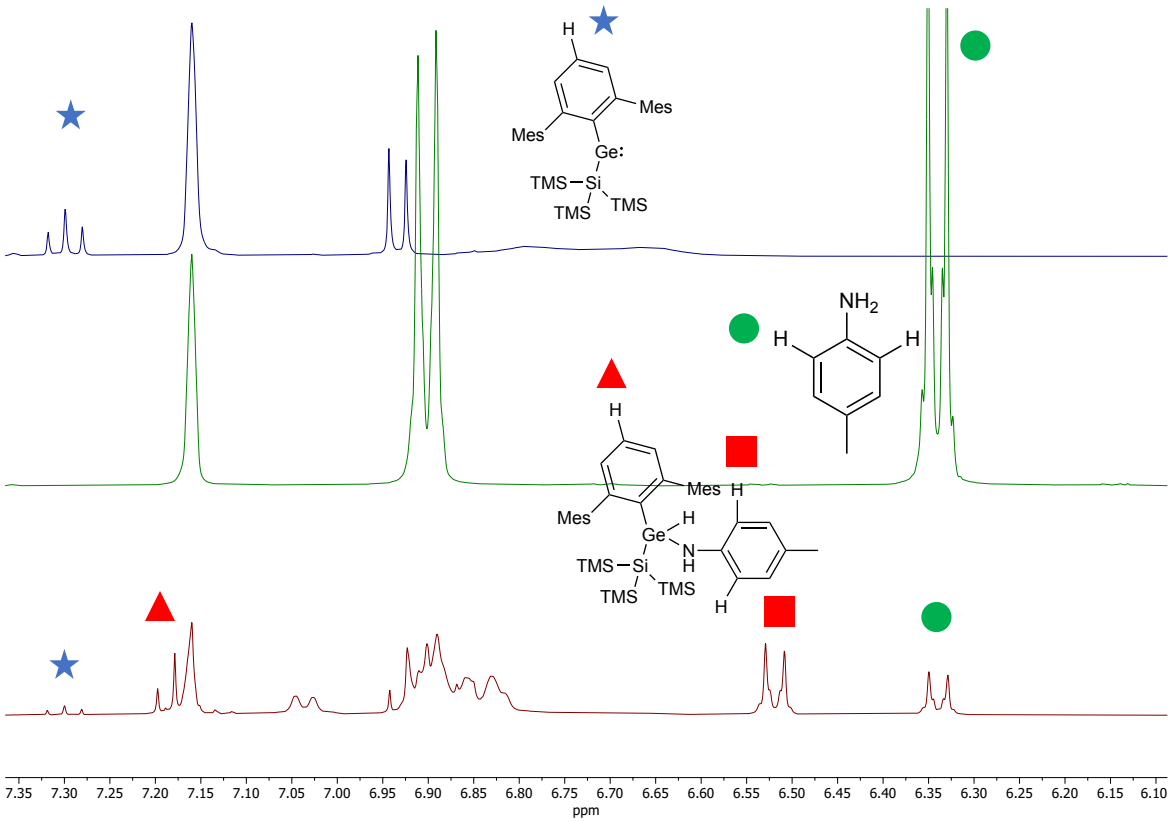


Figure 3-5: Aryl C–H signals in the ^{1}H NMR spectra of species present in the activation of p-toluidine: Top – ^{1}H NMR spectrum of **1.23**. Middle – ^{1}H NMR spectrum of p-toluidine. Bottom – ^{1}H NMR spectrum of the reaction mixture 4 h after the addition of p-toluidine to **1.23**.

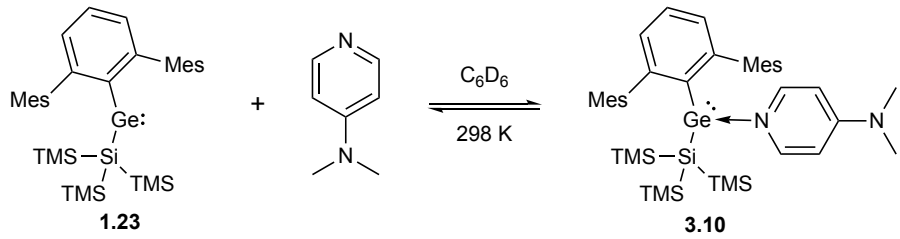
3.2.3 Small Molecule Reactivity of GeAr^{Mes}Si(TMS)$_3$

Once it had been established that **1.23** was able to activate an array of N–H bonds, its reactivity with other small molecules was investigated. In this section, the results of these studies will be documented, and where appropriate compared with similar examples from the literature.

3.2.3.1 Lewis Acidic Behaviour of GeAr^{Mes}Si(TMS)$_3$

As germylenes possess a formally vacant *p*-orbital, reactions of **1.23** with Lewis bases were performed to access the corresponding adducts. When benzene is added to a mixture of **1.23**

and dimethylaminopyridine (DMAP), the formation of an orange solution is immediately observed (Scheme 3-14). The ^{1}H NMR spectrum of the reaction mixture (Figure 3-6) shows a significant change from that of **1.23**, as seen in Figure 3-6. Sharpening of the resonance (at 6.86 ppm) due to the four aromatic protons of the flanking mesityl rings of the terphenyl ligand is observed, along with shifts in the other resonances, suggesting that the adduct, **3.10**, has formed (*p*-H of central terphenyl ring: **3.10** = 7.24 ppm, **1.23** = 7.30 ppm). Only one set of resonances belonging to DMAP are observed in the ^{1}H NMR spectrum (aromatic protons: 8.19 and 5.84 ppm) which integrate in a 3:2 ratio with the ligand resonances of **3.10**. This suggests that free DMAP is in a coordinative equilibrium with the adduct, **3.10**, as has previously been seen with other Lewis bases.[18] Efforts to obtain a crystal suitable for X-ray diffraction to confirm the connectivity of **3.10** have proven unsuccessful, due to the high solubility of **3.10** in hydrocarbon solvents (pentane, toluene).



Scheme 3-14: Coordination of dimethylaminopyridine to aryl(silyl)germylene, **1.23**.

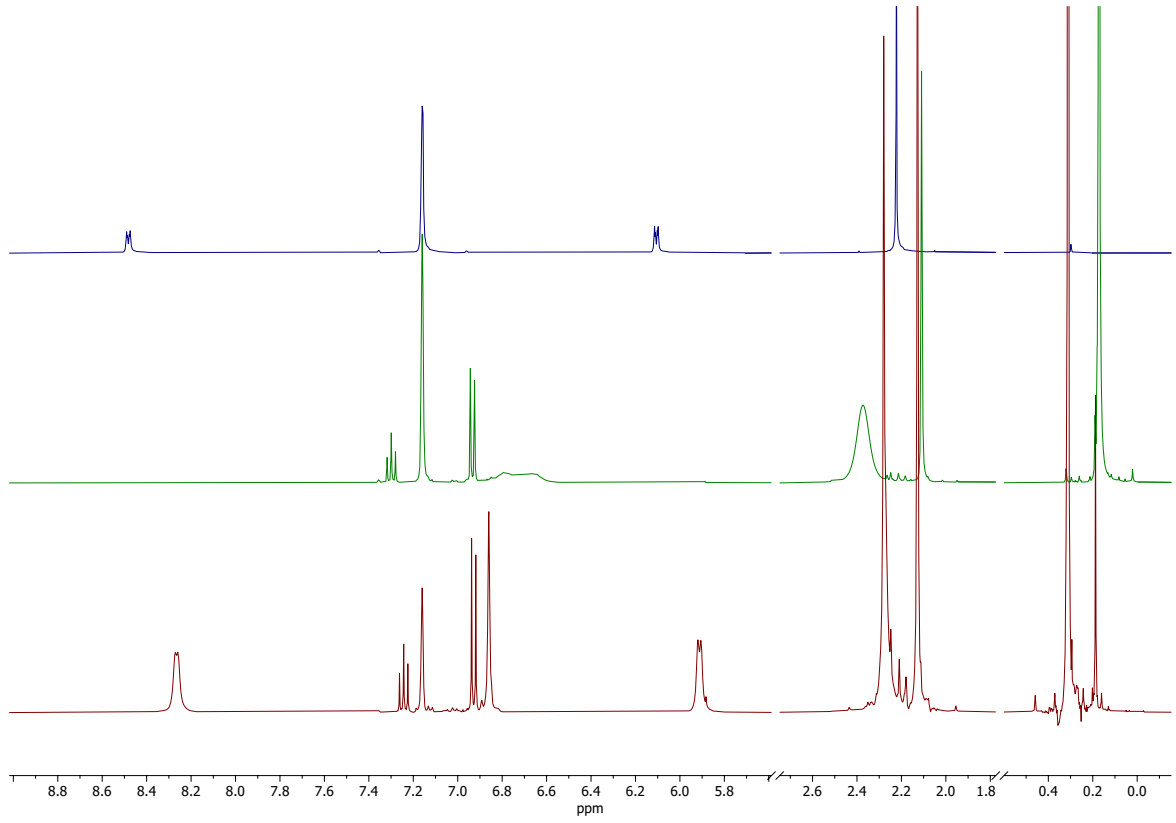
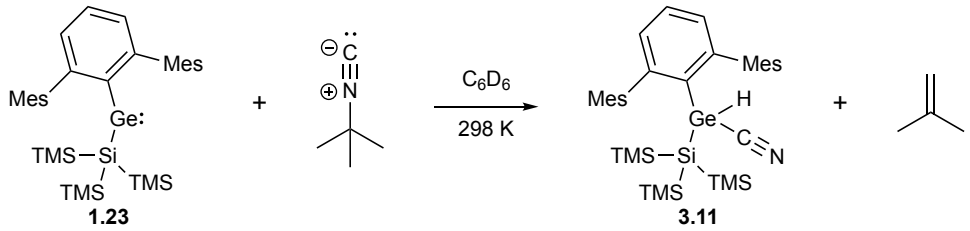


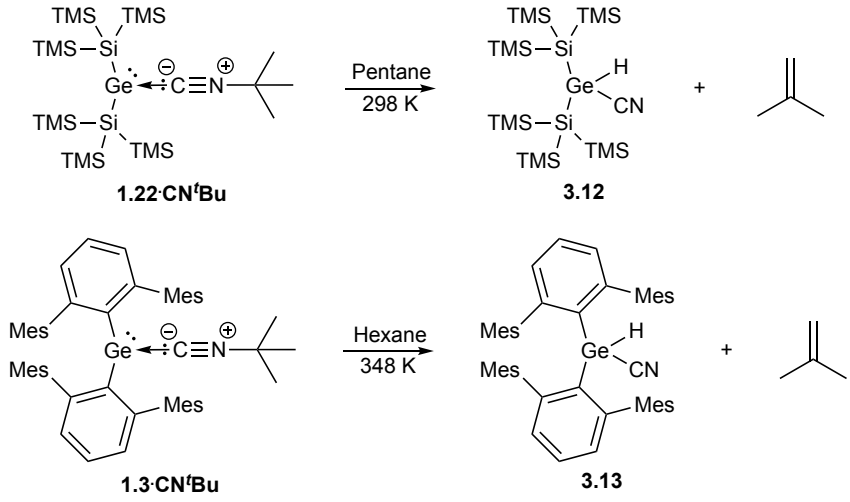
Figure 3-6: Excerpts from three stacked ^{1}H NMR spectra: Top – ^{1}H NMR spectrum of DMAP. Middle – ^{1}H NMR spectrum of **1.23**. Bottom – ^{1}H NMR spectrum of the reaction mixture of **1.23** and DMAP.

Literature precedent exists for the formation of adducts between isocyanides and germylenes, and so the reactivity of **1.23** with *tert*-butylisocyanide (^{t}BuNC) was probed.[18,20] When a solution of ^{t}BuNC is added to a solution of **1.23**, an immediate colour change from teal to yellow is seen (Scheme 3-15). Over the course of 1 h, the reaction mixture decolourises. The identity of the yellow intermediate is difficult to ascertain from *in situ* ^{1}H NMR spectroscopy, but reference to the literature suggests that it is likely to be the coordination complex. [18,20] Analysis of the final product by NMR spectroscopy reveals a germanium hydride peak in the ^{1}H NMR spectrum at 4.53 ppm and a nitrile peak in the ^{13}C NMR spectrum at 124.1 ppm. These data suggest the formation of a Ge(IV) cyanide/hydride species, **3.11**, as has previously been reported in the literature.[18,20] Crystals of **3.11** suitable for X-ray crystallography could be grown from pentane and confirmed the proposed connectivity.



Scheme 3-15: Formation of a Ge(IV) cyanide/hydride species from tert-butylisonitrile and aryl(silyl)germylene, **1.23**.

The crystal structure of **3.11** is depicted below (Figure 3-7). As with compound **3.5** above, the cyanide group is disordered over two positions, indicating that both enantiomers are present in the crystal, and making it effectively impossible to determine the Ge–H position from the difference Fourier map. Additionally, the quality of the X-ray crystal structure data of **3.11** is of insufficient quality to justify discussion of geometric parameters. Nevertheless, the connectivity of **3.11** is confirmed and resembles bis(silyl)germylnitrile, **3.12**, synthesised by Walewska *et al.* and bis(aryl)germylnitrile, **3.13**, synthesised by Brown *et al*. (Scheme 3-16).[18,20]



Scheme 3-16: Top: Synthesis of germylnitrile, **3.12**, from tert-butyl isonitrile germylene adduct, **1.22·CN^{t}Bu**.[20] Bottom: Synthesis of germylnitrile, **3.13**, from tert-butyl isonitrile germylene adduct, **1.3·CN^{t}Bu**.[18]

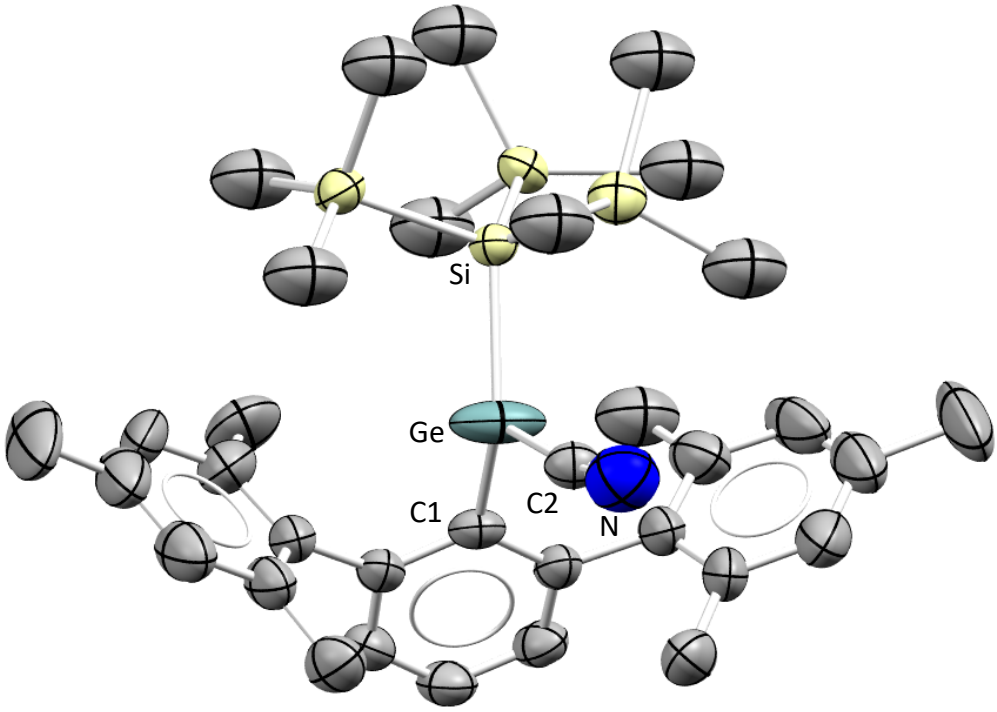
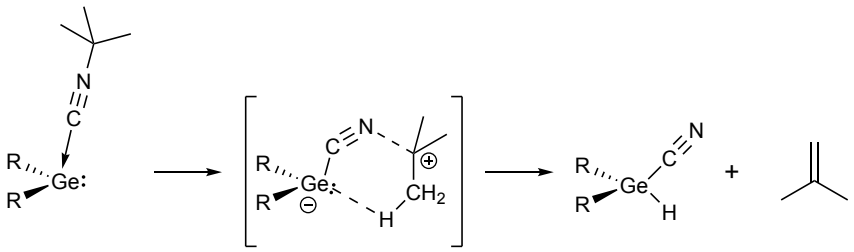


Figure 3-7: Molecular structure of **3.11** as determined by X-ray crystallography. The thermal ellipsoids are set to the 50% probability level. Hydrogen atoms are omitted for clarity. Data of insufficient quality to discuss the geometric parameters of **3.11**.

As mentioned above, there is literature precedent for this type of reactivity of metallylenes with ^{t}BuNC.[18,20–22] One difference in the reaction with **1.23**, as compared to previous germylene examples, is the instability of the intermediate adduct.[18,20] **1.22**·**CN^{t}Bu** decays to **3.12** at room temperature, however full conversion requires two weeks (Scheme 3-16). **1.3**·**CN^{t}Bu** must be heated at 348 K overnight for full conversion to **3.13** (Scheme 3-16). In their 2012 work, Brown *et al.* proposed a mechanism for this reaction based on quantum chemical calculations.[18] Initial coordination of the isocyanide to the germylene is followed by a transition state featuring a formally anionic germanium fragment and a ^{t}Bu cation, which corresponds to concerted C–N bond breaking and Ge–H bond formation.[18] The comparative

lack of stability of the adduct of **1.23** with *tert*-butylisocyanide, as compared to **1.3** and **1.22**, is not clarified when this mechanism is considered. As a higher energy HOMO should lead to most facile C–H activation of the *tert*-butyl group, the calculated mechanism suggests that **1.22·CN^{t}Bu** should transform into **3.12** faster than **3.11** forms from its coordinative adduct (**1.23·CN^{t}Bu)**. The discrepancy of the experimental results from the mechanism necessitates the need for more experiments and calculations to fully ascertain why **3.11** forms so much more rapidly than other related species.

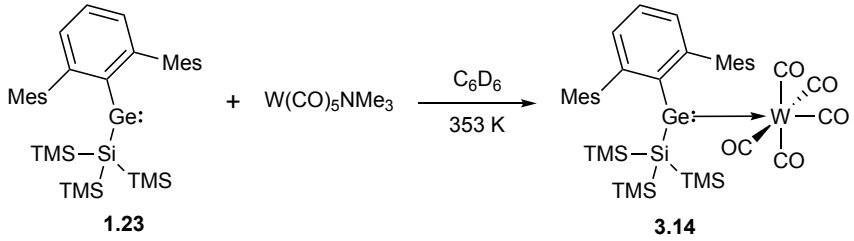


Scheme 3-17: Proposed mechanism for the formation of Ge(IV) cyanide/hydride species from an aryl(silyl)germylene and tert-butylisonitrile, adapted from Brown *et al.*[18]

3.2.3.2 Lewis Basic Behaviour of GeAr^{Mes}Si(TMS)$_3$

Once the Lewis acidity of **1.23** was demonstrated, its ability to behave as a Lewis base was also investigated. When **1.23** and $W(CO)_5NMe_3$ were dissolved together in deuterated benzene, no initial reaction was observed. After 2 d, new terphenyl ligand resonances began to appear in the ^{1}H NMR spectrum (*e.g. p*-H of central terphenyl ring: 7.16 ppm, *m*-H of central terphenyl ring: 6.84 ppm). Heating the reaction mixture to 353 K increased the rate of growth of these resonances (Scheme 3-18). After heating for approximately 20 h in total, the reaction appeared to have gone to completion, and the product, **3.14**, could be isolated as a dark red solid. Analysis of the product by NMR spectroscopy suggested that coordination of the lone pair to the tungsten had taken place, as a reduction of symmetry in the methyl groups of the flanking mesityl rings is seen in the ^{1}H NMR spectrum (**1.23**: 2.20 and 1.94 ppm, **3.14**: 2.44,

2.23, and 2.12 ppm), consistent with the addition of a sterically bulky group to the germanium centre. Crystals of **3.14** suitable for X-ray crystallography could be grown and allow the proposed connectivity to be confirmed.



Scheme 3-18: Adduct formation between an aryl(silyl)germylene, **1.23**, and $W(CO)_5(NMe_3)$.

The crystal structure of **3.14** is depicted below (Figure 3-9). A widening of the angle at the Ge-centre compared to the parent germylene, **1.23**, is observed (**1.23**: 112.5(1)° and 112.7(1)°, **3.14**: 127.70(7)°), as well as a slight increase in the Ge–C and Ge–Si bond lengths (Ge–C: **1.23**, 1.996(3) and 1.997(3) Å; **3.14**, 2.003(2) Å; Ge–Si: **1.23**, 2.439(1) and 2.440(1) Å; **3.14**, 2.4631(8) Å). This reflects the increased steric repulsion brought about by incorporation of the $W(CO)_5$ fragment. The structure of **3.14** can also be compared to two previous examples of germylene-$W(CO)_5$ adducts, one with a bis(aryl)germylene (**3.15**) and the other with a cyclopentadienyl substituted germylene (**3.16**; Figure 3-8). [23,24] The W–Ge bond length measured for **3.14** is 2.5761(4) Å and is slightly shorter than the corresponding distances for **3.15** and **3.16** (2.5934(8) Å and 2.632(4) Å respectively), presumably indicative of the stronger σ-donating ability of **3.14** due to its hypersilyl substituent.

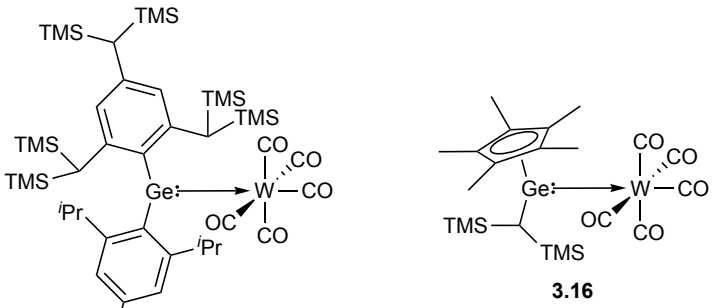


Figure 3-8: Two germylene-tungsten pentacarbonyl adducts, **3.15** and **3.16**.[23,24]

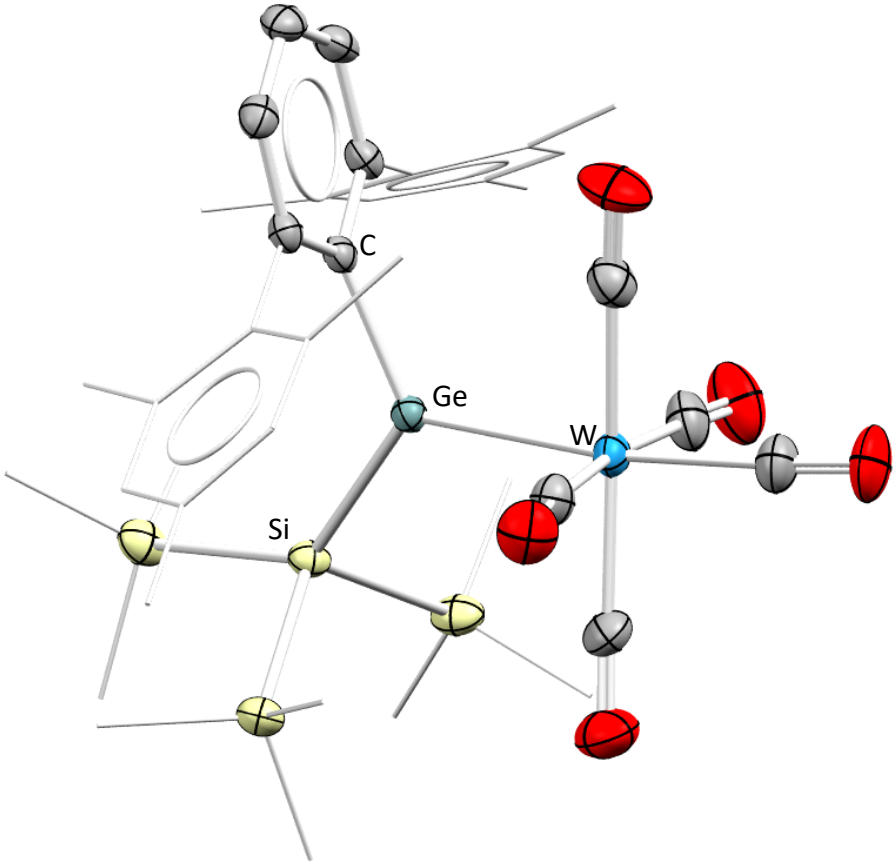
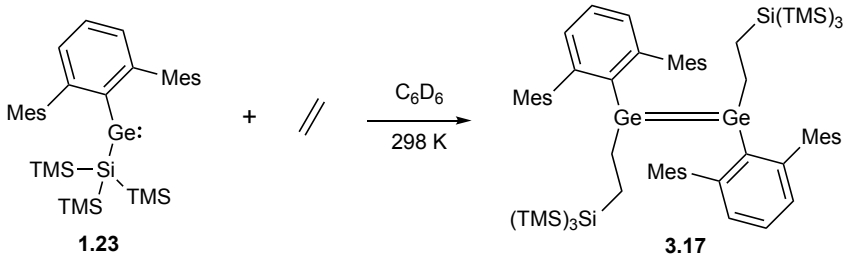


Figure 3-9: Molecular structure of **3.14** as determined by X-ray crystallography. The thermal ellipsoids are set to the 50% probability level. Hydrogen atoms are omitted for clarity. The flanking mesityl rings of the terphenyl ligand and the methyl groups of the hypersilyl ligand are depicted in wireframe for clarity. Key bond lengths (Å) and angles (°): Ge–Si: 2.4631(8), Ge–C: 2.003(2), Ge–W: 2.5761(4), Si–Ge–C: 127.70(7).

3.2.3.3 Reactivity of $GeAr^{Mes}Si(TMS)_3$with Alkenes

Due to the literature precedent for reactivity between metallylenes and unsaturated organic molecules, the behaviour of **1.23** with alkenes was investigated. When a solution of **1.23** is charged with one atmosphere of ethene, an immediate colour change from teal to yellow is observed (Scheme 3-19). This change is accompanied by the precipitation of a yellow solid. This solid proved to be sparingly soluble in all compatible NMR solvents (C_6D_6, tol-d_8 and THF-d_8). Therefore, analysis of the product by NMR spectroscopy could not conclusively determine its identity. However, crystals suitable for X-ray diffraction could be grown and, from these, the connectivity of the product (**3.17**) could be confirmed.



Scheme 3-19: Reaction of aryl(silyl)germylene, **1.23**, with an alkene to form digermene, **3.17**.

The crystal structure of **3.17** is depicted in Figure 3-10. It should be noted that the quality of the X-ray crystal structure of **3.17**, whilst enough to confirm connectivity, is not sufficient to justify discussion of geometric parameters. Despite this shortcoming, the key features of the structure are clear. **3.17** is the first example of a digermene formed from the insertion of an alkene into the Ge–X bond of a germylene. It is thought that the initial step in the reaction is the formation of the germirane, corresponding to a [2+1]-cycloaddition of ethene with **1.23**. This seems likely when considering the 2014 work from Lips *et al.,* in which reversible germirane formation was observed between a bis(aryl)germylene and ethene (Scheme 1-15).[25] However, the Ge–Si bond of **1.23** can then undergo a rapid migratory

insertion of the coordinated ethene, as observed for the silylsilylene of Rieger *et al.* (Scheme 1-16). This is because the formed germirane is likely very unstable.[12] The alkylgermylene so formed is unstable with respect to dimerisation, in contrast to the series of alkylgermylenes synthesised by Jones *et al.*[14] This is likely due to the amido ligand employed by Jones *et al.* being prohibitively bulky and hence preventing dimerisation. For **3.17**, on the other hand, the mesityl terphenyl substituent is not large enough to compensate for the increased flexibility that the -CH_2CH_2- linker provides and therefore dimerisation is seen.[14]

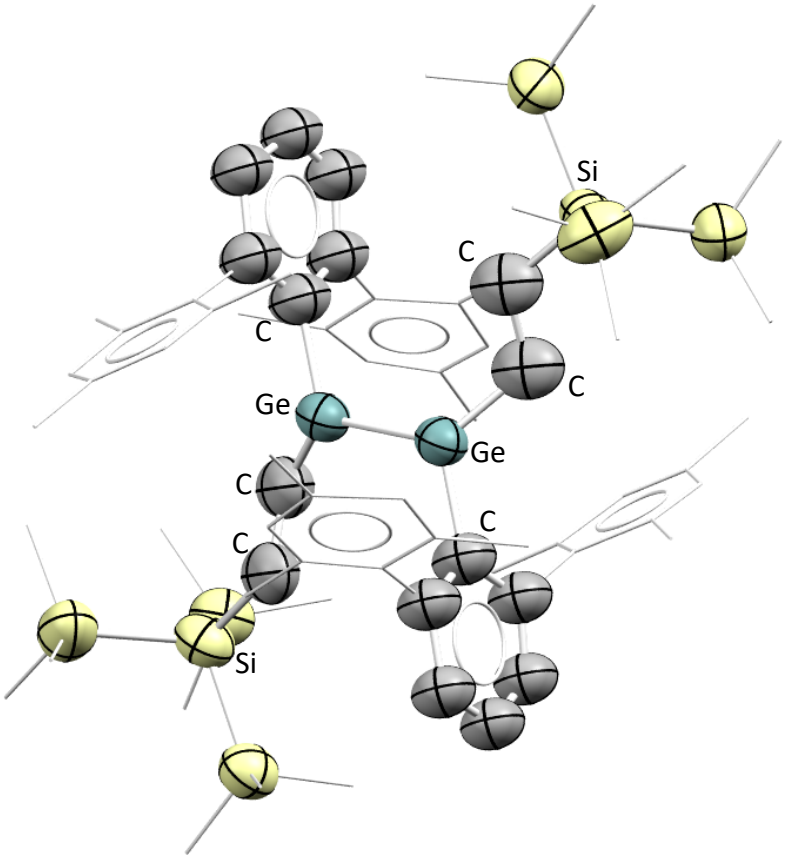
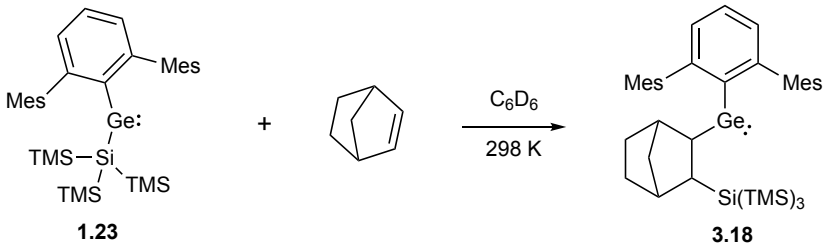


Figure 3-10: Molecular structure of **3.17** as determined by X-ray crystallography. The thermal ellipsoids are set to the 40% probability level. Hydrogen atoms are omitted for clarity. The flanking mesityl rings of the terphenyl ligand and the methyl groups of the hypersilyl ligand are depicted in wireframe for clarity. Data of insufficient quality to discuss the geometric parameters of **3.17**.

To ascertain whether dimerization could be prevented, a bulkier alkene was reacted with aryl(silyl)germylene, **1.23**. When norbornene is added to a solution of **1.23**, an immediate colour change from teal to purple is observed (Scheme 3-20). A reduction of symmetry is observed in the methyl resonances of the flanking mesityl groups of the terphenyl ligand of the new product, **3.18**, (**1.23**: 2.20 and 1.94 ppm, **3.18**: 2.40, 2.25, and 2.15 ppm) which, when considered alongside its purple colour, suggests the formation of a Ge(II) species, rather than a Ge(IV) product (related bis(aryl)germylenes are typically purple in colour).[15] Crystals suitable for X-ray diffraction could be grown and allow the connectivity of the product to be confirmed.



Scheme 3-20: Reaction of norbornene with aryl(silyl)germylene, **1.23**, to yield alkyl(aryl)germylene, **3.18**.

The crystal structure of **3.18** is depicted in Figure 3-11. Unfortunately, the data obtained for **3.18** is only of sufficient quality to discuss the connectivity and not any of the geometric parameters. Unlike **3.17**, **3.18** exists as a monomeric germylene in the solid state. This is likely due to the rigidity of the norbornane fragment which restricts the hypersilyl ligand to a position which disfavours dimerisation after insertion of the alkene into the Ge–Si bond. To date, no examples of cycloadditions between norbornene and heavier carbene analogues have been reported, however the insertion of norbornene into the Sn–H of Sn(II) hydride was reported by Wang *et al.*[26] It is likely the steric bulk of norbornene results in the reaction pathway as proposed by Hadlington *et al.* being followed.[14] In this case, the interaction of the

alkene with the empty orbital of the germylene precedes insertion into the Ge–Si bond, rather than a [2+1]-cycloaddition (as with ethene). More evidence is required to conclusively determine the mechanism of reaction between **1.23** and norbornene.

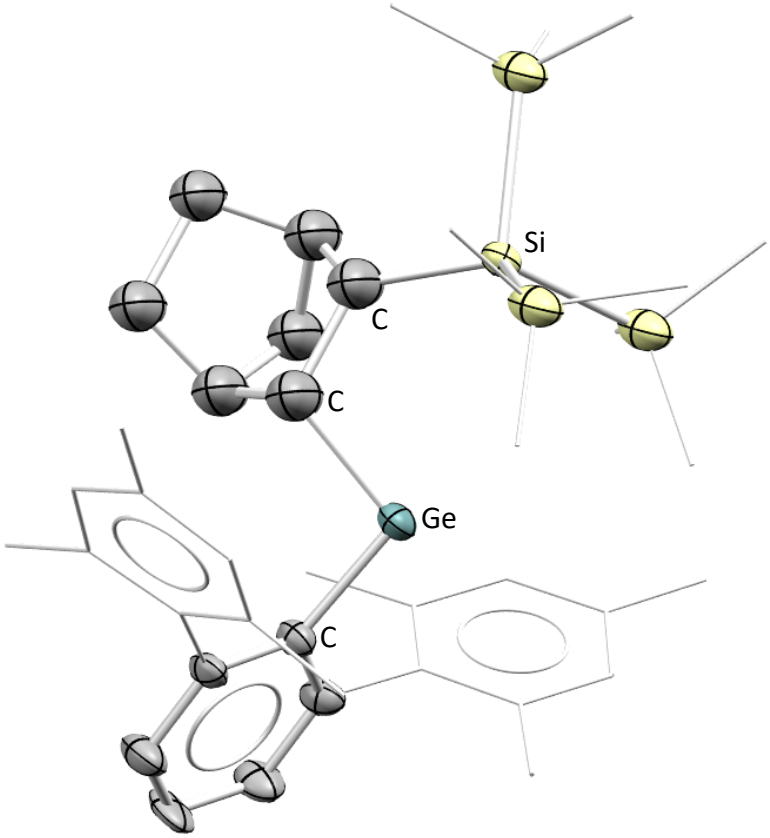
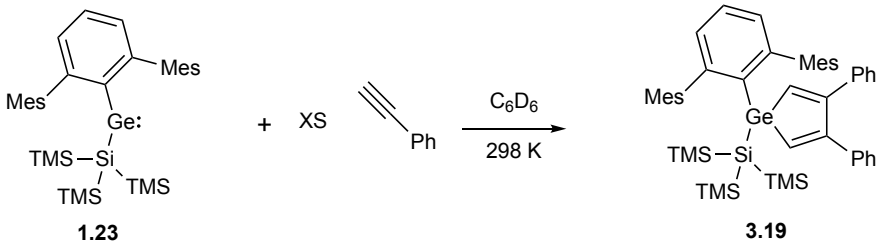


Figure 3-11: Molecular structure of **3.18** as determined by X-ray crystallography. The thermal ellipsoids are set to the 50% probability level. Hydrogen atoms are omitted for clarity. The flanking mesityl rings of the terphenyl ligand and the methyl groups of the hypersilyl ligand are depicted in wireframe for clarity. Data of insufficient quality to discuss the geometric parameters of **3.18**.

3.2.3.4 Reactivity of an Aryl(silyl)germylene with Alkynes

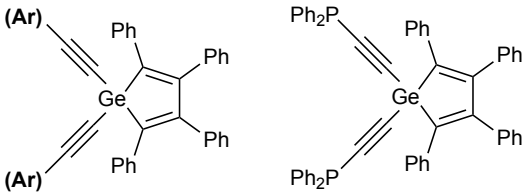
The insertion reactivity displayed with alkenes led to investigation into whether related behaviour would be displayed when **1.23** is combined with alkynes. When an excess of phenyl acetylene is added to a solution of **1.23**, an immediate colour change to purple is seen, followed by slow decolourisation of the solution (Scheme 3-21). Analysis of the colourless

product, **3.19**, by ^{1}H NMR spectroscopy shows an alkenic resonance at 5.62 ppm, which integrates in a 1:3 ratio with each of the three resonances (2.40, 2.25, and 1.86 ppm) due to the C*H*$_3$ groups of the terphenyl ligand. This implies that the product cannot be the result of a [2+1]-cycloaddition or an insertion of the alkyne into the Ge–Si bond since the resonances for these putative products would integrate in a 1:6 ratio. To assess the connectivity of this species, crystals suitable for X-ray diffraction were grown.



Scheme 3-21: Reaction of aryl(silyl)germylene, **1.23**, with an excess of phenylacetylene.

The crystal structure of **3.19** is depicted in Figure 3-13. **3.19** is a germacyclopentadiene that is formed through the reaction of **1.23** with two equivalents of phenylacetylene. A widening of the angle at the germanium centre is seen in **3.19** compared to **1.23** (**3.19**: 126.31(4)°, **1.23**: 112.5(1)° and 112.7(1)°). However, the Ge–C and Ge–Si bonds remain constant within error compared to **1.23** (**3.19**: Ge–C: 1.992(1) Å and Ge–Si: 2.4356(6) Å, **1.23**: Ge–C: 1.996(3) and 1.997(3) Å, and Ge–Si: 2.439(1) and 2.440(1) Å), in contrast with other Ge(IV) species. Despite **3.19** being the first known crystalline example of a germole featuring hydrogens on the 2 and 5-ring positions, the geometry of the germacyclopentadiene fragment is in close agreement with two germoles synthesised by Bandrowsky *et al.,* **3.20** and **3.21** (Figure 3-12).[27] The C=C and C–C bond lengths of **3.19** closely resemble those of **3.20** and **3.21** (Table 3-2). The Ge–C(ring) bond lengths of **3.19** are also equivalent with error to those of **3.20** and **3.21**, despite the greater bulk of the proximal terphenyl and hypersilyl ligands in **3.19**.[27]



3.20 **3.21**

Figure 3-12: Two germoles, **3.20** and **3.21**, synthesised by Bandrowsky *et al*. (**(Ar)** is -C_6H_4F).[27]

Table 3-1: Selected bond lengths (Å) of **3.19**, **3.20**, and **3.21**.[27]

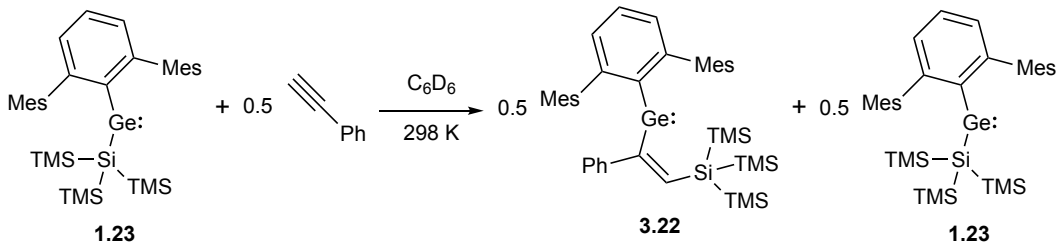
	Ge–C2/C5	**C2=C3, C4=C5**	**C3–C4**
3.19	1.951(1), 1.949(1)	1.346(2), 1.348(2)	1.499(2)
3.20[27]	1.954(1), 1.940(2)	1.362(2)	1.512(2)
3.21[27]	1.929(2), 1.940(3)	1.349(4)	1.516(4)



Figure 3-13: Molecular structure of **3.19** as determined by X-ray crystallography. The thermal ellipsoids are set to the 50% probability level. Hydrogen atoms are omitted for clarity. The flanking mesityl rings of the terphenyl ligand, the methyl groups of the hypersilyl ligand, and the phenyl groups of the germacyclopentadiene are depicted in wireframe for clarity. Key bond lengths (Å) and angles (°): Ge–Si: 2.4356(6), Ge–C1: 1.992(1), Ge–C2: 1.949(1), Ge–C5: 1.951(1), C2–C3: 1.348(2), C4–C5: 1.346(2), C3–C4: 1.499(2), Si–Ge–C1: 126.31(4), C2–Ge–C5: 46.25(4).

As the intermediate colour change to purple was observed in the reaction with phenylacetylene, investigations were carried out to identify this intermediate. Initially, upon addition of half an equivalent of phenylacetylene to a solution of **1.23** (Scheme 3-22), the colour change to purple was again observed, but this time with no subsequent decolourisation. Analysis of the reaction mixture by ^{1}H NMR spectroscopy (Figure 3-14) showed a 1:1 ratio of free germylene (**1.23**) and another species, **3.22**, which contains a terphenyl ligand, as evidenced by the presence of a new diagnostic triplet in the aryl region

(7.24 ppm) corresponding to the *p*-C*H* of the central ring of the terphenyl ligand. A new alkenic resonance was also observed at 7.62 ppm which integrated in a 1:1 ratio when compared to the triplet resonance. The colour of the species persists under these conditions suggesting that this is not a Ge(IV) species resulting from the [2+1]-cycloaddition, since such a species would be expected to be colourless reminiscent of the [2+1]-cycloaddition product isolated by Tokitoh *et al.* (Scheme 1-21) and other Ge(IV) species already documented in this thesis.[28] Therefore it is proposed that the purple product, **3.22**, is formed *via* insertion of PhCCH into the Ge–Si bond of **1.23**.



Scheme 3-22: Reaction of aryl(silyl)germylene, **1.23**, with half an equivalent of phenylacetylene to yield aryl(vinyl)germylene, **3.22**.

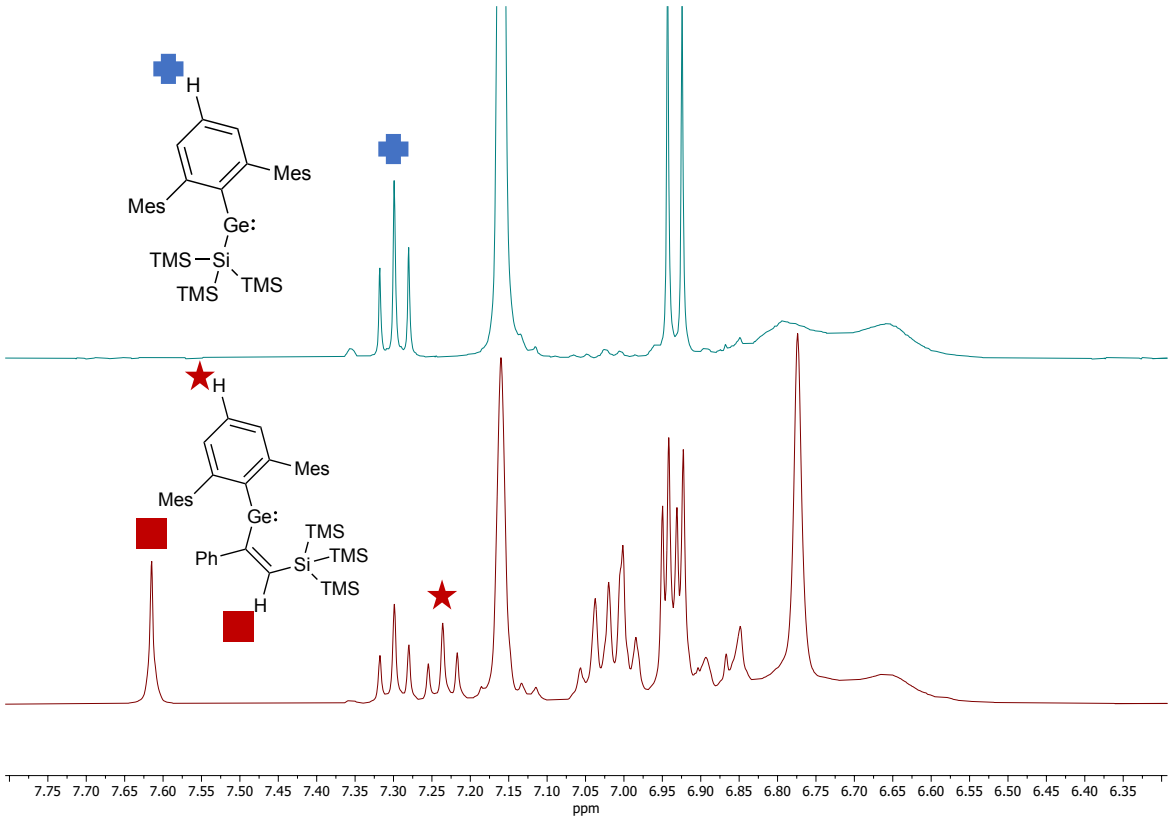
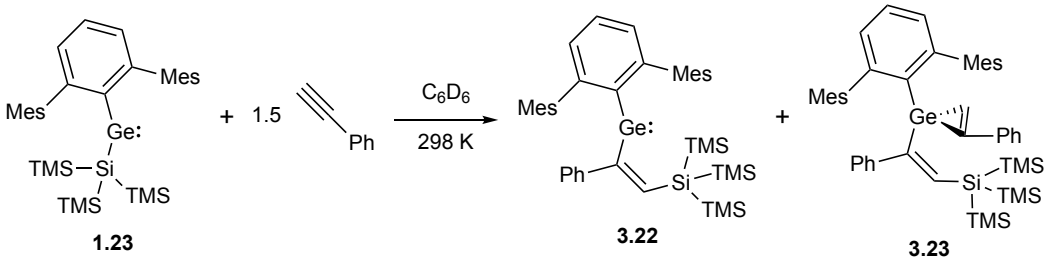


Figure 3-14: Top – ^{1}H NMR spectrum of **1.23**. Bottom – ^{1}H NMR spectrum of the reaction mixture of **1.23** and half an equivalent of phenylacetylene.

To confirm this supposition, one more equivalent of phenyl acetylene was added to the reaction mixture to convert all the remaining free germylene into the insertion product, **3.22** (Scheme 3-23). The colour of the reaction mixture remained purple, however the resonances in the ^{1}H NMR spectrum became significantly broader (Figure 3-15) and two new singlet resonances also appeared at 6.33 and 8.37 ppm. To further aid analysis of the product distribution, single crystals suitable for X-ray diffraction were grown by slow evaporation of the reaction mixture.



Scheme 3-23: Reaction of aryl(silyl)germylene, **1.23**, with one and a half equivalents of phenylacetylene to form Ge(II) and Ge(IV) species.

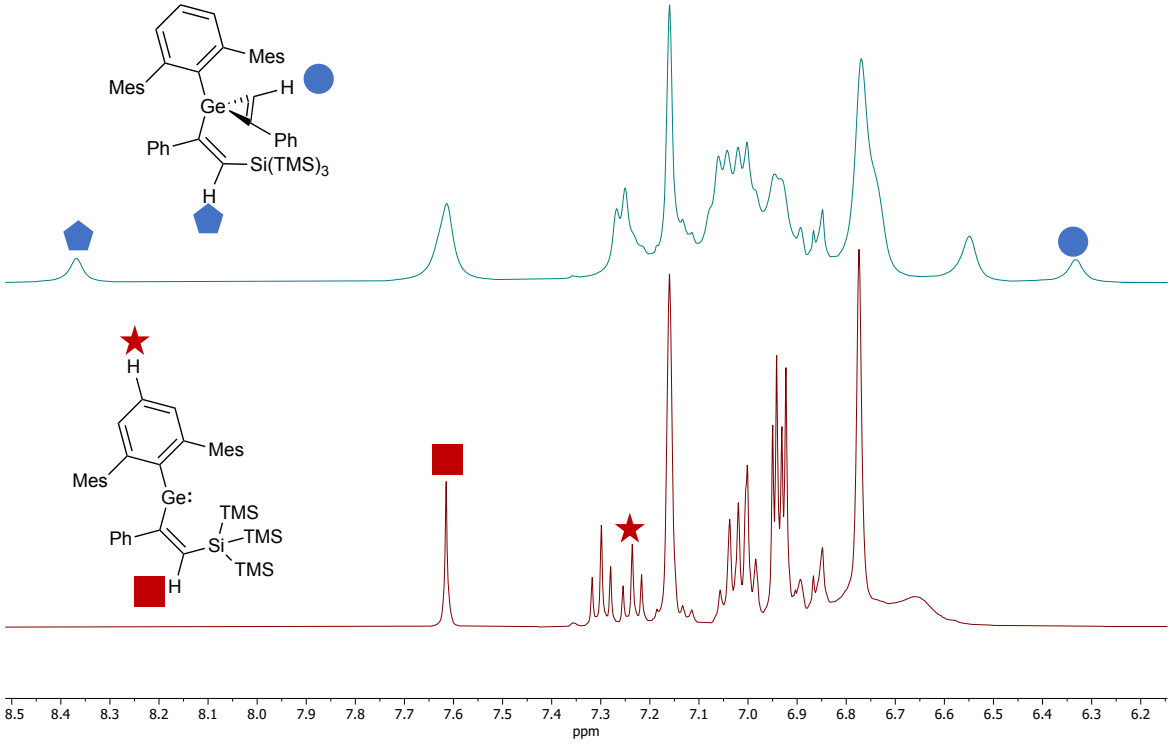


Figure 3-15: Top – ^{1}H NMR spectrum of the reaction mixture of **1.23** and half an equivalent of phenylacetylene. Bottom – ^{1}H NMR spectrum of the reaction mixture of **1.23** and one and a half equivalents of phenylacetylene.

The solid state structure shows two compounds, being a co-crystallite of **3.22** and **3.23** (Scheme 3-23). Therefore, both molecules appear in the asymmetric unit, however the structures of **3.22** and **3.23** appear separately in the figures below (Figure 3-16 and 3-17 respectively) for clarity. Indeed, because of this co-crystallisation, the crystallographic data obtained for both species, while sufficient to prove connectivity, is not of the requisite quality

to discuss geometrical parameters. Inspecting the structure of **3.22** shows that a syn-addition of the alkyne to the Ge–Si bond has occurred, as has been reported in other examples of alkyne addition into Ge–X (X = B, Si, H) bonds.[13,14,20] Additionally, the germanium centre is bonded to the more substituted alkenic carbon, which is also in line with other insertions of alkynes into E–X (E = Ge, Sn and X = B, Si, H) bonds.[13,14,20] It is thought that, as with the reaction of **1.23** with ethene above (Scheme 3-19), the [2+1]-cycloaddition product of phenylacetylene and **1.23** could be the intermediate for this insertion chemistry. Moreover, due to the rigidity of the vinyl group, the hypersilyl ligand is forced into a geometry which disfavours subsequent dimerisation of the germylene, hence why **3.22** is then able to undergo a [2+1]-cycloaddition to form **3.23**. This behaviour is akin to the silylsilylene reported by Rieger *et al.* (Scheme 1-16) in which migratory insertion of a coordinated ethene unit into the Si–Si bond was followed by [2+1]-cycloaddition of another equivalent of ethene.[12] To the best of our knowledge, this is the first example of this mode of reactivity between a germylene and any unsaturated substrate.

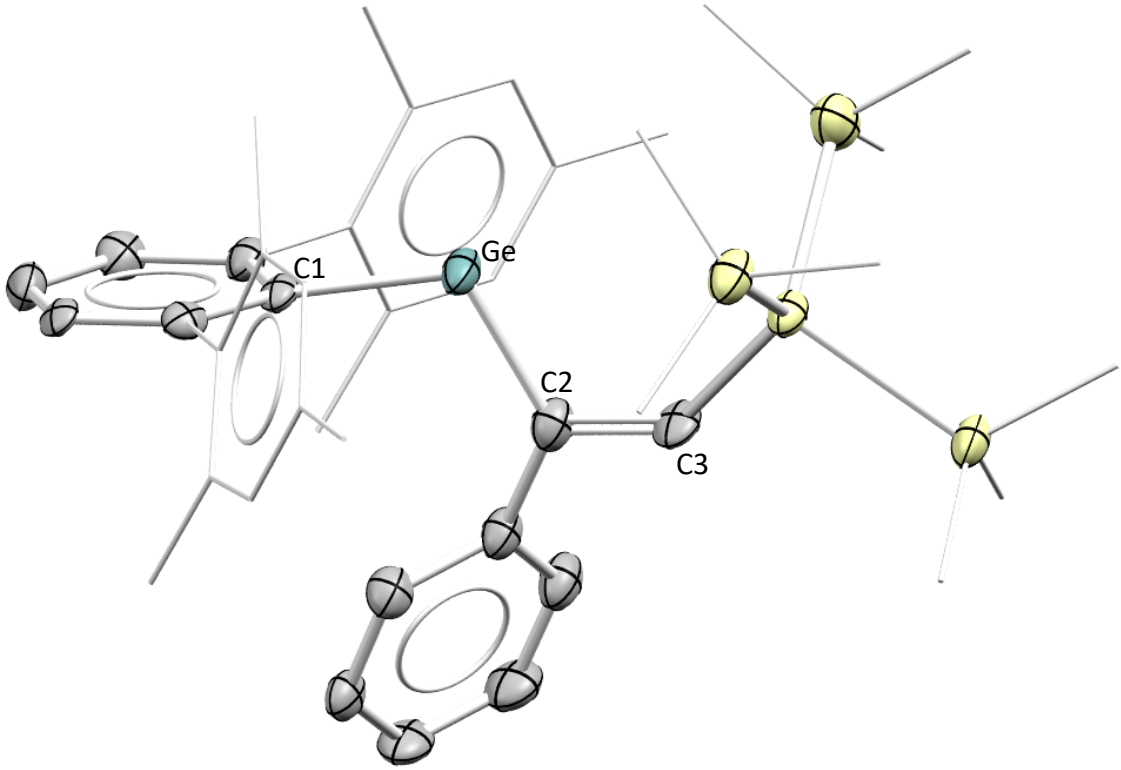


Figure 3-16: Molecular structure of **3.22** as determined by X-ray crystallography. The thermal ellipsoids are set to the 50% probability level. Hydrogen atoms are omitted for clarity. The flanking mesityl rings of the terphenyl ligand, and the methyl groups of the hypersilyl ligand. Data of insufficient quality to discuss the geometric parameters of **3.22**.

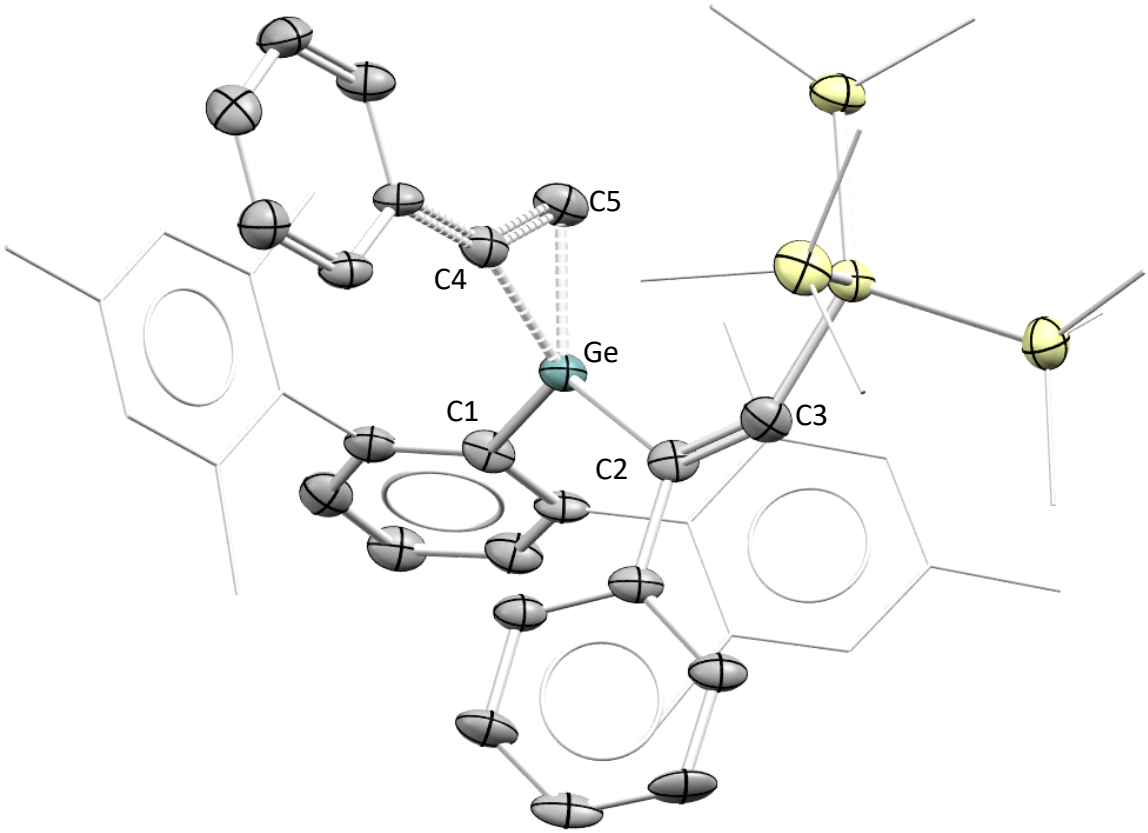
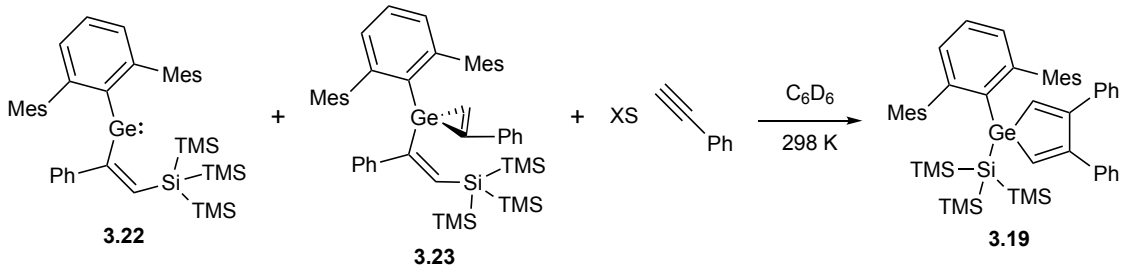


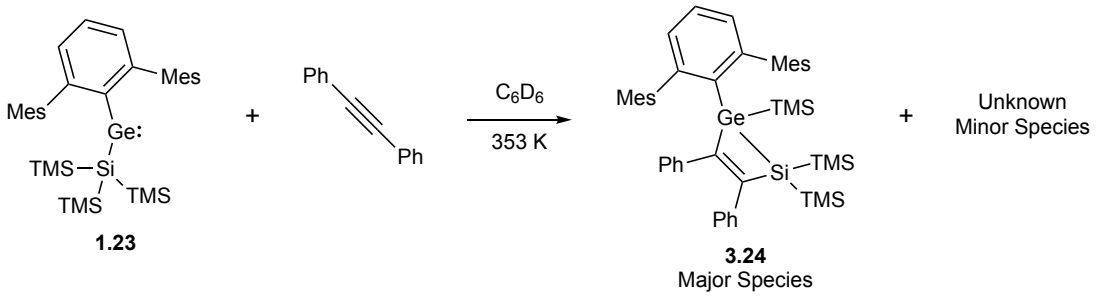
Figure 3-17: Molecular structure of **3.23** as determined by X-ray crystallography. The thermal ellipsoids are set to the 50% probability level. Hydrogen atoms are omitted for clarity. The flanking mesityl rings of the terphenyl ligand, and the methyl groups of the hypersilyl ligand. Data of insufficient quality to discuss the geometric parameters of **3.23**.

An excess of phenylacetylene was added to a C_6D_6 solution containing the residue from the crystallisation which afforded the co-crystal of **3.22** and **3.23** (Scheme 3-24), and the reaction tracked by *in situ* ^{1}H NMR spectroscopy. Immediately after addition, the solution decolourised, suggesting that **3.22** in solution reacts rapidly with phenylacetylene. This is corroborated by the exclusive presence of the resonances due to **3.23** and **3.19** in the ^{1}H NMR spectrum. After one week, only **3.19** remained in solution according to the ^{1}H NMR data, indicating that **3.22** and **3.23** are potentially intermediates in the formation of **3.19** or that the formation of **3.22** and **3.23** from **1.23** is reversible. More research is therefore required to ascertain the mechanism of the formation of **3.19** from phenylacetylene and **1.23**.



Scheme 3-24: Formation of germole, **3.19**, from a combination of a Ge(II) and Ge(IV) species and excess phenyl acetylene.

It was hypothesised that if the bulk of the alkyne was increased the reaction could be stopped at the initial [2+1]-cycloaddition product, and that no insertion into the Ge–Si bond would be seen, as observed by Walewska *et al.* in the reaction between bis(silyl)germylene **1.22** and diphenylacetylene (Schemes 1-19 and 1-20).[20] When diphenylacetylene was reacted with a solution of **1.23** no reaction was observed at room temperature, however after heating at 353 K for 1 h the teal colour of **1.23** began to be discharged (Scheme 3-25). The reaction could be tracked by ^{1}H NMR spectroscopy, and after 2 d of heating at 353 K the reaction seemed to have reached completion. Analysis of the reaction mixture by ^{1}H NMR spectroscopy indicates the presence of a major and minor species (Figure 3-18). The identity of these species has not been determined conclusively because the overlap of peaks in the aromatic region make a full characterisation impossible. However, analysis of the -$SiMe_3$ resonances in the ^{1}H NMR spectrum of the major product (Figure 3-18) suggests that the formation of a silagermacyclobutene could have occurred, as seen by Walewska *et al.* (Schemes 1-19 and 1-20).[20]



Scheme 3-25: Proposed reaction of aryl(silyl)germylene, **1.23**, with diphenylacetylene at 353 K to yield silagermacyclobutene, **3.24**, and an additional minor species.

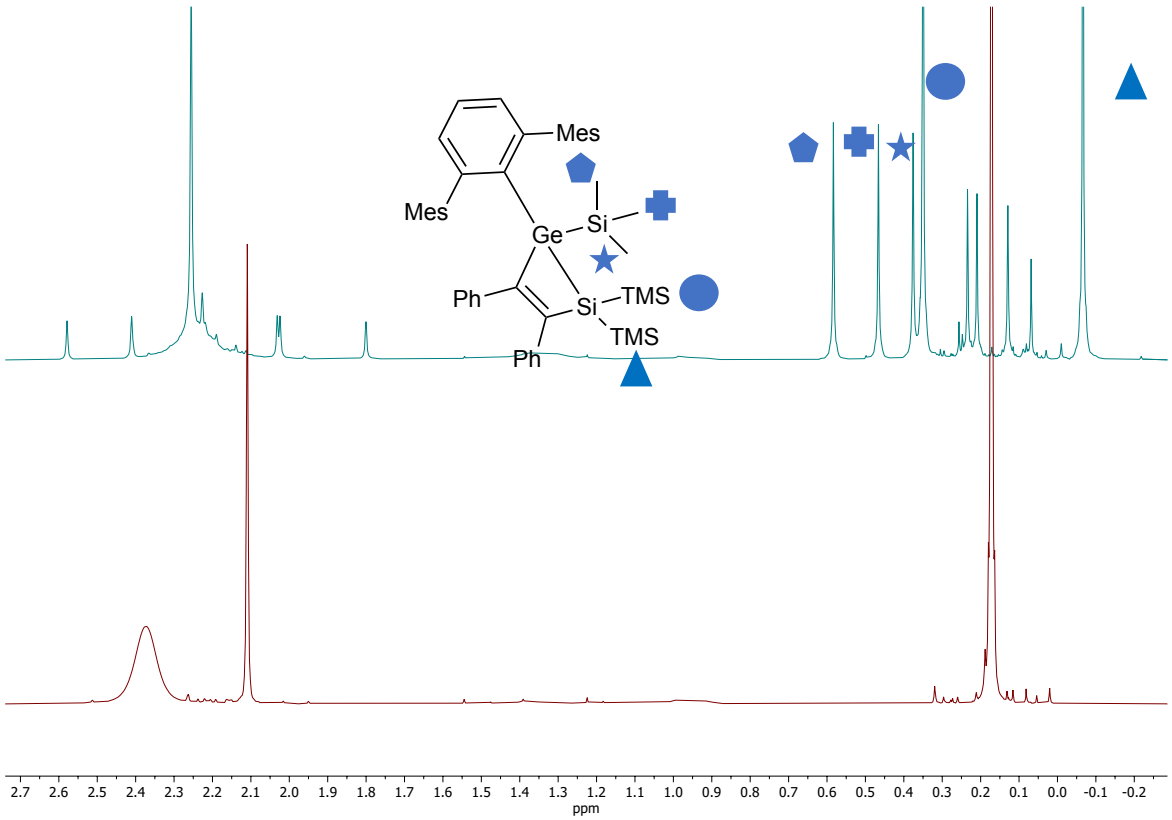


Figure 3-18: Two stacked ^{1}H NMR spectra: Top – ^{1}H NMR spectrum of the reaction mixture of diphenyl acetylene and **1.23** after two days of heating at 353 K. Bottom – ^{1}H NMR spectrum of **1.23.**

3.3 Conclusions

In this chapter, a new synthetic method to access the chlorogermylene, $[GeAr^{Mes}Cl]_2$, was disclosed, allowing it to be synthesised repeatedly and reproducibly (Schemes 3-5 and 3-6). From this precursor, the aryl(silyl)germylene ($GeAr^{Mes}Si(TMS)_3$), **1.23**, could be synthesised in

a straightforward manner (Scheme 3-7), and its reactivity with a variety of small molecules was explored. With monoalkylamines ($MeNH_2$, $^sBuNH_2$, and $^tBuNH_2$), oxidative addition of the N–H bond was found to occur and, in the case of $MeNH_2$, the product $GeAr^{Mes}Si(TMS)_3(H)(NHMe)$ (**3.5**, Scheme 3-9) could be characterised by X-ray crystallography (Figure 3-1). With $^sBuNH_2$ and $^tBuNH_2$, the formation of coordinative intermediates was observed in *in situ* ^1H NMR data (Figures 3-2 and 3-3), preceding oxidative addition of the N–H bond ($^sBuNH_2$: **3.6**, Scheme 3-10; $^tBuNH_2$: **3.7** Scheme 3-11), suggesting that the coordination/proton shuttling mechanism of N–H activation of amines by germylenes proposed by Peng *et al.* is occurring.[7] The reaction of **1.23** with diethylamine (Scheme 3-12) or *p*-toluidine (Scheme 3-13) also produced the respective N–H oxidative addition products. The ability of **1.23** to function as a Lewis acid was investigated through reaction with DMAP (Scheme 3-14) and ^{t}BuNC (Scheme 3-15). With DMAP, the adduct (**3.10**), persists. However, with ^{t}BuNC, C–H activation of the *tert*-butyl group occurs over the course of 1 h at room temperature to yield the Ge(IV) cyanide/hydride species, **3.11**. In addition, the Lewis basicity of **1.23** was demonstrated by the synthesis of the $W(CO)_5$ adduct, **3.14** (Scheme 3-18). Investigations into the reactivity of **1.23** with alkenes were also carried out. With ethene, insertion of the C=C bond into the Ge–Si bond of **1.23** is seen, followed by subsequent dimerisation to yield the digermene, **3.17** (Scheme 3-19). When the bulk of the alkene is increased *e.g.* by using norbornene, insertion of the alkene into the Ge–Si bond is still observed, to form **3.18** (Scheme 3-20). However, due to the greater bulk of the norbornane fragment, dimerisation does not occur. The chemical behaviour of **1.23** with alkynes was also explored. The reaction with excess phenylacetylene was found to couple together two equivalents of the alkyne to yield the germole, **3.19** (Scheme 3-21). However, on exposure of **1.23** to sub-stoichiometric quantities of phenylacetylene, the alkyne was found to insert into

the Ge–Si bond of **1.23** in a *syn*-fashion with the germanium bound to the most substituted carbon to yield the vinylgermylene **3.22** (Scheme 3-22). Adding an additional equivalent of phenylacetylene to **3.22** was found to yield **3.23** (Scheme 3-23), which is formed from the [2+1]-cycloaddition of **3.22** with phenylacetylene. Whilst **3.22** and **3.23** can be observed initially upon the combination of **1.23** and phenylacetylene, prolonged reaction times yield the thermodynamic product *i.e.* germole, **3.19**.

3.4 Characterisation of Novel Materials

3.4.1 Reaction of $GeAr^{Mes}Si(TMS)_3$ with $MeNH_2$ (Scheme 3-9)

To a solution of **1.23** (25 mg, 0.039 mmol) in C_6D_6 (0.40 mL) was added a solution of methylamine in THF (2.0 M, 50 μL, 0.10 mmol). A colour change from teal to colourless was observed. After decolourisation, the volatiles were removed *in vacuo* and the residue extracted with hexane. Slow evaporation of the hexane solution afforded the product as colourless crystals suitable for X-ray crystallography. The product was also characterised by *in situ* ^{1}H NMR spectroscopy. ^{1}H NMR (400 MHz, C_6D_6, 298 K) δ: 7.20 (t, *p*-C*H* Ar^{Mes}, $^3J_{HH}$ = 7.5 Hz, 1H), 6.86 (s, Ar*H*, 6H), 4.92 (d, Ge–*H*, $^3J_{HH}$ = 7.3 Hz, 1H), 2.66 (d, N–CH_3, $^3J_{HH}$ = 6.0 Hz, 3H), 2.24 (s, CH_3-Mes, 6H), 2.18 (s, CH_3-Mes, 6H), 2.11 (s, CH_3-Mes, 6H), 0.18 (s, Si(Si(CH_3)$_3$)$_3$, 27H), -0.50 (quin., N–*H*, $^3J_{HH}$ = 7.0 Hz, 1H) ppm.

3.4.2 Reaction of $GeAr^{Mes}Si(TMS)_3$ with ^{s}BuNH$_2$ (Scheme 3-10)

To a solution of **1.23** (19 mg, 0.030 mmol) in C_6D_6 (0.40 mL) was added ^{s}BuNH$_2$ (9.0 μL, 0.089 mmol) and a colour change from teal to yellow was observed. The reaction was stirred for 12 h at room temperature and the solution decolourised to yield the oxidative addition product, which was characterised by *in situ* ^{1}H NMR spectroscopy. ^{1}H NMR (400 MHz, C_6D_6,

298 K) δ: 7.13 (t, *p*-C*H* Ar^{Mes}, $^{3}J_{HH}$ = 7.5 Hz, 1H), 7.00–6.92 (m, Ar*H*, 3H), 6.87–6.78 (m, Ar*H*, 3H), 3.64–3.62 (m, Ge–*H*, 1H), 2.70–2.52 (m, CN*H*, 1H), 2.41 (s, Mes-CH_3, 3H), 2.32 (s, Mes-CH_3, 3H), 2.24 (s, Mes-CH_3, 3H), 2.23 (s, Mes-CH_3, 3H), 2.19 (s, Mes-CH_3, 3H), 2.03 (s, Mes-CH_3, 3H), 1.07–1.04 (m, ^{s}Bu*H*, 1H), 0.95–0.89 (m, ^{s}Bu*H*, 3H), 0.85–0.73 (m, ^{s}Bu*H*, 4H), 0.29–0.26 (m, Si(CH_3)$_3$, 9H), 0.19–0.16 (m, Si(CH_3)$_3$, 9H), 0.11 (s, Si(CH_3)$_3$, 9H), -0.23 (m, N–*H*, 1H) ppm.

3.4.3 Reaction of $GeAr^{Mes}Si(TMS)_3$ with $^{t}BuNH_2$ (Scheme 3-11)

To a solution of **1.23** (24 mg, 0.038 mmol) in C_6D_6 (0.40 mL) was added $^{t}BuNH_2$ (12 μL, 0.11 mmol) and a colour change from teal to yellow was observed. The reaction was stirred for 12 h at room temperature, and the solution decolourised to yield the oxidative addition product, which was characterised by *in situ* ^{1}H NMR spectroscopy. ^{1}H NMR (400 MHz, C_6D_6, 298 K) δ: 7.12 (t, *p*-C*H* Ar^{Mes}, $^{3}J_{HH}$ = 7.5 Hz, 1H), 7.01 (dd, *m*-C*H* Ar^{Mes}, $^{3}J_{HH}$ = 7.5 Hz, $^{4}J_{HH}$ = 1.6 Hz, 1H), 6.97 (s, Mes-C*H*, 2H), 6.85 (s, Mes-C*H*, 1H), 6.83 (s, Mes-C*H*, 1H), 6.80 (dd, *m*-C*H* Ar^{Mes}, $^{3}J_{HH}$ = 7.5 Hz, $^{4}J_{HH}$ = 1.6 Hz, 1H), 3.69 (s, Ge–*H*, 1H), 2.45 (s, Mes-CH_3, 3H), 2.33 (s, Mes-CH_3, 3H), 2,25 (s, Mes-CH_3, 3H), 2.23–2.21 (m, Mes-CH_3, 6H), 2.00 (s, Mes-CH_3, 3H), 1.13 (s, ^{t}Bu*H*, 9H), 0.98 (s, N–*H*, 1H), 0.28 (s, (Si(CH_3)$_3$, 9H), 0.19 (s, Si(CH_3)$_3$, 9H), 0.13 (s, Si(CH_3)$_3$, 9H) ppm.

3.4.4 Reaction of $GeAr^{Mes}Si(TMS)_3$ with Et_2NH (Scheme 3-12)

To a solution of **1.23** (18 mg, 0.028 mmol) in C_6D_6 (0.40 mL) was added Et_2NH (10 μL, 0.097 mmol) and a colour change from teal to yellow was observed. The reaction was stirred for 12 h at room temperature, and the solution decolourised to yield the oxidative addition product, which was characterised by *in situ* ^{1}H NMR spectroscopy. ^{1}H NMR (400 MHz, C_6D_6, 298 K) δ: 7.12 (t, *p*-C*H* Ar^{Mes}, $^{3}J_{HH}$ = 7.5 Hz, 1H), 6.99 (dd, *m*-C*H* Ar^{Mes}, $^{3}J_{HH}$ = 7.6 Hz, $^{4}J_{HH}$ = 1.5 Hz, 1H), 6.93 (s, Mes-C*H*, 1H), 6.90 (s, Mes-C*H*, 1H), 6.87 (s, Mes-C*H*, 1H), 6.85 (s, Mes-C*H*, 1H),

6.82 (dd, *m*-C*H* Ar^{Mes}, $^{3}J_{HH}$ = 7.6 Hz, $^{4}J_{HH}$ = 1.5 Hz, 1H), 3.73 (s, Ge–*H*, 1H), 2.71 (q, Et-CH_2, $^{3}J_{HH}$ = 7.0 Hz, 4H), 2.36 (s, Mes-CH_3, 3H), 2.27–2.25 (m, Mes-CH_3, 6H), 2.24 (s, Mes-CH_3, 3H), 2.22 (s, Mes-CH_3, 3H), 2.08 (s, Mes-CH_3, 3H), 0.87 (t, Et-CH_2, $^{3}J_{HH}$ = 7.0 Hz, 6H), 0.24 (s, Si(CH_3)$_3$, 9H), 0.19 (s, Si(CH_3)$_3$, 9H), 0.15 (s, Si(CH_3)$_3$, 9H) ppm.

3.4.5 Reaction of $GeAr^{Mes}Si(TMS)_3$ with *p*-Toluidine (Scheme 3-13)

To a solution of **1.23** (18 mg, 0.028 mmol) in C_6D_6 (0.40 mL) was added *p*-toluidine (3.2 mg, 0.029 mmol). The reaction was stirred for 12 h at room temperature, and the solution decolourised to yield the oxidative addition product, which was characterised by *in situ* ^{1}H NMR spectroscopy. ^{1}H NMR (400 MHz, C_6D_6, 298 K) δ: 7.18 (t, *p*-C*H* Ar^{Mes}, $^{3}J_{HH}$ = 7.2 Hz, 1H), 7.04 (d, *m*-C*H* Ar^{Mes}, $^{3}J_{HH}$ = 7.7 Hz, 2H), 6.94–6.80 (m, Ar*H*, 6H), 6.36–6.32 (m, Ar*H*, 2H), 3.73 (s, Ge–*H*, 1H), 2.79 (s, N–*H*, 1H), 2.33 (s, Mes-CH_3, 3H), 2.25 (s, Mes-CH_3, 3H), 2.23 (s, Mes-CH_3, 3H), 2.20 (s, Mes-CH_3, 6H), 2.12 (s, N–CH_3, 6H), 2.02 (s, Mes-CH_3, 3H), 0.24 (s, Si(CH_3)$_3$, 9H), 0.22 (s, Si(CH_3)$_3$, 9H), 0.13 (s, Si(CH_3)$_3$, 9H) ppm.

3.4.6 Synthesis of $GeAr^{Mes}Si(TMS)_3(H)(CN)$, **3.11** (Scheme 3-16)

To a solution of **1.23** (18 mg, 0.028 mmol) in C_6D_6 (0.40 mL) was added a solution of *tert*-butylisonitrile in benzene (0.40 M, 100 μL, 0.040 mmol). An immediate colour change from teal to yellow was observed. The reaction was stirred for 12 h at room temperature, and the reaction mixture decolourised. Volatiles were removed *in vacuo* and the residue extracted with hexane. Slow evaporation of the hexane solution afforded the product as colourless crystals. ^{1}H NMR (500 MHz, C_6D_6, 298 K) δ: 7.14 (t, *p*-C*H* Ar^{Mes}, $^{3}J_{HH}$ = 7.6 Hz, 1H), 6.93 (s, *m*-C*H* Ar^{Mes}, 2H), 6.83 (m, Mes-C*H*, 4H), 4.69 (s, Ge–*H*, 1H), 2.24 (s, Mes-CH_3, 6H), 2.21 (s, Mes-CH_3, 6H), 2.12 (s, Mes-CH_3, 6H), 0.17 (s, Si(SiCH_3)$_3$, 27H) ppm. ^{13}C NMR (126 MHz, C_6D_6, 298 K)

δ: 149.6, 140.5, 137.4, 130.8, 129.6, 129.3, 128.8, 128.3, 124.1, 22.2, 22.0, 21.2, 2.4 ppm. ^{29}Si NMR (100 MHz, C_6D_6, 298 K) δ: -8.4, -106.9 ppm.

3.4.7 Synthesis of $GeAr^{Mes}Si(TMS)_3{\cdot}W(CO)_5$, **3.14** (Scheme 3-18)

1.23 (22 mg, 0.035 mmol) and $W(CO)_5(NMe_3)$ (14 mg, 0.036 mmol) were combined in a J-Youngs tap NMR tube and C_6D_6 (0.40 mL) was added. The reaction was then allowed to heat at 353 K for 24 h. Volatiles were removed *in vacuo* and the residue was extracted into hexane. Slow evaporation of the hexane solution afforded the product as red crystals. ^{1}H NMR (500 MHz, C_6D_6, 298 K) δ: 7.16 (t, *p*-C*H* Ar^{Mes}, $^3J_{HH}$ = 7.5 Hz, 1H), 6.93 (d, *m*-C*H* Ar^{Mes}, $^3J_{HH}$ = 7.4 Hz, 2H), 6.83 (s, Mes-C*H*, 2H), 6.74 (s, Mes-C*H*, 2H), 2.44 (s, Mes-C*H*$_3$, 6H), 2.23 (s, Mes-C*H*$_3$, 6H), 2.12 (s, Mes-C*H*$_3$, 6H), 0.25 (br. s, $Si(Si(CH_3)_3)_3$, 27H) ppm. ^{13}C NMR (126 MHz, C_6D_6, 298 K) δ: 201.6, 196.8, 163.9, 139.2, 135.7, 135.2, 134.7, 133.7, 128.0, 127.9, 127.2, 22.1, 20.3, 18.6, 2.9 ppm. ^{29}Si NMR (100 MHz, C_6D_6, 298 K) δ: -45.9 ppm.

3.4.8 Reaction of $GeAr^{Mes}Si(TMS)_3$ with Ethene (Scheme 3-19)

A solution of **1.23** (26 mg, 0.041 mmol) in C_6D_6 (0.40 mL) was degassed three times using the freeze-pump-thaw method before the headspace was charged with ethene at *ca*. 2 bar. After 5 min the product began to be precipitated out of solution as a yellow powder. Volatiles were removed *in vacuo* and the residue extracted into hexane. Slow evaporation of the hexane solution afforded the product as yellow crystals suitable for X-ray crystallography. The product was also characterised by *in situ* ^{1}H NMR spectroscopy. ^{1}H NMR (400 MHz, C_6D_6, 298 K) δ: 7.36–7.32 (m, Ar*H*, 1H), 7.27–7.21 (m, Ar*H*, 4H), 7.07–7.02 (m, Ar*H*, 2H), 2.71 (s, Mes-C*H*$_3$, 6H), 2.22 (s, Mes-C*H*$_3$, 6H), 2.16 (s, Mes-C*H*$_3$, 6H), 1.78–1.70 (m, -C*H*$_2$, 2H), 1.10–1.04 (m, -C*H*$_2$, 2H), 0.44 (s, $Si(Si(CH_3)_3)_3$, 27H) ppm.

3.4.9 Reaction of $GeAr^{Mes}Si(TMS)_3$ with Norbornene (Scheme 3-20)

1.23 (18 mg, 0.028 mmol) was combined with norbornene (2.7 mg, 0.028 mmol) and the mixture dissolved in C_6D_6 (0.40 mL). An immediate colour change to purple was observed and the reaction was stirred for 12 h at room temperature. Volatiles were removed *in vacuo* and the residue extracted into hexane. Slow evaporation of the hexane solution afforded the product as purple crystals suitable for X-ray crystallography. The product was also characterised by *in situ* ^{1}H NMR spectroscopy. ^{1}H NMR (400 MHz, C_6D_6, 298 K) δ: 7.29 (t, *p*-C*H* Ar^{Mes}, $^3J_{HH}$ = 7.5 Hz, 1H), 6.99 (d, *m*-C*H* Ar^{Mes}, $^3J_{HH}$ = 7.5 Hz, 2H), 6.76 (s, Mes-C*H*, 2H), 6.73 (s, Mes-C*H*, 2H), 2.85 (s, Norborne-*H*, 1H) 2.40 (s, Mes-CH_3, 6H), 2.32 (s, Norborne-*H*, 1H), 2.25 (s, Mes-CH_3, 6H), 2.15 (s, Mes-CH_3, 6H), 2.13–2.09 (m, Norborne-*H*, 1H), 1.62–1.34 (m, Norborne-*H*, 4H), 1.27–1.19 (m, Norborne-*H*, 1H), 0.99–0.85 (m, Norborne-*H*, 2H), 0.18 (s, $Si(Si(CH_3)_3)_3$, 27H) ppm.

3.4.10 Reaction of $GeAr^{Mes}Si(TMS)_3$ with Excess PhCCH (Scheme 3-21)

To a solution of **1.23** (20 mg, 0.032 mmol) in C_6D_6 (0.40 mL) was added an excess of PhCCH (9.0 μL, 0.096 mmol). A colour change from teal to purple and then colourless was seen. After decolourisation the volatiles were removed *in vacuo* and the residue extracted into hexane. Slow evaporation of the hexane solution afforded the product as colourless crystals. ^{1}H NMR (400 MHz, C_6D_6, 298 K) δ: 7.21–7.14 (m, Ar*H*, 7H), 7.06–7.00 (m, Ar*H*, 4H), 7.00–6.95 (m, Ar*H*, 4H), 6.90 (d, *m*-C*H* Ar^{Mes}, $^3J_{HH}$ = 7.5 Hz, 2H), 6.72 (s, Mes-C*H*, 2H), 5.62 (s, Ge-C=C*H*, 2H), 2.40 (s, Mes-CH_3, 6H), 2.25 (s, Mes-CH_3, 6H), 1.86 (s, Mes-CH_3, 6H), 0.21 (s, $Si(Si(CH_3)_3)_3$, 27H) ppm.

3.4.11 Reaction of $GeAr^{Mes}Si(TMS)_3$ with 1 Equiv. of PhCCH (Scheme 3-22)

To a solution of **1.23** (20 mg, 0.032 mmol) in C_6D_6 (0.40 mL) was added PhCCH (3.0 μL, 0.027 mmol) and an immediate colour change to purple was seen. The reaction was stirred for 12 h at room temperature and the insertion product could be characterised by *in situ* ^{1}H NMR spectroscopy. ^{1}H NMR (400 MHz, C_6D_6, 298 K) δ: 7.61 (s, GeC=C*H*, 1H), 7.23 (t, *p*-C*H* Ar^{Mes}, $^3J_{HH}$ = 7.3 Hz, 1H), 7.07–6.97 (m, Ar*H*, 5H), 6.94 (d, *m*-C*H* Ar^{Mes}, $^3J_{HH}$ = 7.3 Hz, 2H), 6.77 (s, Mes-C*H*, 4H), 2.56 (s, Mes-CH_3, 6H), 2.11 (s, Mes-CH_3, 6H), 1.81 (s, Mes-CH_3, 6H), 0.17 (s, $Si(Si(CH_3)_3)_3$, 27H) ppm.

3.5 References

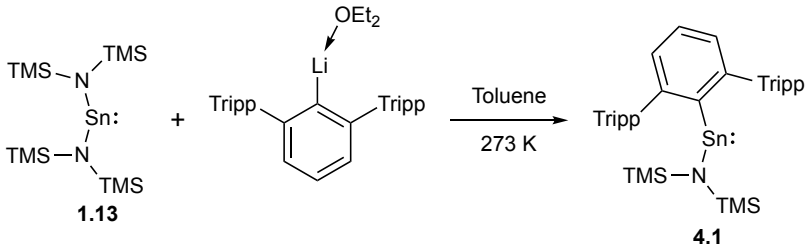
1 Y. Mizuhata, T. Sasamori and N. Tokitoh, *Chem Rev*, 2009, **109**, 3479–3511.
2 J. Zhu, Z. Lin and T. B. Marder, *Inorg Chem*, 2005, **44**, 9384–9390.
3 D. Bourissou, O. Guerret, F. P. Gabbaï and G. Bertrand, *Chem Rev*, 2000, **100**, 39–91.
4 X. Wang, Z. Zhu, Y. Peng, H. Lei, J. C. Fettinger and P. P. Power, *J Am Chem Soc*, 2009, **131**, 6912–6913.
5 J. W. Dube, Z. D. Brown, C. A. Caputo, P. P. Power and P. J. Ragogna, *Chem. Commun.*, 2014, **50**, 1944–1946.
6 K. L. Gullett, T. Y. Lai, C. Y. Chen, J. C. Fettinger and P. P. Power, *Organometallics*, 2019, **38**, 1425–1428.
7 Y. Peng, J.-D. Guo, B. D. Ellis, Z. Zhu, J. C. Fettinger, S. Nagase and P. P. Power, *J Am Chem Soc*, 2009, **131**, 16272–16282.
8 A. V. Protchenko, K. H. Birjkumar, D. Dange, A. D. Schwarz, D. Vidovic, C. Jones, N. Kaltsoyannis, P. Mountford and S. Aldridge, *J Am Chem Soc*, 2012, **134**, 6500–6503.
9 M. Usher, A. V. Protchenko, A. Rit, J. Campos, E. L. Kolychev, R. Tirfoin and S. Aldridge, *Chemistry – A European Journal*, 2016, **22**, 11685–11698.
10 Z. D. Brown, J. D. Guo, S. Nagase and P. P. Power, *Organometallics*, 2012, **31**, 3768–3772.
11 M. Walewska, J. Baumgartner and C. Marschner, *Chemical Communications*, 2014, **51**, 276–278.
12 D. Wendel, W. Eisenreich, C. Jandl, A. Pöthig and B. Rieger, *Organometallics*, 2016, **35**, 1–4.
13 A. V. Protchenko, M. P. Blake, A. D. Schwarz, C. Jones, P. Mountford and S. Aldridge, *Organometallics*, 2015, **34**, 2126–2129.
14 T. J. Hadlington, M. Hermann, G. Frenking and C. Jones, *Chem Sci*, 2015, **6**, 7249–7257.
15 R. S. Simons, L. Pu, M. M. Olmstead and P. P. Power, *Organometallics*, 1997, **16**, 1920–1925.
16 M. E. Alberto, N. Russo and E. Sicilia, *Chemistry - A European Journal*, 2013, **19**, 7835–7846.
17 C. Laurence and J. F. Gal, *Lewis Basicity and Affinity Scales: Data and Measurement*, Wiley Blackwell, 2009.
18 Z. D. Brown, P. Vasko, J. C. Fettinger, H. M. Tuononen and P. P. Power, *J Am Chem Soc*, 2012, **134**, 4045–4048.
19 W. P. Neumann, *Chem Rev*, 1991, **91**, 311–334.
20 M. Walewska, J. Baumgartner, C. Marschner, L. Albers and T. Müller, *Chemistry – A European Journal*, 2016, **22**, 18512–18521.
21 N. Takeda, T. Kajiwara, H. Suzuki, R. Okazaki and N. Tokitoh, *Chemistry – A European Journal*, 2003, **9**, 3530–3543.
22 N. Takeda, H. Suzuki, N. Tokitoh, R. Okazaki and S. Nagase, *J Am Chem Soc*, 1997, **119**, 1456–1457.
23 P. Jutzi, B. Hampel, M. B. Hursthouse and A. J. Howes, *J Organomet Chem*, 1986, **299**, 19–27.

24 N. Tokitoh, K. Manmaru and R. Okazaki, *Organometallics*, 1994, **13**, 167–171.
25 F. Lips, J. C. Fettinger, A. Mansikkamäki, H. M. Tuononen and P. P. Power, *J Am Chem Soc*, 2014, **136**, 634–637.
26 S. Wang, M. L. McCrea-Hendrick, C. M. Weinstein, C. A. Caputo, E. Hoppe, J. C. Fettinger, M. M. Olmstead and P. P. Power, *J Am Chem Soc*, 2017, **139**, 6596–6604.
27 T. L. Bandrowsky, J. B. Carroll and J. Braddock-Wilking, *Organometallics*, 2011, **30**, 3559–3569.
28 T. Sugahara, A. Espinosa Ferao, A. Rey Planells, J. D. Guo, S. Aoyama, K. Igawa, K. Tomooka, T. Sasamori, D. Hashizume, S. Nagase and N. Tokitoh, *Dalton Transactions*, 2020, **49**, 7189–7196.

4 Synthesis of Novel Metallylenes

4.1 Introduction

Whilst silylenes and germylenes are typically synthesised from their tetra or divalent halide precursors, the use of bis(bis(trimethylsilyl)amido) complexes (e.g. $Sn(HMDS)_2$ and $Pb(HMDS)_2$) as starting materials becomes more common as group 14 is descended.[1–5] This stems, at least in part, from the greater solubility of these amido species as compared to the respective halides in hydrocarbon solvents. As a result, less forcing conditions are required and the use of coordinating solvents is avoided, which often makes isolation of the resulting metallylenes more challenging.



Scheme 4-1: Synthesis of amido(aryl)stannylene, **4.1**, from $Sn(HMDS)_2$.[4]

Once synthesised, insight into the electronic structure of metallylenes can be obtained by investigation by UV/vis spectroscopy. The UV/Vis absorption maxima (λ_{max}) of metallylenes are typically attributed to n–p transitions, and therefore act as a guide to the comparative magnitude of the HOMO–LUMO gap in such systems.[4] A longer wavelength is therefore indicative of a smaller HOMO–LUMO gap. This simple view can be complicated by the involvement of ligand orbitals in the electronic structure of the metallylenes, as noted by Power *et al.*[3] Nevertheless, when comparing the absorption maxima of bis(aryl)plumbylene, **4.2**, and aryl(silyl)plumbylene, **4.3**, (λ_{max} = 526 nm and 720 nm respectively), the longer

wavelength of **4.3**, and thus the narrower HOMO–LUMO gap in **4.3**, is a result of the destabilisation of the HOMO by the more electron donating silyl substituent (Figure 4-1).[3,6]

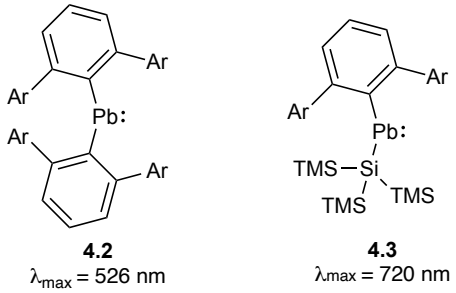
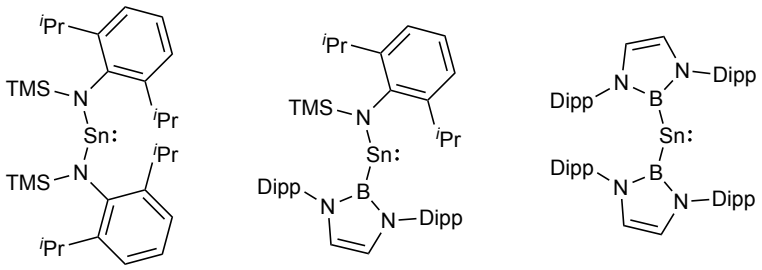


Figure 4-1: The absorption maxima in the UV/spectra of bis(aryl)plumbylene, **4.2**, and aryl(silyl)plumbylene, **4.3**.[3,6]

For stannylenes, ^{119}Sn NMR spectroscopy is also a useful tool to gauge the electronic environment at the tin centre.[7] The chemical shifts of two-coordinate stannylenes can encompass a wide range in ^{119}Sn NMR spectroscopy (δ = -2100 to 4755 ppm), however they are typically downfield shifted as compared to tetramethyl tin, the standard for ^{119}Sn spectroscopy, due to their lower coordination number.[7–9] Also significant in determining the resonances of stannylenes are their paramagnetic contributions to the NMR shift.[10] These contributions become greater, and shift the resonance further downfield, as the HOMO–LUMO gap gets narrower.[10] Evidence for this effect can be seen when comparing the ^{119}Sn resonances of bis(amido), amido(boryl), and bis(boryl)stannylenes (**4.4**, **1.61**, and **1.31** respectively) (Figure 4-2). The downfield shift of **1.31** is a result of the narrow HOMO–LUMO gap of **1.31**, caused by the destabilisation of the HOMO by the two strongly σ-donating boryl substituents.



4.4
^{119}Sn δ = 440 ppm

1.61
^{119}Sn δ = 1918 ppm

1.31
^{119}Sn δ = 4755 ppm

Figure 4-2: Three stannylenes and their associated resonances when investigated by ^{119}Sn NMR spectroscopy.[9,11]

In this chapter, the synthesis of a range of novel metallylenes is reported. Investigation of the structure and bonding of these metallylenes will be carried out by UV/Vis spectroscopy, NMR spectroscopy, and X-ray crystallography. Comparisons with relevant literature examples will be made to demonstrate the difference which result from employing silyl groups as ligands, as well as making comparisons based on comparing two different silyl ligands (-Si(TMS)$_3$ *vs.* -Si(TMS)$_2$(SiPh$_2$^{t}Bu)) to probe the effect of substituent steric bulk on the properties.

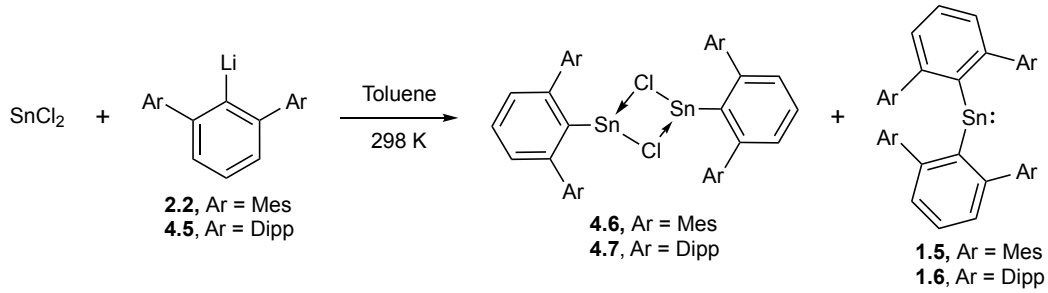
4.2 Results and Discussion

4.2.1 Synthesis of Aryl(silyl)stannylenes

A recent report by Inoue *et al.* of the reversible activation of white phosphorus (Scheme 1-3) shows the capabilities of aryl(silyl)stannylenes in small molecule activation.[12] With this and further small molecule reactivity in mind, the syntheses of two new aryl(silyl)stannylenes was targeted with a view to comparison with related compounds.

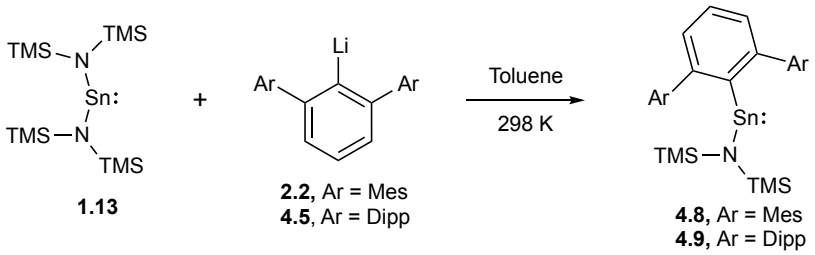
As with aryl(silyl)germylene (GeAr^{Mes}Si(TMS)$_3$), **1.23**, initial attempts to access aryl(silyl)stannylenes were made *via* chlorostannylene precursors, **4.6** ([Sn(Ar^{Mes})Cl]$_2$) and **4.7** ([Sn(Ar^{Dipp})Cl]$_2$), which had previously been reported in the literature by Simons *et al.*[3,13]

However, despite repeated attempts, this route failed to yield **4.6** and **4.7** cleanly (Scheme 4-2), with the reaction mixture invariably contaminated with the corresponding bis(aryl)stannylenes (**1.5** and **1.6**). This finding was attributed to the greater solubility of the mono-substituted arylstannylenes, **4.6** and **4.7**, compared to $SnCl_2$ in toluene. Hence, as the concentrations of **4.6** or **4.7** grow in solution through the course of the reaction, they can undergo a further salt metathesis reaction with one equivalent of aryllithiate (**2.2** or **4.5**) to yield the corresponding bis(aryl)stannylene (**1.5** or **1.6**).



Scheme 4-2: The reaction between tin dichloride and terphenyl lithiate (**2.2** or **4.5**) to yield chlorostannylene (**4.6** or **4.7**), contaminated with bis(aryl)stannylene (**1.5** or **1.6**).

Rather than cleanly access the chlorostannylenes, **4.6** and **4.7**, *via* their corresponding bis(aryl)stannylene precursors, **1.5** and **1.6**, (as used in the synthesis of chlorogermylene ($[Ge(Ar^{Mes})Cl]_2$), **2.3**, (Schemes 3-5 and 3-6)), a different tin(II) starting material was employed. It was decided to use tin bis(bis(trimethylsilyl)amide), **1.13**, as the Sn(II) source since Power *et al.* had previously succeeded in synthesising aryl(amido)stannylene, **4.1**, *via* a similar route with no hint of any bis(aryl)stannylene formation (Scheme 4-1).[4] When the terphenyl lithiates, **2.2** and **4.5**, were combined with **1.13** in toluene and stirred overnight, a red suspension formed in each case (Scheme 4-3). After filtration, the product could be isolated (for both terphenyl ligands) as a red solid in yields of up to 80% with no contamination from the corresponding bis(aryl)stannylene (Scheme 4-3).



Scheme 4-3: Synthesis of two aryl(amido)stannylenes, **4.8** and **4.9**, from their corresponding lithiates and tin bis(bis(trimethylsilyl)amide).

Crystals suitable for X-ray crystallography of both **4.8** and **4.9** could be grown from a toluene and pentane solution respectively (Figures 4-3 and 4-4) and allowed the geometric parameters of the two stannylenes to be compared to the previously synthesised system, **4.1**.[4] Key bond lengths and angles of **4.8**, **4.9**, and **4.1** are summarised in Table 4-1. The lengths of all three Sn–C bond lengths are equivalent with error and are consistent with a Sn(II) centre bonded to a terphenyl ligand. As such they are very similar to the Sn–C bonds in the bis(terphenyl)stannylenes **1.5**, **1.6**, and **1.7** (Figure 1-9) (Sn–C: 2.225(5), 2.255(2), and 2.250(4) Å respectively).[3,10,12,14,15] A clear trend can also be observed in the bond angles at the tin centre. As the steric bulk of the flanking aryl group is increased (Mes < Dipp < Tripp), the angle at the tin centre widens due to the greater repulsion forcing the ligands apart. However, comparing the ^{119}Sn NMR shifts of **4.8** and **4.1** (**4.8**: 1192.6 ppm, **4.1**[4]: 1196.8 ppm) indicates that the widening of the angle does not have a large impact on the HOMO–LUMO gap of the two stannylenes. Unfortunately, attempts to measure the ^{119} Sn NMR resonance of **4.9** have been unsuccessful, potentially due to the resonance being too broad at room temperature.

Table 4-1: Selected bond lengths (Å) and angles (°) for the compounds **4.8**, **4.9**, and **4.1**.[4]

	Sn–C	Sn–N	C–Sn–N
4.8	2.242(4)	2.111(4)	103.6(1)
4.9	2.222(3)	2.074(9)	107.3(2)
4.1[4]	2.225(5)	2.094(5)	108.4(2)

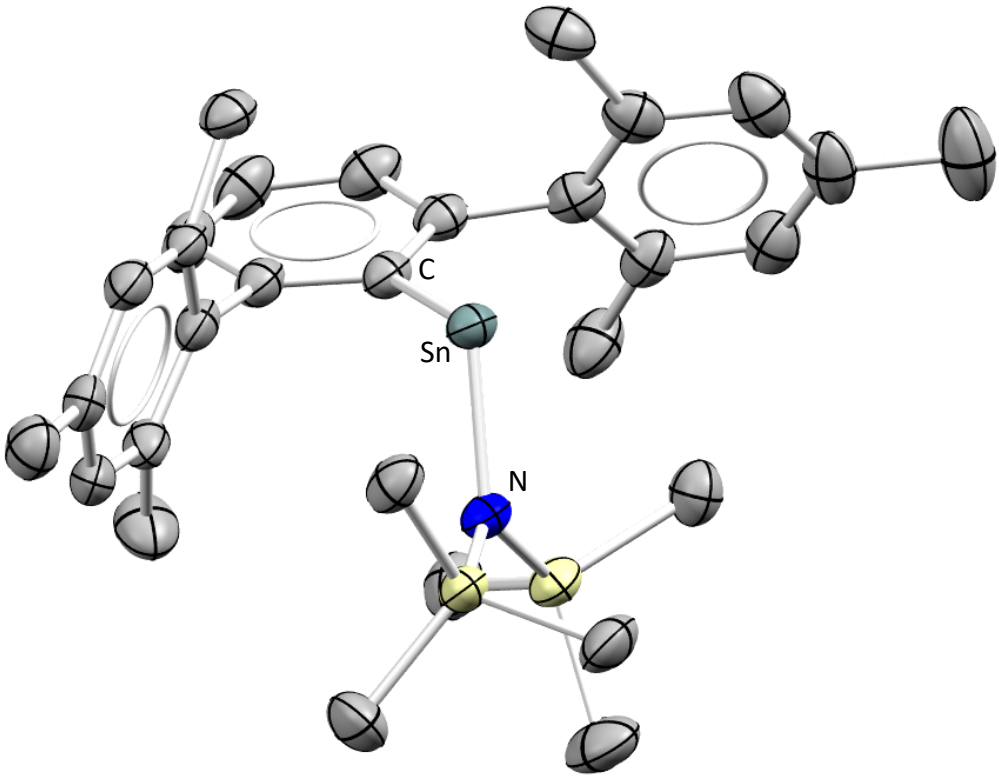


Figure 4-3: Molecular structure of **4.8** as determined by X-ray crystallography. The thermal ellipsoids are set at the 50% probability level. Hydrogen atoms are omitted for clarity. Key bond lengths and angles detailed in Table 4-1.

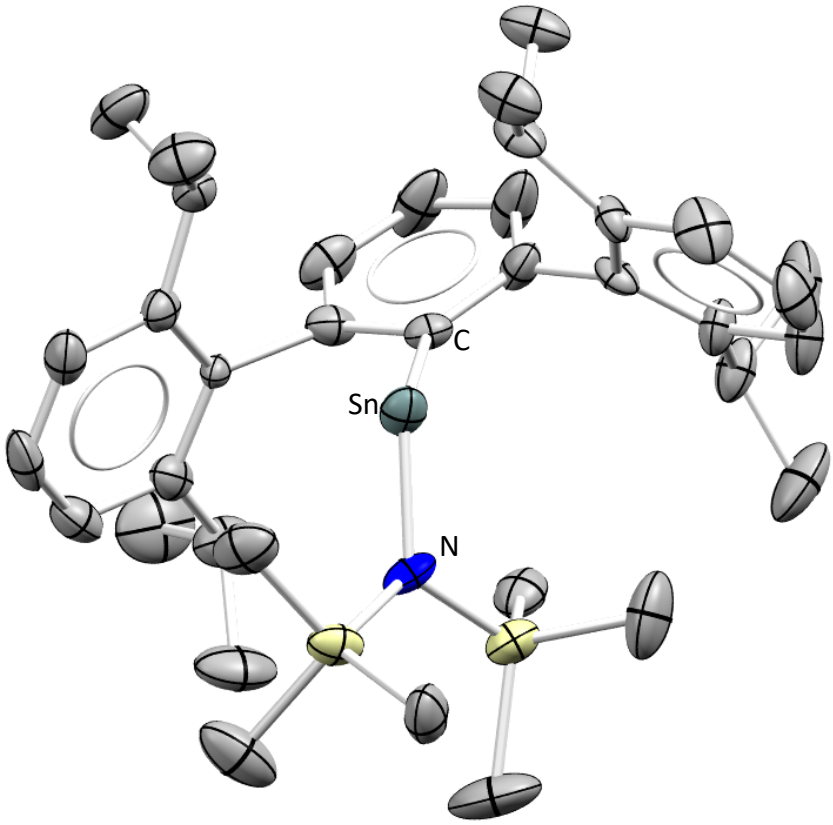
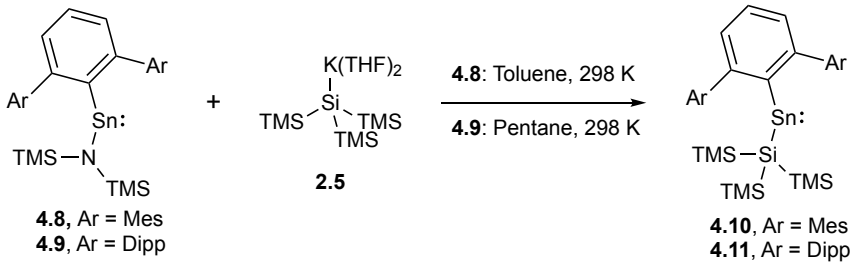


Figure 4-4: Molecular structure of **4.9** as determined by X-ray crystallography. The thermal ellipsoids are set at the 50% probability level. Hydrogen atoms are omitted for clarity. Key bond lengths and angles detailed in Table 4-1.

From **4.8** and **4.9**, the facile syntheses of the corresponding aryl(silyl)stannylenes, **4.10** and **4.11**, are possible, as depicted in Scheme 4-4. The different solvent choice (**4.8**: toluene, **4.9** pentane) for these two reactions reflects the greater solubility of **4.11** in aromatic solvents as compared to **4.10**. Isolation of **4.11** was therefore easier from pentane. Nevertheless, combination of either **4.8** or **4.9** with $K(THF)_2Si(TMS)_3$, **2.5**, in the appropriate solvent resulted in immediate formation of a dark green suspension. After stirring the reaction mixtures overnight and subsequent filtration, the desired products could be isolated as blue crystals. In the case of **4.11**, it was found that removal of the volatiles *in vacuo*, followed by re-extraction of the residue into pentane at 195 K, was necessary to generate the product

free from the KHMDS side product. In addition, crystals of both **4.10** and **4.11** suitable for X-ray crystallography could be obtained from pentane to allow comparison of geometric parameters with other aryl(silyl)metallylenes.[6,12,13]



Scheme 4-4: Synthesis of two aryl(silyl)stannylenes, **4.10** and **4.11**, from the corresponding aryl(amido)stannylenes, **4.8** and **4.9**, and potassium hypersilyl.

The structures of **4.10** and **4.11** are shown below (Figures 4-5 and 4-6). Key bond lengths and angles along with those for related literature compounds are detailed in Table 4-2. It is clear from the data that **4.10** and **4.11** closely resemble the previously synthesised aryl(silyl)stannylene $SnAr^{Mes}Si^tBu_3$, **1.11**, reported by Inoue *et al.*[12] The longer Sn–Si bond length of **1.11** (2.6981(17) Å), compared to **4.10** and **4.11** (2.6407(7) and 2.6524(6) Å), is presumably due to the greater proximal steric bulk of the supersilyl ligand (in **1.11**), $-Si^tBu_3$, compared to the hypersilyl ligand $SiTMS_3$ (in **4.10** and **4.11**). The slight difference in Sn–Si bond lengths is due to the different steric profiles of the hypersilyl and supersilyl ligands. Analysis of the three stannylenes by ^{119}Sn NMR spectroscopy shows a dramatic difference in their chemical shifts. While **4.10** and **4.11** display similar shifts (2793.1 and 2834.0 ppm respectively), **1.11** gives rise to a resonance at 197.3 ppm.[12] This difference could potentially be attributed to the use of THF-d_8 as the NMR solvent for **1.11**, compared to C_6D_6 for **4.10** and **4.11**. Solvent effects are known to be large in ^{119}Sn NMR spectroscopy and could be exaggerated in this case because the THF could coordinate to the tin centre, dramatically affecting the observed resonance.[16] This is borne out by comparison of the UV/Vis absorption

maxima for **4.10** and **1.11**. Both have similar values of λ_{max} (**4.10**: 638 nm, **1.11**: 674 nm), indicating that the electronic structure of the two stannylenes is very similar.

Trends in the structure and bonding of heavier metallylenes as a function of metal can be gleaned through comparison of **4.10** with its germylene, **1.23**, and plumbylene, **4.3**, analogues.[6,13] The lengthening of the E–C and E–Si bonds down the group is consistent with the increase in covalent radii of the elements as group 14 is descended. Furthermore, there is less s/p mixing in the heavier group 14 elements and therefore the angle at the metal centre narrows down the group and approaches 90°.

Table 4-2: Selected bond lengths (Å) and angles (°) for **4.10**, **4.11**, **1.11**, **1.23**, and **4.3**.[6,12,13]

	E–C	**E–Si**	**C–E–Si**
4.10	2.189(3)	2.6407(7)	109.75(6)
4.11	2.212(2)	2.6524(6)	111.66(5)
1.11[12]($SnAr^{Mes}Si^{t}Bu_3$)	2.217(5)	2.6981(17)	113.50(14)
1.23[13]($GeAr^{Mes}SiTMS_3$)	1.997(3)	2.440(1)	112.6(1)
4.3[6] ($PbAr^{Mes}SiTMS_3$)	2.290(4)	2.7120(12)	109.17(11)

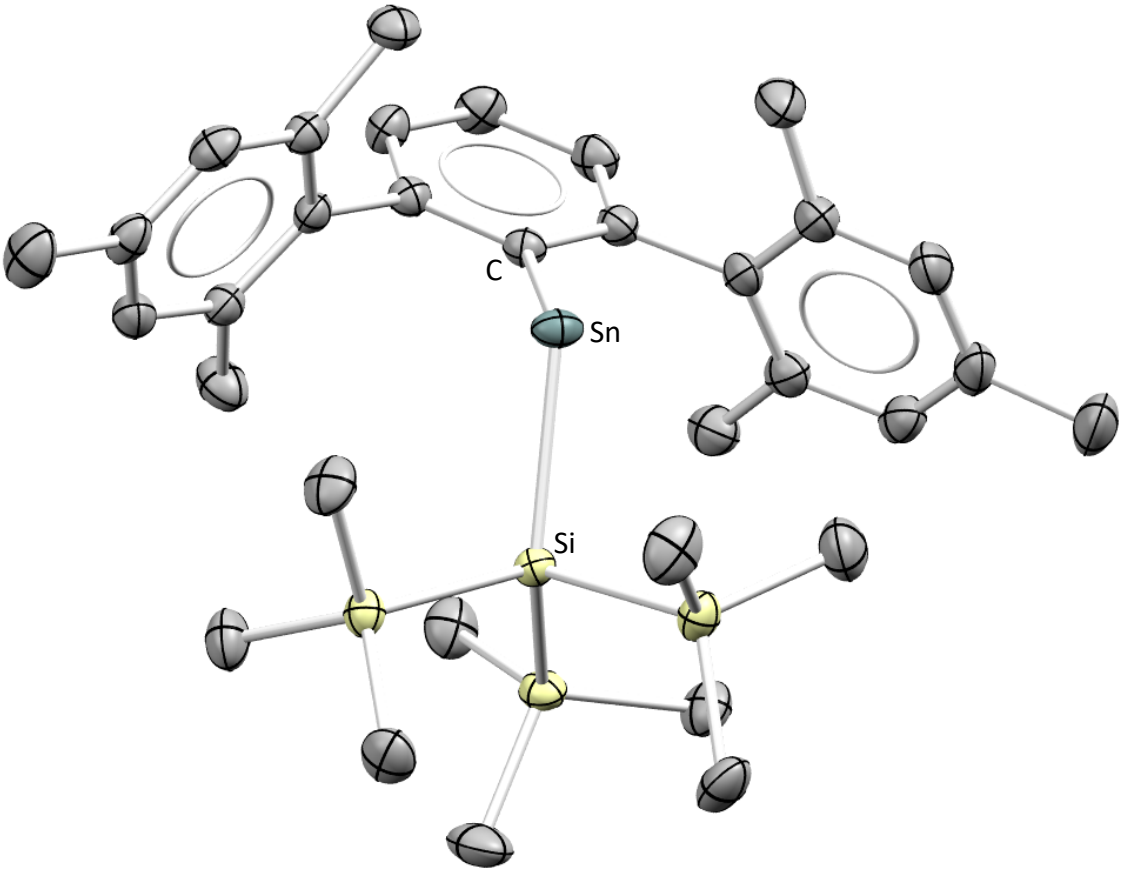


Figure 4-5: Molecular structure of **4.10** as determined by X-ray crystallography. The thermal ellipsoids are set at the 50% probability level. Hydrogen atoms are omitted for clarity. Key bond lengths and angles detailed in Table 4-2.

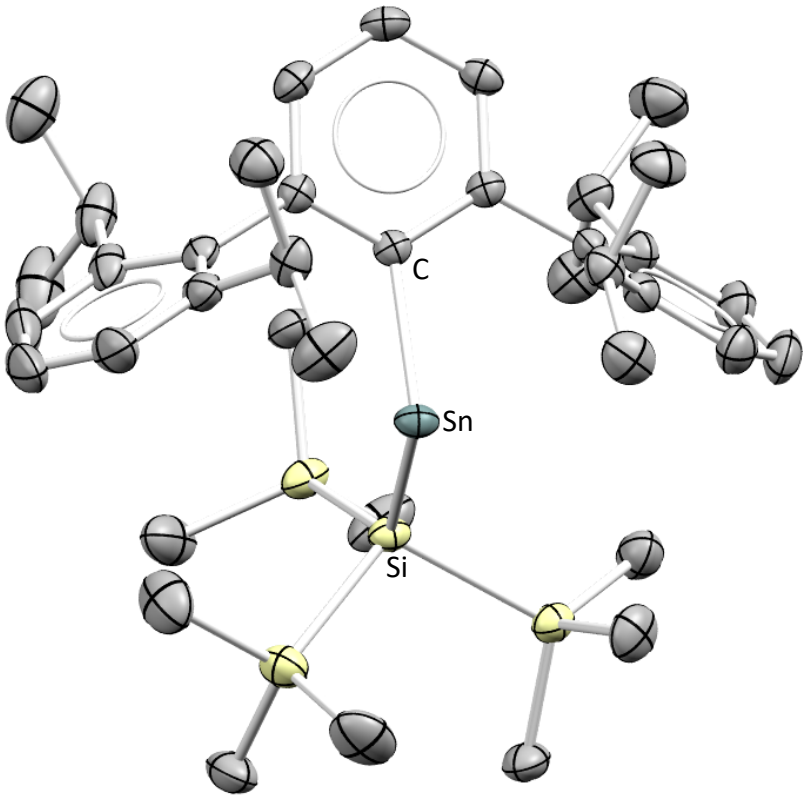


Figure 4-6: Molecular structure of **4.11** as determined by X-ray crystallography. The thermal ellipsoids are set to the 50% probability level. Hydrogen atoms are omitted for clarity. Key bond lengths and angles detailed in Table 4-2.

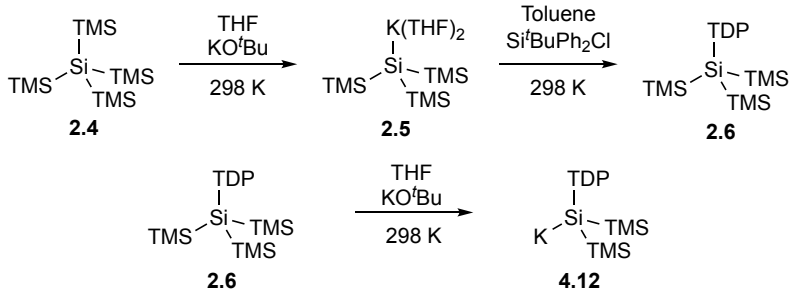
4.2.2 Synthesis of Bis(silyl)metallylenes

Analysis of the literature shows that there are only three crystallographically characterised examples of acyclic bis(silyl)metallylenes.[5,17] Two (one plumbylene and one stannylene) were synthesised by insertion of a silylene into the E–N bonds of the corresponding $E(HMDS)_2$ precursor.[17] The other, a bis(hypersilyl)plumbylene, **1.10**, was synthesised in 1995 by Klinkhammer *et al.*[5] As mentioned above, the synthesis of the tin analogue, **1.8**, was attempted and, while this species is thought to be present in solution, it exists as the corresponding distannene, **1.9**, in the solid state (Figure 1-11). The stability of the corresponding germanium analogue is even lower; it can only be accessed when stabilised by

a Lewis base and, in the absence of a base, forms a disilagermirane (Scheme 1-5).[18,19] Intrigued as to the range of small reactivity that bis(silyl)metallylenes would be capable of, their synthesis was attempted.

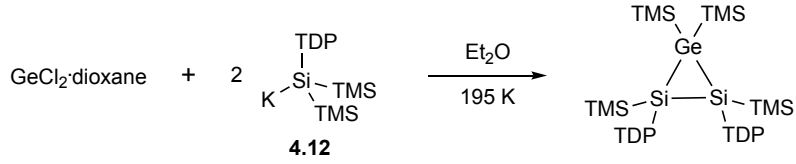
4.2.2.1 Attempted Synthesis of a Bis(silyl)germylene

It was hypothesised that using a different silyl ligand would allow the isolation of a usable bis(silyl)germylene. The silyl-substituent would need to be bulkier than the hypersilyl ligand (-Si(TMS)$_3$), to disfavour the dimerisation of the stannylene, as had been observed by Klinkhammer *et al.* in the formation of distannene **1.9** (Figure 1-11).[5] It was thought that the silyl ligand, -Si(TMS)$_2$(Si^{t}BuPh$_2$), reported by Kunz *et al.,* might be ideal.[20] Substitution of one of the trimethylsilyl groups of the hypersilyl ligand with a [-Si^{t}BuPh$_2$] fragment not only increases the steric bulk of the ligand but also reduces the number of Si–TMS bonds into which the metallylene can insert. This should reduce the likelihood of decomposition of the formed metallylene through migration of -TMS groups, as was observed by Stalke *et al.* in the attempted synthesis of a bis(silyl)germylene (Scheme 1-5), which instead yielded the disilagermirane, **1.21**.[18] The ligand can be synthesised *via* a method adapted from the syntheses reported by Baumgartner *et al.* and Kunz *et al.*[20,21] The tetrasilane precursor, **2.6**, was synthesised in a one-pot reaction from tetrakis(trimethylsilyl)silane, **2.4** (Scheme 4-5). Once isolated, combination with potassium *tert*-butoxide in THF cleanly afforded the potassium silanide, **4.12** (Scheme 4-5).



Scheme 4-5: Top – Synthesis of silane, **2.6**, from tetrakis(trimethylsilyl)silane via a one-pot procedure. Bottom – Synthesis of potassium silanide, **4.12**, from **2.6** (TDP is -Si(^{t}Bu)(Ph)$_2$).

To gauge whether this might be a viable way of synthesising a bis(silyl)germylene, an *in situ* NMR experiment was performed. **4.12** and $GeCl_2$·dioxane were suspended in C_6D_6, mirroring previous attempts to synthesise bis(silyl)germylenes, and an immediate colour change to orange was observed.[18,19] Through analysis of the reaction mixture by ^{1}H NMR spectroscopy, it was possible to see that a reaction had occurred, however the exact nature of the process is unclear due to the complex array of overlapping peaks present in the spectrum. The reaction was attempted at 195 K with diethyl ether as the solvent in an attempt to reduce the complexity of the ^{1}H NMR data. However, no change in reactivity was seen, with the same orange solution forming at 195 K and studies of the reaction mixture by *in situ* ^{1}H NMR spectroscopy still showing a complex mixture of products. It is proposed that, as with the bis(hypersilyl)germylene, $Ge(Si(TMS)_3)_2$, the formation of a disilagermirane could also occur for the bulkier germylene. Attempts to isolate single crystals of the product(s) of this reaction *via* slow evaporation or by storage of concentrated solutions at 243 K yielded nothing, presumably due to the high solubility of these systems.

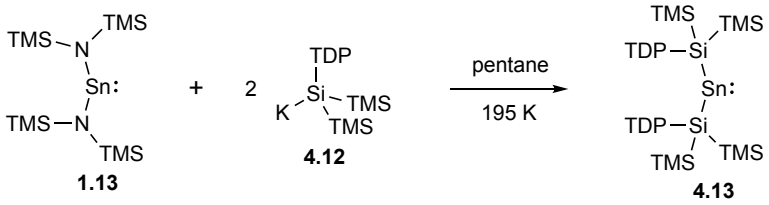


Scheme 4-6: Proposed formation of a disilagermirane from the attempted synthesis of a bis(silyl)germylene.

The synthesis of the bis(silyl)germylene was also attempted using $Ge(HMDS)_2$ as the precursor because the tin and lead analogues had previously been used in the synthesis of bis(silyl)metallylenes.[5] However, combination of the **4.12** with $Ge(HMDS)_2$ afforded no reaction, despite forcing conditions being employed (elevated temperatures). This lack of reactivity was postulated to be due to the Ge–N bond of $Ge(HMDS)_2$ being stronger than the Sn–N and Pb–N bonds of its heavier analogues, thereby presenting a more significant kinetic barrier to reaction.

4.2.2.2 Synthesis of a Bis(silyl)stannylene

As the synthesis of a bis(silyl)stannylene (in solution at least) had already been achieved by Klinkhammer *et al.*, this synthetic route was followed in initial studies to assess the feasibility of the method.[5] The addition of a solution of **1.13** to a suspension of **4.12** at 195 K leads to the immediate formation of a lime green suspension (Scheme 4-7). As the reaction mixture was warmed to 273 K, the suspension changed colour to dark red/brown. Similar observations were reported by Klinkhammer *et al.*, however no explanation was offered as to what causes the colour change.[5] From this suspension, the crude product could be isolated following filtration and removal of volatiles *in vacuo*. Analysis of the crude product by ^{1}H NMR spectroscopy suggested the formation of the target stannylene, or the corresponding distannene, on the basis of one set of ligand resonances (e.g. one ^{t}Bu resonance at 0.86 ppm and one TMS resonance at 0.20 ppm) in the ^{1}H spectrum. After re-extraction of the residue into pentane at 195 K, followed by filtration, the product could be isolated as dark red crystals suitable for X-ray crystallography, which allowed the connectivity of the product **4.13** to be confirmed.



Scheme 4-7: Synthesis of a bis(silyl)stannylene, **4.13**, from $Sn(HMDS)_2$ and potassium silanide, **4.12**.

The molecular structure of **4.13** is depicted in Figure 4-7; key geometric parameters of **4.13**, as well as some pertinent literature comparisons, are detailed in Table 4-3.[3,9] Unlike the bis(hypersilyl)stannylene reported by Klinkhammer *et al.*, **4.13** exists as the free stannylene in both solution and the solid state (closest Sn–Sn distance: 10.4 Å), highlighting the importance of steric bulk in preventing dimerisation.[5] Indeed, the bulk of the silyl ligand can also be seen in the angle adopted at the tin centre, which is much wider than that of the bis(aryl)stannylene, **1.5** (reported by Power *et al.*), even despite the longer Sn–X bonds.[3] The wide angle adopted at the metal centre, combined with the strong σ-donating silyl substituents, suggest that the HOMO–LUMO gap of **4.13** should be narrow. However, efforts to gauge this by ^{119}Sn NMR spectroscopy have proved futile, even when conducting the measurement at 195 K with the aim of sharpening the resonance. In addition, analysis by UV/Vis shows a λ_{max} of 425 nm, significantly lower than would be expected considering the angle at the metal centre, potentially suggesting some ligand effects affecting the transition.[3]

Table 4-3: Selected bond lengths (Å) and angles (°) for **4.13**, **1.31**, and **1.5**.[3,9]

	Sn–X1	**Sn–X2**	**X1–Sn–X2**
4.13	2.6590(8)	2.6463(8)	121.71(3)
1.31[9] ($Sn(BNDippCH)_2)_2$)	2.285(8)	2.294(8)	118.8(3)
1.5[3] ($Sn(Ar^{Mes})_2$)	2.225(5)	2.225(5)	114.7(2)

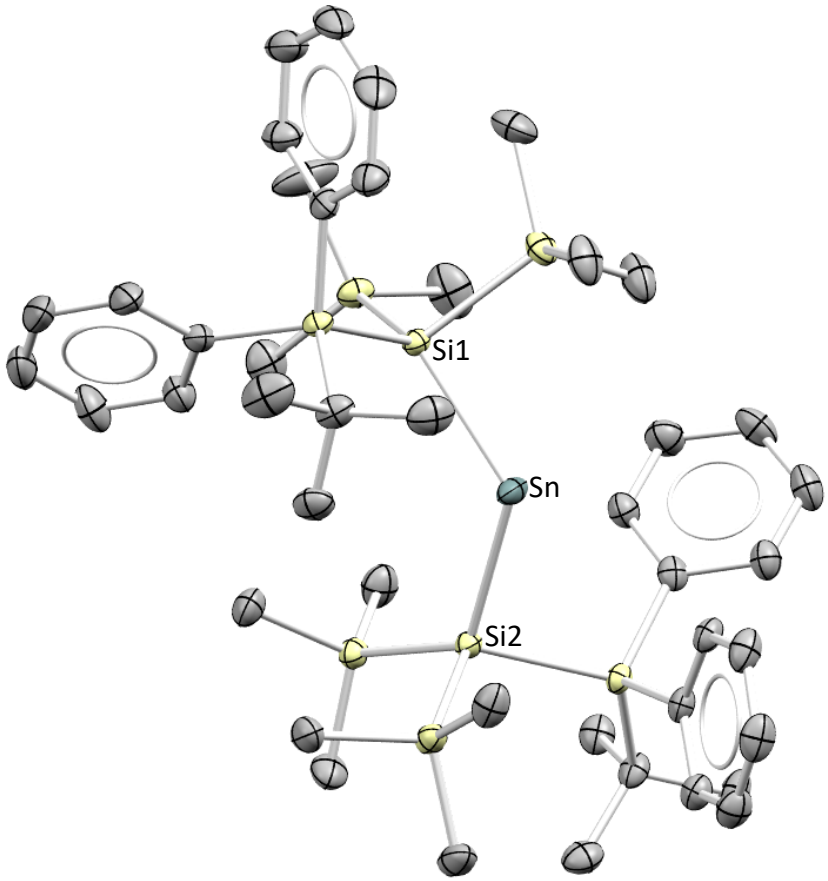
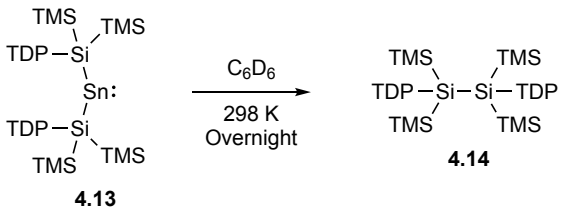


Figure 4-7: Molecular structure of **4.13** as determined by X-ray crystallography. The thermal ellipsoids are set to the 50% probability level. Hydrogen atoms are omitted for clarity. Key bond lengths and angles detailed in Table 4-3.

4.13 is not stable in solution at room temperature. This is evidenced by the formation of a tin mirror on the surfaces of vessels at ambient temperatures for prolonged periods (overnight or longer). This instability is not seen in the solid state, as illustrated by the fact that crystalline samples of **4.13** which were left for months (in an inert atmosphere glovebox) appear unchanged when investigated by solution-phase NMR spectroscopy. When **4.13** decomposes in solution, the formation of the tin mirror is accompanied by the slow decolourisation of the solution. Investigation of the new species formed by ^{1}H NMR spectroscopy shows the formation of a new set of ligand resonances (e.g. one ^{t}Bu resonance at 1.30 ppm and one TMS resonance at 0.35 ppm). As one product is apparently elemental tin, it is conceivable that the symmetrical pattern of resonances in the ^{1}H NMR spectrum belong to the product of a reductive elimination process, *i.e.* two silyl ligands coupled together. From this colourless solution, crystals suitable for X-ray diffraction could be grown, which allowed the connectivity of **4.14** to be confirmed.



Scheme 4-8: Reductive elimination of disilane, **4.14**, from bis(silyl)stannylene, **4.13**.

The molecular structure of **4.14** is shown below (Figure 4-8). Unfortunately, the X-ray diffraction data obtained is not of sufficient quality to discuss the geometrical parameters of **4.14**. However, it does confirm that **4.13** decays in solution, by reductive elimination, to yield elemental tin and the sterically encumbered hexasilyl-disilane, **4.14**.

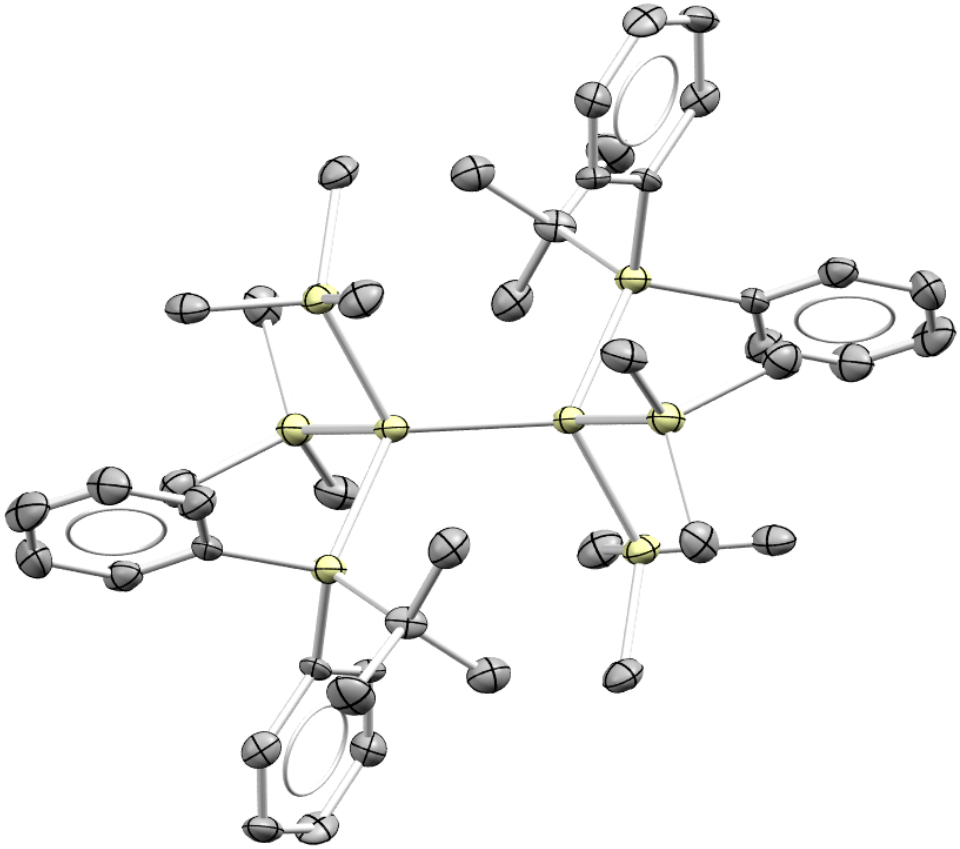
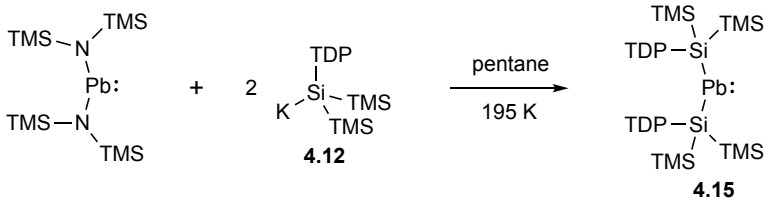


Figure 4-8: Molecular structure of **4.14** as determined by X-ray crystallography. The thermal ellipsoids are set at the 50% probability level. Hydrogen atoms are omitted for clarity. Data of insufficient quality to discuss the geometric parameters of **4.14**.

4.2.2.3 Synthesis of a Bis(silyl)plumbylene

As Klinkhammer *et al.* had already disclosed the synthesis of a bis(silyl)plumbylene, the attempts to synthesise the plumbylene analogue of **4.13** were based considerably on their method.[5] Analogous to the synthesis of **4.13**, a solution of $Pb(HMDS)_2$ in pentane was added to a stirred suspension of **4.12** in pentane at 195 K (Scheme 4-9). An orange suspension is formed immediately. As the suspension is warmed to 273 K, a colour change to dark red is observed. The crude product can be accessed from this solution by removal of the volatiles *in vacuo*, and analysis of the residue by ^{1}H NMR spectroscopy shows the formation of a new set of ligand resonances (e.g. ^{t}Bu resonance at 0.98 ppm, TMS resonance at 0.36 ppm) suggesting

that the desired plumbylene has been formed. Re-extraction of the crude product into pentane at 195 K, and subsequent crystallisation from this solution, was found to be essential to access the product cleanly. Crystals of **4.15** suitable for X-ray crystallography could be grown in this manner and allow confirmation of the connectivity of the product **4.15**.



Scheme 4-9: Synthesis of bis(silyl)plumbylene, **4.15**, from $Pb(HMDS)_2$.

The molecular structure of **4.15** is shown below (Figure 4-9) and key geometric parameters for **4.15** and **1.10** are detailed in Table 4-4.[5] Comparison of the structures of **4.15** and **4.13** shows the change in bonding as group 14 is descended, with a lengthening of the E–Si bonds (2.722(1) and 2.737(1) Å *vs.* 2.6590(8) and 2.6463(8) Å respectively). However, since the lengthening is small, the angle at the metallylene centre remains similar between the two metallylenes (121.61(3)° *vs.* 121.71(3)° respectively). Insight into the differences between the hypersilyl ligand (-$Si(TMS)_3$) and the bulkier silyl ligand (-$Si(TMS)_2(SiPh_2{}^tBu)$) can be seen by comparing **4.15** with **1.10**. Not only are the Pb–Si bonds longer in **4.15**, but a significant widening is seen at the metal centre (**4.15**: 121.61(3)°, **1.10**: 113.56(10)°), indicating the greater steric bulk of the new silyl ligand compared to its hypersilyl counterpart.

Table 4-4: Selected bond lengths (Å) and angles (°) for **4.15** and **1.10**.[5]

	Pb–Si1	**Pb–Si2**	**Si1–Pb–Si2**
4.15	2.722(1)	2.737(1)	121.61(3)
1.10[5] ($Pb(SiTMS_3)_2$)	2.700(3)	2.704(3)	113.56(10)

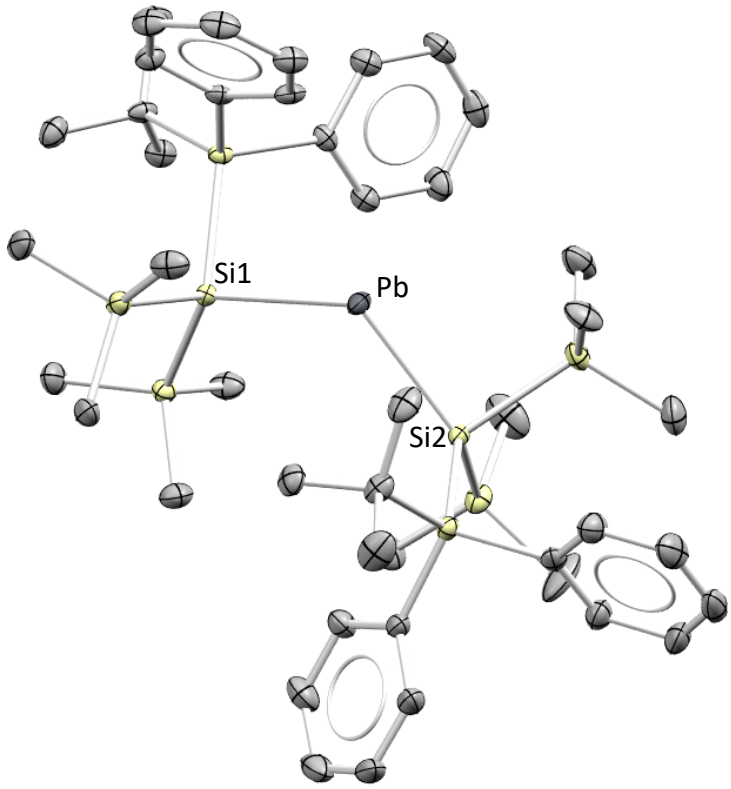
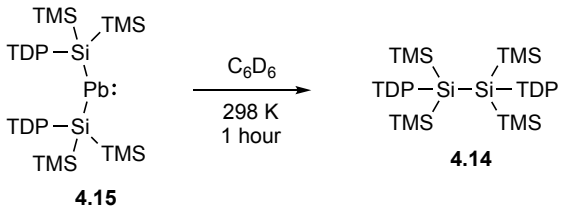


Figure 4-9: Molecular structure of **4.15** as determined by X-ray crystallography. The thermal ellipsoids are set at the 50% probability level. Hydrogen atoms are omitted for clarity. Key bond lengths and angles detailed in Table 4-4.

As with **4.13**, **4.15** is unstable in solution at ambient temperature. In fact, **4.15** is less stable than **4.13**, as evidenced by the formation of a lead mirror after *circa* 1 h when **4.15** is stored

at ambient temperature as a solution in benzene or hexane. The same phenomenon was observed by Lappert *et al.* when they demonstrated that their bis(silyl)plumbylene, **4.17** (Figure 4-10), was less stable in solution than the tin analogue, **4.16** (Figure 4-10).[17] Additionally, it was reported that **4.17** was unstable in the solid state, however this was not observed with **4.15**.[17]



Scheme 4-10: Reductive elimination of disilane, **4.14**, from bis(silyl)plumbylene, **4.15**.

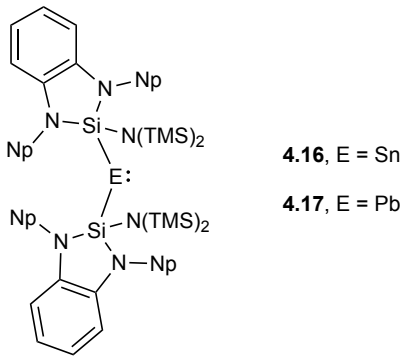
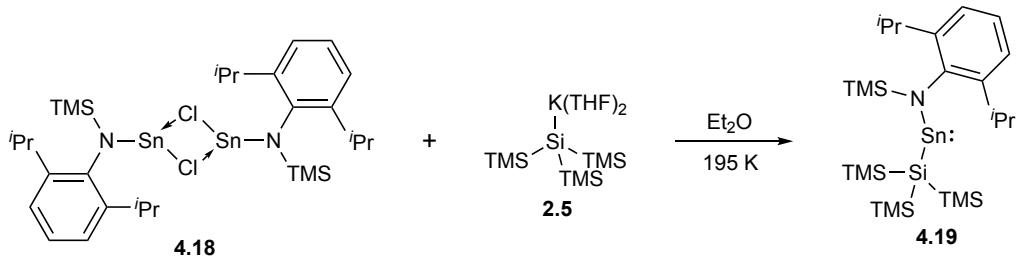


Figure 4-10: Bis(silyl)stannylene, **4.16**, and bis(silyl)plumbylene, **4.17**, synthesised by Lappert et al. (Np is $-CH_2{}^tBu$).[17]

4.2.3 Synthesis of Amido(silyl)stannylenes

The amido(silyl)silylene, $Si(N(Dipp)(TMS)(Si(TMS)_3)$, reported by Protchenko *et al.* is the first and only example of an acyclic amido(silyl)metallylene in the literature.[22] It was hypothesised that an amido(silyl)stannylene would act as a good point of comparison to **4.10**, **4.11**, and **4.13**. The synthesis of the stannylene analogue, $Sn(N(Dipp)(TMS)(Si(TMS)_3)$, of the silylene reported by Protchenko *et al.* was therefore attempted.[22]

The precursor, chloride bridged Sn(II) species $[Sn(N(Dipp)(TMS))Cl]_2$, **4.18**, was straightforwardly synthesised *via* literature procedures.[23–25] An initial trial experiment was carried out in a J-Youngs NMR tube with deuterated solvent so that the composition of the reaction mixture could be investigated by ^1H NMR spectroscopy. Upon addition of C_6D_6 to a solid mixture of the two precursors, an immediate colour change to black was seen and *in situ* NMR measurements showed a complex mixture of products. It was thought that the product could be temperature sensitive, so the reaction was performed at lower temperatures. Dropwise addition of a diethyl ether solution of **2.5** to a suspension of the Sn(II) precursor, **4.18**, in diethyl ether at 195 K resulted in the immediate formation of an orange suspension (Scheme 4-11). This colour persisted while the reaction mixture was kept at 195 K, however on warming to 273 K a colour change to green was observed. Volatiles were removed *in vacuo,* and the residue extracted into pentane. It was observed that any solution above the level of the ice bath slowly turned brown. The reason for this decomposition is unknown, however it highlights the importance of maintaining low temperatures throughout the course of the reaction. From the pentane solution, blue crystals suitable for X-ray crystallography could be grown which allowed the connectivity of the product, **4.19**, to be determined.



Scheme 4-11: Synthesis of amido(silyl)stannylene, **4.19**.

The molecular structure of **4.19** is depicted in Figure 4-11. The key geometric parameters of **4.19**, and the related amido(boryl)stannylene, **1.61**, reported by Protchenko *et al.* are detailed

in Table 4-5.[9] The Sn–N bond lengths of the two amidostannylenes are in good agreement. However, the angle at the tin centre is wider for **4.19**, presumably reflecting the greater steric bulk of the hypersilyl ligand. Unfortunately, despite repeated attempts, analysis of **4.19** by ^{119}Sn NMR spectroscopy did not yield a detectable resonance, potentially due to excessive broadness. However, it could also be due to the instability of **4.19**, as demonstrated by the colour changes shown at temperatures above 273 K.

Table 4-5: Selected bond lengths (Å) and angles (°) for **4.19** and **1.61**.[9]

	Sn–B/Si	**Sn–N**	**B/Si–Sn–N**
4.19	2.652(1)	2.067(3)	112.7(1)
1.61[9](Sn(BNDippCH)$_2$(N(Dipp)(TMS)))	2.335(5)	2.069(3)	106.7(2)

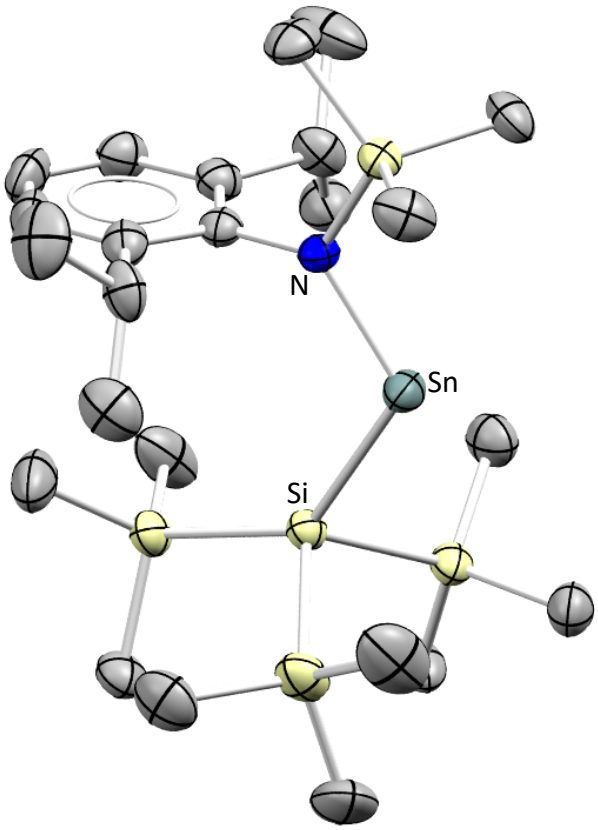
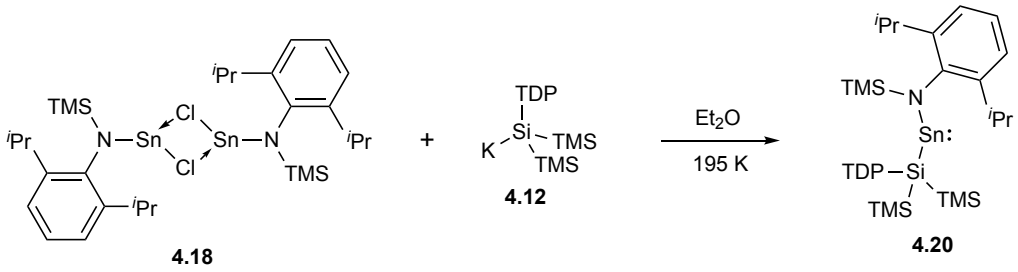


Figure 4-11: Molecular structure of **4.19** as determined by X-ray crystallography. The thermal ellipsoids are set at the 50% probability level. Hydrogen atoms are omitted for clarity. Key bond lengths and angles are detailed in Table 4-5.

As **4.19** is thermally unstable, attempts to synthesise an amido(silyl)stannylene with a bulkier silyl ligand were undertaken. When a diethyl ether solution of **4.12** is added dropwise to a solution of **4.18** in diethyl ether at 195 K, a dark orange suspension is formed. The colour of solution persists at this low temperature, however as the reaction mixture is warmed up to 273 K it is accompanied by a colour change in the suspension to dark red/purple. The volatiles were removed from this solution *in vacuo* and the residue was analysed by ^{1}H NMR spectroscopy. The spectrum showed the formation of one major species which had a ratio of intensities of amido:silyl resonances of 1:1, suggesting the formation of the desired stannylene, **4.20**. This product also appeared to be stable at elevated temperatures given that

heating the NMR sample at 353 K overnight had no visible effect on the solution or the resonances observed in the ^{1}H NMR spectrum. Unfortunately, crystals suitable for X-ray crystallography could not be obtained for this species, due to the high solubility of **4.20** in the solvents used (benzene, and pentane).



Scheme 4-12: Synthesis of amido(silyl)stannylene, **4.20**.

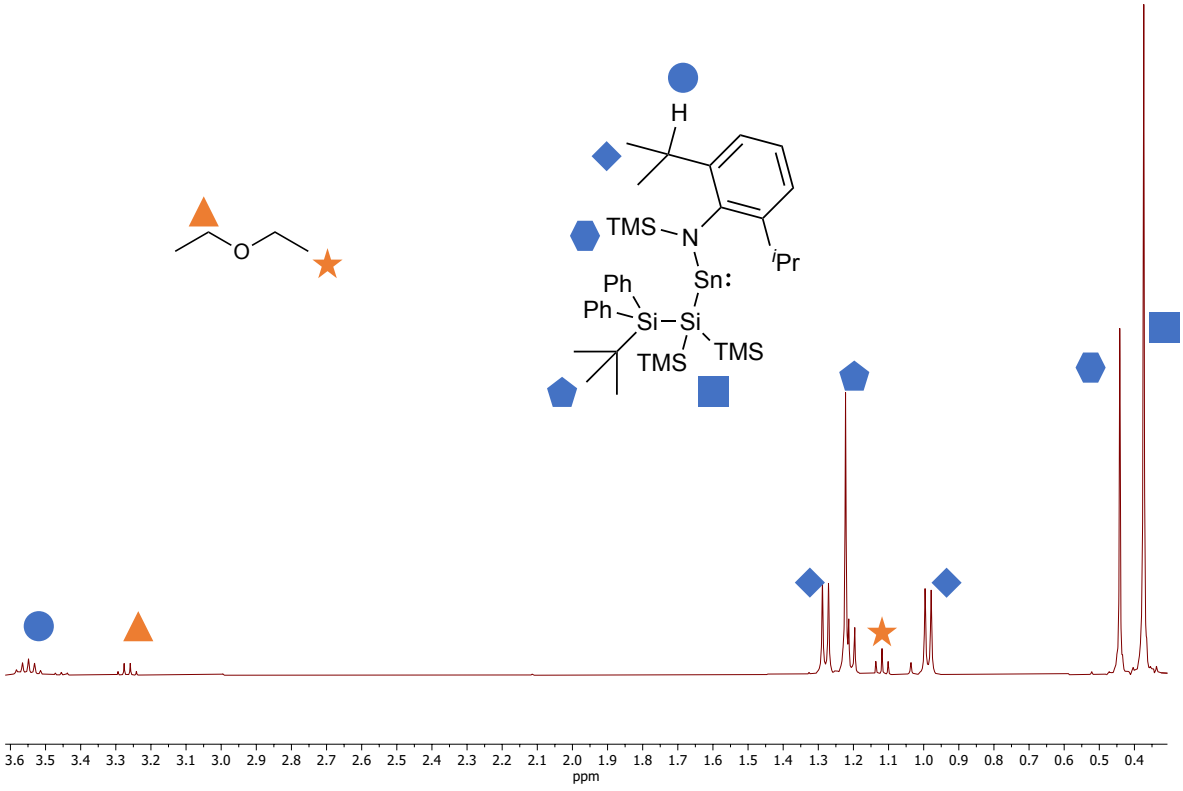


Figure 4-12: Excerpt from the ^{1}H NMR spectrum of **4.20** in C_6D_6, diagnostic resonances are highlighted.

4.3 Conclusions

In this chapter, the synthesis of several novel metallylenes are reported. The aryl(amido)stannylenes, **4.8** (Sn(Ar^{Mes})(HMDS)) and **4.9** (Sn(Ar^{Dipp})(HMDS) have been synthesised (Scheme 4-3) and compared to the known aryl(amido)stannylene, **4.1** (Sn(Ar^{Tripp})(HMDS).[4] **4.1** was found to have a wider angle at the tin centre in the solid state than **4.8** or **4.9** (108.4(2)°, 103.6(1)°, and 107.3(2)° respectively), due to the greater bulk of the aryl ligand. This appears to have a negligible effect on the electronic structure of the stannylenes, however as evidenced by the similar values of the ^{119}Sn NMR resonances of **4.1** and **4.8** (1197 ppm and 1193 ppm respectively).[4] The aryl(silyl)stannylenes, **4.10** (Sn(Ar^{Mes})($Si(TMS)_3$)) and **4.11** (Sn(Ar^{Dipp})($Si(TMS)_3$)), were also synthesised (Scheme 4-4) and compared with the aryl(silyl)stannylene, **1.11** (Sn(Ar^{Mes})($Si(^tBu)_3$)).[12] The ^{119}Sn NMR chemical shifts of **4.10**, **4.11**, and **1.10** are very different (2793 ppm, 2834 ppm, and 197 ppm respectively), however this is likely a solvent effect (**4.10** and **4.11** measured in C_6D_6, **1.11** measured in THF-d_8).[12] The synthesis of a series of bis(silyl)metallylenes was also attempted. Combination of the potassium silanide, **4.12** ($KSi(TMS)_2(Si^tBuPh_2)$), with $GeCl_2$·dioxane in diethyl ether resulted in a complex mixture of products. The corresponding stannylene, **4.13** ($Sn(Si(TMS)_2(Si^tBuPh_2))_2$) however, could be prepared (Scheme 4-7) and was found to have a very wide angle at the metal centre in the solid state (127.71(3)°) by single crystal X-ray crystallography. The plumbylene, **4.15** ($Pb(Si(TMS)_2(Si^tBuPh_2))_2$), was also synthesised (Scheme 4-9) and compared to the bis(silyl)plumbylene, **1.10** ($Pb(Si(TMS)_3)_2$). **4.15** was found to have a significantly wider angle at the lead centre than **1.10** (121.61(3)° and 113.56(10)° respectively), reflecting the greater steric bulk of the silyl ligand of 4.15 (-$Si(TMS)_2(Si^tBuPh_2)$

vs. -Si(TMS)$_3$). Finally, the aryl(amido)stannylene, **4.19** (Sn(N(Dipp)(TMS))(Si(TMS)$_3$)), was synthesised (Scheme 4-11) and is the first example of an acylic amido(silyl)stannylene.

4.4 Characterisation of Novel Materials

4.4.1 Synthesis of SnAr^{Mes}HMDS, **4.8** (Scheme 4-3)

2.2 (1.0 g, 3.1 mmol) and **1.13** (1.4 g, 3.1 mmol) were combined in a Schlenk flask and toluene (30 mL) added at room temperature. The resulting mixture was allowed to stir for 12 h at room temperature and then filtered. The filtrate was concentrated *in vacuo* to incipient crystallisation and stored at 243 K to afford the product as a red solid. A second crop of the product could be obtained by concentrating the mother liquor *in vacuo* to incipient crystallisation and storing at 243 K. Overall yield: 1.4 g, 75 %. ^{1}H NMR (400 MHz, C_6D_6, 298K) δ: 7.25 (t, *p*-C*H* Ar^{Mes}, $^3J_{HH}$ = 7.6 Hz, 1H), 7.04 (d, *m*-C*H* Ar^{Mes}, $^3J_{HH}$ = 7.5 Hz, 2H), 6.83 (s, Mes-C*H*, 4H), 2.32 (s, Mes-C*H$_3$*, 12H), 2.15 (s, Mes-C*H$_3$*, 6H), -0.02 (s, N(SiC*H$_3$*)$_2$, 18H) ppm. ^{13}C NMR (101 MHz, C_6D_6) δ: 184.5, 146.1, 137.8, 137.2, 136.8, 130.4, 129.9, 127.8, 22.1, 21.0, 6.1 ppm (as reported by Fischer *et al.*).[26] ^{29}Si NMR (99 MHz, C_6D_6, 298 K) δ: -0.8 ppm. ^{119}Sn NMR (187 MHz, C_6D_6, 298 K) δ: 1192.6 ppm. EA: Anal. Calcd. For $C_{30}H_{43}NSi_2Sn$: C, 60.81; H, 7.31; N, 2.36; found: C, 60.91; H, 7.27; N,2.34.

4.4.2 Synthesis of SnAr^{Dipp}HMDS, **4.9** (Scheme 4-3)

4.5 (1.0 g, 2.5 mmol) and **1.13** (1.1 g, 2.5 mmol) were combined as solids, toluene (50 mL) added, and the reaction mixture stirred for 12 h at room temperature. The resulting red suspension was filtered, and volatiles then removed *in vacuo.* The residue was extracted into pentane (30 mL) and filtered. The filtrate was concentrated to incipient crystallisation and stored at 243 K to afford the product as a red solid. A second crop of the product could be

obtained by concentrating the mother liquor *in vacuo* to incipient crystallisation and storing at 243 K. Overall yield: 1.3 g, 78%. NMR data as reported by Fischer *et al.*[26] ^{1}H NMR (400 MHz, C_6D_6, 298K) δ: 7.34–7.32 (m, Ar*H*, 2H), 7.26–7.23 (m, Ar*H*, 3H), 7.20–7.18 (m, Ar*H*, 4H), 3.28 (sept, ^{i}Pr-*H*, $^{3}J_{HH}$ = 6.8 Hz, 4H), 1.38 (d, ^{i}Pr-C*H*$_3$, $^{3}J_{HH}$ = 6.8 Hz, 12H), 1.06 (d, ^{i}Pr-C*H*$_3$, $^{3}J_{HH}$ = 6.7 Hz, 12H), 0.02 (s, N(SiC*H*$_3$)$_2$, 18H) ppm. ^{13}C NMR (101 MHz, C_6D_6) δ: 185.3, 147.6, 144.8, 137.4, 131.6, 129.5, 126.8, 124.2, 31.3, 27.1, 23.0, 6.2 ppm. EA: Anal. calcd. For $C_{30}H_{43}NSi_2Sn$: C, 63.90; H, 8.19; N, 2.07; found: C, 61.06; H, 8.23; N, 2.56.

4.4.3 Synthesis of $SnAr^{Mes}Si(TMS)_3$, **4.10** (Scheme 4-4)

4.8 (0.50 g, 0.84 mmol) and **2.5** (0.24 g, 0.84 mmol) were combined as solids, toluene (30 mL) added, and the reaction mixture stirred at room temperature for 12 h. The resulting dark green suspension was filtered, and the filtrate concentrated *in vacuo* to incipient crystallisation. Storage at 243 K afforded the product as a blue crystalline solid. A second crop of the product could be obtained by concentrating the mother liquor *in vacuo* to incipient crystallisation and storing at 243 K. Overall yield: 0.50 g, 87%. ^{1}H NMR (400 MHz, C_6D_6, 298 K) δ: 7.36 (t, *p*-C*H* Ar^{Mes}, $^{3}J_{HH}$ = 7.5 Hz, 1H), 7.05 (d, *m*-C*H* Ar^{Mes}, $^{3}J_{HH}$ = 7.5 Hz, 2H), 6.82 (br. s, Mes-C*H*, 2H), 6.65–6.64 (br. s, Mes-C*H*, 2H), 2.41–2.37 (m, Mes-C*H*$_3$, 12H), 2.11 (s, Mes-C*H*$_3$, 6H) 0.21 (s, Si(SiC*H*$_3$)$_3$, 27H) ppm. ^{13}C NMR (101 MHz, C_6D_6) δ: 179.2, 146.0, 137.8, 136.4, 130.2, 129.6, 129.5, 128.7, 22.2, 21.2, 4.7 ppm (as reported by Fischer *et al.*).[27] ^{29}Si NMR (99 MHz, C_6D_6, 298 K) δ: -4.5, -39.7 ppm (as reported by Fischer *et al.*).[27] ^{119}Sn NMR (187 MHz, C_6D_6, 298 K) δ: 2793.1 ppm. EA Anal. calcd. for $C_{33}H_{52}Si_4Sn$: C, 58.30; H, 7.71; found: C, 57.81; H, 7.82.

4.4.4 Synthesis of $SnAr^{Dipp}Si(TMS)_3$, **4.11** (Scheme 4-4)

4.9 (140 mg, 0.20 mmol) and **2.5** (58 mg, 0.20 mmol) were combined in a Schlenk flask and pentane (3 mL) added at room temperature. The reaction mixture was stirred for 12 h at room temperature. After filtration, volatiles were removed *in vacuo*. The residue was extracted into pentane at 195 K (3 x 2 mL), and the solution concentrated to incipient crystallisation and stored at 243 K to yield the product as blue crystals suitable for X-ray crystallography. Yield: 110 mg, 74%. ^{1}H NMR (500 MHz, C_6D_6, 298 K) δ: 7.34–7.31 (m, Ar*H*, 1H), 7.26–7.24(m, Ar*H*, 2H), 7.20(t, *p*-C*H* Dipp, $^3J_{HH}$ = 7.6 Hz, 2H), 7.08 (d, *m*-C*H* Dipp, $^3J_{HH}$ = 7.6 Hz, 4 H), 3.34 (sept, ^{i}Pr-*H*, $^3J_{HH}$ = 6.9 Hz, 4H), 1.35 (d, ^{i}Pr-C*H*$_3$, $^3J_{HH}$ = 6.9 Hz, 12H), 1.09 (d, ^{i}Pr-C*H*$_3$, $^3J_{HH}$ = 6.7 Hz, 12H), 0.22 (s, Si(SiC*H*$_3$)$_3$, 27H) ppm. ^{13}C NMR (126 MHz, C_6D_6, 298 K) δ: 183.3, 146.8, 144.5, 136.1, 130.9, 129.1, 128.0, 126.7, 124.0, 30.8, 26.0, 24.8, 5.4, 5.2, 5.0, 4.9 ppm. ^{29}Si NMR (99 MHz, C_6D_6, 298 K) δ: -4.1, -30.4 ppm. ^{119}Sn NMR (187 MHz, C_6D_6, 298 K) δ: 2834.0 ppm. EA Anal. calcd. for $C_{39}H_{64}Si_4Sn$: C, 61.31; H, 8.44; found: C, 58.64; H, 7.24.

4.4.5 Synthesis of $Sn(Si(TMS)_2(Si^tBuPh_2))_2$, **4.13** (Scheme 4-7)

To a stirred suspension of **4.12** (2.4 g, 4.6 mmol) in pentane (50 mL) at 195 K was added dropwise a solution of **1.13** (1.0 g, 2.3 mmol) also in pentane (50 mL). After addition, the reaction was stirred at 195 K for 1 h to yield a green suspension. The reaction mixture was then allowed to warm to 273 K and filtered. Volatiles from the filtrate were removed *in vacuo*, and the residue extracted into pentane at 195 K. The resulting brown suspension was removed by filtration, and the filtrate concentrated to incipient crystallisation and stored at 243 K to afford the product as a dark red crystalline solid. Yield: 0.42 g, 19.2%. ^{1}H NMR (500 MHz, C_6D_6, 298 K) δ: 7.71–7.66 (m, Ar*H*, 8 H), 7.07–6.94 (m, Ar*H*, 12H), 0.86 (s, ^{t}Bu-*H*, 18H), 0.20 (s, Si(SiC*H*$_3$)$_3$, 36H) ppm. ^{13}C NMR (126 MHz, C_6D_6, 298 K) δ: 136.5, 136.3, 134.6, 134.4,

127.2, 127.0, 126.1, 125.7, 125.3, 27.4, 26.9, 20.5, 18.8, 12.0, 5.0, 3.1 ppm. ^{29}Si NMR (99 MHz, C_6D_6, 298 K) δ: 10.4, -3.3, -46.0 ppm. EA Anal. calcd. for $C_{44}H_{74}Si_8Sn$: C, 55.84; H, 7.88; found: C, 54.26; H, 7.62.

4.4.6 Synthesis of $Pb(Si(TMS)_2(Si^tBuPh_2))_2$, **4.15** (Scheme 4-9)

To a stirred suspension of **4.12** (50 mg, 0.11 mmol) in pentane (5.0 mL) at 195 K was added dropwise a solution of $Pb(HMDS)_2$ (29 mg, 0.055 mmol) also in pentane (10 mL). After addition, the reaction mixture was stirred at 195 K for 1 h to yield an orange suspension. The reaction mixture was allowed to warm to 273 K and then filtered. Volatiles were removed *in vacuo*, and the residue extracted into pentane at 195 K. The resulting red suspension was filtered, and the filtrate concentrated to incipient crystallisation, and stored at 243 K to afford the product as a dark red crystalline solid. Due to the instability of **4.15** in solution it could only be characterised by ^{1}H NMR spectroscopy. Yield: 8.5 mg, 15%. ^{1}H NMR (400 MHz, C_6D_6, 298 K) δ: 7.64–7.57 (m, Ar*H*, 8H), 7.11–6.96 (m, Ar*H*, 12H), 0.98 (s, ^{t}Bu-*H*, 18H), 0.36 (s, $Si(SiC\mathit{H}_3)_3)_3$, 36H) ppm.

4.4.7 Synthesis of $Sn(N(Dipp)(TMS))Si(TMS)_3$, **4.19** (Scheme 4-11)

A solution of **2.5** (160 mg, 0.55 mmol) in benzene (3.0 mL) was added dropwise to a suspension of **4.18** (220 mg, 0.28 mmol) also in benzene (2.0 mL) at room temperature. The reaction mixture was stirred for 5 min before volatiles were removed *in vacuo.* The residue was extracted into pentane at 195 K and the resulting suspension was removed by filtration. The filtrate was concentrated to incipient crystallisation and stored at 243 K to afford the product as blue crystals suitable for X-ray crystallography. To isolate the product cleanly, these crystals were washed with HMDSO at 195 K. Yield: 61 mg, 50%. ^{1}H NMR (400 MHz, C_6D_6,

298 K) δ: 7.15–7.12 (m, Ar*H*, 2H), 7.05–7.00 (m, Ar*H*, 1H), 3.60 (sept, ^{i}Pr-*H*, $^{3}J_{HH}$ = 6.9 Hz, 2H), 1.26 (d, ^{i}Pr-C*H*$_3$, $^{3}J_{HH}$ = 6.9 Hz, 6H), 1.11 (d, ^{i}Pr-C*H*$_3$, $^{3}J_{HH}$ = 6.9 Hz, 6H), 0.38 (s, Si(C*H*$_3$)$_3$, 27H) ppm. ^{13}C NMR (126 MHz, C_6D_6, 298 K) δ: 150.9, 146.9, 143.3, 127.7, 124.4, 123.9, 123.5, 122.9, 27.7, 27.3, 26.3, 25.4, 23.4, 23.2, 4.7, 4.5, 4.4, 4.3, 4.3, 3.5 ppm. ^{29}Si NMR (99 MHz, C_6D_6, 298 K) δ: 6.4, 2.4, -5.0, -42.1 ppm.

4.4.8 Reaction of [Sn(N(Dipp)(TMS))Cl]$_2$ with KSi(TMS)$_2$(Si^{t}BuPh$_2$) (Scheme 4-12)

A solution of **4.12** (65 mg, 0.12 mmol) in diethyl ether (1.0 mL) was added dropwise to a solution of **4.18** (50 mg, 0.062 mmol) also in diethyl ether (1.0 mL). The reaction mixture was cooled to 195 K and allowed to stir for 1 h. The reaction mixture was then heated to 273 K and the volatiles removed *in vacuo.* The residue was then extracted into C_6D_6 and the product was characterised by ^{1}H NMR spectroscopy. ^{1}H NMR (400 MHz, C_6D_6, 298 K) δ: 7.89–7.83 (m, Ar*H*, 4H), 7.22–7.01 (m, Ar*H*, 9H), 3.55 (sept, ^{i}Pr-*H*, $^{3}J_{HH}$ = 6.8 Hz, 2H), 1.28 (d, ^{i}Pr-C*H*$_3$, $^{3}J_{HH}$ = 6.5 Hz, 6H), 1.22 (s, ^{t}Bu-*H*, 9H), 0.99 (d, ^{i}Pr-C*H*$_3$, $^{3}J_{HH}$ = 6.5 Hz, 6H), 0.44 (s, Si(C*H*$_3$)$_3$, 9H), 0.37 (s, Si(Si(C*H*$_3$)$_3$)$_2$, 18H) ppm.

4.5 References

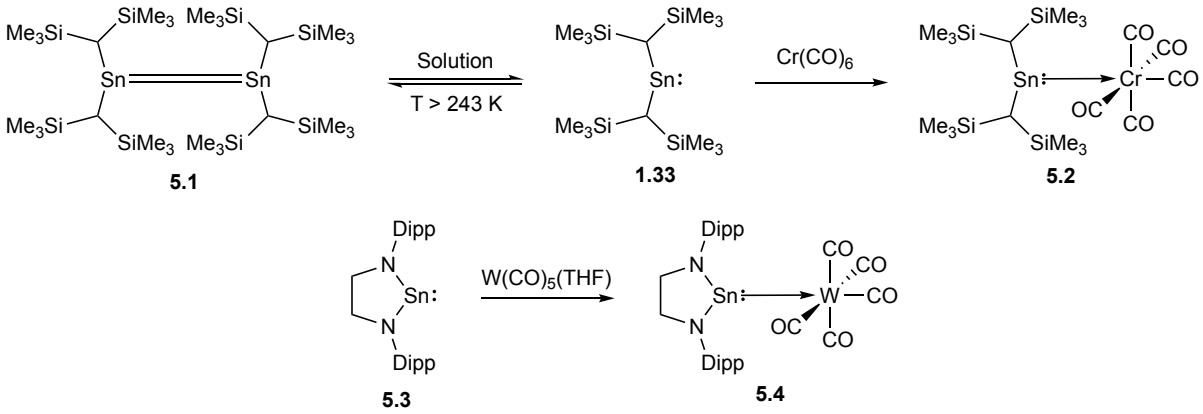
1 A. Jana, I. Objartel, H. W. Roesky and D. Stalke, *Inorg Chem*, 2009, **48**, 798–800.
2 M. Denk, R. Lennon, R. Hayashi, R. West, A. V. Belyakov, H. P. Verne, A. Haaland, M. Wagner and N. Metzler, *J Am Chem Soc*, 1994, **116**, 2691–2692.
3 R. S. Simons, L. Pu, M. M. Olmstead and P. P. Power, *Organometallics*, 1997, **16**, 1920–1925.
4 L. Pu, M. M. Olmstead, P. P. Power and B. Schiemenz, *Organometallics*, 1998, **17**, 5602–5606.
5 K. W. Klinkhammer and W. Schwarz, *Angewandte Chemie International Edition in English*, 1995, **34**, 1334–1336.
6 J. Klett, K. W. Klinkhammer and M. Niemeyer, *Chemistry - A European Journal*, 1999, **5**, 2531–2536.
7 D. Agustin and M. Ehses, *Comptes Rendus. Chimie*, 2009, **12**, 1189–1227.
8 P. Jutzi and R. Dickbreder, *J Organomet Chem*, 1989, **373**, 301–306.
9 A. V. Protchenko, K. H. Birjkumar, D. Dange, A. D. Schwarz, D. Vidovic, C. Jones, N. Kaltsoyannis, P. Mountford and S. Aldridge, *J Am Chem Soc*, 2012, **134**, 6500–6503.
10 P. Wilfling, K. Schittelkopf, M. Flock, R. H. Herber, P. P. Power and R. C. Fischer, *Organometallics*, 2015, **34**, 2222–2232.
11 J. R. Babcock, L. Liable-Sands, A. L. Rheingold and L. R. Sita, *Organometallics*, 1999, **18**, 4437–4441.
12 D. Sarkar, C. Weetman, D. Munz and S. Inoue, *Angewandte Chemie International Edition*, 2021, **60**, 3519–3523.

13 M. Usher, A. V. Protchenko, A. Rit, J. Campos, E. L. Kolychev, R. Tirfoin and S. Aldridge, *Chemistry – A European Journal*, 2016, **22**, 11685–11698.
14 A. J. Valentine, A. M. Geer, L. J. Taylor, A. M. Teale, K. E. Wood, H. E. L. Williams, W. Lewis, S. P. Argent, J. McMaster and D. L. Kays, *Dalton Transactions*, 2021, **50**, 722–728.
15 G. H. Spikes, Y. Peng, J. C. Fettinger and P. P. Power, *Z Anorg Allg Chem*, 2006, **632**, 1005–1010.
16 P. J. Smith and L. Smith, *Inorganica Chimica Acta Reviews*, 1973, **7**, 11–33.
17 B. Gehrhus, P. B. Hitchcock and M. F. Lappert, *Angewandte Chemie International Edition in English*, 1997, **36**, 2514–2516.
18 A. Heine and D. Stalke, *Angewandte Chemie International Edition in English*, 1994, **33**, 113–115.
19 M. Walewska, J. Baumgartner and C. Marschner, *Chemical Communications*, 2014, **51**, 276–278.
20 T. Kunz, O. Şahin and A. Schnepf, *Z Anorg Allg Chem*, 2022, **648**, e202200081.
21 J. Hlina, F. Stella, M. A. Meshgi, C. Marschner and J. Baumgartner, *Molecules 2016, Vol. 21, Page 1079*, 2016, **21**, 1079.
22 A. V Protchenko, A. D. Schwarz, M. P. Blake, C. Jones, N. Kaltsoyannis, P. Mountford, S. Aldridge, A. V Protchenko, A. D. Schwarz, M. P. Blake, P. Mountford, S. Aldridge, N. Kaltsoyannis and C. Jones, *Angewandte Chemie International Edition*, 2013, **52**, 568–571.
23 A. Schulz, A. Villinger and A. Westenkirchner, *Inorg Chem*, 2013, **52**, 11457–11468.
24 M. Á. Fuentes, A. Zabala, A. R. Kennedy and R. E. Mulvey, *Chemistry – A European Journal*, 2016, **22**, 14968–14978.
25 M. Brynda, R. Herber, P. B. Hitchcock, M. F. Lappert, I. Nowik, P. P. Power, A. V. Protchenko, A. Růžička and J. Steiner, *Angewandte Chemie International Edition*, 2006, **45**, 4333–4337.
26 M. Fischer, M. M. D. Roy, L. L. Wales, M. A. Ellwanger, A. Heilmann and S. Aldridge, *J Am Chem Soc*, 2022, **144**, 8908–8913.
27 M. Fischer, M. M. D. Roy, Lewis. L. Wales, M. A. Ellwanger, C. McManus, A. F. Roper, A. Heilmann and S. Aldridge, *Angewandte Chemie International Edition*, 2022, **61**, e202211616.

5 Small Molecule Reactivity of Novel Stannylenes

5.1 Introduction

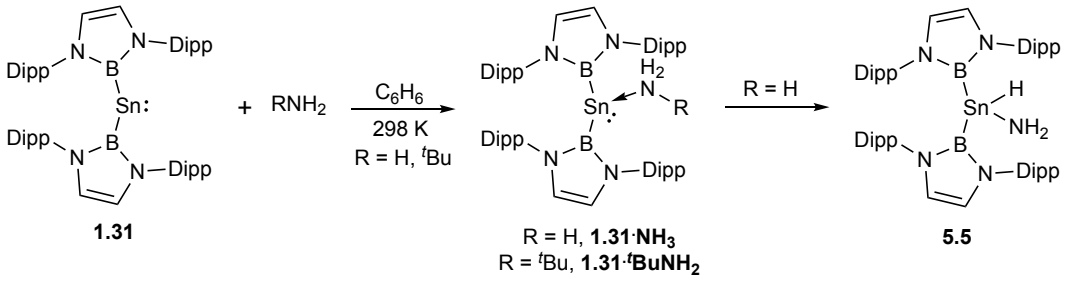
Investigations into the reactivity of stannylenes have been underway for over half a century.[1] Initial research from Lappert *et al.* on the coordination chemistry of the bis(alkyl)stannylene, **1.33**, (which is in equilibrium with its dimer, **5.1**, in solution) demonstrated the Lewis basicity of stannylenes (Scheme 5-1).[2] The literature probing the Lewis basicity of stannylenes has expanded over subsequent decades and has shown them to be versatile donors capable of coordinating to a range of metal centres.[3–6]



Scheme 5-1: Top – Equilibrium between distannene, **5.1**, and its stannylene monomer, **1.33**, with subsequent coordination to a chromium centre.[2] Bottom – Coordination of an N-heterocyclic stannylene, **5.3**, to a tungsten centre to yield adduct, **5.4**.[3]

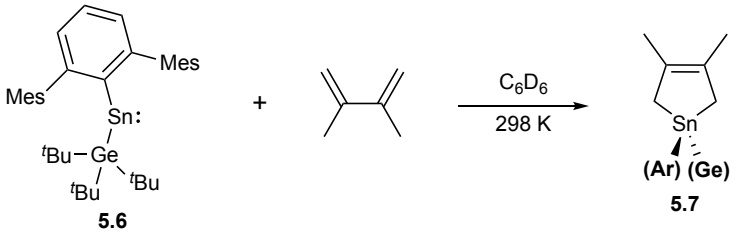
However, the reactivity of stannylenes extends to more than just coordination chemistry. Stannylenes can also behave as Lewis acids, as seen in the reaction between bis(boryl)stannylene, **1.31**, and amines (Scheme 5-2). When **1.31** is reacted with ammonia, NH_3, or *tert*-butylamine, $^tBuNH_2$, coordination is observed from the nitrogen lone pair into the formally vacant p-orbital of **1.31**. With $^tBuNH_2$, the reaction stops at the coordination complex, but with NH_3, oxidative addition of one of the N–H bonds then occurs *via* a proposed

proton shuttling mechanism (Schemes 1-11 and 1-12). Such transition metal like behaviour displayed by **1.31** is an exciting development and shows the importance of minimising the HOMO–LUMO gap of stannylenes to access new reactivity.



Scheme 5-2: Coordination of amines to **1.31**, followed by subsequent oxidative addition of an N–H bond in the case of ammonia.[7]

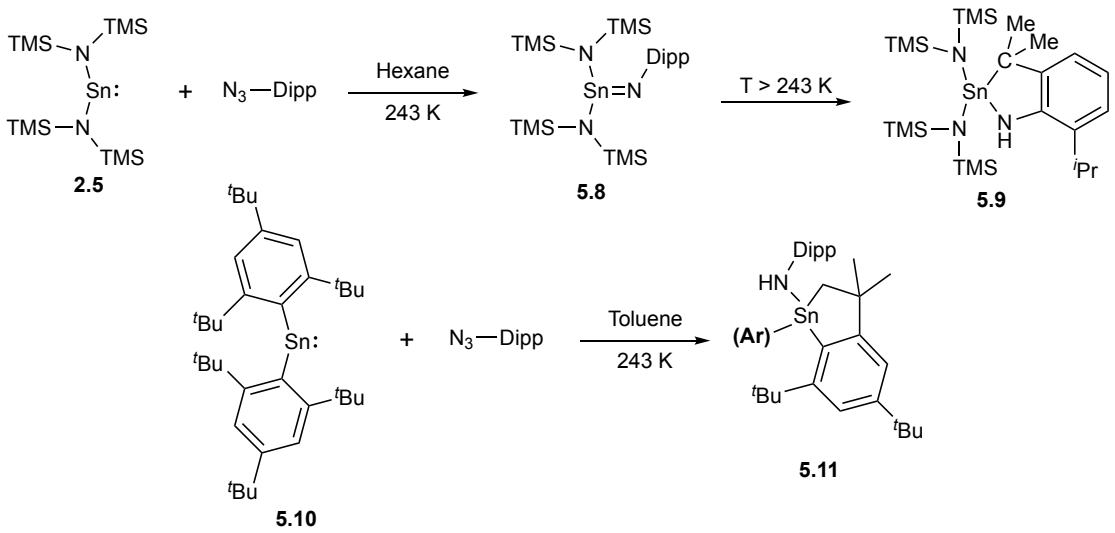
Stannylenes are also capable of performing [4+1]-cycloadditions with conjugated dienes, as is to be expected considering their Lewis ambiphilicity.[8,9] An early example of this reactivity was shown in the 2001 work of Power *et al.,* in which stannacycle **5.7** was synthesised *via* the [4+1]-cycloaddition of aryl(germyl)stannylene **5.6** with dimethylbutadiene (Scheme 5-3).[10] Reactions such as this have proved to be a useful way to trap metallylenes in solution given that cyclisation is typically rapid and the resulting products are significantly more stable and hence easier to isolate.[8–11]



Scheme 5-3: The [4+1]-cycloaddition of **5.6** with 2,3-dimethyl-1,3-butadiene (**(Ar)** is $-C_6H_3$-2,6-(C_6H_2-2,4,6-Me_3)$_2$ and **(Ge)** is $-Ge(^tBu)_3$).[10]

Organoazides are another class of reagent whose reactivity with stannylenes has been extensively investigated.[12–16] The potential products of these reactions include stanna-imines

containing a Sn=N double bond, however these species are often very reactive. Thus, while one example of a stanna-imine, **5.8**, can be isolated at 243 K and crystallographically characterised, warming to room temperature causes C–H activation to yield **5.9** (Scheme 5-4).[12] A similar phenomenon is reported by Fooken *et al.* in the synthesis of **5.10** through the reaction of bis(aryl)stannylene, **5.11**, with diisopropylphenyl azide (Scheme 5-4).[13] The high reactivity of the putative tin-nitrogen double bond suggests that other E–H bond activation chemistry is possible, such as with the N–H bond of amines.



Scheme 5-4: Top – Formation of stanna-imine, **5.8**, with subsequent C–H activation across the Sn=N bond at temperatures greater than 243 K.[12] Bottom – Formation of stannacycle, **5.11**, from the C–H activation across a transient Sn=N bond (**(Ar)** is – C_6H_2-2,4,6-(^{t}Bu)$_3$).[13]

In this chapter, the reactivity of two stannylenes, **4.10** and **4.13**, with a range of small molecules (e.g. amines, alkenes, diketones, dienes) will be explored. Investigations into the structure and bonding of the products of these reactions will be carried out using X-ray crystallography and multinuclear NMR spectroscopy.

5.2 Results and Discussion

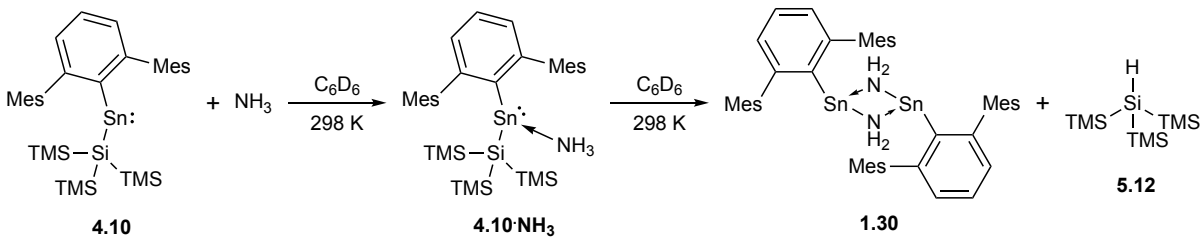
5.2.1 Reactivity with N–H Bonds

Bis(aryl)stannylene, **1.6**, reacts with NH_3 to form an amido bridged Sn(II) complex (Scheme 1-11).[17] It was thought that by substitution of one or two aryl ligands with the more σ-donating silyl ligands, not only would the HOMO–LUMO gap decrease, making the stannylene more reactive, but also the formed Sn(IV) state would be stabilised, as demonstrated by Protchenko *et al.* in the reaction between bis(boryl)stannylene **1.31** and NH_3 (Scheme 5-2).[7]

5.2.1.1 $SnAr^{Mes}Si(TMS)_3$

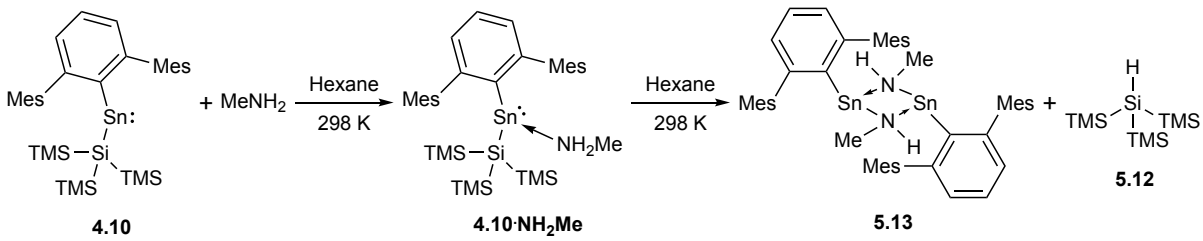
A solution of **4.10** in C_6D_6 was degassed and exposed to one atmosphere of ammonia at ambient temperature (Scheme 5-5), resulting in an immediate colour change from teal to yellow. Analysis of the reaction mixture by ^{1}H NMR spectroscopy shows the formation of new species, **4.10·NH₃**, which has ligand resonances with the same pattern as **4.10** but slightly shifted (e.g. *p*-H of central terphenyl ring: **4.10**, 7.05 ppm; **4.10·NH₃**, 6.89 ppm) or more symmetrical (e.g. *m*-H of central terphenyl ring: **4.10**, 6.82 and 6.64 ppm; **4.10·NH₃**, 6.81 ppm). A broad singlet resonance corresponding to the ammonia protons is also seen (-0.03 ppm) which integrates in a 7:1 ratio with the *p*-H of central terphenyl ring resonance of **4.10·NH₃**. This is shifted from the resonance of free ammonia in C_6D_6 (-0.14 ppm). These data suggest that **4.10·NH₃** is the adduct of ammonia and aryl(silyl)stannylene **4.10**, akin to the bis(boryl)stannylene amine adducts **1.31·NH₃** and **1.31·^{t}BuNH₂** (Scheme 5-2).[7] After 12 h, the reaction mixture decolourises, and investigations of the colourless solution by ^{1}H NMR spectroscopy show the growth of new resonances in the spectrum. These match the

amido-bridged Sn(II) complex, **1.30**, reported by Power *et al.* (Scheme 1-11), and the protonated silyl ligand **5.12**, $HSi(TMS)_3)_3$, (Si–*H*: 2.52 ppm).[17,18] Attempts to unequivocally confirm the connectivity of **4.10·NH₃** were stymied by the coordinative equilibrium between **4.10** and NH_3. This was evidenced by the regeneration of **4.10** whenever a solution of **4.10·NH₃** was exposed to vacuum. This phenomenon also serves to make the clean isolation of **4.10·NH₃** challenging, since NMR samples are invariably contaminated with **4.10** and **1.30**. Attempts to isolate **4.10·NH₃** as a crystalline solid only yield **1.30** due to the presence of excess NH_3 facilitating onward reactivity.



Scheme 5-5: Formation of a Sn(II) bridged amido dimer, **1.30**, via the intermediate adduct, **4.10·NH₃**.

Methylamine can also react with **4.10**. A solution of methylamine was added to a hexane solution of **4.10** and an immediate colour change from teal to yellow occurred (Scheme 5-6). After 12 h, the reaction mixture was completely decolourised. Investigation of the reaction mixture by ^1H NMR spectroscopy reveals a new quartet at 1.62 ppm and doublet at 1.25 ppm (due to the methylamine fragment) which integrate in an equimolar ratio with a new set of terphenyl ligand resonances with the same pattern as those of **1.30**. When taken together with the absence of any obvious tin hydride signals, and the presence of **5.12** (Si–*H*: 2.52 ppm), this suggests the formation of the amido-bridged Sn(II) species, **5.13**. Crystals suitable for X-ray crystallography were grown and allow confirmation of the proposed connectivity of **5.13** (Figure 5-1).



Scheme 5-6: Formation of a Sn(II) bridged amido dimer, **5.13**, via the intermediate adduct **4.10·NH$_2$Me**.

The molecular structure of **5.13** is shown in Figure 5-1 and a list of key geometric parameters (together with those of **1.30**, as reported by Peng *et al.*) are detailed in Table 5-1.[17] Both **5.13** and **1.30** are amido bridged Sn(II) species, with Sn–C bond lengths similar to the aryl(amido)stannylenes, **4.8** and **4.9** reported above (**5.13**: 2.264(5) Å, **4.8**: 2.242(4) Å, **4.9**: 2.222(3) Å). The methyl groups of the methylamine fragments adopt a trans-configuration about the Sn_2N_2 plane. This arrangement allows the methyl group to point away from the proximal mesityl ring.

Table 5-1: Selected bond lengths (Å) and angles (°) for the compounds **5.13** and **1.30**.[17]

	N1–Sn1–N2	**N1–Sn2–N2**	**Sn1-N1**	**Sn1-N2**	**Sn2-N1**	**Sn1–N1–Sn2**
5.13	79.3(2)	79.3(2)	2.225(4)	2.238(5)	2.238(5)	100.7(2)
1.30[17]	75.49(7)	75.87(8)	2.222(2)	2.223(2)	2.214(2)	100.51(8)
	C1–Sn1–N1	**C2–Sn2–N2**	**Sn1–C1**	**Sn2–C2**	**Sn2–N2**	**Sn1–N2–Sn2**
5.13	96.4(2)	96.4(2)	2.264(5)	2.264(5)	2.225(4)	100.7(2)
1.30[17]	95.03(8)	93.99(8)	2.240(3)	2.230(3)	2.212(2)	100.56(8)

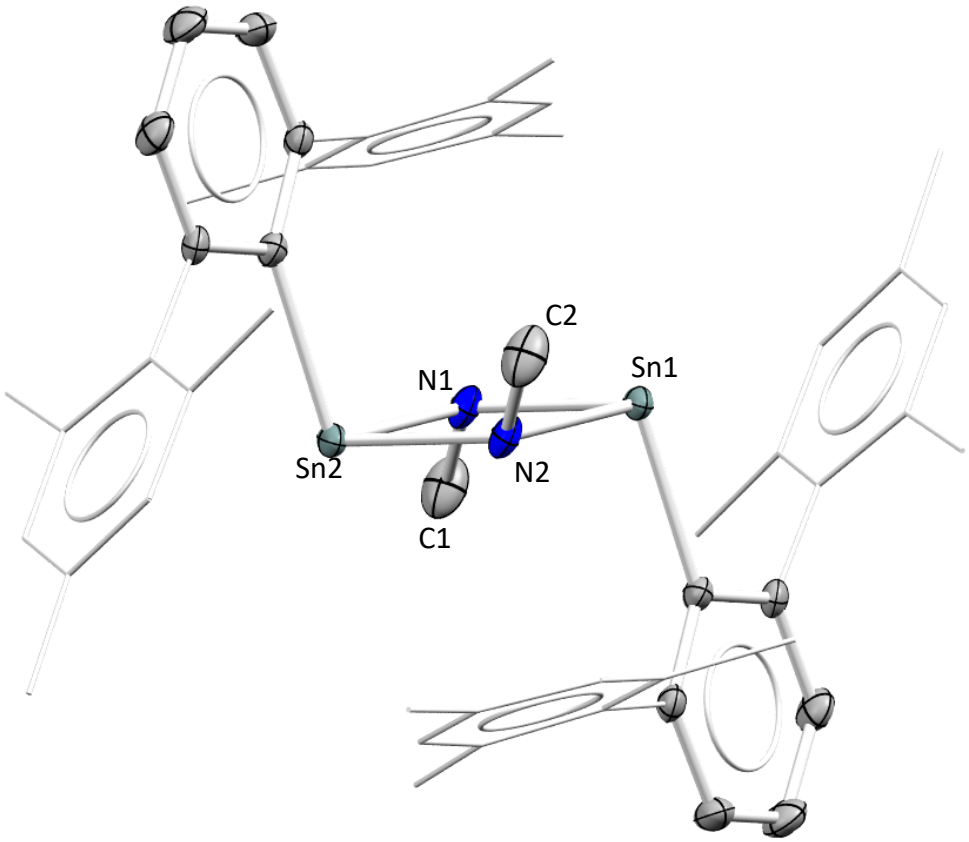
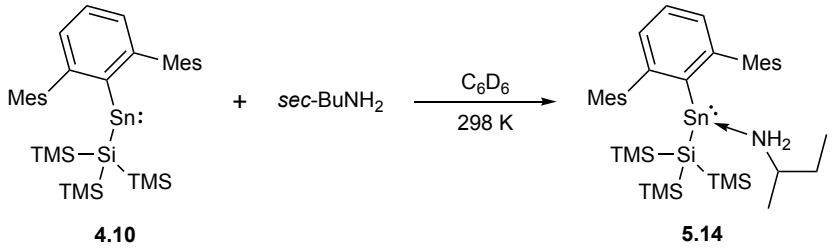


Figure 5-1: Molecular structure of **5.13** as determined by X-ray crystallography. Thermal ellipsoids are set at the 50% probability level. Hydrogen atoms are omitted for clarity. The flanking mesityl rings of the terphenyl ligands are depicted in wireframe for clarity. Key bond lengths and angles are detailed in Table 5-1 above.

As in the case of the related germylene system, **1.23**, it was thought increasing the steric bulk of the amine might allow the reaction to be halted at the formation of coordination complex. To probe this hypothesis, the reactivity of **4.10** with *sec*-butylamine, $^{s}BuNH_2$, was investigated. A solution of **4.10** in C_6D_6 in an NMR tube was combined with $^{s}BuNH_2$ (Scheme 5-7) and an immediate colour change to yellow was seen, reminiscent of the reactions of **4.10** with ammonia and methylamine. However, in this case, the yellow reaction mixture does not decolourise and no onward reaction was observed. Analysis of the reaction mixture by ^{1}H NMR spectroscopy shows the formation of new ligand resonances (e.g. *p*-H of central aryl ring of terphenyl ligand: 7.29 ppm) which integrate in equimolar fashion with the new doublet

and triplet resonances (at 0.82 and 0.66 ppm, respectively) corresponding to the methyl groups of a $^{s}BuNH_2$ unit. This evidence suggests that the product of this reaction, **5.14**, is the coordination complex of **4.10** with $^{s}BuNH_2$.



4.10 **5.14**

Scheme 5-7: Adduct, **5.14**, formation from the reaction of **4.10** with sec-butylamine.

As proposed for the reaction between **4.10** and other amines, it is thought that **5.14** is in equilibrium with **4.10** and *sec*-butylamine. Removal of volatiles *in vacuo* results in the regeneration of **4.10**. Indeed, when crystals of **5.14** were obtained, redissolution of the solid results in the regeneration of **4.10** and *sec*-butylamine, which persistently contaminates any attempts to obtain clean NMR data for **5.14**. Nevertheless, crystals of **5.14** suitable for X-ray crystallography could be grown and confirm the proposed connectivity.

The molecular structure of **5.14** is displayed below (Figure 5-2), and key geometric parameters together with those of two related literature compounds are detailed in Table 5-2.[7] Comparison of **5.14** with its precursor, **4.10**, shows a lengthening of Sn–C (**5.14**: 2.271(2) Å, **4.10**: 2.189(3) Å) and Sn–Si bonds (**5.14**: 2.7504(8) Å, **4.10**: 2.6407(7) Å) and a slight widening of the angle at the tin centre (**5.14**: 112.98(6)°, **4.10**: 109.75(6)°). The Sn–N bond length is in close agreement with the two amine bis(boryl)stannylene adducts, **1.31·NH₃** and **1.31·^{t}BuNH₂**, synthesised by Protchenko *et al.* (Scheme 5-2) (**5.14**: 2.364(2) Å, **1.31·NH₃**: 2.355(3) Å, **1.31·^{t}BuNH₂**: 2.350(2) Å).[7] In addition, the near perpendicular alignment of the amine to the

Sn–C–Si plane (98.06(9)° and 91.61(6)°) indicates that the adduct is formed by donation of the lone pair of the amine nitrogen into the formally empty p-orbital of **4.10**.

Table 5-2: Selected bond lengths (Å) and angles (°) for the compounds **5.14**, **1.31·NH$_3$**, **1.31·^{t}BuNH$_2$**.[7]

	Sn–C/B	Sn–Si/B	Sn–N	B/C–Sn–Si/B	B/C–Sn–N	B/Si–Sn–N
5.14	2.271(2)	2.7504(8)	2.364(2)	112.98(6)	98.06(9)	91.61(6)
1.31·NH$_3$	2.311(3)	2.306(3)	2.355(3)	119.3(1)	92.4(1)	94.6(1)
1.31·^{t}BuNH$_2$	2.323(2)	2.338(2)	2.350(2)	118.3(1)	90.3(1)	95.4(1)

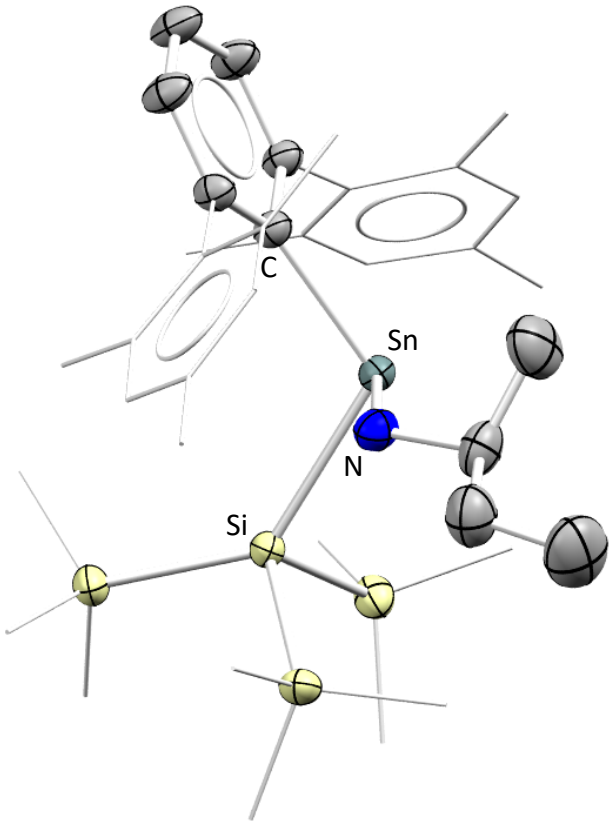
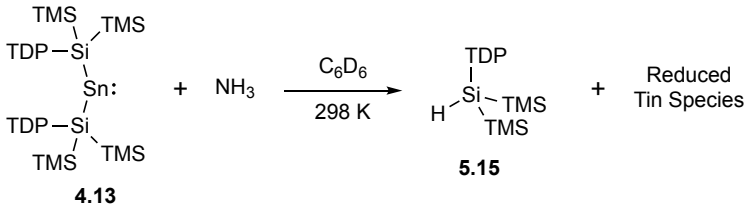


Figure 5-2: Molecular structure of **5.14** as determined by X-ray crystallography. Thermal ellipsoids are set at the 50% probability level. Hydrogen atoms are omitted for clarity. The flanking mesityl rings of the terphenyl ligand and the methyl groups of the hypersilyl ligand are depicted in wireframe for clarity. Key bond lengths and angles detailed in Table 5-2.

5.2.1.2 $Sn(Si(TMS)_2(Si^tBuPh_2))_2$

A solution of **4.13** in C_6D_6 was degassed and the headspace exposed to one atmosphere of ammonia at ambient temperature (Scheme 5-8). An immediate colour change to orange was observed. Analysing the reaction mixture by ^1H NMR spectroscopy shows one major product which gives rise to a singlet resonance corresponding to one proton at 2.92 ppm (Figure 5-3). This resonance is thought to arise from the Si–H of the protonated silyl ligand, **5.15**, as it is in close agreement with the literature value (2.94 ppm).[19] After 4-5 h, the solution begins to precipitate dark solid, suggesting the formation of insoluble reduced tin species, although

these are not detectable in the ^{1}H NMR spectrum. The formation of **5.15** is proposed to occur as a result of reductive elimination from the oxidative addition product (as observed with the bis(boryl)stannylene, **1.31** (Scheme 5-2)).[7] The precipitation of black tin metal was also observed by Protchenko *et al*. in the oxidative addition of ammonia by **1.31**, consistent with the instability of these Sn(IV) systems and indicating that a similar process could be occurring with **4.13** and ammonia. Further work is necessary to unequivocally determine what happens in this reaction.



Scheme 5-8: Formation of protonated ligand, **5.15**, from the reaction of **4.13** with ammonia.

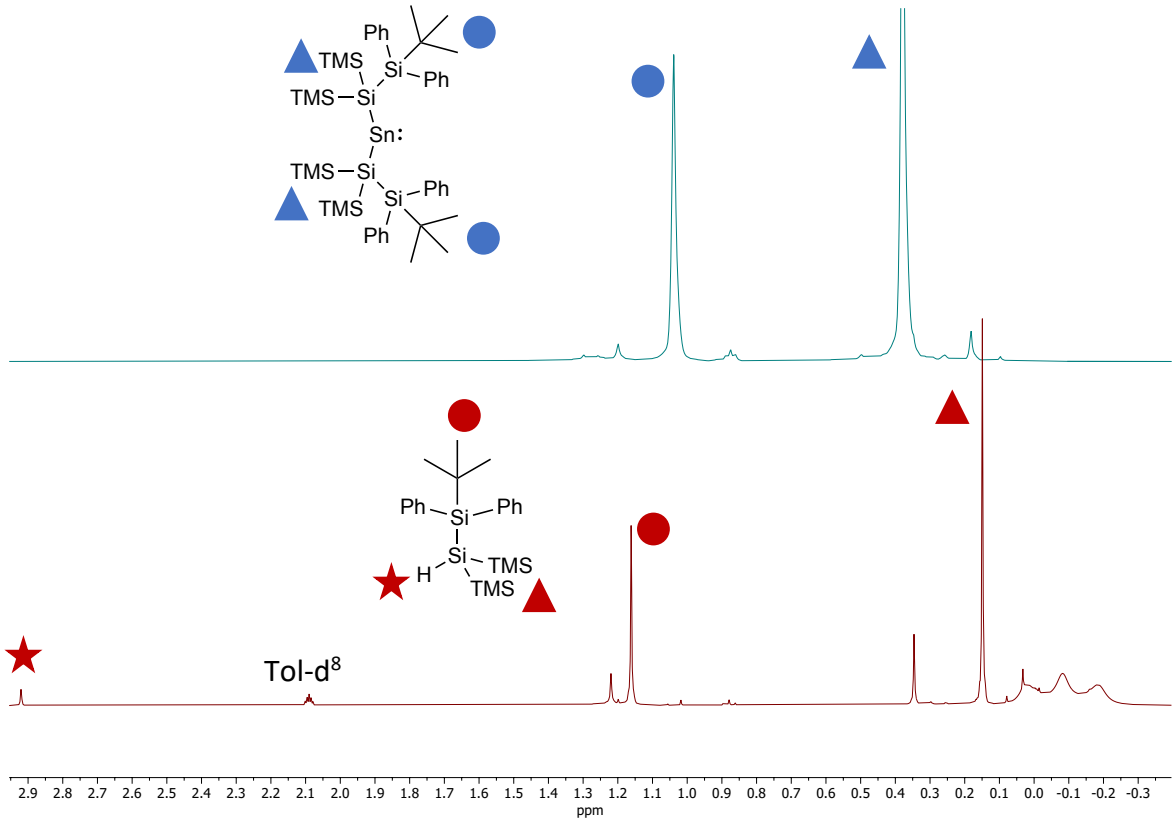


Figure 5-3: Top – ^{1}H NMR spectrum of **4.13** before addition of ammonia. Bottom – ^{1}H NMR spectrum of the reaction mixture between **4.13** and ammonia to form **5.15**.

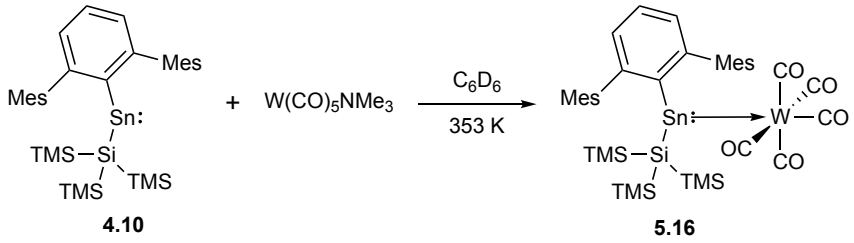
5.2.2 Reactivity with Lewis Acids

As group 14 is descended, the lone pair of a metallylene is stabilised as it becomes more s-orbital like in character.[20] Nevertheless, there is a wealth of literature detailing the coordination chemistry of stannylenes.[2,21] In order to probe the Lewis basicity of **4.10** and **4.13**, their reactivity with a range of Lewis acids was investigated.

5.2.2.1 $W(CO)_5NMe_3$

To gauge the strength of **4.10** as a Lewis base, the reaction with $W(CO)_5NMe_3$ was performed, since other $W(CO)_5$ adducts of stannylenes were known.[3,22] Combining the two solids in an NMR tube and suspending in C_6D_6 allowed the reaction to be tracked by *in situ* ^{1}H NMR spectroscopy. After 2 d at room temperature, no reaction was observed. The reaction mixture

was therefore heated to 353 K and after 1 h, new resonances could be seen growing in the ^{1}H NMR spectrum. After 24 h, the reaction had reached completion (Scheme 5-9). These NMR data suggest that the tin centre had become more sterically crowded, given that the new resonances indicate a reduction of symmetry compared to the resonances of **4.10** (e.g. *o*-CH_3 of flanking terphenyl rings: **4.10**, 2.18 ppm; **5.16**, 2.26 and 2.44 ppm) consistent with complexation to $W(CO)_5$. Crystals suitable for X-ray diffraction could be grown from the reaction mixture and confirm the proposed connectivity.



Scheme 5-9: Formation of adduct, **5.16**, from the reaction of **4.10** with $W(CO)_5NMe_3$.

The molecular structure of **5.16** is shown in Figure 5-4 and key geometric parameters, along with those for N-heterocyclic stannylene adduct, **5.4**, synthesised by Wass *et al.* (Scheme 5-1), for comparison, are detailed in Table 5-3 below.[3] The adduct **5.16** is formed by the donation of the lone pair of **4.10** to the tungsten centre, as evidenced by the planar distribution of the three groups around the tin centre (sum of angles: 359.94°). This feature offers a notable contrast with amine adduct, **5.14** (sum of angles: 302.65°). As with **3.12** above (Scheme 3-18), coordination to the tungsten does not dramatically alter the structure of stannylene fragment (Sn–C: **4.10,** 2.189(3) Å; **5.16**, 2.183(3) Å; Sn–Si: **4.10**, 2.6407(7) Å; **5.16**, 2.6323(9) Å). The Sn–W bond length (2.7603(4) Å) of **5.16** is longer than that of **5.4** (2.6889(3) Å), presumably due to the greater steric bulk of the stannylene **4.10**. The resonances observed in the ^{119}Sn NMR spectra of the two compounds are also markedly

different (**5.16**: 1954 ppm, **5.4**[3]*:* 462 ppm), likely due to the greater σ-donating capacity of the substituents in **5.16**.

Table 5-3: Selected bond lengths (Å) and angles (°) for the compounds **5.16**, **5.4**.[3]

	Sn–C	Sn–Si	Sn–W	C–Sn–Si	C/N–Sn–W	Si/N–Sn–W
5.16	2.183(3)	2.6323(9)	2.7603(4)	120.94(8)	116.31(8)	122.69(2)
5.4 [3]	N/A	N/A	2.6889(3)	N/A	138.20(2)	138.20(2)

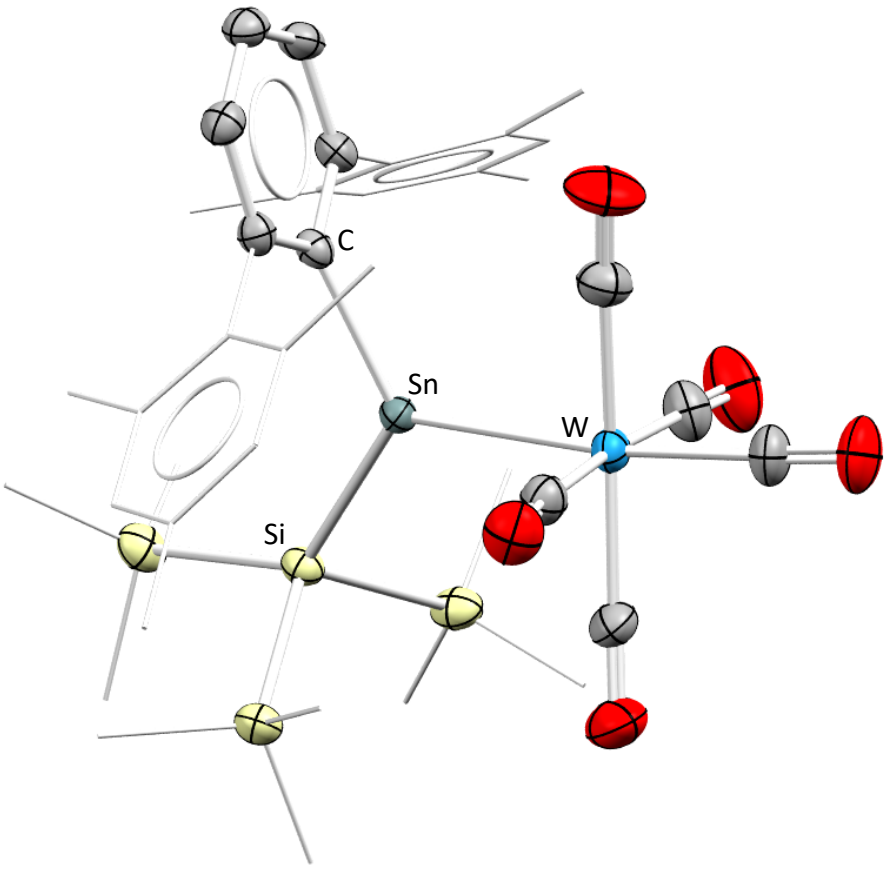
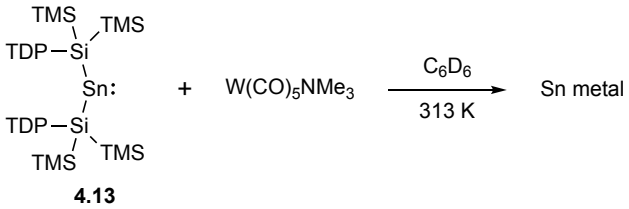


Figure 5-4: Molecular structure of **5.16** as determined by X-ray crystallography. The thermal ellipsoids are set to the 50% probability level. Hydrogen atoms are omitted for clarity. The flanking mesityl rings of the terphenyl

ligand and the methyl groups of the hypersilyl ligand are depicted in wireframe for clarity. Key bond lengths and angles are documented in Table 5-3 above.

In order to compare the donor strengths of **4.10** and **4.13**, the reaction of **4.13** with $W(CO)_5NMe_3$ was attempted. Due to the greater σ-donating capacity of the silyl substituent, (which potentially makes **4.13** a better σ-donor), it was envisaged that the reaction between **4.13** and $W(CO)_5NMe_3$ would proceed at ambient temperatures, meaning that decomposition of **4.13** would not occur. However, upon dissolution of the two solids, no reaction was seen at ambient temperature, despite reaction times of over a week. The reaction mixture was therefore warmed to 313 K (Scheme 5-10). However, even this mild temperature increase was enough to initiate the production of elemental tin from the reaction mixture, suggesting that **4.13** is decomposing. Despite its Lewis basicity being postulated to be greater than that of **4.10**, it is likely that the very large steric bulk of **4.13** prevents access to its coordination complex with $W(CO)_5NMe_3$ at temperatures below that at which it decomposes.

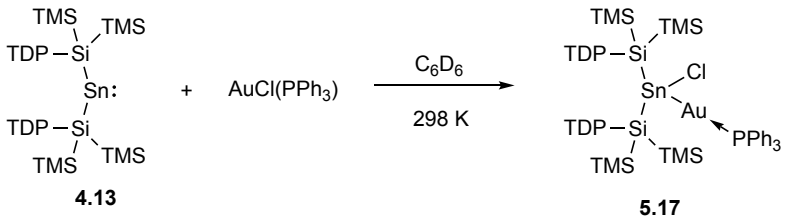


Scheme 5-10: Decomposition of **4.13** to form tin metal at elevated temperatures in the presence of $W(CO)_5NMe_3$.

5.2.2.2 $Au(PPh_3)Cl$

Since the steric bulk of **4.13** precluded its coordination to $W(CO)_5$, the reaction with a sterically less encumbered gold(I) chloride complex was investigated to see if a Sn–Au bond could be obtained. Combination of **4.13** and $Au(PPh_3)Cl$ in an NMR tube and dissolution in C_6D_6 resulted in a colour change to yellow, without the use of elevated temperatures

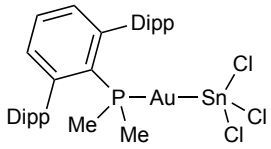
(Scheme 5-11). Tracking the reaction by ^{31}P NMR spectroscopy shows the formation of a new resonance at 46.6 ppm, which has ^{119}Sn satellites (J_{Sn-P} = 1396.7 Hz), slightly shifted from the resonance of the starting material (32.9 ppm).[23] This suggests that the phosphine ligand is still bound to an Au(I) centre, which is itself bound to a tin atom, rather than being in solution as free PPh_3 (^{31}P NMR chemical shift: -5.0 ppm).[24] In addition, the ^{1}H NMR resonance corresponding to the -$SiMe_3$ groups on the silyl ligand splits into two resonances in the product (0.40 and 0.39 ppm), suggesting a less symmetric environment. The lowering of symmetry in the ^{1}H NMR data and the ^{31}P data suggests that the oxidative addition of the Au–Cl has occurred at the tin centre to form the Sn(IV) product, **5.17**, which contains an Au(I) moiety with a triphenyl phosphine ligand. Crystals of **5.17**, suitable for X-ray diffraction, could be grown from the reaction mixture, allowing the proposed connectivity to be confirmed.



Scheme 5-11: Oxidative addition by **4.13** of a Au–Cl bond to form **5.17**.

The molecular structure of **5.17** is depicted in Figure 5-6 and key geometric parameters, along with related literature examples ($Sn(HMDS)_2(Cl)Au(THT)$ (**1.18**) synthesised by Cabeza *et al.* (Scheme 1-5) and $SnCl_3Au(PMe_2Ar^{Dipp})$ (**5.18**) synthesised by Campos *et al.* (Figure 5-5)), are detailed in Table 5-4.[25,26] The structure of **5.17** can be seen to result from the oxidative addition of the Au–Cl bond in $Au(PPh_3)Cl$ at the tin centre. Unlike the adduct **5.16**, a pseudo-tetrahedral geometry is adopted at the tin centre which acts formally as an X-type stannyl ligand. The near linear angle at the gold atom of **5.17** (175.97(3)°) is indicative of a gold(I) species. A slight lengthening of the Sn–Si bonds (**5.17**: 2.676(1) Å and 2.664(1) Å,

4.13: 2.6590(8) Å and 2.6463(8) Å) and a widening of the angle at the tin centre (**5.17**: 136.34(4)°, **4.13**: 121.71(3)°) are observed compared to **4.13**. While this widening is expected on formation of a Sn(IV) species, the bond lengthening is thought to be due to steric repulsion from the bulky triphenyl phosphine ligand. This is also demonstrated in the significantly longer Sn–Au (2.6119(6) Å) bond than literature comparisons, e.g. **1.18** (2.5711(5) Å) and **5.18** (2.5438(9) Å).[25,26] However, the Au–P bond length of **5.17** (2.341(1) Å) is in good agreement with that of **5.18** (2.321(2) Å).[26]



5.18

Figure 5-5: Au(I) complex synthesised by Campos *et al.* relevant bond lengths and angles in Table 5-4 below.[26]

Table 5-4: Selected bond lengths (Å) and angles (°) of **5.17** and related literature examples.[25,26]

	Sn–Si1/2	**Sn–Au**	**Sn–Cl**	**Au–P**	**Si1–Sn–Si2**	**Sn–Au–P**
5.17	2.676(1), 2.664(1)	2.6119(6)	2.448(1)	2.341(1)	136.34(4)	175.97(3)
5.18[26]	N/A	2.5438(9)	2.417(7)	2.321(2)	N/A	151.65(5)
1.18[25]	N/A	2.5711(5)	2.412(2)	N/A	N/A	N/A

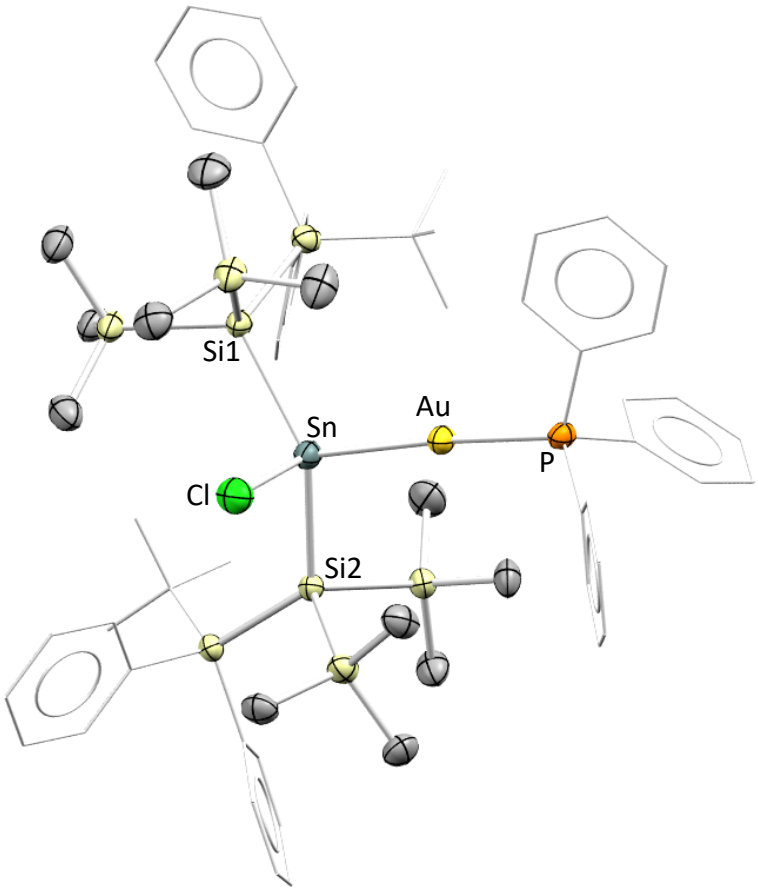


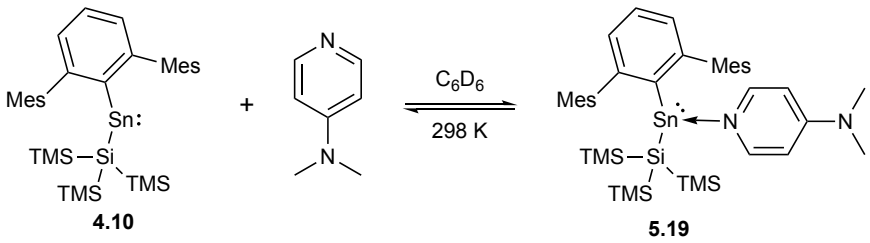
Figure 5-6: Molecular structure of **5.17** as determined by X-ray crystallography. The thermal ellipsoids are set to the 50% probability level. Hydrogen atoms are omitted for clarity. Phenyl and tert-butyl groups are depicted in wireframe for clarity. Key bond lengths and angles are detailed in Table 5-4 above.

5.2.3 Reactivity with Lewis Bases

The formally vacant p-orbitals of stannylenes allude to their ability to behave as Lewis acids, as has already been demonstrated in the formation of coordination complex **5.14**. Interested in seeing what effect substituent choice might have on their Lewis acidity, the reactivity of **4.10** and **4.13** towards Lewis bases was also probed.

5.2.3.1 Dimethylaminopyridine (DMAP)

The reactivity of **4.10** and **4.13** was investigated with DMAP. When **4.10** was added to a solution of excess DMAP in C_6D_6, an immediate colour change from teal to green was seen (Scheme 5-12). Investigation of the reaction mixture by ^{1}H NMR spectroscopy shows the formation of a new species, **5.19**, with sharp ligand resonances (e.g. *m*-H of the flanking terphenyl ligand rings: **4.10**, 6.82 and 6.64 ppm; **5.19**, 6.77 ppm) and a slight shifting of other ligand resonances (e.g. *p*-H of the central terphenyl ligand ring (Figure 5-7): **4.10**, 7.36 ppm; **5.19**, 7.30 ppm). Only one set of DMAP resonances are observed in the ^{1}H NMR spectrum (aryl C–H: 8.32 and 6.00 ppm, N–CH_3: 2.18 ppm), despite being in excess, and these are noticeably shifted from the resonances of free DMAP (Aryl C–H: 8.48 and 6.11 ppm, N–CH_3: 2.23 ppm). These data suggest that **5.19** is probably the coordination complex of **4.10** and DMAP, and that the coordinated DMAP is in rapid exchange with free DMAP in solution.



Scheme 5-12: Adduct, **5.19**, formation from the reaction between **4.10** and DMAP.

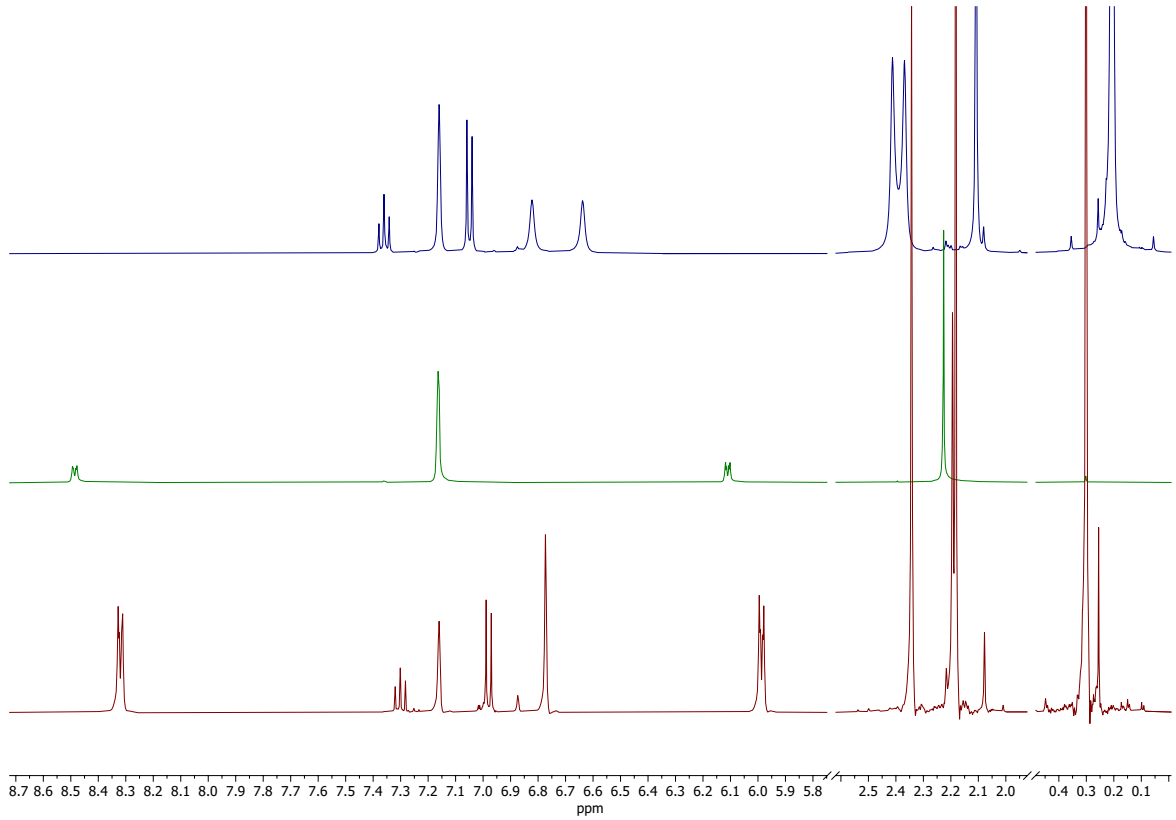
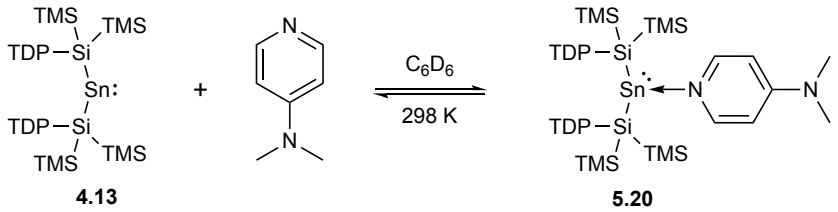


Figure 5-7: Top – Excerpts from a ^{1}H NMR spectrum of **4.10**. Middle – Excerpts from a ^{1}H NMR spectrum of DMAP. Bottom – Excerpts from a ^{1}H NMR spectrum of the reaction between **4.10** and DMAP.

With a view to probing whether **4.13** is more Lewis acidic than **4.10**, the reactivity of **4.13** with DMAP was also investigated. When an excess of DMAP is added to a solution of **4.13** in C_6D_6, an immediate colour change from brown to orange is observed (Scheme 5-13). Analysis of the reaction mixture by ^{1}H NMR spectroscopy suggests that coordination occurs to form **5.20** (as with **5.19** above) because new ligand resonances (e.g. ^{t}Bu group of ligands: **4.13**, 1.04 ppm; **5.20**, 1.34 ppm) are observed, as well as one set of shifted DMAP resonances (aryl C–H: 8.35 and 5.96 ppm, N–CH_3: 2.07 ppm). Of particular interest is the broadening of the resonances in the ^{1}H NMR spectrum, corresponding to the trimethylsilyl groups of the silyl substituent and all of the DMAP resonances (Figure 5-8). This phenomenon suggests that like **4.10**, **4.13** is in a coordinative equilibrium with DMAP. Unfortunately, single crystals of **5.20**

suitable for X-ray diffraction could not be grown, which was thought to be due to the presence of DMAP in solution ultimately affecting the solubility of **5.20**.



Scheme 5-13: Adduct, **5.20**, formation from the reaction between bis(silyl)stannylene, **4.13**, and DMAP.

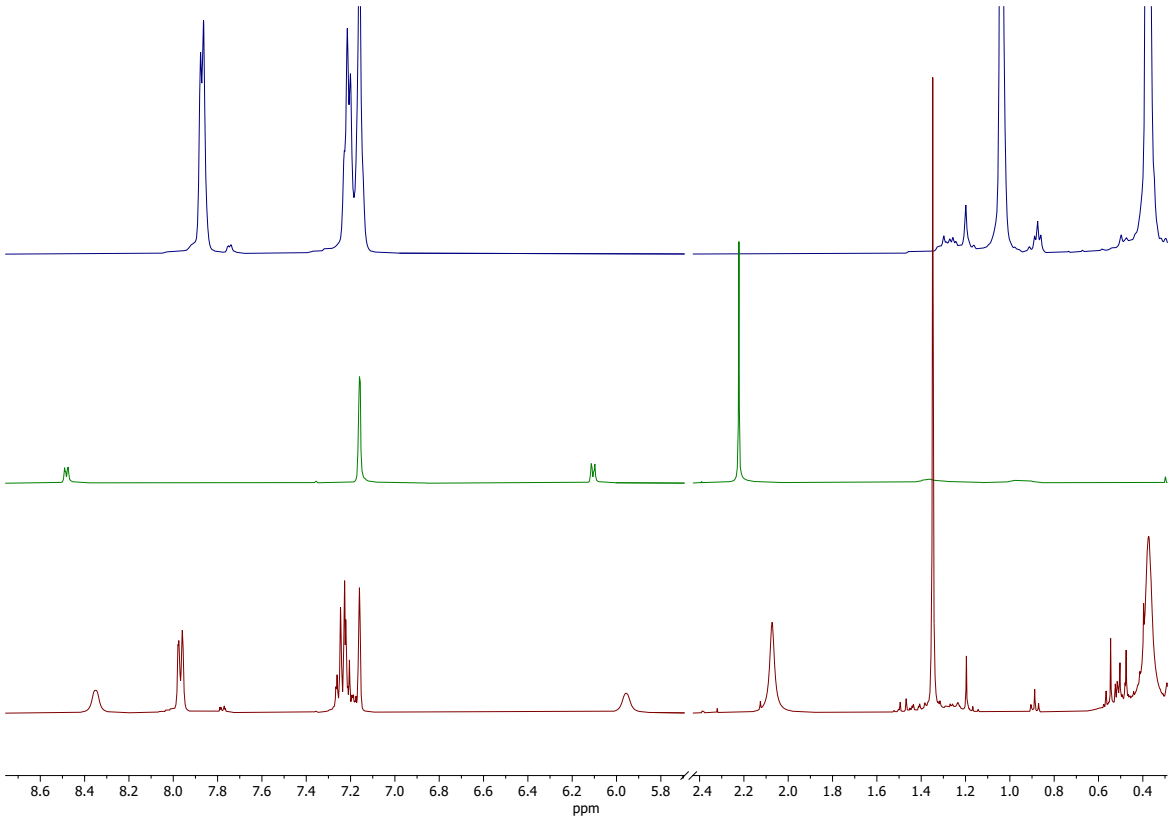
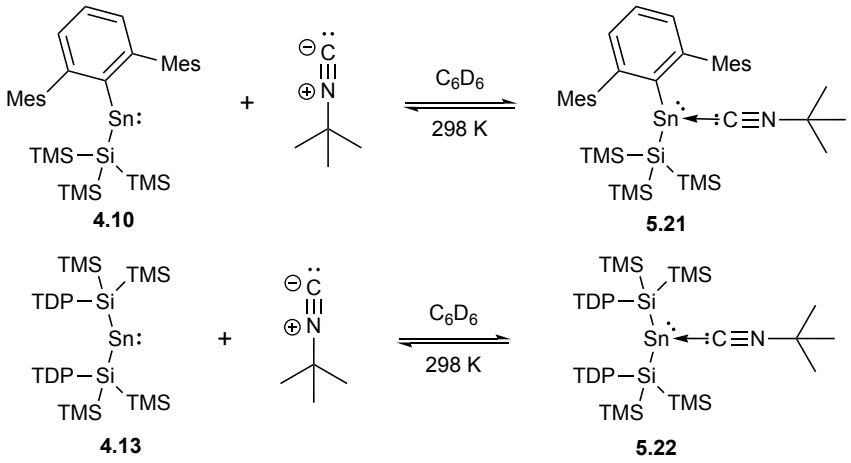


Figure 5-8: Signals in the ^{1}H NMR spectra of species present in the reaction between **4.13** and DMAP: Top – Excerpts from a ^{1}H NMR spectrum of **4.13**. Middle – Excerpts from a ^{1}H NMR spectrum of DMAP. Bottom – Excerpts from a ^{1}H NMR spectrum of the reaction between **4.13** and DMAP.

5.2.3.2 Tertbutylisonitrile

The use of a stronger Lewis base, ^{t}BuNC, was also trialled to see whether the coordinative equilibria could be shifted more towards the respective adducts, allowing their isolation and

structural characterisation. However, this was not the case. Instead similar colour changes are observed when solutions of **4.10** and **4.13** in C_6D_6 are combined with an excess of a (protio) benzene solution of ^{t}BuNC (Scheme 5-14). In both cases, it is proposed that coordination occurs to form the adducts **5.21** (**4.10** and ^{t}BuNC) and **5.22** (**4.13** and ^{t}BuNC). This was evidenced by analysis of both the reaction mixtures by *in situ* ^{1}H NMR spectroscopy, which showed new ligand resonances corresponding to the adduct (**5.20** or **5.21**) and only one resonance due to ^{t}BuNC (**5:20** ^{t}BuNC shift: 0.88 ppm; **5:21** ^{t}BuNC shift: 0.97 ppm), despite ^{t}BuNC being in excess in both reaction mixtures (2:1 ratio of intensities compared to ligand resonances for **5.21** and **5.22**) (Figures 5-9 and 5-10). This implies that the ^{t}BuNC which reacts with **4.10** or **4.13**, must be in fast exchange with free (unreacted) ^{t}BuNC, or otherwise two ^{t}BuNC resonances would be observed. Therefore, it is likely that this is a coordinative process, particularly considering the two literature examples of ^{t}BuNC coordination at a germylene centre reported by Power *et al.* and Walewska *et al.* ($GeAr^{Mes}_2$ (**1.3**) and $Ge(Si(TMS)_3)_2$ (**1.22**) (Scheme 3-16)).[27,28]



Scheme 5-14: Reactions of **4.10** and **4.13** with ^{t}BuNC to form the corresponding adducts **5.21** and **5.22** respectively.

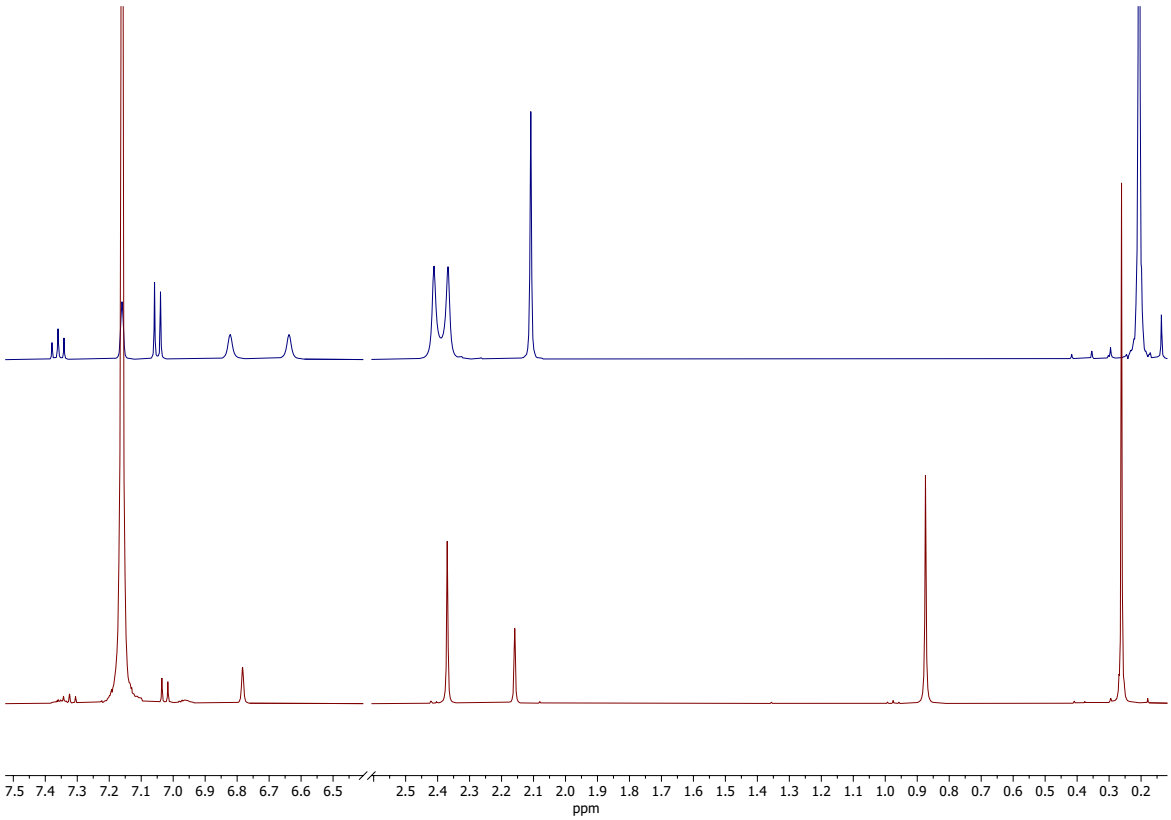


Figure 5-9: Signals in the ^{1}H NMR spectra of species present in the reaction between **4.10** and ^{t}BuNC: Top – Excerpts from the ^{1}H NMR spectrum of **4.10**. Bottom – Excerpts from the ^{1}H NMR spectrum of the reaction between **4.10** and ^{t}BuNC.

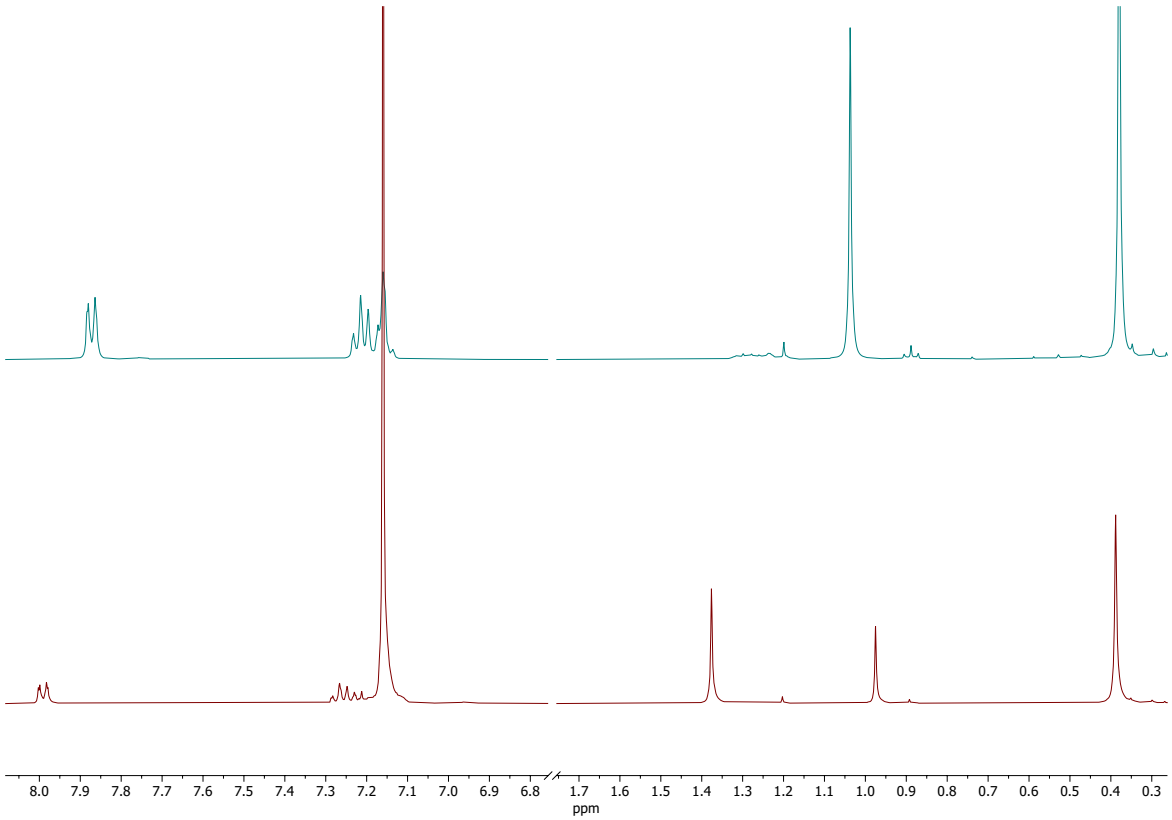


Figure 5-10: Signals in the ^{1}H NMR spectra of species present in the reaction between **4.13** and ^{t}BuNC: Top – Excerpts from the ^{1}H NMR spectrum of **4.13**. Bottom – Excerpts from the ^{1}H NMR spectrum of the reaction between **4.13** and ^{t}BuNC.

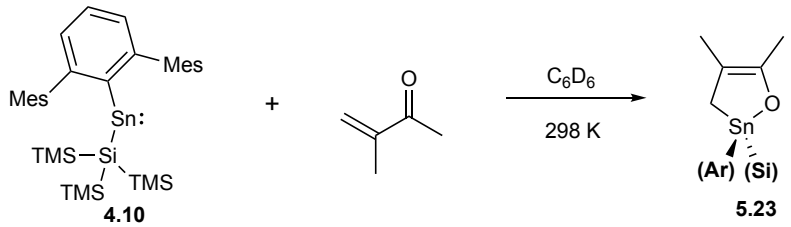
5.2.4 Reactivity with Dienes and Heterodienes

As the literature already documents that metallylenes can undergo cycloadditions with a range of unsaturated organic substrates, the reactivity of the novel stannylenes **4.10** and **4.13** towards α,β-unsaturated compounds (namely diketones and dienes) were investigated.[8,9,11]

5.2.4.1 α,β-Unsaturated Ketones

When methylisopropenyl ketone (MIPK) was added to a C_6D_6 solution of **4.10**, an immediate colour change from teal to yellow occurs (Scheme 5-15). Investigation of the reaction mixture by multinuclear NMR spectroscopy implies that the Sn(IV) cycloaddition product, **5.23**, has been formed (Figure 5-11). Particularly indicative is the ^{13}C NMR spectrum, in which a singlet resonance is observed at 29.4 ppm, corresponding to the CH_2 group bonded to the Sn centre,

which features diagnostic ^{119}Sn satellites ($^{1}J_{Sn-C}$ = 259.4 Hz). Unfortunately, attempts to grow crystals suitable for X-ray diffraction to fully confirm the connectivity have so far proved unsuccessful, as **5.23** was found to decompose in solution even when maintained at 243 K.



Scheme 5-15: The [4+1]-cycloaddition of MIPK and 4.10 (**(Ar)** is $-C_6H_3$-2,6-(C_6H_2-2,4,6-Me_3)$_2$ and **(Si)** is $-Si(SiMe_3)_3$).

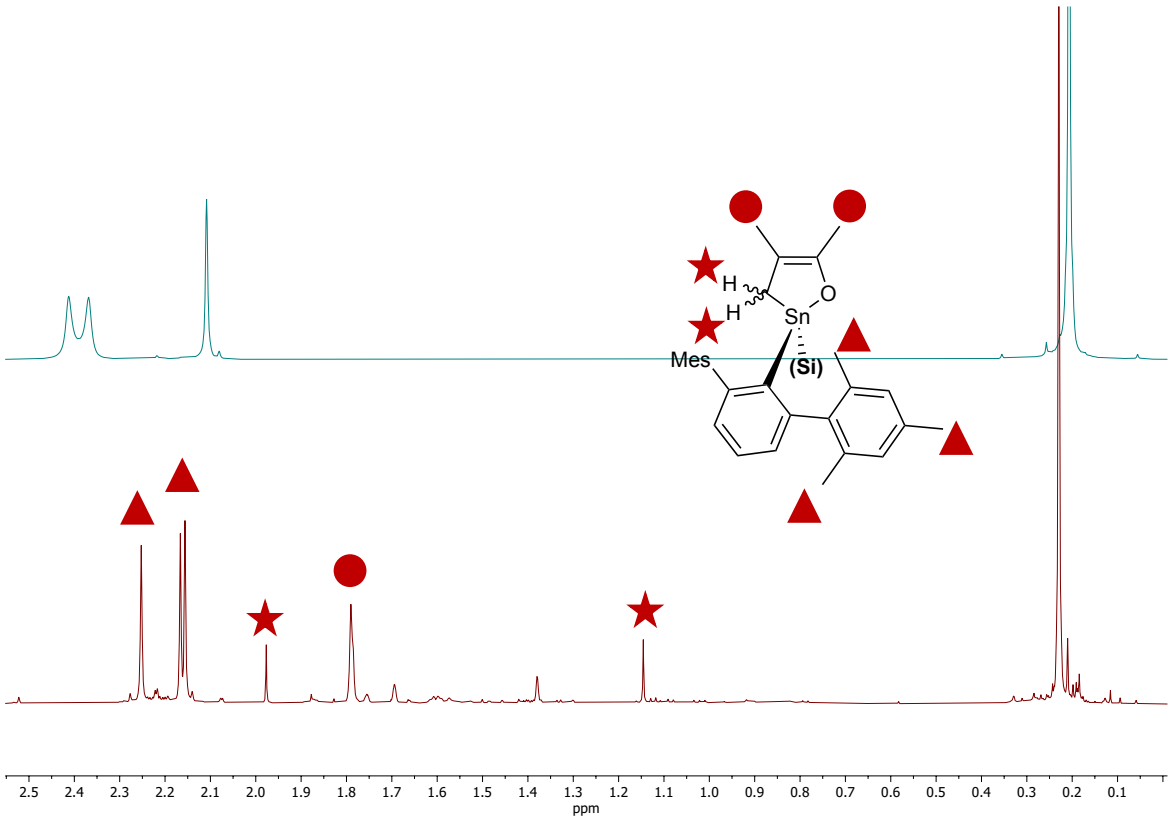
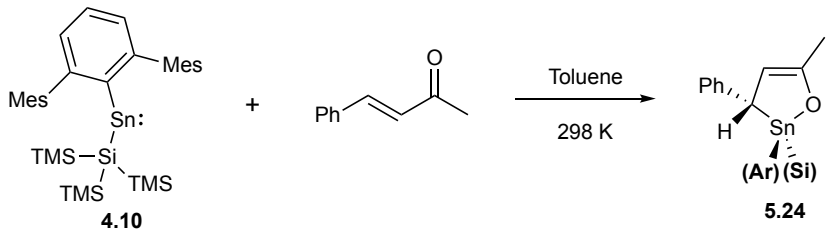


Figure 5-11: Top – Excerpt from the ^{1}H NMR spectrum of **4.13**. Bottom – Excerpt from the ^{1}H NMR spectrum of the reaction between **4.13** and MIPK.

The reaction between **4.10** and a bulkier α,β-unsaturated ketone was then investigated to elucidate the effect of steric bulk on the cycloaddition. As with **5.23** above, upon addition of

methylstyryl ketone, MSK, to a solution of the stannylene, an immediate colour change from teal to yellow occurs (Scheme 5-16). No notable difference between the rates of reaction of **4.10** with MIPK or MSK could be discerned, as both reactions occurred immediately. Investigation of the reaction mixture by ^{1}H NMR spectroscopy shows the formation of one major species, **5.24**. The two singlet resonances in the ^{1}H NMR spectrum at 4.70 and 3.96 ppm correspond to the vinylic proton and aliphatic proton, respectively, of the stannacycle formed *via* [4+1]-cycloaddition. Further evidence that cycloaddition occurs can be obtained through ^{13}C NMR spectroscopy. A new singlet resonance appears at 46.5 ppm with ^{119}Sn satellites ($^{1}J_{Sn-C}$ = 233.7 Hz), implying that it is adjacent to the Sn centre. Crystals suitable for X-ray diffraction could be grown which allowed the stereochemistry of **5.24** to be confirmed.



Scheme 5-16: The [4+1]-cycloadditon of **4.10** with methylstyrylketone (**(Ar)** is – C_6H_3-2,6-(C_6H_2-2,4,6-Me_3)$_2$ and **(Si)** is –$Si(SiMe_3)_3$).

The molecular structure of **5.24** is depicted below (Figure 5-12). **5.24** is formed from the [4+1]-cycloaddition of **4.10** with MSK, and is the only stereoisomer seen in the crystal. The widening of the C1–Sn–Si angle is seen from **4.10** to **5.24** (109.75(6)° to 119.73(6)°) and is consistent with the smaller Sn(IV) centre forcing the ligands further apart in angular terms. The heterocyclic ring of **5.24** is almost planar (sum of the internal angles = 539.6°), potentially because the bulk of the phenyl ring bonded to the stannacycle disfavours the adoption of an envelope conformation. The magnitudes of the internal torsion angles Sn–O–C4–C3 and Sn–C2–C3–C4 (4.6(3)° and 8.4(3)° respectively) further evidence the near planarity of the

stannacycle. The presence of the phenyl ring may explain why the other stereoisomer, resulting from the cycloaddition of methylstyryl ketone to **4.10**, is not seen. If the phenyl group of the stannacycle were to point towards the terphenyl ligand, a large steric clash with the flanking mesityl group of the terphenyl ligand would likely result (Figure 5-12).

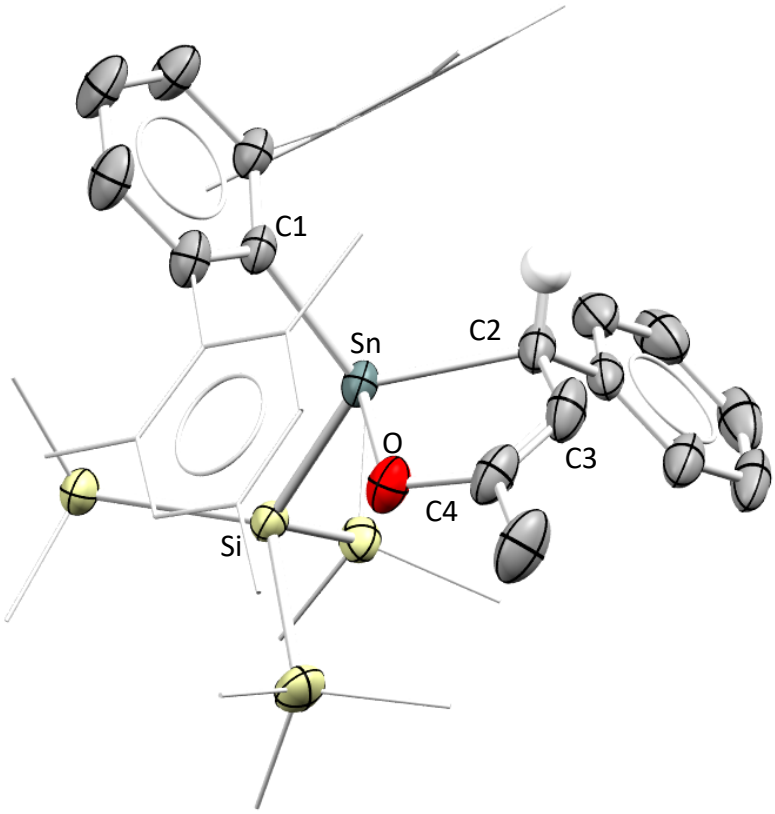
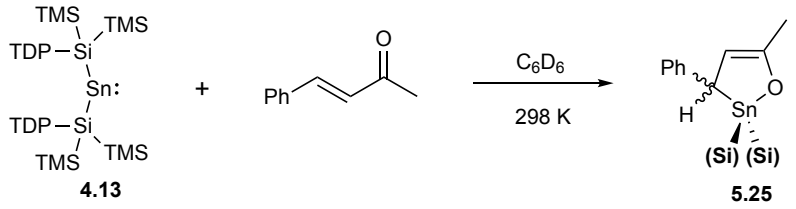


Figure 5-12: Molecular structure of **5.24** as determined by X-ray crystallography. The thermal ellipsoids are set to the 50% probability level. Hydrogen atoms (except for the C–H at the chiral carbon) are omitted for clarity. The flanking mesityl rings of the terphenyl ligand and the methyl groups of the hypersilyl ligand are depicted in wireframe for clarity. Key bond lengths (Å) and angles (°): Sn–C1: 2.188(2), Sn–Si: 2.6076(8), Sn–C2: 2.205(3), Sn–O: 2.039(2), C1–Sn–Si: 119.73(6), C2–Sn–O: 85.25(9).

The addition of C_6D_6 to a mixture of **4.13** and excess methylstyryl ketone results in a colour change from dark brown to orange over the course of approximately 5 min (Scheme 5-17). Investigation of the reaction mixture by ^{1}H NMR spectroscopy (Figure 5-13) implies that a

[4+1]-cycloaddition has taken place to yield the stannacycle product, **5.25**. Inspection of the pattern of resonances shows a reduction in symmetry from **4.13** to **5.25**. The ^{t}Bu (**4.13**, 1.04 ppm; **5.25**, 1.31 and 1.11 ppm) and TMS signals (**4.13**, 0.38 ppm; **5.25**, 0.44, 0.37, 0.29, 0.19 ppm) are split, indicative of a loss of symmetry on the NMR timescale. In addition, these ligand resonances integrate in an equimolar ratio with a new resonance corresponding to the methyl group of the stannacycle ring of **5.25** (1.88 ppm). Finally, two new singlet resonances appear in the ^{1}H NMR spectrum at 5.02 and 4.98 ppm, which correspond to the vinylic and aliphatic protons of the resultant stannacycle ring. Confirmation of the proposed connectivity of **5.25** could not be obtained as it was found to be unstable in solution, even when maintained at 243 K.



Scheme 5-17: The [4+1]-cycloadditon of **4.13** with methylstyrylketone (**(Si)** is –Si(SiMe$_3$)$_2$(Si^{t}BuPh$_2$)).

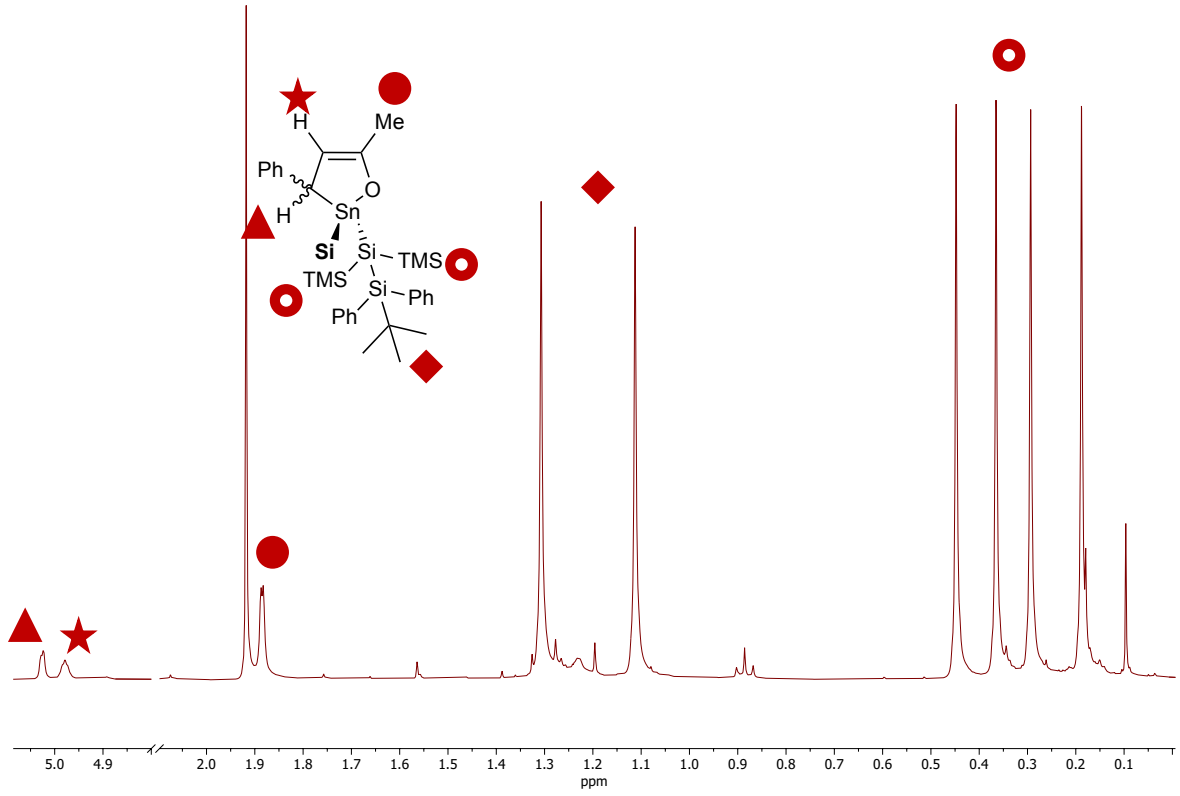
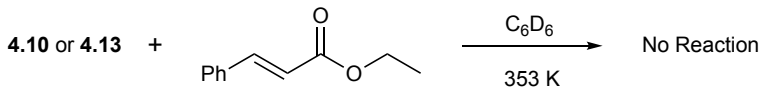


Figure 5-13: Excerpts from a ^{1}H NMR spectrum of the reaction mixture formed between bis(silyl)stannylene, **4.13** and methylstyryl ketone.

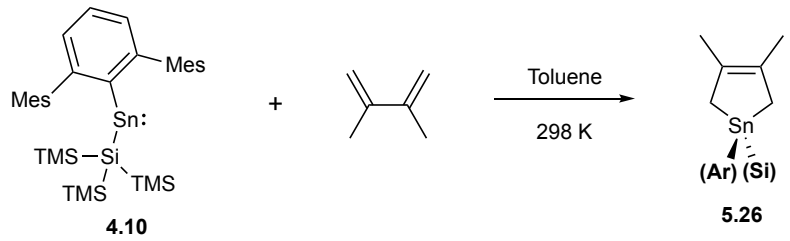
The reactivity of both **4.10** and **4.13** with an α,β-unsaturated ester, ethyl cinnamate, was also investigated (Scheme 5-18). It was found that, even with prolonged heating at 353 K, no reaction was observed. This is thought to be due to the ester having a less nucleophilic O-centre at the carbonyl group than a ketone due to the resonance forms of the ester and, as a result, is less able to perform the pericyclic cycloaddition.



Scheme 5-18: No observed reactivity between ethyl cinnamate and aryl(silyl)stannylene, **4.10**, or bis(silyl)stannylene, **4.13**.

5.2.4.2 Dienes

When butadiene is added to a C_6D_6 solution of **4.10** no immediate colour change is seen, however over the course of 24 h the reaction mixture slowly decolourises. The expected product for this reaction, as with the α,β-unsaturated ketones above, is the Sn(IV) [4+1]-cycloaddition product, **5.26** (Scheme 5-19). Analysis of the product by NMR spectroscopy allows this to be confirmed. Particularly indicative is the ^{13}C NMR spectrum of **5.26** which features a singlet resonance at 28.5 ppm with ^{119}Sn satellites ($^1J_{Sn-C}$ = 251.2 Hz), corresponding to the two CH_2 groups bonded to the tin centre. Furthermore, the resonance in the ^{119}Sn NMR spectra at -79 ppm is indicative of a Sn (IV) species compared to 2793 ppm for **4.10**. Colourless crystals of **5.26** suitable for X-ray crystallography could also be grown, allowing confirmation of the proposed connectivity.



Scheme 5-19: The [4+1]-cycloaddition of aryl(silyl)stannylene, **4.10**, with 2,3-dimethyl-1,3-butadiene (**(Ar)** is $-C_6H_3$-2,6-(C_6H_2-2,4,6-$Me_3)_2$ and **(Si)** is $-Si(SiMe_3)_3$).

The molecular structure of **5.26** was determined by X-ray crystallography and is depicted below (Figure 5-14). Key geometric parameters of **5.26** along with relevant literature examples (**5.24** (Figure 5-11) and $SnAr^{Mes}Ge(^tBu)_3(CH_2C(Me)C(Me)CH_2)$, **5.7**, synthesised by Power *et al.* (Scheme 5-3)) are detailed in Table 5-5.[10] As expected, based on the NMR data, **5.26** is the [4+1]-cycloaddition product, and adopts a more typical envelope conformation within the stannacycle when compared to **5.24**. This is exemplified by the much wider torsion angles of 23.3(2)° and 21.3(2)° (Sn–C1–C2–C3 and Sn–C4–C3–C2) as compared to 4.6(3)° and

8.4(3)° for **5.24**. The presence of the double bond in the heterocycle is clearly visible to the significantly shorter C2–C3 bond length (1.342(3) Å) as compared to the other C–C bond lengths within the metallacycle (1.514(3) and 1.515(3) Å). The structure of **5.26** is similar to that of the stannacyclopentene, $SnAr^{Mes}Ge(^{t}Bu)_3(CH_2C(Me)C(Me)CH_2)$, **5.7**.[10] The Sn–C1 and Sn-C4 bond lengths are in good agreement for both **5.26** and **5.7** (2.166(2) and 2.172(2) Å *vs.* 2.157(5) and 2.171(4) Å respectively), as are the C–Sn–C bite angles (82.82(7)° and 80.9(2)° respectively).[10]

Table 5-5: Selected bond lengths (Å) and angles (°) of **5.26** and releated compounds.[10]

	Sn–C1	**Sn–C4/O**	**O/C4–Sn–C1**	**C2–C3**
5.26	2.166(2)	2.172(2)	82.82(7)	1.342(3)
5.24	2.205(3)	2.039(2)	85.25(9)	1.337(4)
5.7[10]	2.157(5)	2.171(4)	80.9(2)	1.324(8)

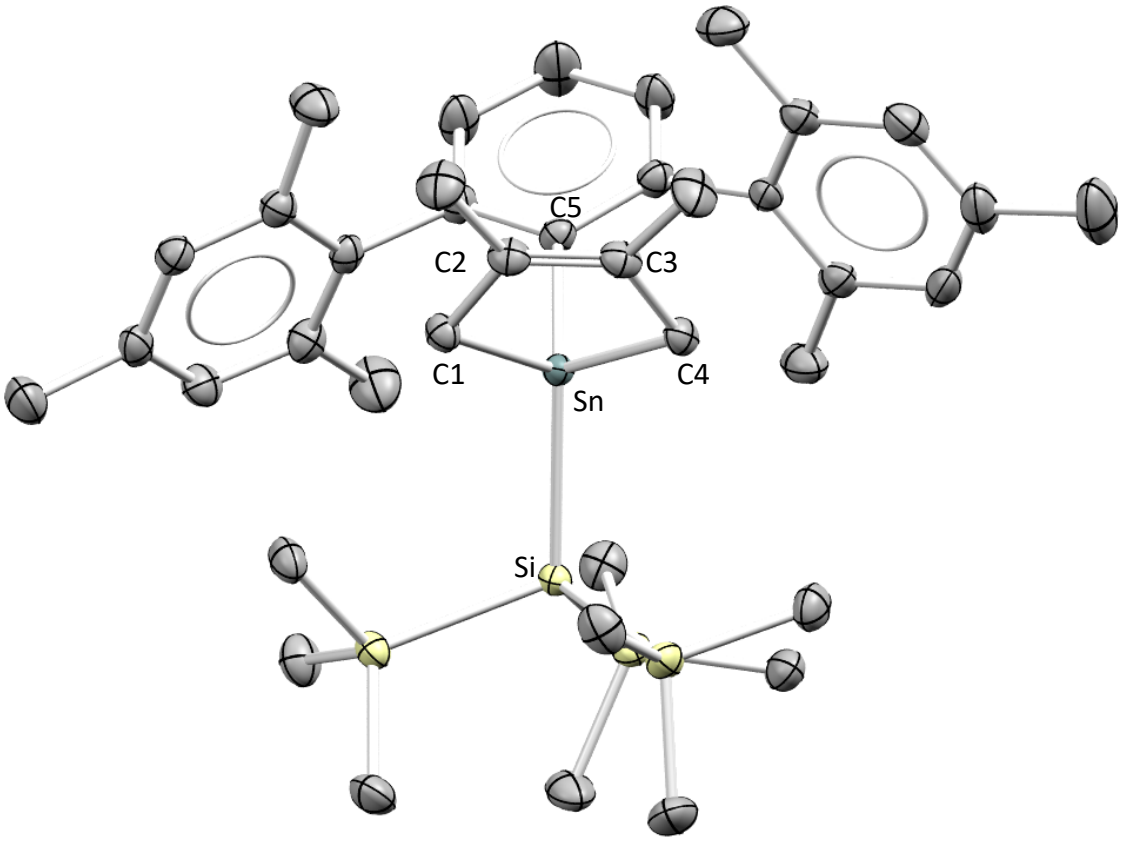


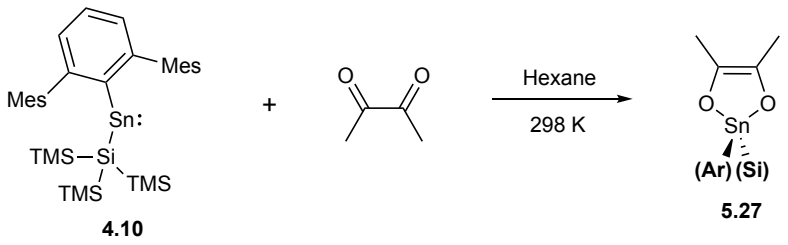
Figure 5-14: Molecular structure of **5.26** as determined by X-ray crystallography. The thermal ellipsoids are set to the 50% probability level. Hydrogen atoms are omitted for clarity. Key bond lengths (Å) and angles (°) not detailed in Table 5-5 above: Sn–Si: 2.6225(6), Sn–C5: 2.189(2), Si–Sn–C5: 121.33.

When the bulkier diene, 1,4-diphenylbutadiene, was reacted with **4.10**, no reaction was seen, even after prolonged heating at 353 K. It is reasonable to suggest that the greater bulk of the diene precluded sufficiently close enough approach to the stannylene to allow for orbital overlap.

5.2.4.3 Diketones

Diacetyl, MeC(O)C(O)Me, was added to a C_6D_6 solution of **4.10**, leading to an immediate colour change to orange. Analysis of the reaction mixture by NMR spectroscopy indicates that the expected [4+1]-cycloaddition product, **5.27**, is formed (Scheme 5-20). The ^{1}H NMR

spectrum displays new resonances which indicate that **5.27** possesses a plane of symmetry on the NMR timescale (e.g. a singlet resonance for the *o*-CH_3 groups of the flanking terphenyl ligand rings at 2.20 ppm; and a singlet for the C–H protons of the silyl ligand at 0.21 ppm) consistent with the expected cycloaddition product (Figure 5-15). A new singlet resonance at 1.90 ppm, which corresponds to the two methyl groups of the metallacycle, is also consistent with this assignment. The ^{119}Sn NMR spectrum features a resonance at 50.8 ppm, *i.e.* very similar to the resonances of the other [4+1]-cycloaddition products **5.24** and **5.26** (94.1 and -78.5 ppm respectively). Unfortunately, crystals suitable for X-ray crystallography could not be grown to confirm the connectivity of the species as **5.27** was found to decompose in solution even when maintained at 243 K.



Scheme 5-20: The [4+1]-cycloaddition of aryl(silyl)stannylene, **4.10**, with diacetyl (**(Ar)** is $–C_6H_3$-2,6-(C_6H_2-2,4,6-$Me_3)_2$ and **(Si)** is $–Si(SiMe_3)_3$).

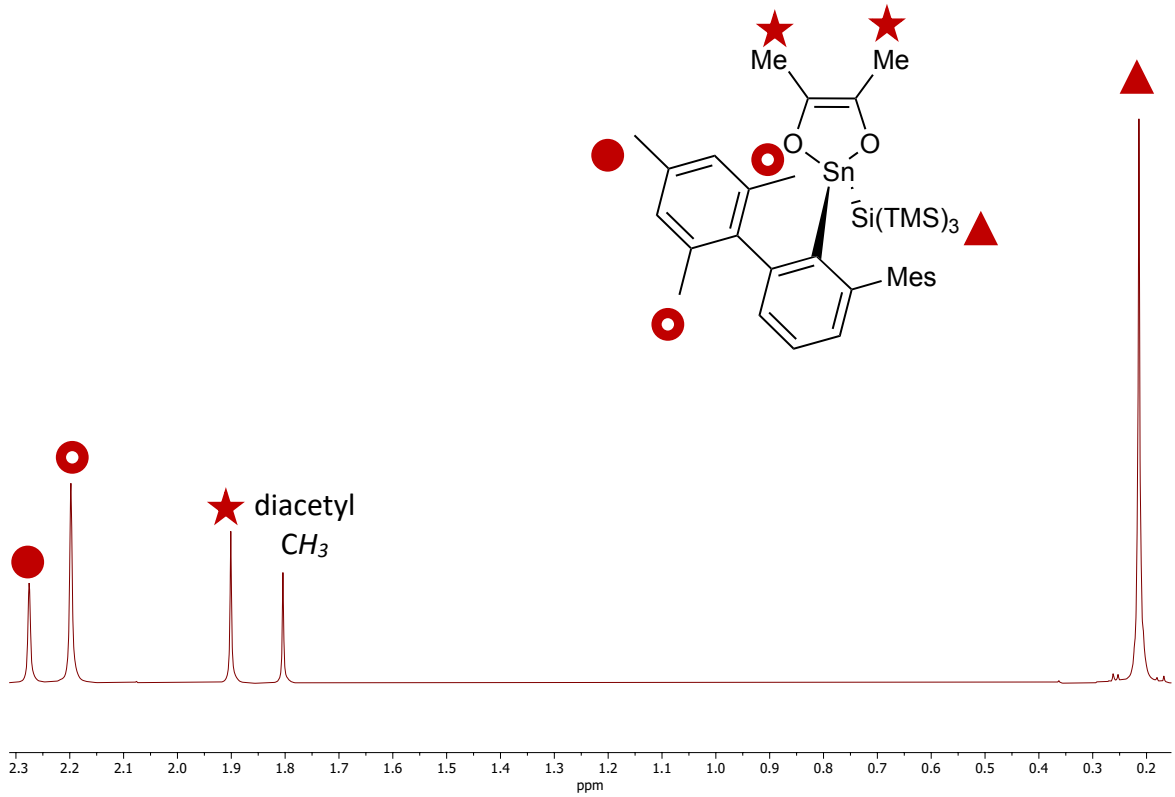
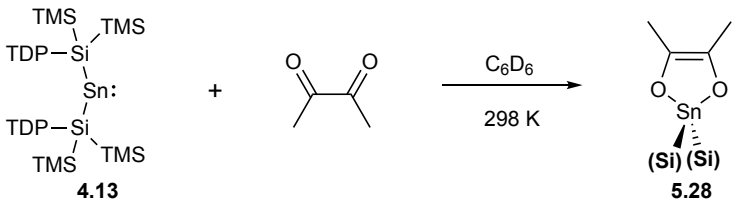


Figure 5-15: Excerpt from the ^{1}H NMR spectrum of the reaction between aryl(silyl)stannylene, **4.10**, and diacetyl.

The reaction between diacetyl and bis(silyl)stannylene, **4.13**, was also investigated. When the two reagents were combined, an immediate colour change to red was seen, and analysis of the product by ^{1}H NMR spectroscopy implied that a cycloaddition reaction had occurred (Scheme 5-21). A new singlet resonance in the ^{1}H NMR spectrum at 2.11 ppm (Figure 5-16) corresponds to the methyl groups of the resulting metallacycle, **5.28** (integrating as six protons with respect to the ligand resonances). Despite **5.28** also being unstable in solution, crystals suitable for X-ray diffraction were able to be grown at 243 K and allowed the proposed connectivity to be confirmed.



Scheme 5-21: The [4+1]-cycloadditon of bis(silyl)stannylene, **4.13**, with diacetyl (**(Si)** is $-Si(SiMe_3)_2(Si^tBuPh_2)$).

The molecular structure of **5.28** is depicted below (Figure 5-16). As suggested by the ^1H NMR data, **5.28** is the expected [4+1]-cycloaddition product. As with **5.24**, the metallacycle component of **5.28** adopts a planar conformation (sum of internal angles = 539.6°), as opposed to the envelope conformation seen in **5.26**. This is apparent from the torsion angles of 4.5(2)° and 4.6(2)° for Sn–O1–C1–C2 and Sn–O2–C2–C1, respectively. The Sn–O bond lengths measured for **5.28** (Sn–O1: 2.023(2) Å and Sn–O2: 2.023(1)) are slightly shorter than that of **5.24** (2.039(2) Å), potentially reflecting the reduced steric repulsion in **5.28**.

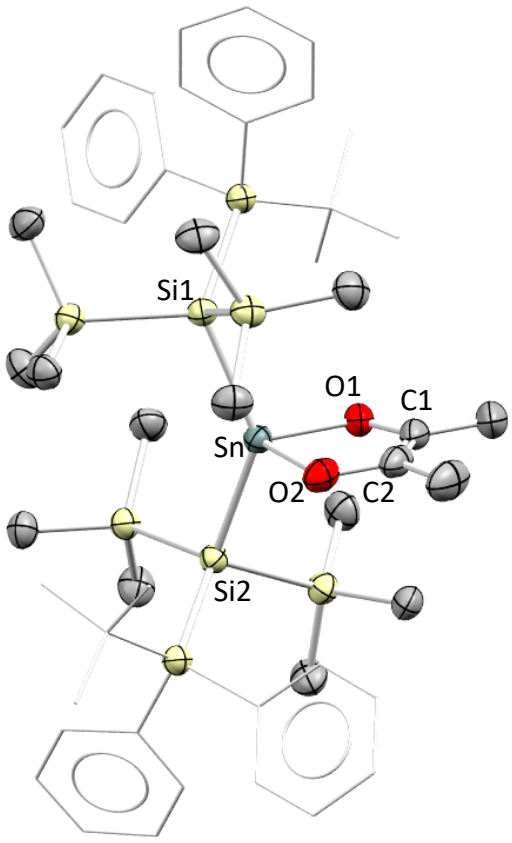


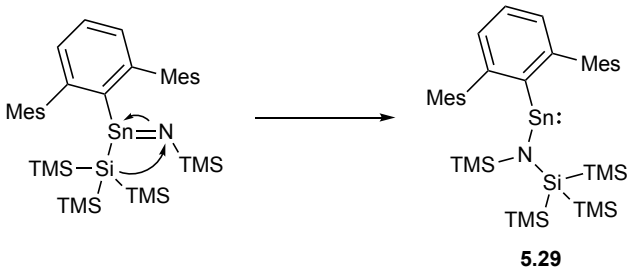
Figure 5-16: Molecular structure of **5.28** as determined by X-ray crystallography. The thermal ellipsoids are set to the 50% probability level. Hydrogen atoms are omitted for clarity. Phenyl and tert-butyl groups are depicted in wireframe for clarity. Key bond lengths (Å) and angles (°): Sn–Si1: 2.6491(6), Sn–Si2: 2.6314(5), Sn–O1: 2.023(2), Sn–O2: 2.023(1), C1–C2: 1.330(3), Si1–Sn–Si2: 139.71(2), O1–Sn–O2: 83.26(6).

5.2.5 Reactivity with Azides

Having documented the migratory ability of the Ge–Si bond of aryl(silyl)germylene, **1.23**, in Chapter 3, research was undertaken to see whether similar behaviour might occur with intrinsically weaker Sn–Si bonds. Initial studies with this goal focussed on the reactivity of **4.10** and **4.13** with organoazides, since it was thought that the transient stanna-imines, when formed, were likely to undergo migration chemistry.[12–14]

5.2.5.1 Trimethylsilylazide

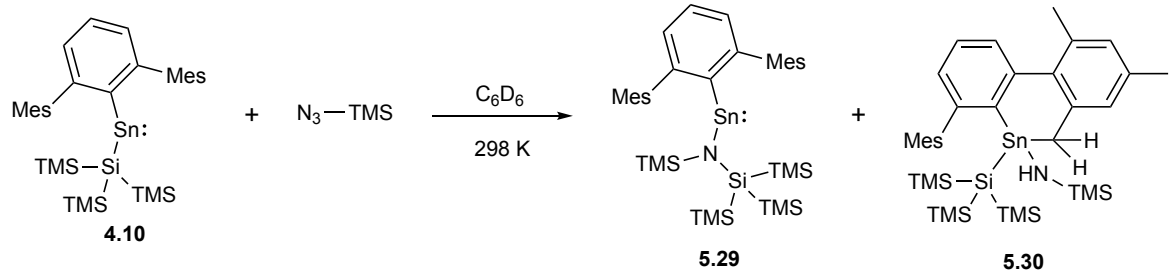
When trimethylsilylazide, $TMSN_3$, was added to a solution of **4.10**, a colour to change to yellow was observed with the concurrent evolution of gas. Analysis of the reaction mixture by ^{1}H NMR spectroscopy shows the formation of a major and minor species. The resonances of the major species, **5.29** (Scheme 5-23), have a similar distribution to **4.10** (e.g. one resonance corresponding to: *o*-CH_3 groups of the flanking terphenyl ligand rings at 2.31 ppm and a single signal for the *p*-CH_3 groups of the flanking terphenyl ligand rings at 2.18 ppm). This suggests that the symmetry of **5.29** (major product) is retained from the starting material, as would occur from the 1,2-migration of the silyl substituent (-Si($SiTMS_3$)$_3$) from Sn to N in a postulated stanna-imine intermediate (Scheme 5-22).



Scheme 5-22: Proposed mechanism of formation of the major product, **5.29**, of the reaction between aryl(silyl)stannylene **4.10** and $TMSN_3$.

However, further NMR evidence proved challenging to interpret due to persistent contamination of the minor species, **5.30** (Scheme 5-23). The lower solubility of **5.30** in aromatic solvents allowed it to be obtained in isolation, free from **5.29**, meaning that good quality characterisation data could be obtained. Analysis of **5.30** by ^{1}H NMR spectroscopy shows two doublet resonances (both integrating as one proton) in the aliphatic region of the ^{1}H NMR spectrum (at 2.88 ppm and 2.59 ppm), both of which possess ^{119}Sn satellites ($^2J_{Sn-H}$ = 93.8 and 36.7 Hz respectively). In addition, the presence of five singlet resonances

(2.30, 2.27, 2.23, 2.22, and 2.15 ppm), all integrating to three protons, in the aliphatic region corresponding to the other methyl groups of the terphenyl ligand, suggests that a C–H activation of one of the methyl groups has occurred. Further evidence for this hypothesis is provided in the ^{13}C NMR spectrum, in which a resonance at 27.3 ppm with ^{119}Sn satellites ($^{1}J_{Sn-C}$ = 250.7 Hz) indicates the presence of a Sn–C bond. It is known in the literature that transient stanna-imines can undergo intermolecular C–H activation, and these NMR data suggest that this has also occurred in the formation of **5.30**.[12] Crystals suitable for X-ray diffraction could be grown from both **5.29** and **5.30** and allow the proposed connectivity to be confirmed in each case.



Scheme 5-23: Reaction of aryl(silyl)stannylene, **4.10**, with trimethylsilyl azide to form **5.29** and **5.30**.

The molecular structure of **5.30** is depicted below (Figure 5-17). The tin centre is shown to feature a distorted tetrahedral coordination environment resulting from the C–H activation of one of the mesityl methyl groups across the Sn–N bond of a transient intermediate stanna-imine. **5.30** has shorter bonds to the aryl and silyl ligands than the parent stannylene **4.10** (Sn–C: **5.30**, 2.175(2) Å; **4.10**, 2.189(3) Å; Sn–Si: **5.30**, 2.5915(8) Å; **4.10**, 2.6407(7) Å). These two substituents are also spread further apart in angular terms (**5.30**: 125.04(5)°; **4.10**: 109.75(6)°), characteristic of the formation of a Sn(IV) species. In addition, the formed Sn–C and Sn–N bonds of **5.30** (2.172(2) Å and 2.044(1) Å respectively) are in good agreement

with the other crystallographically characterised example of C–H activation across a stanna-imine, *i.e.* **5.11** (Sn–C: 2.137(4) Å and Sn–N: 2.084(3) Å) (Scheme 5-11).[13]

Table 5-6: Selected bond lengths (Å) and angles (°) of **5.30** and **5.11**.[13]

	Sn–C2	**Sn–N**	**C2–Sn–N**
5.30	2.172(2)	2.044(1)	107.99(6)
5.11[13]	2.137(4)	2.084(3)	N/A

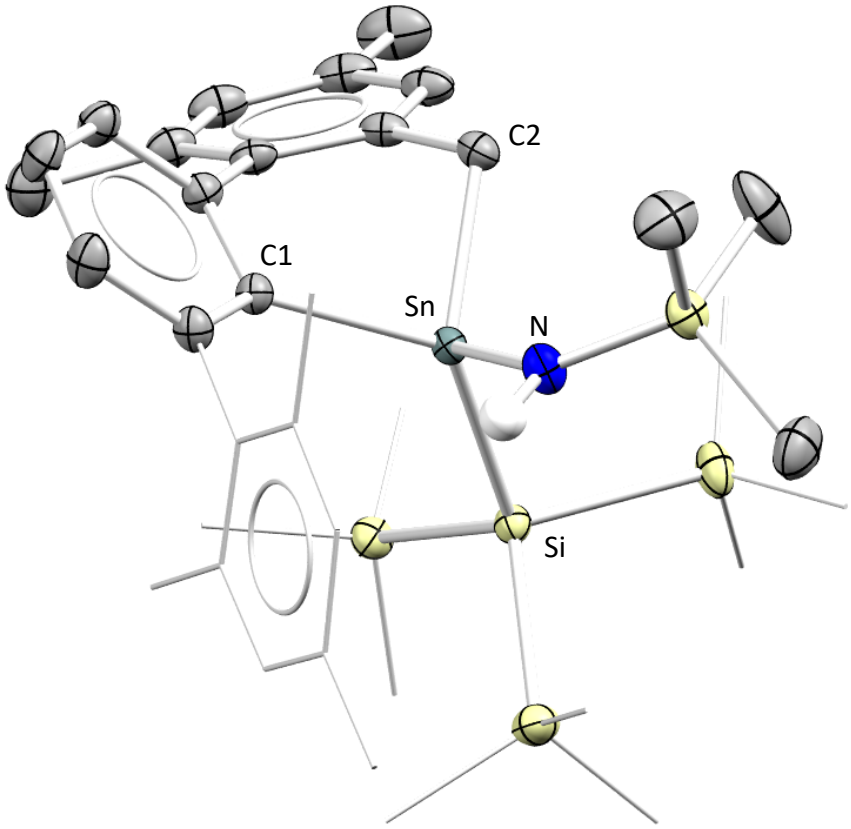


Figure 5-17: Molecular structure of **5.30** as determined by X-ray crystallography. The thermal ellipsoids are set to the 50% probability level. Hydrogen atoms (except for the N–H) are omitted for clarity. One of the flanking mesityl rings of the terphenyl ligand and the methyl groups of the hypersilyl ligand are depicted in wireframe

for clarity. Key bond lengths (Å) and angles (°): Sn–Si: 2.5915(8), Sn–C1: 2.175(2), Sn–C2: 2.172(2), Sn–N: 2.044(1), Si–Sn–C1: 125.04(5), N–Sn–C2: 107.99(6).

The molecular structure of **5.29** is depicted below (Figure 5-18). As stated above, **5.29** is thought to form *via* the migration of the silyl group from Sn to the N of the proposed stanna-imine intermediate. The bond lengths and angles of **5.29** are in close agreement with the two amido stannylenes synthesised above, **4.8** ($SnAr^{Mes}HMDS$) and **4.9** ($SnAr^{Dipp}HMDS$), as can be seen in Table 5-7 below. The wider C–Sn–N bond angle of **5.29** (112.23(8)°) is presumably due to the hypersilyl substituent being bulkier than the trimethylsilyl substituents found in **4.8** and **4.9**.

Table 5-7: Selected bond lengths (Å) and angles (°) of **5.29**, **4.8** and **4.9**.

	Sn–C	**Sn–N**	**C–Sn–N**
5.29	2.221(2)	2.092(2)	111.23(8)
4.8	2.242(4)	2.111(4)	103.6(1)
4.9	2.222(3)	2.074(9)	107.3(2)

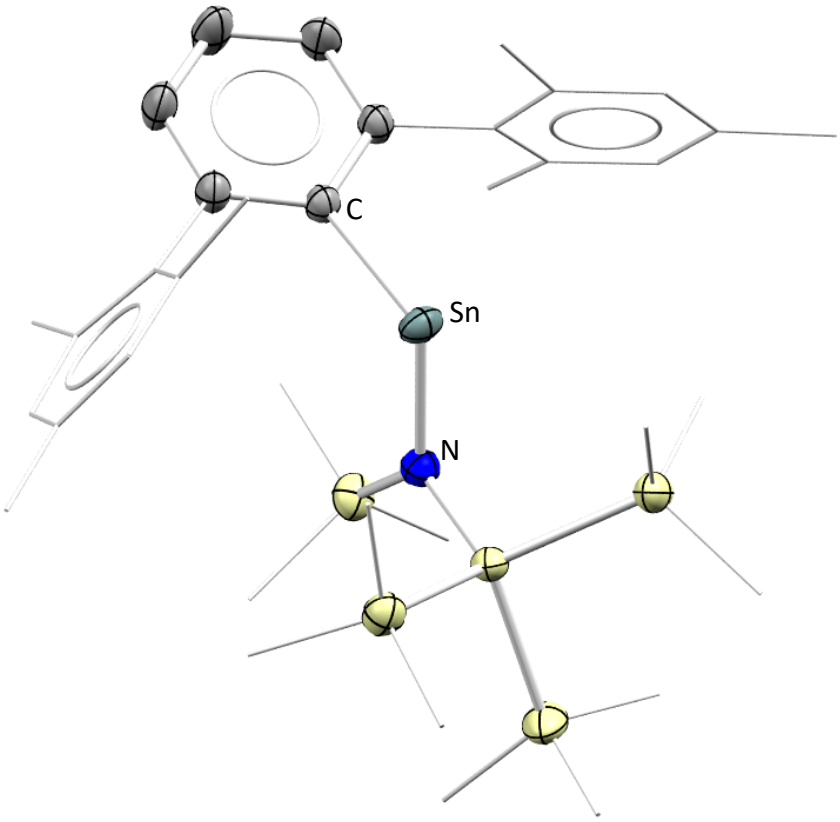
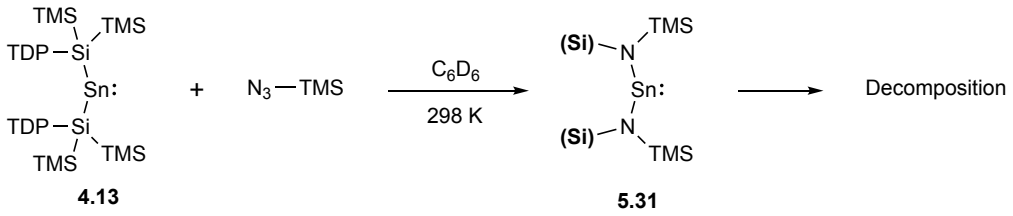


Figure 5-18: Molecular structure of **5.29** as determined by X-ray crystallography. The thermal ellipsoids are set to the 50% probability level. Hydrogen atoms are omitted for clarity. The flanking mesityl rings of the terphenyl ligand and the methyl groups of all the trimethylsilyl fragments are depicted in wireframe for clarity. Key bond lengths and angles are detailed in Table 5-6 above.

When an excess of $TMSN_3$ was added to a solution of bis(silyl)stannylene **4.13**, a colour change from brown to green was observed, accompanied by the release of a gas (presumably N_2) (Scheme 5-24). After 3 d, the reaction mixture underwent another colour change to yellow. Tracking the progress of the reaction by ^1H NMR spectroscopy suggests the initial product that formed, is the result of the reaction of **4.13** with two equivalents of $TMSN_3$ (Scheme 5-24) to form the bis(amido)stannylene ($Sn(N(TMS)(Si(TMS)_2(Si^tBuPh_2)))_2$) **5.31**. Two resonances are seen (at 1.22 ppm and 1.23 ppm), which correspond to the two *tert*-butyl groups of the silyl substituents ($Si(TMS)_2(Si^tBuPh_2)$) of **5.31**. These integrate in an equimolar ratio with two resonances at 0.38 ppm and 0.29 ppm which are proposed to correspond to

the trimethylsilyl groups of **5.31** (Scheme 5-19). However, after prolonged reaction times, these resonances disappear and a more complex array of signals grows in, suggesting that additional reactivity occurs. Unfortunately, so far all attempts to isolate the intermediates in this reaction have proved unsuccessful due to how readily **5.31** decomposes.



Scheme 5-24: Reaction of bis(silyl)stannylene, **4.13**, with trimethylsilylazide to form **5.31** which subsequently decays (**(Si)** is -Si(TMS)$_2$(Si^{t}BuPh$_2$)).

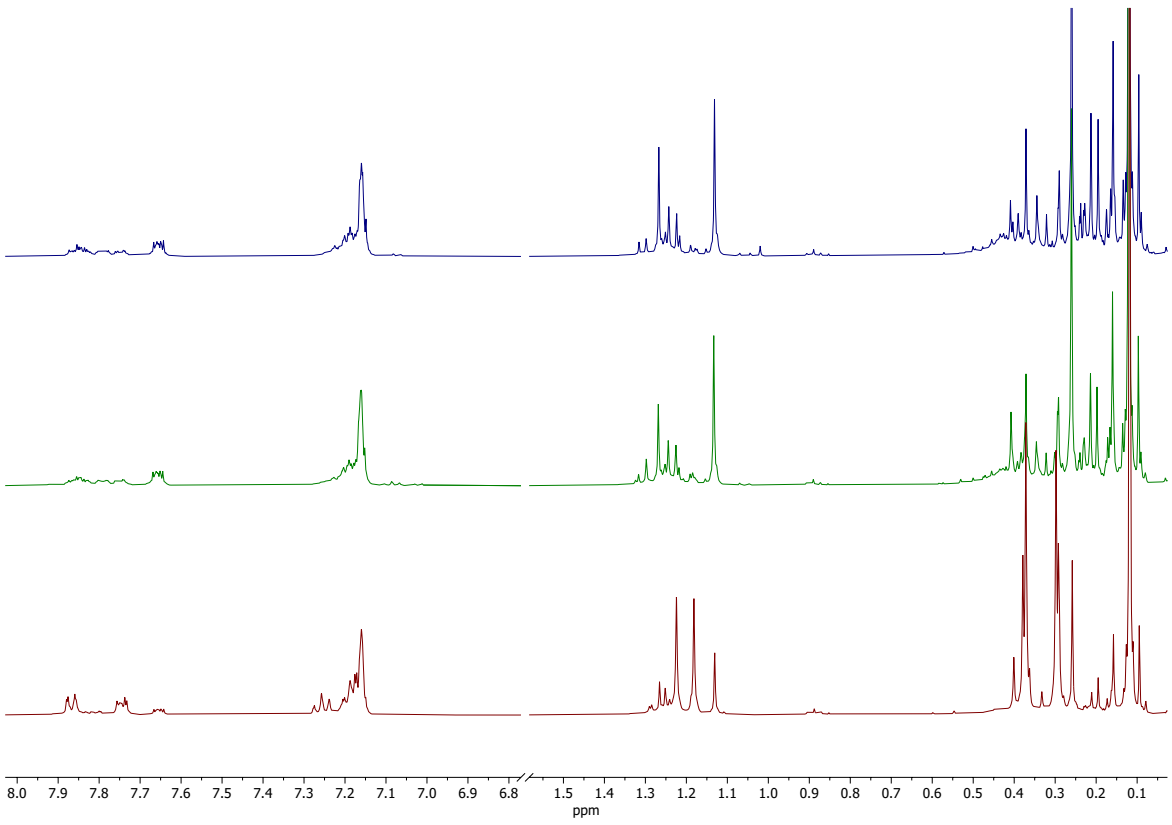
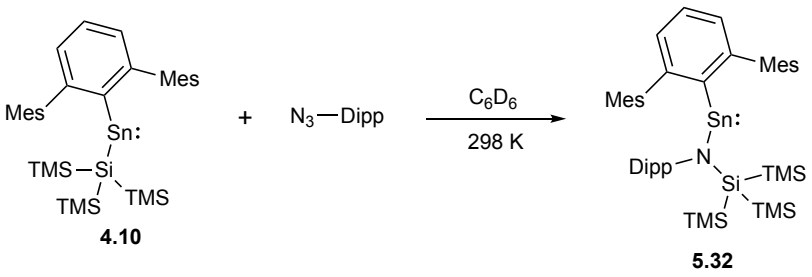


Figure 5-19: Signals in the ^{1}H NMR spectra of species present in the activation of TMSN$_3$: Top – Extract from a ^{1}H NMR spectrum of the reaction between **4.13** and TMSN$_3$ after twenty-four hours. Middle – Extract from a ^{1}H NMR spectrum of the reaction between **4.13** and TMSN$_3$ after twelve hours. Bottom – Extract from a ^{1}H NMR spectrum of the reaction between **4.13** and TMSN$_3$ immediately after combination.

5.2.5.2 Diisopropylphenylazide

The reaction of diisopropylphenyl azide, $DippN_3$, with **4.10**, leads to a colour change from teal to dark orange, accompanied by the release of a gas (presumably N_2) (Scheme 5-25). Analysis of the reaction mixture by ^1H NMR spectroscopy shows the formation of just one species, $SnAr^{Mes}N(Dipp)Si(TMS)_3$ (**5.32**), resulting from the migration of the silyl substituent from the Sn centre to the N of a proposed transient stanna-imine (Scheme 5-25). This is evidenced by the Ar^{Mes} ligand resonances of **5.32** (e.g. *para*-C*H*$_3$ of mesityl rings: 2.21 ppm) integrating in an equimolar ratio with the new septet resonance of the Dipp group (3.29 ppm) of **5.32**. The lack of C–H activation in this case is most likely due to the steric bulk of the azide preventing approach of the methyl group to the putative stanna-imine function. Single crystals suitable for X-ray crystallography could be grown from hexane and allow the proposed connectivity of **5.32** to be confirmed.



Scheme 5-25: Reaction of aryl(silyl)stannylene, **4.10**, with diisopropylphenyl azide.

The molecular structure of **5.32** is depicted below (Figure 5-20). As with compound **5.29** ($SnAr^{Mes}N(TMS)Si(TMS)_3$) above, **5.32** is thought to form by migration of the silyl substituent from Sn to the N of a transient stanna-imine. The bond lengths associated with the Sn centre of **5.32** are equal within error to those of **5.29** (Sn–C: **5.32**, 2.20(3) Å; **5.29**, 2.221(2) Å; Sn–N: **5.32**, 2.085(3) Å; **5.29**, 2.092(2) Å), whereas **5.32** has a slightly wider angle at the tin centre (**5.32**: 112.03(9)°; **5.29** 111.23(8)°) presumably due to the bulkier amide substituent.

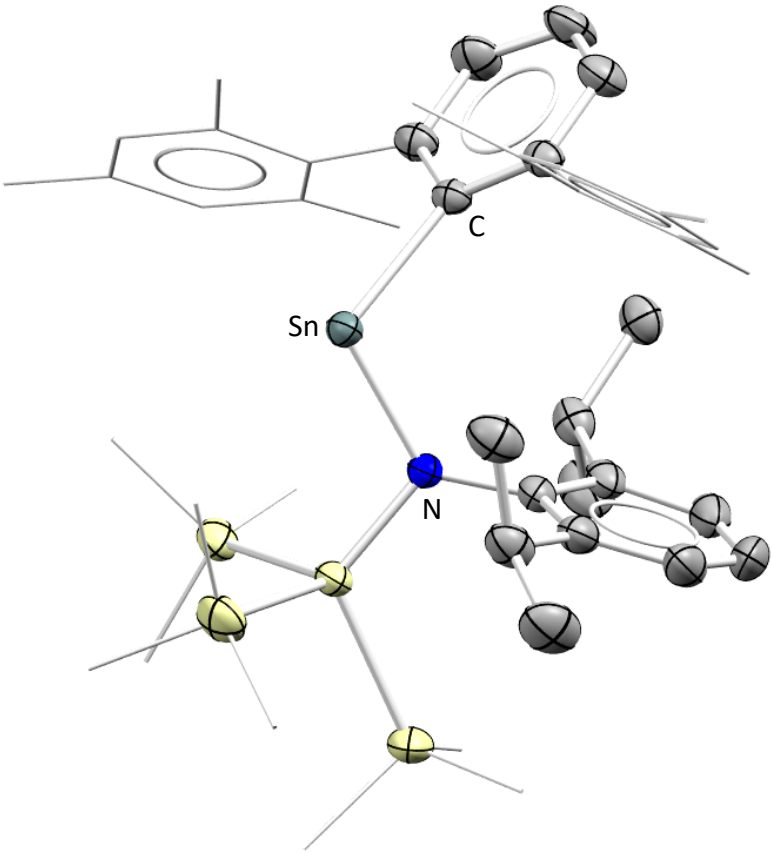
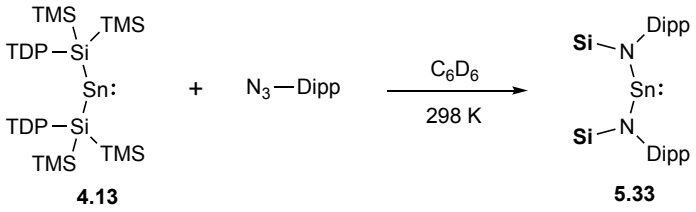


Figure 5-20: Molecular structure of **5.32** as determined by X-ray crystallography. The thermal ellipsoids are set to the 50% probability level. Hydrogen atoms are omitted for clarity. The flanking mesityl rings of the terphenyl ligand and the methyl groups of the hypersilyl ligand are depicted in wireframe for clarity. Key bond lengths (Å) and angles (°): Sn–C: 2.20(3), Sn–N: 2.085(3), C–Sn–N: 112.03(9).

The reaction of **4.13** with $DippN_3$ was also investigated because it was thought that the greater bulk of the azide would stabilise the product with respect to onward decomposition. Upon addition of $DippN_3$ to a C_6D_6 solution of **4.13,** a colour change from brown to green was observed. On this occasion the colour persists after 12 h. Tracking the reaction by ^1H NMR spectroscopy confirms that no significant decay of the initially formed resonances was observed. As with the reaction between **4.13** and $TMSN_3$ above (Scheme 5-24), it is thought that **4.13** reacts with two equivalents of $DippN_3$ to yield the bis(amido)stannylene ($Sn(N(Dipp)(Si(TMS)_2(Si^tBuPh_2)))_2$), **5.33**, (Scheme 5-26). This is evidenced by the new aliphatic Dipp resonances (septet CH: 3.74 ppm and doublet CH_3: 1.38 and 1.33 ppm) which integrate

in a 1:1 ratio with the silyl ligand resonances (e.g. the ^{t}Bu group of -Si(SiMe$_3$)$_2$(Si^{t}BuPh$_2$): 1.14 ppm; the TMS groups of -Si(SiMe$_3$)$_2$(Si^{t}BuPh$_2$): 0.11 ppm) (Figure 5-21). Unfortunately, attempts to isolate this product as a solid and obtain more conclusive characterisation data have proved unsuccessful due to the high solubility of **5.33** in organic solvents (HMDSO, pentane, hexane, and toluene).



Scheme 5-26: Reaction of bis(silyl)stannylene, **4.13**, with diisopropylphenyl azide.

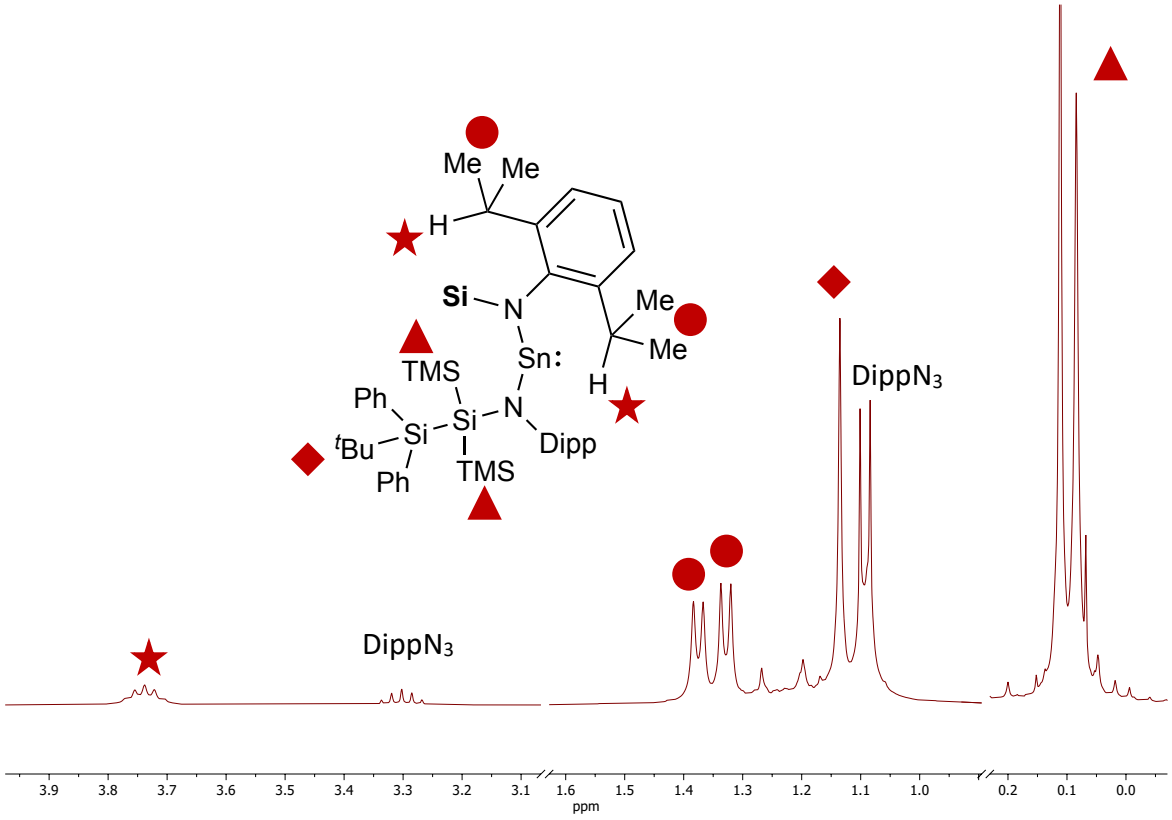
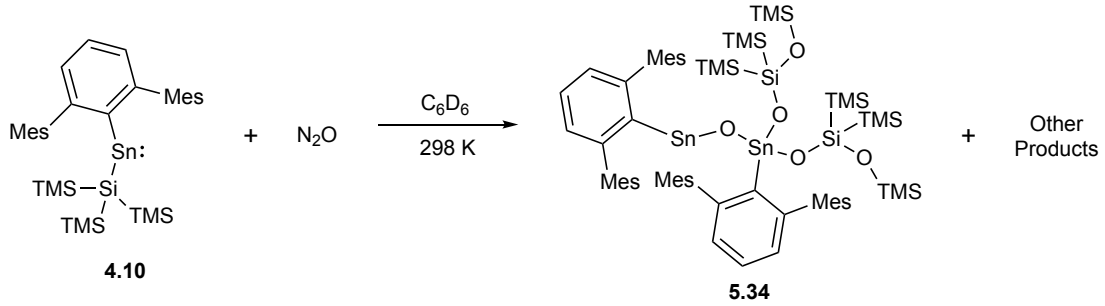


Figure 5-21: Excerpts from the ^{1}H NMR spectrum of the reaction between bis(silyl)stannylene, **4.13**, and diisopropylphenylazide.

5.2.6 Attempted Formation of a Stannanone

The reactions of **4.10** and **4.13** with azides serve to demonstrate the lability of the Sn–Si bond. To investigate whether the same migration chemistry would occur with transient Sn–O moieties, the reactions of **4.10** and **4.13** with N_2O were probed.

For both **4.10** and **4.13**, a C_6D_6 solution of the stannylene was exposed to one atmosphere of nitrous oxide at ambient temperature. An immediate colour change was observed with both **4.10** and **4.13**, as well as the release of a gas (presumably N_2), confirming that a reaction was occurring. Indeed, analysis of the reaction mixtures of **4.10** and **4.13** by ^{1}H NMR spectroscopy showed the formation of many species, the identities of which proved impossible to ascertain unequivocally. However, orange crystals suitable for X-ray diffraction could be grown from the reaction of **4.10** with N_2O (Scheme 5-27), which helps to elucidate why the NMR data proved so complex.



Scheme 5-27: Reaction of **4.10** with nitrous oxide to yield **5.34** as well as other products.

The molecular structure of **5.34** is depicted below (see Figure 5-22). As can be seen crystallographically, **5.34** is a mixed Sn(II)/Sn(IV) compound which results from the reaction of two and a half equivalents of N_2O with **4.10**. That oxygen can insert not only into the Sn–Si bond, but also into the Si–Si bonds of the hypersilyl ligand may explain why the NMR data obtained for the reaction mixtures of both **4.10** and **4.13** are so complicated. The differences

in geometric parameters for the two tin centres reflect their different oxidation states. Sn1 gives rise to longer Sn–C and Sn–O bond lengths than Sn2 (2.25(1) Å and 2.037(5) Å *vs.* 2.164(6) Å and 1.944(5) Å respectively) and features a smaller O–Sn–C angle (107.5(4)° *vs.* 119.4(2)°), as is expected for the larger Sn(II) atom. The mechanism of formation of **5.34** is unknown, however the first step of the reaction most likely involves the formation of a transient stannanone (*cf.* reactions with azides) which can then undergo tin to oxygen migration of a silyl group, driven thermodynamically by Si–O bond formation.

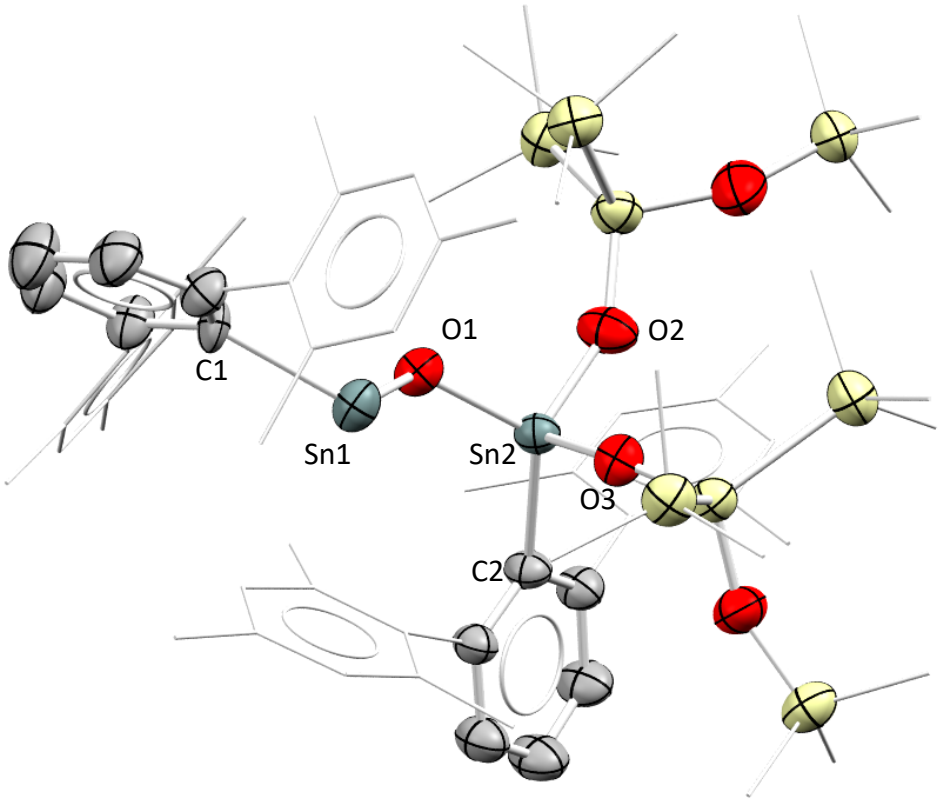
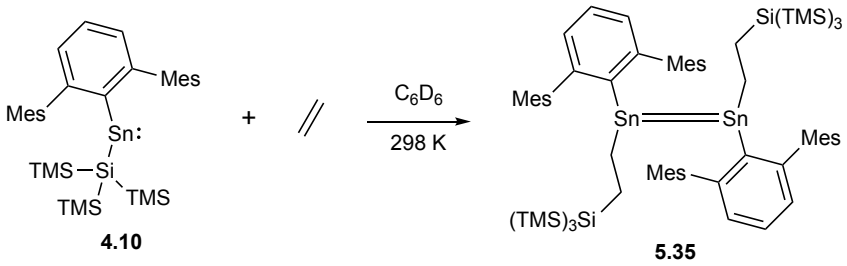


Figure 5-22: Molecular structure of **5.34** as determined by X-ray crystallography. The thermal ellipsoids are set to the 50% probability level. Hydrogen atoms are omitted for clarity. The flanking mesityl rings of the terphenyl ligands and the methyl groups of the trimethylsilyl fragments are depicted in wireframe for clarity. Key bond lengths (Å) and angles (°): Sn1–C1: 2.25(1), Sn1–O1: 2.037(5), Sn2–O1: 1.944(5), Sn2–C2: 2.164(6), Sn2–O2: 1.968(5), Sn2–O3: 1.928(5), C1–Sn1–O1: 107.5(4), C2–Sn2–O1: 119.4(2), O2–Sn2–O3: 102.0(2).

5.2.7 Reactivity with Alkenes

Having observed the lability of the Sn–Si bonds in both **4.10** and **4.13** to insertion of azides and nitrous oxide, their reactivity with alkenes was investigated. Due to its structural similarity to aryl(silyl)germylene, **1.23**, the reactivity of **4.10** with ethene was initially investigated. A C_6D_6 solution of **4.10** was exposed to one atmosphere of ethene at ambient temperature (Scheme 5-28). An immediate colour change to red was observed, followed by the precipitation of a red powder from the reaction mixture. The rapidity of the reaction and mildness of the conditions is a marked contrast to the reaction of the bis(aryl)stannylene, **1.6**, with ethene (Scheme 1-18) as reported by Power *et al.*, for which heating at 333 K for 12 h is required.[29] This difference in reactivity could be attributed to the narrower HOMO–LUMO gap of **4.10**. Analysis of the reaction mixture by ^{1}H NMR spectroscopy shows the growth of two new triplet resonances at 1.12 and 1.08 ppm, which arise from the -CH_2CH_2- chain resulting from ethene insertion into the Sn–Si bond. Crystals of the product suitable for X-ray crystallography could be grown, allowing the proposed connectivity of **5.35** to be confirmed.



Scheme 5-28: Insertion of ethene into the Sn–Si bond of aryl(silyl)stannylene, **4.10**, and subsequent dimerisation to form **5.35**.

The molecular structure of **5.35** is shown below (Figure 5-23). Key geometric parameters and related literature data for $[Sn(CHTMS_2)_2]_2$ (**5.1**), $[Sn(Si(TMS)_3)_2]_2$ (**1.9**), and $SnAr^{Dipp}(CH_2CH_2Ar^{Dipp})$ (**1.42**) are detailed in Table 5-8.[29–31] The structure of **5.35** confirms that

4.10 reacts in a similar fashion with ethene as **1.23** does ($GeAr^{Mes}Si(TMS)_3$) (Scheme 3-19), *i.e.* insertion of the alkene into the Sn–Si bond followed by dimerisation. As is observed for previously reported distannenes, **5.35** has a *trans*-bent structure (C4–Sn2–Sn1–C2 and C6–Sn2–Sn1–C1 torsion angles: 53.9(2)°), with each tin centre adopting a trigonal pyramidal coordination environment.[29–31] The Sn–Sn bond length of **5.35** is 2.7710(6) Å, which is similar to that measured for **5.1**, $[Sn(CHTMS_2)_2]_2$), (2.764(2) Å) (Scheme 5-1), and **1.9**, $[Sn(Si(TMS)_3)_2]_2$, (2.8247(6) Å) (Figure 1-11) (see Table 5-8).[30,31] The length of the C–C bond associated with the ethylene unit of **5.35** is 1.524(8) Å, which agrees with that reported for **1.42** ($SnAr^{Dipp}(CH_2CH_2Ar^{Dipp})$) by Power *et al.* (Scheme 1-18), (1.542(13) Å) and is indicative of a C–C single bond.[29]

Table 5-8: Selected bond lengths (Å), angles (°), and torsions (°) of **5.35** and other related literature compounds.[29–31]

	Sn1–Sn2	**C2–C3** **C5–C6**	**C4–Sn2–Sn1–C2** **C6–Sn2–Sn1–C1**	**C1–Sn1–C2** **C4–Sn2–C5**
5.35	2.7710(6)	1.524(8)	53.9(2)	107.0(2)
1.42[29]	N/A	1.542(13)	N/A	N/A
5.1[31]	2.764(2)	N/A	N/A	112.0
1.9[30]	2.8247(6)	N/A	28.6	120.46(4)

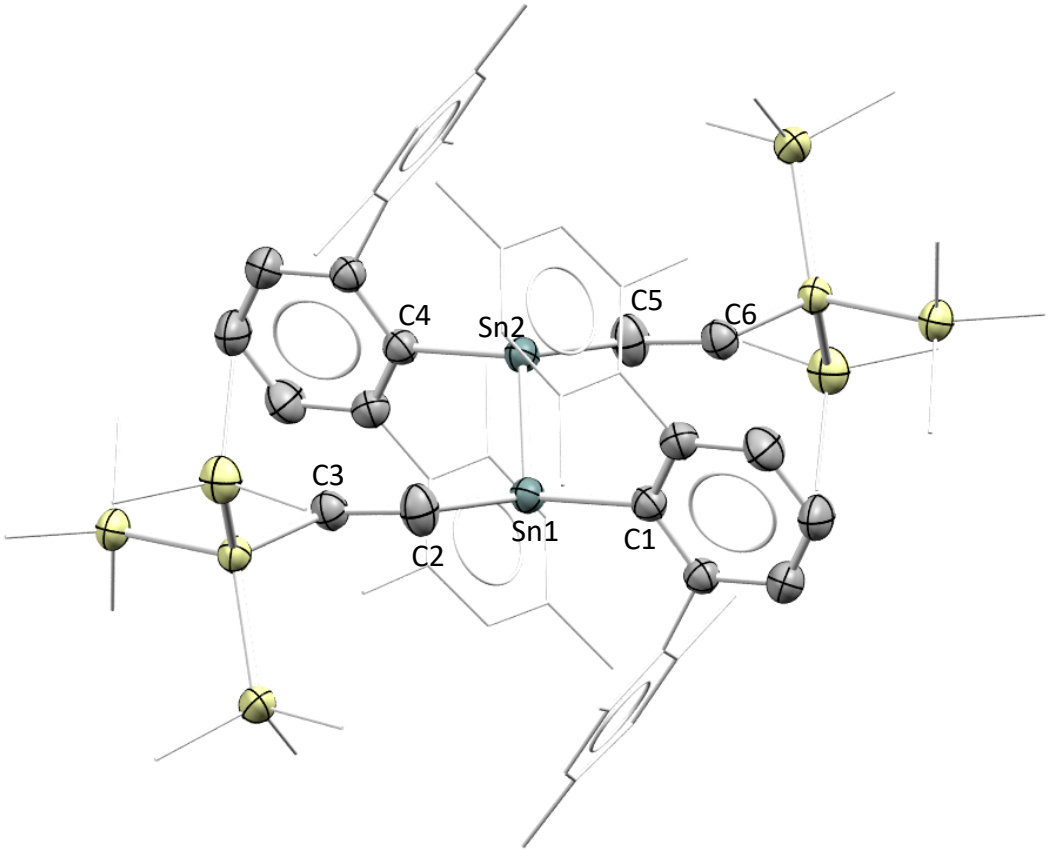


Figure 5-23: Molecular structure of **5.35** as determined by X-ray crystallography. The thermal ellipsoids are set to the 50% probability level. Hydrogen atoms are omitted for clarity. The flanking mesityl rings of the terphenyl ligands and the methyl groups of the hypersilyl ligands are depicted in wireframe for clarity. Key bond lengths are detailed above in Table 5-6.

The reactivity of **4.10** with bulkier alkenes (cyclopentene, *tert*-butylethylene, and norbornene) was also investigated since it was hoped that the stannylenes resulting from insertion would remain monomeric, as observed in the insertion of norbornene into the Ge–Si bond of aryl(silyl)germylene **1.23** ($GeAr^{Mes}Si(TMS)_3$) to yield monomeric **3.14** (Scheme 3-20). However, no reactivity was observed with any of the alkenes with **4.10**, even when more forcing conditions were employed. The greater steric bulk of these alkenes could explain the lack of reactivity. In their 2019 work, Power *et al.* proposed a mechanism for the reaction of **1.6** with ethene, in which pre-coordination of the alkene to the empty p-orbital on the stannylene is the first mechanistic step (see Scheme 1-17).[29] With this mechanism in mind, it

makes sense that this pre-coordination would be more disfavoured as the steric bulk of the alkene increases, and therefore why no reactivity is observed.

5.3 Conclusions

In this chapter, the reactivity of some novel stannylenes towards small molecules has been explored. The reactions between **4.10** ($SnAr^{Mes}Si(TMS)_3$) and smaller amines (NH_3 and $MeNH_2$) resulted in the formation of Sn(II) bridged amido species, **1.30** ($[SnAr^{Mes}NH_2]_2$) and **5.13** ($[SnAr^{Mes}NHMe]_2$), rather than the corresponding N–H oxidative addition products. When **4.10** was reacted with $^{s}BuNH_2$, only adduct formation occurred, yielding **5.14** ($^{s}BuNH_2{\cdot}SnAr^{Mes}Si(TMS)_3$). Even when **4.13** ($Sn(Si(TMS)_2(Si^{t}BuPh_2))_2$) was reacted with ammonia, with its two strong sigma donating silyl ligands, the oxidative addition products were still not seen and only the protonated ligand **5.15** ($HSi(TMS)_2(Si^{t}BuPh_2)$) could be identified. The ability of **4.10** to act as a Lewis base was confirmed by the formation of the adduct, **5.16** ($W(CO)_5{\cdot}SnAr^{Mes}Si(TMS)_3$), however a comparison of donor strength with **4.13** could not be achieved due to the instability of **4.13** at elevated temperatures which precludes coordination at tungsten. However, **4.13** was found to be able to oxidatively add an Au–Cl bond to yield **5.17** ($(PPh_3Au)(Cl)Sn(Si(TMS)_2(Si^{t}BuPh_2))_2$. The reactivity of **4.10** and **4.13** with DMAP and $^{t}BuNC$ was also explored, resulting in coordination of the Lewis bases to the formally vacant 5p-orbitals of **4.10** and **4.13**. **4.10** was found to be capable of [4+1]-cycloadditions with unsaturated systems (methylisopropenyl ketone (**5.23**), methylstyryl ketone (**5.24**), butadiene (**5.26**), and MeC(O)C(O)Me (**5.27**)). Similarly, **4.13** was found to be capable of [4+1]-cycloadditions with methylstyryl ketone (**5.25**) and MeC(O)C(O)Me (**5.28**). The reaction between **4.10** and $TMSN_3$ was found to yield two products: the aryl(amido)stannylene **5.29** ($SnAr^{Mes}N(TMS)(Si(TMS)_3)$) and the mesityl ligand

C–H activation product **5.30** ($SnSi(TMS)_3(NH(TMS)(Ar^{Mes}\text{-}CH_2))$), both of which are thought to form *via* the onward reaction of a putative stanna-imine intermediate. When **4.10** reacts with the bulkier azide, $DippN_3$, only the aryl(amido)stannylene, **5.32**, ($SnAr^{Mes}N(Dipp)(Si(TMS)_3)$) is observed. **4.13** also reacts with $DippN_3$ to yield the bis(amido)stannylene **5.33** ($Sn(N(Dipp)(Si(TMS)_2(Si^tBuPh_2)))_2$), resulting from the uptake of two equivalents of azide. Finally, **4.10** was found to be capable of the insertion of ethene into the Sn–Si bond, which was then followed by dimerisation to yield distannene **5.35** ($[SnAr^{Mes}(CH_2CH_2Si(TMS)_3)]_2$).

5.4 Characterisation of Novel Materials

5.4.1 Reaction of $SnAr^{Mes}Si(TMS)_3$ with Methylamine (Scheme 5-6)

To a solution of **4.10** (40 mg, 0.059 mmol) in THF (1.5 mL) was added a THF solution of methylamine (30 μL, 2.0 M) at room temperature with stirring. A colour change to yellow was seen immediately and the reaction was stirred at room temperature for 30 min. Volatiles were removed *in vacuo* and the resulting yellow residue extracted into hexane. The solution was concentrated to incipient crystallisation and stored at 243 K to afford crystals of the product, **5.13**, suitable for X-ray crystallography. **5.13** was also characterised by ^{1}H NMR spectroscopy. ^{1}H NMR (400 MHz, C_6D_6, 298 K) δ: 7.20 (t, *p*-C*H* Ar^{Mes}, $^3J_{HH}$ = 7.5 Hz, 1H), 6.86 (d, *m*-C*H* Ar^{Mes}, $^3J_{HH}$ = 7.5 Hz, 2H), 6.81 (s, Mes-C*H* 4H), 2.23–2.18 (m, Mes-CH_3, 18H), 1.62 (q, N*H*Me, $^3J_{HH}$ = 6.7 Hz, 1H), 1.25 (d, NHCH_3, $^3J_{HH}$ = 6.8 Hz, 3H).

5.4.2 Synthesis of $SnAr^{Mes}Si(TMS)_3{\cdot}NH_2{}^sBu$, **5.14** (Scheme 5-7)

To a solution of **4.10** (20 mg, 0.029 mmol) in toluene (0.20 mL) was added *sec*-butylamine (0.10 mL, 0.99 mmol) at room temperature. The reaction mixture was stirred for 30 min before being cooled to 243 K, whereupon the product could be isolated cleanly as orange

crystals. ^{1}H NMR (400 MHz, C_6D_6, 298 K) δ: 7.28 (t, *p*-C*H* Ar^{Mes}, $^{3}J_{HH}$ = 7.5 Hz, 1H), 6.96 (d, *m*-C*H* Ar^{Mes}, $^{3}J_{HH}$ = 7.5 Hz, 2H), 6.81 (s, Mes-C*H*, 4H), 2.35 (s, Mes-C*H*$_3$, 12H), 2.16 (s, Mes-C*H*$_3$, 6H), 1.29–1.17 (m, ^{s}Bu-*H*, 1H), 1.10 (s, ^{s}Bu-*H*, 2H), 1.05–0.94 (m, ^{s}Bu-*H*, 1H), 0.82 (d, ^{s}Bu-*H*, $^{3}J_{HH}$ = 6.4 Hz, 3H), 0.66 (t, ^{s}Bu-*H*, $^{3}J_{HH}$ = 7.4 Hz, 3H), 0.31 (s, Si(SiC*H*$_3$)$_3$, 27H) ppm. ^{13}C NMR (101 MHz, C_6D_6, 298 K) δ 146.8, 138.6, 135.2, 134.6, 127.5, 127.0, 126.4, 126.2, 48.4, 30.3, 20.1, 19.3, 8.7, 3.5 ppm.

5.4.3 Synthesis of $SnAr^{Mes}Si(TMS)_3{\cdot}W(CO)_5$, **5.16** (Scheme 5-9)

4.10 (15 mg, 0.022 mmol) and $W(CO)_5(NMe_3)$ (8.9 mg, 0.023 mmol) were combined in an NMR tube equipped with a J-Young valve and C_6D_6 (0.40 mL) was added. The reaction mixture was heated at 353 K for 24 h. Volatiles were removed *in vacuo* and the residue extracted into hexane. Slow evaporation of the hexane solution afforded the product as red crystals suitable for X-ray crystallography. ^{1}H NMR (500 MHz, C_6D_6, 298 K) δ: 7.23 (t, *p*-C*H* Ar^{Mes}, $^{3}J_{HH}$ = 7.5 Hz, 1H), 6.93 (d, *m*-C*H* Ar^{Mes}, $^{3}J_{HH}$ = 7.6 Hz, 2H), 6.84 (s, Mes-C*H*, 2H), 6.76 (s, Mes-C*H*, 2H), 2.44 (s, Mes-C*H*$_3$, 3H), 2.26 (s, Mes-C*H*$_3$, 3H), 2.10 (s, Mes-C*H*$_3$, 3H), 0.25 (s, Si(SiC*H*$_3$)$_3$, 27H) ppm. ^{13}C NMR (126 MHz, C_6D_6, 298 K) δ: 201.5, 198.2, 144.1, 137.1, 136.0, 135.8, 134.5, 129.5, 129.2, 128.7, 128.5, 127.2, 22.6, 21.3, 19.9, 4.0 ppm. ^{119}Sn NMR (187 MHz, C_6D_6, 298 K) δ: 1954.7 ppm.

5.4.4 Reaction of $Sn(Si(TMS)_2(Si^tBuPh_2))_2$ with $AuPPh_3Cl$ (Scheme 5-11)

4.13 (30 mg, 0.031 mmol) and $AuPPh_3Cl$ (16 mg, 0.031 mmol) were combined in an NMR tube equipped with a J-Young valve and C_6D_6 (0.40 mL) was added. The reaction mixture was stored at room temperature for 12 h. Volatiles were removed *in vacuo* and the residue extracted into hexane. The resulting suspension was filtered and the product, **5.17**, isolated as brown

crystals suitable for X-ray diffraction by slow evaporation of filtrate. **5.17** was also characterised by *in situ* ^{1}H and ^{31}P NMR spectroscopy. ^{1}H NMR (400 MHz, C_6D_6, 298 K) δ: 8.04–7.92 (m, Ar*H*, 8H), 7.54–7.47 (m, Ar*H*, 8H), 7.27–7.21 (m, Ar*H*, 4H), 7.14–6.98 (m, Ar*H*, 15H), 1.46 (s, ^{t}Bu-*H*, 18H), 0.40 (s, Si(SiC*H*$_3$)$_3$, 18H), 0.39 (s, Si(SiC*H*$_3$)$_3$, 18H) ppm. ^{31}P NMR (162 MHz, C_6D_6, 298 K) δ: 46.6 ppm.

5.4.5 Synthesis of SnAr^{Mes}Si(TMS)$_3$(C(H$_2$)C(Me)C(Me)O), **5.23** (Scheme 5-15)

Excess methyl isopropenyl ketone (11 μL, 0.11 mmol) was added to a suspension of **4.10** (33 mg, 0.049 mmol) in C_6D_6 (0.40 mL), leading to an immediate colour change from teal to pale yellow. Removal of volatiles *in vacuo* afforded the product as a pale yellow solid. ^{1}H NMR (600 MHz, C_6D_6, 298 K) δ: 7.21 (t, *p*-C*H* Ar^{Mes}, $^{3}J_{HH}$ = 7.5 Hz, 1H), 6.89 (d, *m*-C*H* Ar^{Mes}, $^{3}J_{HH}$ = 7.5 Hz, 2H), 6.88 (br. d, Mes-C*H*, 4H), 2.24 (s, Mes-C*H*$_3$, 6H), 2.15 (br. d, Mes-C*H*$_3$, 12H), 1.97 (s, Sn-C*H*,1H), 1.78 (m, C(C*H*3), 6H), 1.14 (s, Sn-C*H*, 1H), 0.22 (s, Si(SiC*H*$_3$)$_3$, 27H) ppm. ^{13}C NMR (151 MHz, C_6D_6, 298 K) δ: 153.6, 149.4, 146.9, 140.6, 137.0, 129.9, 129.0, 128.9, 128.6, 98.5, 29.8, 22.0, 22.0, 20.9, 19.6, 18.3, 3.7 ppm. ^{29}Si NMR (79 MHz, C_6D_6, 298 K) δ: −6.3, −109.4 ppm. ^{119}Sn NMR (149 MHz, C_6D_6, 298 K) δ: 72.6 ppm.

5.4.6 Synthesis of SnAr^{Mes}Si(TMS)$_3$(C(H)(Ph)C(H)C(Me)O), **5.24** (Scheme 5-16)

4.10 (96 mg, 0.14 mmol) and methyl styryl ketone (21 mg, 0.14 mmol) were combined as solids, toluene (5.0 mL) added, and the reaction mixture stirred at room temperature for 1 h. Over this time, the reaction mixture become pale yellow in colour. Volatiles were removed *in vacuo* and the residue extracted into hexane. The hexane solution was concentrated to incipient crystallisation and stored at 243 K to yield the product as pale-yellow crystals suitable for X-ray crystallography. Yield: 68 mg, 58 %. ^{1}H NMR (600 MHz, C_7D_8, 298 K) δ: 7.17

(t, *p*-C*H* Ar^{Mes}, $^{3}J_{HH}$ = 7.5 Hz, 1H), 7.08 (d, Ar*H*, $^{3}J_{HH}$ = 7.5 Hz, 1H), 7.02 (t, Ar*H*, $^{3}J_{HH}$ = 7.5 Hz, 2H), 6.97 (d, Ar*H*, $^{3}J_{HH}$ = 7.5 Hz, 1H), 6.88 (t, Ar*H*, $^{3}J_{HH}$ = 7.5 Hz, 1H), 6.95 – 6.72 (m, Mes-C*H*, 4H), 6.60 (d, *m*-C*H* Ar^{Mes}, $^{3}J_{HH}$ = 7.5 Hz, 2H), 4.70 (s, C(Me)-C*H*, 1H), 3.96 (s, Sn-C*H* 1H), 2.32 (br. d, Mes-CH_3, 6H), 2.31 (s, Mes-CH_3, 6H), 2.03 (br. d, Mes-CH_3, 6H), 1.67 (d, C(CH_3), 3H), 0.07 (s, Si(SiCH_3)$_3$, 27H) ppm. ^{13}C NMR (151 MHz, C_7D_8, 298 K) δ: 163.5, 148.0, 146.9, 137.7, 137.4, 129.7, 129.3, 129.1, 128.4, 128.2, 128.1, 128.0, 125.6, 124.5, 97.2, 46.9, 24.4, 24.3, 21.9, 21.7, 21.1, 20.8, 4.1, 4.0 ppm. ^{29}Si NMR (79 MHz, C_7D_8, 298 K) δ: −6.5, −100.0 ppm. ^{119}Sn NMR (149 MHz, C_7D_8, 298 K) δ: 94.1 ppm.

5.4.7 Reaction of $Sn(Si(TMS)_2(Si^tBuPh_2))_2$ with PhC(H)C(H)COMe (Scheme 5-17)

To a solution of **4.13** (14 mg, 0.015 mmol) in C_6D_6 (0.40 mL) was added methyl styryl ketone (2.2 mg, 0.015 mmol). A colour change from dark brown to orange was observed over 5 min. The product, **5.25**, was characterised by *in situ* ^{1}NMR spectroscopy. ^{1}H NMR (400 MHz, C_6D_6, 298 K) δ: 7.90–7.86 (m, Ar*H*, 4H), 7.82–7.78 (m, Ar*H*, 2H), 7.65–7.60 (m, Ar*H*, 2H), 7.55–7.50 (m, Ar*H*, 2H), 7.28 (s, Ar*H*, 1H), 7.13–7.09 (m, Ar*H*, 6H), 7.04–6.99 (m, Ar*H*, 8H), 5.03 (s, Sn–C*H*, 1H), 4.98 (s, C=C*H*, 1H), 1.88 (s, C=C(CH_3), 3H), 1.31 (s, ^{t}Bu-*H*, 9H), 1.11 (s, ^{t}Bu-*H*, 9H), 0.45 (s, SiCH_3, 9H), 0.36 (s, SiCH_3, 9H), 0.29 (s, SiCH_3, 9H), 0.19 (s, SiCH_3, 9H) ppm.

5.4.8 Synthesis of $SnAr^{Mes}Si(TMS)_3(C(H_2)C_2Me_2C(H_2))$, 5.26 (Scheme 5-19)

To a solution of **4.10** (85 mg, 0.13 mmol) in toluene (5.0 mL) was added excess 2,3-dimethyl-1,3-butadiene (0.02 mL, 0.18 mmol). The reaction mixture was stirred for 3 d at room temperature, during which time it decolourised. Removal of the volatiles *in vacuo* afforded the product as an off-white powder. Crystals of **5.26** suitable for X-ray crystallography could be obtained by storage of a concentrated hexane solution at 280 K.

Yield: 29 mg, 30 %. ^{1}H NMR (600 MHz, C_6D_6, 298 K) δ: 7.20 (t, *p*-C*H* Ar^{Mes}, $^{3}J_{HH}$ = 7.5 Hz, 1H), 6.91 (s, Mes-C*H*, 4H), 6.89 (d, *m*-C*H* Ar^{Mes},$^{3}J_{HH}$ = 7.5 Hz, 2H), 2.24 (s, Mes-CH_3, 6H), 2.17 (s, Mes-CH_3, 12H), 1.75 (s, C(CH_3), 6H), 1.62 (d, Sn-CH_2, $^{2}J_{HH}$ = 15.4 Hz, 2H), 1.34 (d, Sn-CH_2, $^{2}J_{HH}$ = 15.4 Hz, 2H), 0.24 (s, Si(SiCH_3)$_3$, 27H) ppm. ^{13}C NMR (151 MHz, C_6D_6, 298 K) δ: 150.5, 142.5, 142.1, 136.8, 136.4, 131.9, 128.8, 128.7, 128.4, 28.5, 22.8, 21.2, 21.2, 4.4 ppm. ^{29}Si NMR (79 MHz, C_6D_6, 298 K) δ: −7.1, −122.7 ppm. ^{119}Sn NMR (149 MHz, C_6D_6, 298 K) δ: -78.5 ppm.

5.4.9 Synthesis of Sn(Ar^{Mes})(Si(TMS)$_3$)(OC_2Me_2O), **5.27** (Scheme 5-20)

To a stirred solution of **4.10** (100 mg, 0.15 mmol) in hexane (5.0 mL) was added an excess of MeC(O)C(O)Me (15 μL, 0.17 mmol), which was accompanied by an immediate colour change from teal to orange. After stirring for 1 h, the reaction mixture was concentrated to incipient crystallisation and then stored at 280 K to afford the product as orange crystals suitable for X-ray crystallography. ^{1}H NMR (400 MHz, C_6D_6, 298 K) δ: 7.21 (t, *p*-C*H* Ar^{Mes}, $^{3}J_{HH}$ = 7.5 Hz, 1H), 6.92 (s, Mes-C*H*, 4H), 6.92 (d, *m*-C*H* Ar^{Mes}, $^{3}J_{HH}$ = 7.5 Hz, 2H), 2.28 (s, Mes-CH_3, 6H), 2.20 (s, Mes-CH_3, 12H), 1.90 (s, C(CH_3), 6H), 0.22 (s, SiCH_3, 27H) ppm. ^{13}C NMR (151 MHz, C_6D_6, 298 K) δ: 151.2, 148.5, 142.0, 139.3, 136.6, 132.6, 130.3, 128.5, 128.1, 21.8, 21.3, 16.4, 2.7 ppm. ^{29}Si NMR (79 MHz, C_6D_6, 298 K) δ: −16.4, −96.1 ppm. ^{119}Sn NMR (149 MHz, C_6D_6, 298 K) δ: 50.8 ppm.

5.4.10 Reaction of Sn(Si(TMS)$_2$(Si^{t}BuPh$_2$))$_2$ with MeC(O)C(O)Me (Scheme 5-21)

To a solution of **4.13** (23 mg, 0.024 mmol) in C_6D_6 (0.40 mL) was added MeC(O)C(O)Me (0.10 mL, 1.2 mmol). An immediate colour change from brown to red was observed and the reaction mixture stirred for 30 min. Volatiles were removed *in vacuo* and the residue redissolved in minimal pentane. The resulting suspension was filtered and the product, **5.28**,

obtained as red crystals suitable for X-ray crystallography, by the slow evaporation of the solvent from the filtrate. **5.28** was also characterised by *in situ* ^{1}H NMR spectroscopy. ^{1}H NMR (400 MHz, C_6D_6 , 298 K) δ: 7.90–7.82 (m, Ar*H*, 8H), 7.29–7.15 (m, Ar*H*, 12H), 2.11 (s, C(C*H*$_3$), 6H), 1.30 (s, ^{t}Bu-*H,* 18H), 0.32 (m, Si(SiC*H*$_3$)$_3$, 36H) ppm.

5.4.11 Synthesis of Sn(Ar^{Mes})(N(TMS)(Si(TMS)$_3$)), **5.29** (Scheme 5-23)

To a solution of **4.10** (30 mg, 0.044 mmol) in C_6D_6 (0.40 mL) was added $TMSN_3$ (5.8 μL, 0.044 mmol). An immediate colour change from teal to yellow was observed along with gas evolution. Volatiles were removed *in vacuo* and the residue dissolved in minimal hexane. Storage of the concentrated solution at 243 K afforded two types of crystals (orange and colourless) suitable for X-ray crystallography. Data for **5.29**, the orange crystals, as reported by Fischer *et al.*[32] ^{1}H NMR (400 MHz, C_6D_6, 298 K) δ: 7.27–7.23 (m, Ar*H*, 1H), 7.07–7.05 (m, Ar*H*, 2 H), 6.80–6.79 (m, Mes-C*H*, 4H), 2.31 (s, Mes-C*H*$_3$, 12H), 2.18 (s, Mes-C*H*$_3$, 6H), 0.22 (s, Si(SiC*H*$_3$)$_3$, 27H), 0.13 (s, N(SiMe$_3$)$_2$, 9H) ppm. ^{13}C NMR (101 MHz, C_6D_6, 298 K) δ: 187.1, 145.8, 138.4, 130.3, 130.2, 22.0, 21.1, 6.9, 3.2 ppm. ^{29}Si NMR (80 MHz, C_6D_6, 298 K) δ: 5.5, -16.4, -38.3 ppm.

5.4.12 Synthesis of SnSi(TMS)$_3$(NH(TMS)(Ar^{Mes}-CH$_2$), **5.30** (Scheme 5-23)

A similar method was followed as that for **5.29**. Data for **5.30**, the colourless crystals, suitable for X-ray crystallography, as reported by Fischer *et al*.[32] ^{1}H NMR (400 MHz, C_6D_6, 298 K) δ: 7.23–7.20 (m, Ar*H*, 1H), 6.90–6.88 (m, Ar*H*, 2H), 6.86–6.85 (m, Ar*H*, 4H), 2.88 (d, Sn-C(H)*H*, $^{2}J_{HH}$ = 11.2 Hz, 1H), 2.59 (d, Sn-C(H)*H*, $^{2}J_{HH}$ = 11.2 Hz, 1H), 2.30 (s, Mes-C*H*$_3$, 3H), 2.27 (s, Mes-C*H*$_3$, 3H), 2.23 (s, Mes-C*H*$_3$, 3H), 2.22 (s, Mes-C*H*$_3$, 3H), 2.15 (s, Mes-C*H*$_3$, 3H), 0.16 (s, SiC*H*$_3$, 36H), -0.99 (s, Sn-N*H*, 1H) ppm. ^{13}C NMR (101 MHz, C_6D_6, 298 K) δ: 149.8, 147.4, 145.9, 141.9,

138.9, 137.4, 136.8, 136.7, 136.6, 135.6, 130.6, 130.1, 129.4, 128.5, 128.4, 27.3, 23.2, 23.1, 22.8, 21.1, 21.0, 4.3, 3.1 ppm. ^{29}Si NMR (80 MHz, C_6D_6, 298 K) δ: 3.4, -7.4 -121.4 ppm. EA Anal. calcd. for $C_{36}H_{61}NSi_5Sn$: C, 56.37; H, 8.02; N, 1.83; found: C, 55.80; H, 7.42; N, 1.61.

5.4.13 Synthesis of $SnAr^{Mes}N(Dipp)(Si(TMS)_3)$, **5.32** (Scheme 5-25)

To a solution of **4.10** (40 mg, 0.059 mmol) in C_6D_6 (0.40 mL) was added a solution of $DippN_3$ (12 mg, 0.059 mmol) in C_6D_6 (0.30 mL). Immediate gas evolution and a colour change from teal to red was observed. Volatiles were then removed *in vacuo* and the residue extracted into hexane. The resulting suspension was filtered and the filtrate concentrated to incipient crystallisation then stored at 243 K to yield the product as dark orange/red crystals suitable for X-ray crystallography. Yield: 32 mg, 67%. Data for **5.32** as reported by Fischer *et al.*[32] ^{1}H NMR (400 MHz, C_6D_6, 298 K) δ: 7.06–7.03 ppm (m, Ar*H*, 1H), 6.98–6.90 (m, Ar*H*, 3H), 6.83–6.81 (m, Ar*H*, 2H), 6.75 (s, Mes-C*H*, 4H), 3.29 (sept, ^{i}Pr-*H*, $^3J_{HH}$ = 6.5 Hz, 2H), 2.21 (s, Mes-C*H*$_3$, 6H), 2.10 (s, Mes-C*H*$_3$, 12H), 1.26 (d, ^{i}Pr-C*H*$_3$, $^3J_{HH}$ = 6.7 Hz, 6H), 0.57 (d, ^{i}Pr-C*H*$_3$, $^3J_{HH}$ = 6.7 Hz, 6H), 0.14 (s, Si(SiC*H*$_3$)$_3$, 27H) ppm. ^{13}C NMR (101 MHz, C_6D_6, 298 K) δ: 188.4, 152.7, 147.3, 142.3, 138.8, 137.3, 137.3, 131.6, 129.7, 128.0, 124.2, 123.7, 28.5, 27.9, 27.1, 22.4, 21.1, 3.2 ppm. ^{29}Si NMR (80 MHz, C_6D_6, 298 K) δ: -15.7, -31.5 ppm. ^{119}Sn NMR (149 MHz, C_6D_6,298 K) δ: -99.0 ppm.

5.4.14 Reaction of $Sn(Si(TMS)_2(Si^tBuPh_2))_2$ with $DippN_3$ (Scheme 5-26)

To a solution of **4.13** (23 mg, 0.024 mmol) in C_6D_6 (0.40 mL) was added $DippN_3$ (11 mg, 0.055 mmol), and an immediate colour change from brown to green was seen. The reaction was stirred for 12 h and the product, **5.33**, then characterised by *in situ* ^{1}H NMR spectroscopy. ^{1}H NMR (400 MHz, C_6D_6, 298 K) δ: 7.90–7.82 (m, Ar*H*, 4H), 7.24–7.17 (m, Ar*H*,

6H), 7.02–6.91 (m, Ar*H*, 3H), 3.74 (sept, ^{i}Pr-*H*, $^{3}J_{HH}$ = 6.9 Hz, 2H), 1.38 (d, ^{i}Pr-C*H*$_3$, $^{3}J_{HH}$ = 6.6 Hz, 6H), 1.33 (d, ^{i}Pr-C*H*$_3$, $^{3}J_{HH}$ = 6.6 Hz, 6H), 1.14 (s, ^{t}Bu-*H,* 9H), 0.11 (s, SiC*H*$_3$, 18H) ppm.

5.4.15 Reaction of $SnAr^{Mes}Si(TMS)_3$ with Ethene (Scheme 5-28)

A solution of **4.10** (70 mg, 0.10 mmol) in benzene (15 mL) was degassed three times using the freeze-pump-thaw method, and the headspace then charged with ethene at *ca*. 2 bar and the reaction mixture stirred. After 5 min, the product began to precipitate out of solution. The reaction mixture was then concentrated *in vacuo* to precipitate additional product, which could be isolated by filtration. This crude product, **5.35**, was extracted into toluene and concentrated *in vacuo* before being stored at 280 K to afford the product as red crystals suitable for X-ray crystallography. **5.5** was also characterised by *in situ* ^{1}H NMR spectroscopy. ^{1}H NMR (400 MHz, C_6D_6, 298 K) δ: 7.29 (t, *p*-C*H* Ar^{Mes}, $^{3}J_{HH}$ = 7.5 Hz, 1H), 7.01 (d, *m*-C*H* Ar^{Mes}, $^{3}J_{HH}$ = 7.5 Hz, 1H), 6.91 (s, Mes-C*H*, 2H), 6.76 (d, *m*-C*H* Ar^{Mes}, $^{3}J_{HH}$ = 7.5, 1H), 6.68 (s Mes-C*H*, 2H), 2.38 (s, Mes-C*H*$_3$, 6H), 2.23 (s, Mes-C*H*$_3$, 3H), 2.18 (s, Mes-C*H*$_3$, 3H), 2.11 (s, Mes-C*H*$_3$, 6H), 1.12 (t, C-C*H*$_2$, 2H), 1.08 (t, C-C*H*$_2$, 2H), 0.30 (s, Si(SiC*H*$_3$)$_3$, 27H) ppm.

5.5 References

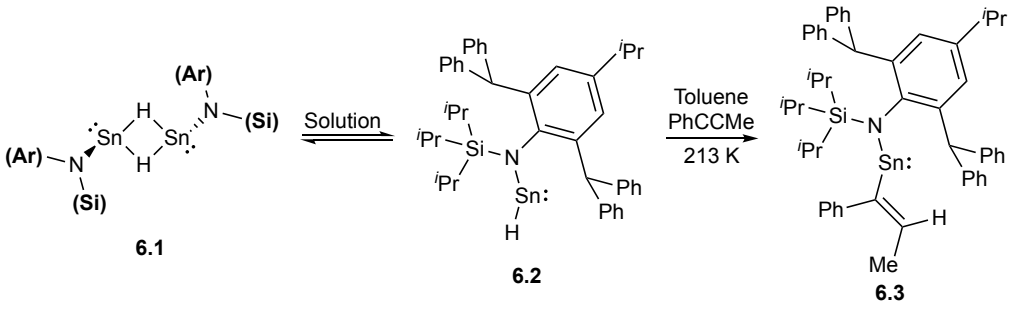
1 P. J. Davidson, A. Hudson, M. F. Lappert and P. W. Lednor, *J Chem Soc Chem Commun*, 1973, 829–830.
2 J. D. Cotton, P. J. Davison, D. E. Goldberg, M. F. Lappert and K. M. Thomas, *J Chem Soc Chem Commun*, 1974, 893–895.
3 S. M. Mansell, R. H. Herber, I. Nowik, D. H. Ross, C. A. Russell and D. F. Wass, *Inorg Chem*, 2011, **50**, 2252–2263.
4 M. F. Lappert and R. S. Rowe, *Coord Chem Rev*, 1990, **100**, 267–292.
5 A. V. Zabula, T. Pape, A. Hepp and F. E. Hahn, *Dalton Transactions*, 2008, **43**, 5886–5890.
6 A. V. Zabula, T. Pape, A. Hepp and F. Ekkehardt Hahn, *Organometallics*, 2008, **27**, 2756–2760.
7 A. V. Protchenko, J. I. Bates, L. M. A. Saleh, M. P. Blake, A. D. Schwarz, E. L. Kolychev, A. L. Thompson, C. Jones, P. Mountford and S. Aldridge, *J Am Chem Soc*, 2016, **138**, 4555–4564.
8 K. Hillner and W. P. Neumann, *Tetrahedron Lett*, 1986, **27**, 5347–5350.
9 R. Marx, W. P. Neumann and K. Hillner, *Tetrahedron Lett*, 1984, **25**, 625–628.
10 W. Setaka, K. Sakamoto, M. Kira and P. P. Power, *Organometallics*, 2001, **20**, 4460–4462.
11 M. Schriewer and W. P. Neumann, *J Am Chem Soc*, 1983, **105**, 897–901.
12 G. Ossig, A. Meller, S. Freitag and R. Herbst-Irmer, *J Chem Soc Chem Commun*, 1993, 497–499.
13 U. Fooken, W. Saak and M. Weidenbruch, *J Organomet Chem*, 1999, **579**, 280–284.

14 H. Grützmacher and H. Pritzkow, *Angewandte Chemie International Edition in English*, 1991, **30**, 1017–1018.
15 A. Schulz, M. Thomas and A. Villinger, *Dalton Transactions*, 2018, **48**, 125–132.
16 P. Švec, Z. Padělková, M. Alonso, F. De Proft and A. Růžička, *Can J Chem*, 2014, **92**, 434–440.
17 Y. Peng, J.-D. Guo, B. D. Ellis, Z. Zhu, J. C. Fettinger, S. Nagase and P. P. Power, *J Am Chem Soc*, 2009, **131**, 16272–16282.
18 S. Kyushin, H. Sakurai and H. Matsumoto, *Chem Lett*, 1998, **27**, 107–108.
19 T. Kunz, O. Şahin and A. Schnepf, *Z Anorg Allg Chem*, 2022, **648**, e202200081.
20 Y. Mizuhata, T. Sasamori and N. Tokitoh, *Chem Rev*, 2009, **109**, 3479–3511.
21 D. Agustin and M. Ehses, *Comptes Rendus. Chimie*, 2009, **12**, 1189–1227.
22 A. K. Swarnakar, M. J. Ferguson, R. McDonald and E. Rivard, *Dalton Transactions*, 2016, **45**, 6071–6078.
23 P. L. Ang, V. H. Nguyen and J. H. K. Yip, *Dalton Transactions*, 2022, **51**, 3081–3095.
24 H. J. Lawson and J. D. Atwood, *J Am Chem Soc*, 1989, **111**, 6223–6227.
25 J. A. Cabeza, J. M. Fernández-Colinas, P. García-Álvarez and D. Polo, *Inorg Chem*, 2012, **51**, 3896–3903.
26 N. Hidalgo, S. Bajo, J. J. Moreno, C. Navarro-Gilabert, B. Q. Mercado and J. Campos, *Dalton Transactions*, 2019, **48**, 9127–9138.
27 Z. D. Brown, P. Vasko, J. C. Fettinger, H. M. Tuononen and P. P. Power, *J Am Chem Soc*, 2012, **134**, 4045–4048.
28 M. Walewska, J. Baumgartner, C. Marschner, L. Albers and T. Müller, *Chemistry – A European Journal*, 2016, **22**, 18512–18521.
29 T. Y. Lai, J. D. Guo, J. C. Fettinger, S. Nagase and P. P. Power, *Chemical Communications*, 2019, **55**, 405–407.
30 K. W. Klinkhammer and W. Schwarz, *Angewandte Chemie International Edition in English*, 1995, **34**, 1334–1336.
31 D. E. Goldberg, D. H. Harris, M. F. Lappert and K. M. Thomas, *J Chem Soc Chem Commun*, 1976, 261–262.
32 M. Fischer, M. M. D. Roy, Lewis. L. Wales, M. A. Ellwanger, C. McManus, A. F. Roper, A. Heilmann and S. Aldridge, *Angewandte Chemie International Edition*, 2022, **61**, e202211616.

6 The Alkyne Insertion Chemistry of Silylstannylenes

6.1 Introduction

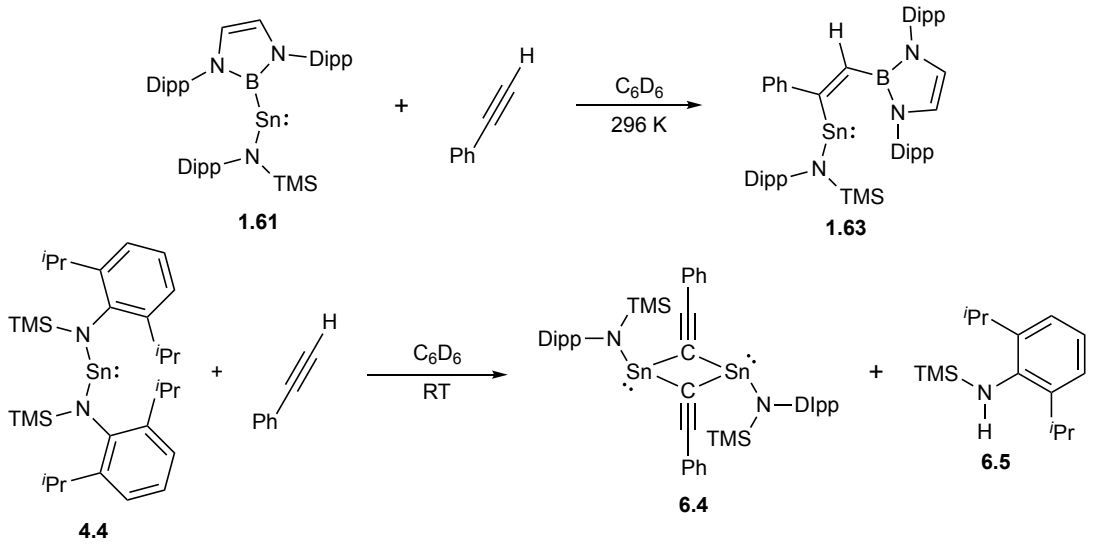
As documented in the introduction (Section 1.3.4.3), alkynes can react with stannylenes in a variety of ways, including by insertion into the Sn–X bonds of stannylenes (Schemes 1-22 and 1-23).[1–4] In their 2015 paper, Hadlington *et al.* described the hydrostannylation of 1-phenylprop-1-yne (PhCCMe) by a tin(II) hydride, **6.2**, (Scheme 6-1).[4] The reaction proceeds rapidly (within "several" minutes) at ambient conditions to yield the alkenylstannylene, **6.3**, as the E-isomer with the Sn-bound hydride transferred to the methyl-substituted alkenic carbon.[4] The reaction is regio- and stereospecific for **6.3**, in stark contrast to the hydroboration of alkynes with boranes, which typically gives a mix of regioisomers, depending on the borane substituents.[5] The reaction of PhCCMe with excess **6.2** does not, however, lead to double hydrometallation of the alkyne, yielding only **6.3**, which the authors attribute to the steric bulk of the amido ligand employed.[4]



Scheme 6-1: Hydrostannylation of 1-phenylprop-1-yne by tin(II) hydride, **6.2** (**(Ar)** is $-C_6H_2$-2,6-$(CH(Ph)_2)_2$-4-(^{i}Pr) and **(Si)** is $-Si(^iPr)_3$).

Insertions of alkynes into the Sn–B/Ge bonds of boryl- and germylstannylenes are also possible (Scheme 6-2), illustrating that this mode of reactivity is not restricted to tin(II) hydrides.[2,3] However, ligand choice is still important when designing systems capable of

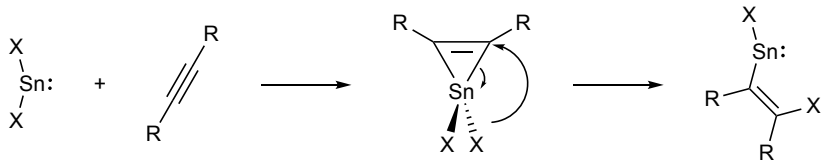
undergoing alkyne insertion. This is illustrated by the divergent reactivity displayed towards phenylacetylene by amido(boryl)stannylene, **1.61**, and bis(amido)stannylene, **4.4**, disclosed by Protchenko *et al.* in their 2015 report.[3] The reaction between **1.61** and phenylacetylene (Scheme 6-2) yields alkenylstannylene, **1.63**, both stereo- and regiospecifically.[3] **1.63** is the Z-isomer, and the boryl ligand is bound to the least hindered alkenic carbon, mirroring the stereochemistry seen in the formation of alkenylstannylene, **6.3** (Scheme 6-1).[3,4] However, the reaction between bis(amido)stannylene, **4.4**, and phenylacetylene does not yield the corresponding insertion product. Instead, a protonolysis reaction occurs to yield a Sn(II) species featuring bridging acetylide groups, **6.4**, and the protonated amido ligand, **6.5**. This reactivity is reminiscent of behaviour reported by Harris *et al.* on the reaction of a Sn(II) amide with phenylacetylene, and suggests this chemistry is a feature of stannylenes with Sn–N bonds.[6]



Scheme 6-2: Top – Insertion of phenylacetylene into the Sn–B bond of amido(boryl)stannylene, **1.61**. Bottom – Reaction of phenylacetylene with bis(amido)stannylene, **4.4**.

The stereospecificity of the products resulting from the insertion of alkynes into the Sn–X bonds of stannylenes reported in the literature has prompted speculation into the mechanism

of the reaction.[2,3] One proposed mechanism (Scheme 6-3) suggests that the reaction proceeds *via* initial cycloaddition of the alkyne (to form a Sn(IV) species) followed by migration of the X-substituent to yield the alkenyl stannylene. This mechanism offers an explanation of the stereochemistry of the products and finds mechanistic precedent in the known examples of cycloaddition of stannylenes (and their lighter congeners) with alkynes. More work is required to definitively prove this mechanism and ascertain its generality.[1,7–9]



Scheme 6-3: Proposed mechanism of insertion of alkynes into the Sn–X bonds of stannylenes.

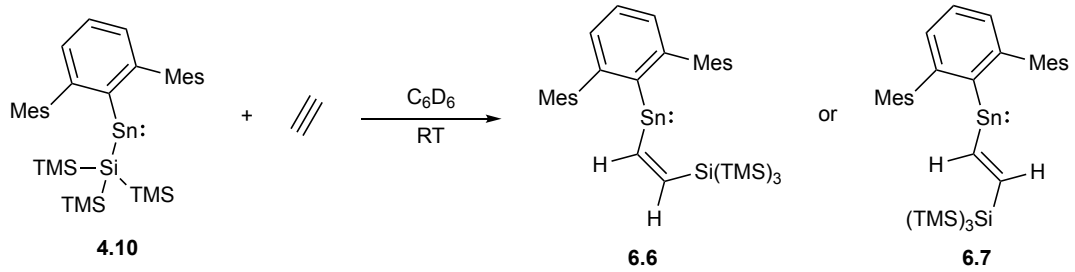
Encouraged by the reactivity of alkynes with aryl(silyl)germylene, **1.23**, in addition to the insertion chemistry with azides displayed by aryl(silyl)stannylene, **4.10**, the reactivity of silylstannylenes with alkynes was investigated. This chapter documents the irreversible insertion of a wide range of alkynes into the Sn–Si bonds of silylstannylenes, along with null reactions which confirm the importance of ligand choice in achieving this behaviour. Additionally, the first examples of *reversible* insertion of alkynes into Sn–X bonds will be disclosed, and the thermodynamics of these processes compared with related reactions. Finally, a mechanism for the silylstannylation reaction is proposed, based on quantum chemical calculations, which agrees with the experimental results disclosed in this chapter and other results from the literature.

6.2 Results and Discussion

6.2.1 Irreversible Alkyne Insertion

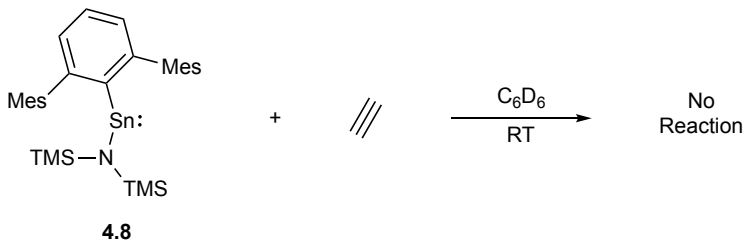
6.2.1.1 Acetylene

Exposure of a solution of aryl(silyl)stannylene, **4.10**, to one atmosphere of acetylene leads to an immediate colour change from teal to red. Analysis of the reaction mixture by NMR spectroscopy suggests that the acetylene has inserted into the Sn–Si bond of the stannylene (Scheme 6-4). Diagnostic evidence is provided by the roofed doublets in the ^{1}H NMR spectrum (9.50 and 8.06 ppm), which show $^{1}J_{CH}$ coupling to the resonances in the ^{13}C NMR spectrum assigned to the Sn–*C* (202.0 ppm) and Si–*C* (δ = 177.5 ppm) units respectively. These signals correspond to the alkenic protons of the insertion product, **6.6** or **6.7**. The coupling constant ($^{3}J_{HH}$ = 16.7 Hz) is suggestive of a *trans*-alkene; however, the presence of pendant Si- and Sn-derived groups may affect this. Notably, in their 1978 work, Seyferth *et al.* reported that *trans*-1-trimethylsilyl-2-trimethylstannylethene possesses a $^{3}J_{HH}$ alkenic coupling constant of 22.0 Hz, *i.e.* significantly above the range of a typical *trans*-alkene ($^{3}J_{HH}$ = 11-18 Hz).[10,11] Furthermore, all reported examples of the insertion of alkynes into the E–X bonds of metallylenes to date have yielded the *syn*-addition product (Schemes 1-20, 1-21, 1-22, 1-23, 1-24, and 6-1).[2–4,7,12,13] Therefore, it is proposed that the reaction between **4.10** and acetylene most likely affords the *cis*-alkene product, **6.6**. Unfortunately, conclusive confirmation of the geometry of the product by single crystal X-ray diffraction could not be obtained due to the solubility of the product in organic solvents (pentane, hexane, and toluene).



Scheme 6-4: Insertion of acetylene into the Sn–Si bond of **4.10**, to yield either **6.6** or **6.7.**

The reaction between the aryl(amido)stannylene, **4.8**, and acetylene was also investigated. When a C_6D_6 solution of **4.8** was charged with one atmosphere of acetylene, no immediate visual change in the reaction mixture was observed. Similarly, when the reaction mixture was investigated by *in situ* ^{1}H NMR spectroscopy, no changes in the starting material resonances were detected either. The absence of insertion chemistry observed between **4.8** and acetylene could stem from the inability of **4.8** to form the requisite metallacyclopropene intermediate to produce the insertion product, as proposed by Protchenko *et al.*[3] Furthermore, **4.8** does not show the same protonolysis chemistry demonstrated by Protchenko *et al.,* in which the bis(amido)stannylene, **4.4**, reacts with phenylacetylene to form a dimeric alkynylstannylene and the corresponding aniline (Scheme 6-2).

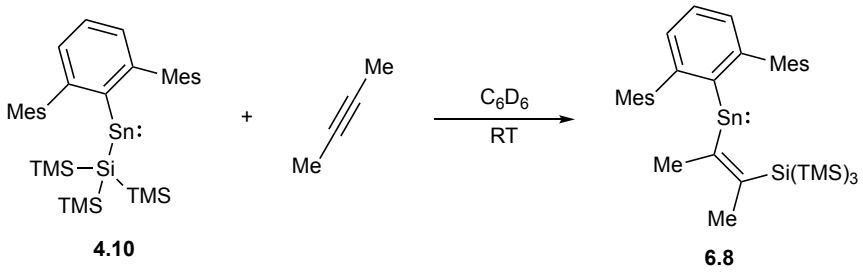


Scheme 6-5: Null reaction observed between **4.8** and acetylene.

6.2.1.2 But-2-yne

Upon addition of but-2-yne to aryl(silyl)stannylene, **4.10**, no immediate colour change was seen. However, after 2 d at room temperature, the formation of a purple solution was

observed. Analysis of the reaction mixture by ^{1}H NMR spectroscopy showed the formation of two new singlet resonances (2.53 and 1.87 ppm) corresponding to the methyl groups of the alkenyl functionality, presumably formed from the insertion of but-2-yne into the Sn–Si bond of **4.10** to yield the alkenylstannylene, **6.8** (Scheme 6-6). These resonances of **6.8** integrate in a 3:1 ratio with the triplet resonance (7.35 ppm) corresponding to the *para*-substituted proton of the central aromatic ring of the terphenyl ligand, thereby confirming the stoichiometry of the reaction. While confirmation of the stereochemistry of **6.8** could not be achieved by NMR spectroscopy, crystals of **6.8**, suitable for single crystal X-ray diffraction, could be grown which allow the geometry of **6.8** in the solid state to be confirmed conclusively.



Scheme 6-6: Insertion of but-2-yne into the Sn–Si bond of **4.10** to give **6.8**.

The molecular structure of **6.8** is depicted below (Figure 6-1). Accordingly, **6.8** is shown to be formed as the result of the *syn*-insertion of but-2-yne into the Sn–Si bond of **4.10**, in agreement with previously reported examples of alkyne insertion into the Sn–X bonds of stannylenes.[2–4] **6.8** features a narrower angle at the tin centre compared to **4.10** (100.33(2)° vs. 109.75(6)°), presumably due to the reduced steric repulsion at the tin centre brought about by the new vinyl substituent. The similar Sn–C(aryl) bond lengths measured for **6.8** and **4.10** (2.200(5) Å and 2.189(3) Å respectively) indicate that they are both Sn(II) compounds. **6.8** can be compared to two previous examples of compounds formed by insertion of

phenylacetylene into a Sn–X bond: alkenyl(amido)stannylene, **1.63**, synthesised by Protchenko *et al.* (Scheme 6-2), and alkenyl(aryl)stannylene, **1.65**, synthesised by Maudrich *et al.* (Scheme 1-24).[2,3] The Sn–C(alkenyl) distance measured for **6.8** (2.163(4) Å) is shorter than those of **1.63** and **1.65** (2.254(4) Å and 2.214(4) Å respectively) presumably due to the presence of the smaller methyl group bonded to the tin-bound alkenyl carbon in **6.8**, compared to the phenyl groups of **1.63** and **1.65**.

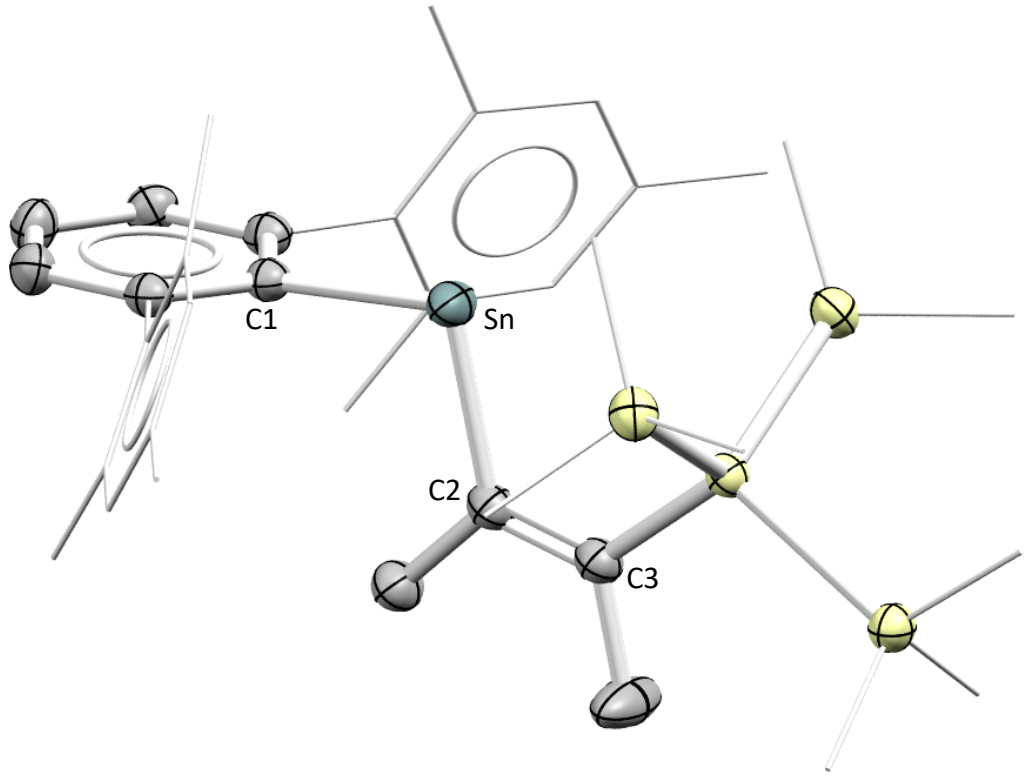
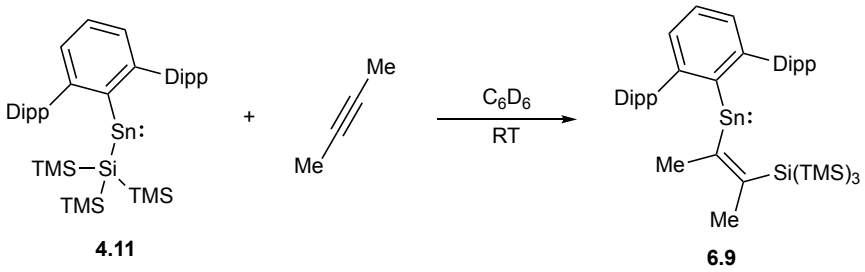


Figure 6-1: Molecular structure of **6.8** as determined by X-ray crystallography. Thermal ellipsoids are set at the 50% probability level. Hydrogen atoms are omitted for clarity. The flanking mesityl rings of the terphenyl ligand and the methyl groups of the hypersilyl ligand are depicted in wireframe for clarity. Key bond lengths (Å) and angles (°): Sn–C1: 2.200(5), Sn–C2: 2.163(4), C2–C3: 1.347(2), C1–Sn–C2: 100.33(2).

When but-2-yne is added to a C_6D_6 solution of the bulkier (Dipp-substituted) aryl(silyl)stannylene, **4.11**, no immediate reaction was observed (as with **4.10**). However,

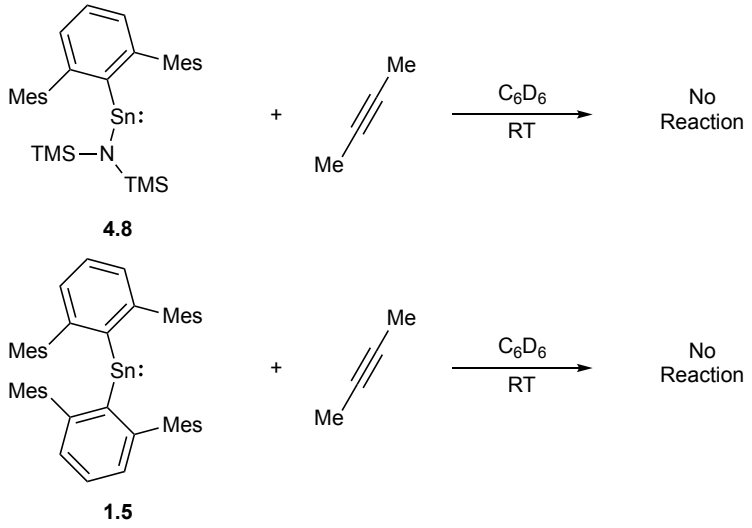
after several days the reaction mixture gradually becomes deep purple in colour. Investigation by ^{1}H NMR spectroscopy suggests that the product of this reaction, **6.9**, is the result of the corresponding insertion of but-2-yne into the Sn–Si bond of **4.11** (Scheme 6-7). This is evidenced by the generation of two new singlet resonances (2.64 and 1.94 ppm), corresponding to the methyl groups of the alkene functionality of **6.9**, which are in accordance with new ligand resonances of **6.9** (TMS protons: 0.10 ppm). It is proposed that **6.9**, like **6.8**, is formed *via* the *syn*-addition of but-2-yne into the Sn–Si bond. However, attempts to grow crystals suitable for single crystal X-ray diffraction to confirm this geometry proved unsuccessful due to the greater solubility imparted by the diisopropylphenyl groups of **6.9** (as compared to the mesityl groups of **6.8**).



Scheme 6-7: Proposed formation of **6.9** by insertion of but-2-yne into the Sn–Si bond of **4.11**.

The reactivity of aryl(amido)stannylene, **4.8**, and bis(aryl)stannylene, **1.5**, with but-2-yne was also investigated. However, as above (Scheme 6-5), it was found that the Sn–C and Sn–N bonds of these species were not amenable to the insertion chemistry demonstrated by the Sn–Si bonds of **4.10** and **4.11** with but-2-yne. That **1.5** does *not react* with but-2-yne is particularly noteworthy, given that in 2019 Lai *et al.* documented the insertion of ethylene into the Sn–C bond of a bulkier bis(aryl)stannylene, **1.6** (Scheme 1-17) and, in the same report, found **1.5** to be unreactive towards ethylene.[14] The authors attribute this difference to the narrower HOMO–LUMO gap of **1.6**, owing to the wider angle adopted at the tin centre.[14] This

conclusion is also in agreement with the cycloaddition/migration mechanism proposed by Protchenko *et al*.[3] These results therefore suggest that alkyne insertion into the Sn–C or Sn–N bond of a stannylene could be feasible, provided that the HOMO–LUMO gap of the stannylene is sufficiently narrow.

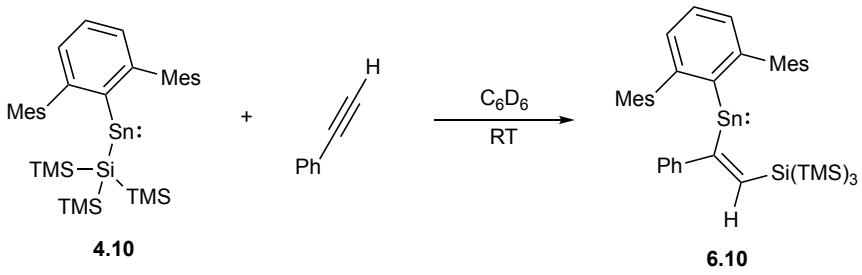


Scheme 6-8: Top – Null reaction between but-2-yne and **4.8**. Bottom – Null reaction between but-2-yne and **1.5**.

6.2.1.3 Phenylacetylene

When phenylacetylene was added to a solution of aryl(silyl)stannylene, **4.10**, an immediate colour change from teal to purple was seen. Analysis of the product, **6.10**, by NMR spectroscopy suggests that, as with but-2-yne, phenylacetylene inserts into the Sn–Si bond of **4.10** (Scheme 6-9). This assignment is supported by the appearance of an alkenic-H signal at δ = 7.28 ppm in the ^{1}H NMR spectrum, which integrates in a 1:1 ratio with the resonance due to the *para*-H of the central ring of the terphenyl ligand of **6.10** (7.26 ppm). The ^{13}C NMR spectrum of **6.10** shows two resonances at 218.3 ppm (Sn–*C*) and 179.7 ppm (Si–*C*). However, only the Si–*C* resonance couples to the alkenic resonance in the ^{1}H NMR data, implying that the silyl group is bonded to the least hindered alkenic carbon. Single crystals suitable for

X-ray crystallography could be grown and allow the proposed regio- and stereochemistry of **6.10** to be confirmed.



Scheme 6-9: Insertion of phenylacetylene into the Sn–Si bond of **4.10** to give **6.10**.

The molecular structure of **6.10** is depicted below (Figure 6-2) and confirms that it is formed by the *syn*-insertion of phenylacetylene into the Sn–Si bond of **4.10**. The connectivity of **6.10** confirms the inferences made from the NMR data and replicates the stereo- and regioselectivity reported by both Hadlington *et al.* and Protchenko *et al.* (Schemes 6-1 and 6-2).[3,4] This selectivity is presumably derived from the mechanism of the insertion of the alkyne into the Sn–X bond and will be discussed in further detail below. When the structure of **6.10** is compared to that of the aryl(alkenyl)stannylene, **6.8** (formed from the insertion of but-2-yne into the Sn–Si bond of **4.10**), a wider angle is observed at the tin centre (**6.10**: 103.79(8)°, **6.8**: 100.33(2)°). This is thought to result from the greater steric repulsion between the terphenyl ligand and the pendant phenyl group of the alkene moiety in **6.10** and is further exemplified in the longer Sn–C(alkenyl) bond length of **6.10** (**6.10**: 2.209(2) Å; **6.8**: 2.163(4) Å).

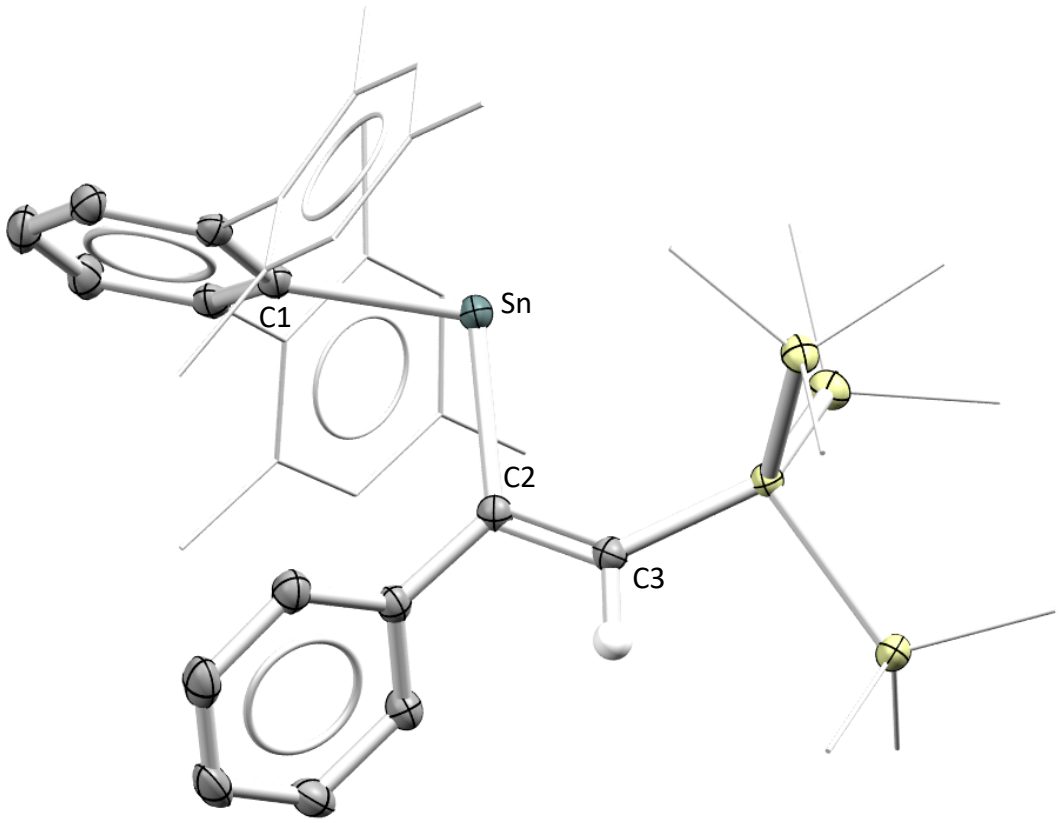
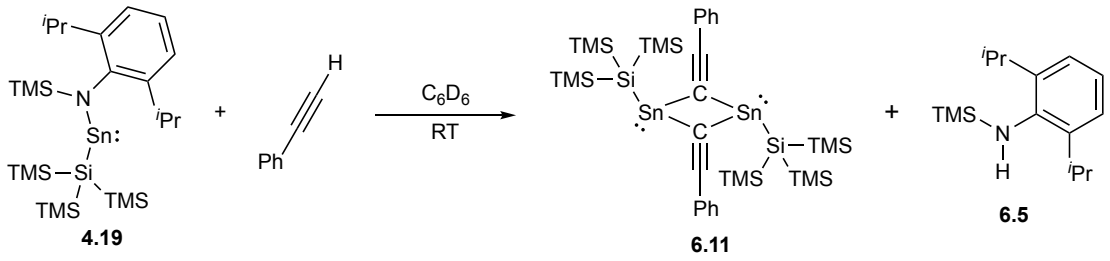


Figure 6-2: Molecular structure of **6.10** as determined by X-ray crystallography. Thermal ellipsoids are set at the 50% probability level. All hydrogen atoms, except for the alkenic proton, are omitted for clarity. The flanking mesityl rings of the terphenyl ligand and the methyl groups of the hypersilyl ligand are depicted in wireframe for clarity. Key bond lengths (Å) and angles (°): Sn–C1: 2.219(2), Sn–C2: 2.209(2), C2–C3: 1.348(2), C1–Sn–C2: 103.79(8).

The reactivity of amido(silyl)stannylene, **4.19**, with phenylacetylene was also investigated. Combining phenylacetylene with a C_6D_6 solution of **4.19** resulted in an immediate colour change from teal to orange (Scheme 6-10). Analysis of the reaction mixture by *in situ* NMR spectroscopy shows the appearance of an amine resonance at 2.00 ppm which integrates in an equimolar ratio with new aliphatic diisopropylphenyl ligand resonances (isopropyl C–*H*: 3.45 ppm, isopropyl methyl groups: 1.21 ppm). This suggests that the aniline, HN(Dipp)(TMS) **6.5**, has been formed (Scheme 6-10). The formation of **6.5** is likely *via* a protonolysis reaction, as observed between phenylacetylene and a bis(amido)stannylene,

4.4, (Scheme 6-2) by Protchenko *et al.*[3] This reaction pathway would likely produce a (dimeric) alkynylstannylene, **6.11**, as the other product. A change in the hypersilyl proton resonances in the ^{1}H NMR data of the reaction mixture (0.11 ppm) compared to **4.19** (0.38 ppm) is detected, but these data alone are not sufficient to confirm the synthesis of **6.11**. The aromatic region of the *in situ* ^{1}H NMR spectrum is difficult to interpret due to the presence of the amine co-product **6.5**. Attempts to isolate **6.11** have also proved unsuccessful due to persistent contamination with **6.5**. The presence of the aniline is also thought to help solubilise **6.11** in aliphatic solvents and has therefore stymied attempts to obtain **6.11** as single crystals suitable for X-ray diffraction.

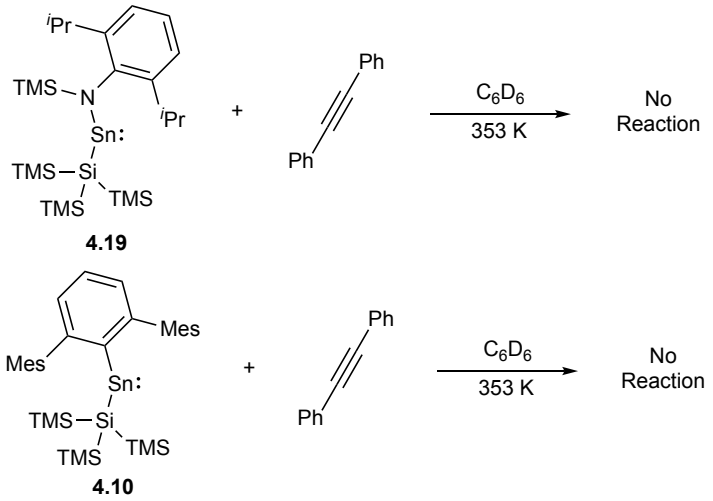


Scheme 6-10: Proposed products from the reaction between amido(silyl)stannylene, **4.19**, and phenylacetylene.

That no evidence of insertion is observed between phenylacetylene and **4.19** is a marked contrast to the reactivity of amido(boryl)stannylene, **1.61**, reported by Protchenko *et al.* (Scheme 6-2).[3] This divergence suggests that the Sn–Si bond of **4.19** is less labile to insertion than the Sn–B bond of **1.61**. One explanation for this result could be that the π-accepting ability (albeit weak) of the boryl ligand serves to stabilise an intermediate in the insertion mechanism, or more simply that **1.61** has a narrower HOMO–LUMO gap than **4.19** and therefore is able to undergo insertion by phenylacetylene. However, given the similar σ-donating abilities of boryl and silyl ligands, as well as the wider angle at the tin centre of

4.19 (112.7(1)°) compared to **1.61** (106.7(2)°), it seems unlikely that such a large difference in reactivity would be observed. This could suggest that a different mechanism is at work.[15]

To eliminate the possibility of protonolysis, the reaction between **4.19** and diphenylacetylene was explored. However, despite prolonged periods of heating at elevated temperatures, no reaction was observed. To determine whether this lack of insertion is purely a consequence of the amido ligand employed in **4.19**, aryl(silyl)stannylene, **4.10**, was also reacted with diphenylacetylene. However, once more, no reaction was observed despite heating the reaction mixture to 353 K for 14 d. These null reactions imply that the steric profile of the hypersilyl ligand, used in both **4.10** and **4.19**, prevents the insertion chemistry of these silylstannylenes with alkynes.

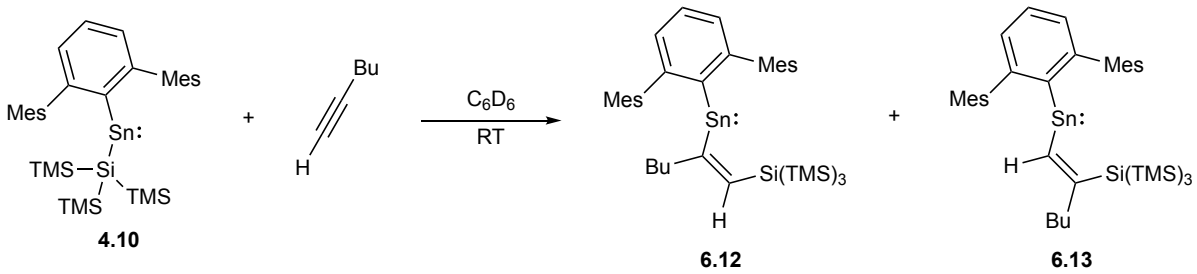


Scheme 6-11: Top – No observed reactivity between amido(silyl)stannylene, **4.19**, and diphenylacetylene. Bottom – No observed reactivity between aryl(silyl)stannylene, **4.10**, and diphenylacetylene.

6.2.1.4 Hex-1-yne

In contrast to the unreactive nature of but-2-yne detailed above, when hex-1-yne is added to a C_6D_6 solution of aryl(silyl)stannylene, **4.10**, an immediate colour change from teal to purple is seen (Scheme 6-12). Investigation of the reaction mixture by ^{1}H NMR spectroscopy shows

the formation of a major product, **6.12**, and a minor species, **6.13**. Both products give rise to alkenic resonances (**6.12**: 7.37 ppm, **6.13**: 7.77 ppm) which integrate in a 1:1 ratio with new terphenyl ligand resonances (*meta*-H of central aryl ring of terphenyl ligand: **6.12**, 7.09 ppm; **6.13**, 7.02 ppm), suggesting that both products result from the insertion of hex-1-yne into the Sn–Si bond of **4.10**. Considering the wealth of evidence, both in the literature and in this thesis, which demonstrates the *syn*-addition of alkynes into the E–X bonds of metallylenes, it is proposed that **6.12** and **6.13** are both Z-alkenes.[2–4,7,8,13] The formation of **6.12** is more favoured than **6.13** as demonstrated by its greater concentration in the *in situ* ^{1}H NMR spectrum (Figure 6-3). Based on this observation it is hypothesised that in **6.12**, the silyl group is attached to the least hindered alkenic carbon (Scheme 6-12), as this is the only regiochemistry which has been observed in examples of alkyne insertion into Sn–X bonds (e.g. **4.10** and PhCCH (Scheme 6-9)). [2–4,7,8] However, NMR experiments to confirm the proposed connectivities of **6.12** and **6.13** have so far proved difficult to perform due to the rapidity with which both species decay under ambient conditions (Figure 6-3). The formation of two products is at odds with the reaction between phenylacetylene and **4.10**, to yield **6.10**, discussed above. It is also at odds with the insertion of phenylacetylene into the Sn–B bond of amido(boryl)stannylene (Scheme 6-2), **1.61**, from which only the *syn*-addition product (with boryl attachment to the least hindered carbon) is obtained. The difference in selectivity could be due to the greater steric bulk of the phenyl group of the phenylacetylene compared to the butyl chain of hex-1-yne, which dramatically disfavours the formation of the other regioisomer for phenylacetylene. Additionally, the greater electronic similarity between alkyl/H substituents could result in silyl-group migration to the more substituted carbon being more favoured.



Scheme 6-12: Reaction of hex-1-yne with aryl(silyl)stannylene, **4.10**, to yield two insertion products.

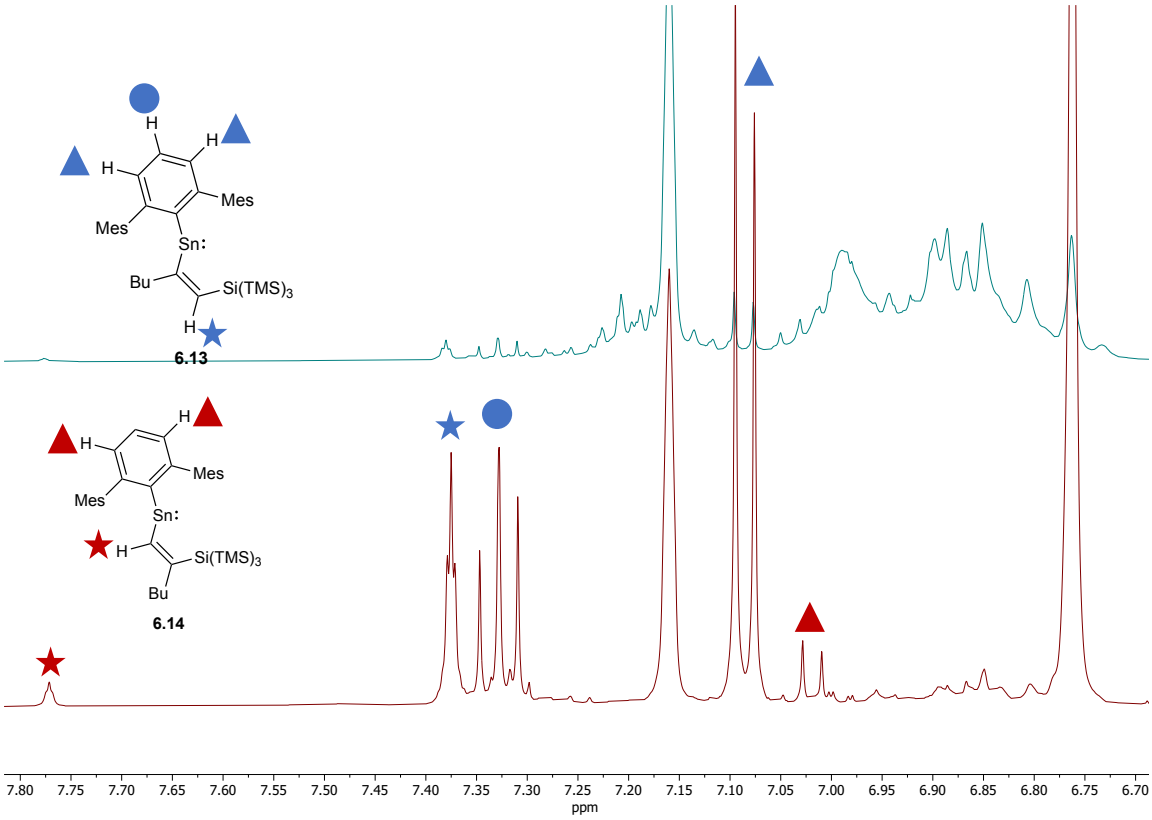
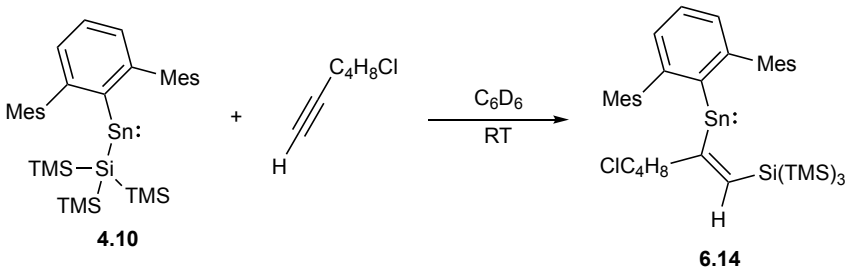


Figure 6-3: Aryl C–H signals in the ^{1}H NMR spectra of species present in the reaction with hex-1-yne: Top – ^{1}H NMR spectrum of reaction mixture after 1 h. Bottom – ^{1}H NMR spectrum of the reaction mixture immediately after the combination of reagents.

The reactivity of **4.10** with 6-chlorohex-1-yne was also examined to see whether the substitution of the chlorine for a proton affects the product distribution. After addition of the alkyne to a C_6D_6 solution of **4.10**, the reaction mixture became purple in colour over the course of 4 h (Scheme 6-13). Analysis of the reaction by ^{1}H NMR spectroscopy shows the

growth of only one new alkenic proton resonance (7.39 ppm), similar to the alkenic shift measured for **6.12** above (7.37 ppm). This new resonance integrates in an equimolar ratio with the novel terphenyl ligand shifts (e.g. *para*-H of central phenyl ring: 7.33 ppm, *meta*-H of central phenyl ring: 7.09 ppm) in the ^{1}H NMR spectrum. This evidence suggests that the product of the reaction, **6.14**, is formed as a result of the insertion of the alkyne into the Sn–Si bond of **4.10** (Scheme 6-13). While the connectivity of **6.14** could not be confirmed, the change in specificity of the reactions between **4.10** and hex-1-yne or 6-chlorohex-1-yne shows how sensitive the reaction mechanism is towards the bulk (and electronic structure) of the alkyne.

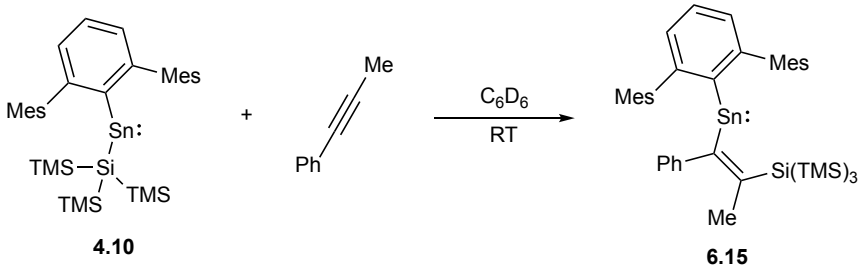


Scheme 6-13: Reaction of aryl(silyl)stannylene, **4.10**, with 6-chlorohex-1-yne to yield proposed product, **6.14**.

6.2.1.5 1-Phenylprop-1-yne

When phenylpropyne was added to a solution of aryl(silyl)stannylene, **4.10**, a colour change from teal to purple was observed over the course of 10 h (Scheme 6-14). Analysis of the product, **6.15**, by ^{1}H NMR spectroscopy shows the appearance of new terphenyl ligand resonances (e.g. *para*-H of central ring of terphenyl ligand: 7.22 ppm, *meta*-H of central ring of terphenyl ligand: 6.95 ppm) which integrate in an equimolar ratio with a singlet resonance at 1.73 ppm. The latter resonance is proposed to correspond to the methyl group of the alkenyl functionality formed *via* insertion of 1-phenylprop-1-yne into the Sn–Si bond of **4.10**,

to yield **6.15**. Crystals of the product, **6.15**, suitable for single crystal X-ray diffraction could be obtained and allowed connectivity to be determined.



Scheme 6-14: Insertion of phenylpropyne into the Sn–Si bond of **4.10** to give **6.15**.

The molecular structure of **6.15** is depicted below (Figure 6-4). The quality of the X-ray data, whilst sufficient to confirm connectivity, does not merit discussion of geometrical parameters. Nevertheless, **6.15** forms as a result of the *syn*-insertion of 1-phenylprop-1-yne into the Sn–Si bond of **4.10**. That **6.15** is the Z-isomer, and the silyl group is attached to the least hindered alkenic carbon, is in close agreement with other crystallographically characterised alkyne insertion products disclosed in this thesis (**3.12**, **3.13**, **6.8**, and **6.10**) as well as previous literature examples of alkyne insertions into metallylene-ligand bonds.[2,3,7,12,13]

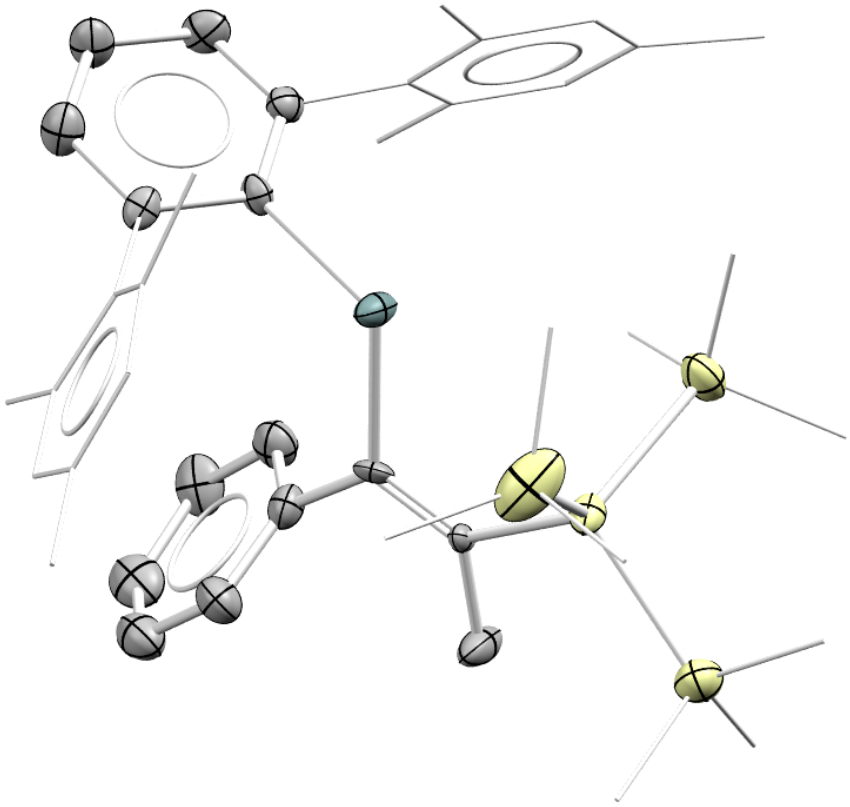
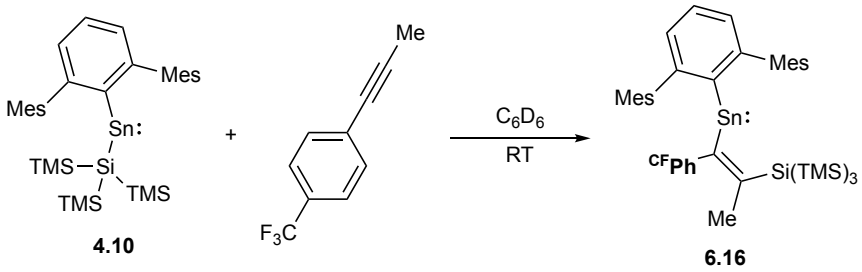


Figure 6-4: Molecular structure of **6.15** as determined by X-ray crystallography. Hydrogen atoms are omitted for clarity. The flanking mesityl rings of the terphenyl ligand and the methyl groups of the hypersilyl ligand are depicted in wireframe for clarity. Data of insufficient quality to discuss the geometric parameters of **6.15**.

6.2.1.6 1-(Prop-1-ynl)-4-Trifluoromethylbenzene

When 1-(prop-1-ynl)-4-trifluoromethylbenzene, $CF_3(C_6H_4)CCMe$, was added to a toluene solution of aryl(silyl)stannylene, **4.10**, no immediate reactivity was observed. However, over the course of 10 h, a colour change was observed from teal to purple. Analysis of the product of this reaction by ^{19}F NMR spectroscopy shows the formation of a new species with a resonance at (-61.4 ppm), slightly shifted from the starting material (-62.5 ppm). Further analysis by ^{1}H NMR spectroscopy suggests that insertion of the alkyne into the Sn–Si bond of **4.10** has occurred (Scheme 6-15). This is evidenced by the formation of a singlet resonance at 1.72 ppm, corresponding to the methyl group of the alkenyl functionality of the product, **6.16**. This resonance integrates in an equimolar ratio with a new signal at 7.18 ppm (3:1 ratio of

intensities) which is due to the *para*-H of the central phenyl ring of the terphenyl ligand of **6.16**. Crystals suitable for single crystal X-ray diffraction could be grown, allowing the connectivity of **6.16** to be confirmed.



Scheme 6-15: Insertion of phenylpropyne into the Sn–Si bond of aryl(silyl)stannylene, **4.10**, to give **6.16** (**Ph^{CF}** is $-C_6H_4$-4-(CF_3)).

The molecular structure of **6.16** is depicted below (Figure 6-5) and confirms that it is formed from the *syn*-addition of $CF_3(C_6H_4)CCMe$ across the Sn–Si bond of **4.10**. As with the crystallographically characterised examples above, the silyl group is attached to the least hindered carbon atom. The Sn–C(alkenyl) bond length of (2.181(2) Å) is similar to the values seen in those measured for insertion products **6.8** and **6.10** (2.163(4) and 2.209(2) Å), formed by insertion of but-2-yne and phenylacetylene, respectively. The slightly larger angle at the tin centre for **6.16**/**6.10** and **6.8** (103.70(8)°/103.79(8)° and 100.33(2)°) is presumably due to the increased bulk of the pendant aryl rings compared to the methyl group of **6.8**.

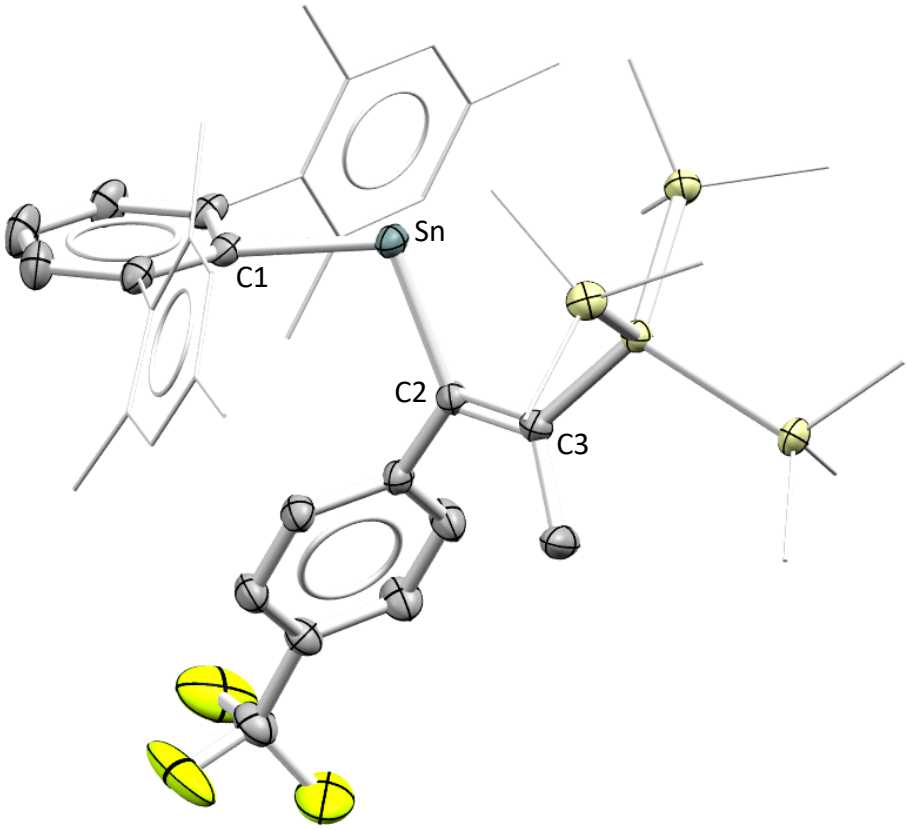
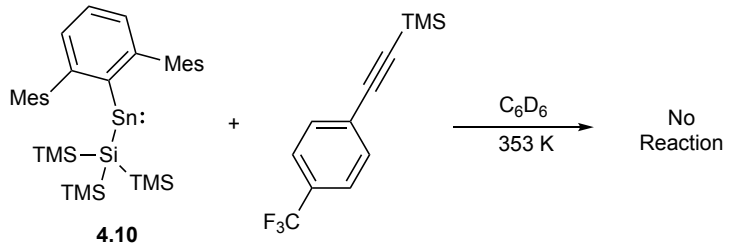


Figure 6-5: Molecular structure of **6.16** as determined by X-ray crystallography. Thermal ellipsoids are set at the 50% probability level. Hydrogen atoms are omitted for clarity. The flanking mesityl rings of the terphenyl ligand and the methyl groups of the hypersilyl ligand are depicted in wireframe for clarity. Key bond lengths (Å) and angles (°): Sn–C1: 2.219(2), Sn–C2: 2.181(2), C2–C3: 1.355(3), C1–Sn–C2: 103.70(8).

To further investigate the effect of steric bulk on the insertion chemistry of **4.10** with alkynes, the reaction with $CF_3(C_6H_4)CCSiMe_3$ was attempted. After combination of the reagents, no reaction was seen, even after 10 d. Moreover, heating the reaction mixture to 353 K also did not yield a reaction, suggesting that this alkyne is too bulky for the reaction to proceed.

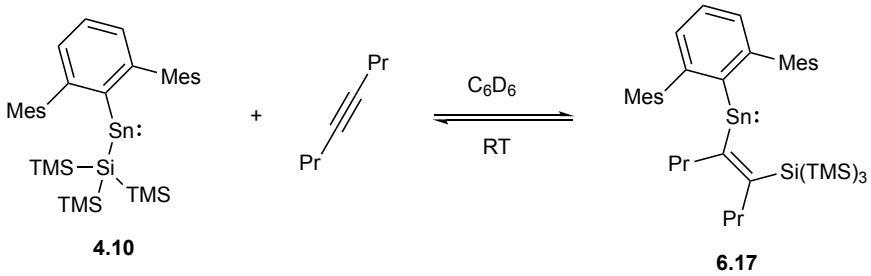


Scheme 6-16: No observed reactivity between aryl(silyl)stannylene, **4.10**, and 1-trimethylsilyl-2-(4-trifluoromethylphenyl)-ethyne.

6.2.2 Reversible Alkyne Insertion

6.2.2.1 Aryl(silyl)stannylene **4.10** and Oct-4-yne

Upon addition of an excess of oct-4-yne to a C_6D_6 solution of aryl(silyl)stannylene, **4.10**, no immediate change was seen. However, after 3 h the solution turns a deeper shade of blue. Investigation of the reaction mixture by ^{1}H NMR spectroscopy shows the resonances due to **4.10** along with signals corresponding to a new species. A triplet resonance (7.32 ppm), a doublet resonance (7.08 ppm), and a singlet resonance (6.87 ppm), due to the terphenyl ligand of the insertion product **6.17** (Scheme 6-17), integrate in an equimolar ratio with a triplet resonance (0.75 ppm). This is thought to be due to one of the -CH_3 groups of the propyl chains being bound to the alkene function. **6.17** is proposed to be the Z-isomer of the alkene based on the results so far obtained in this thesis. Despite leaving the reaction for several days with the alkyne in excess, analysis of the reaction mixture by *in situ* ^{1}H NMR spectroscopy indicated that conversion of **4.10** did not go to completion, as evidenced by the 10:1 ratio of intensities of the resonances corresponding to the *meta*-substituted protons of the terphenyl ligands of **4.10** and **6.17**.

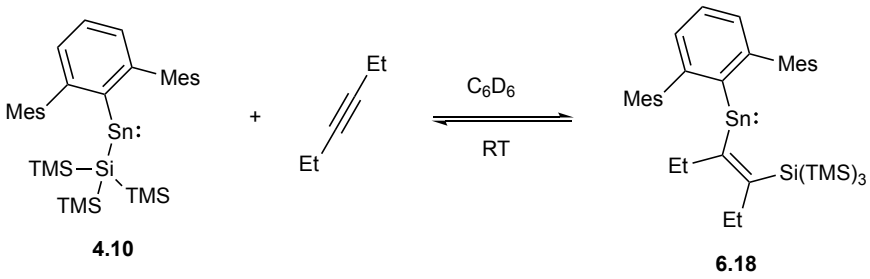


Scheme 6-17: Reversible insertion of oct-4-yne into the Sn–Si bond of aryl(silyl)stannylene, **4.10**.

Intrigued as to why the reaction did not go to completion, investigations were carried out to ascertain whether **6.17** was in equilibrium with **4.10** and oct-4-yne. The reaction of **4.10** and three equivalents of oct-4-yne in C_6D_6 was allowed to equilibrate at ambient conditions. Analysis by *in situ* ^{1}H NMR spectroscopy showed the ratio of intensities of the *meta*-substituted protons of the terphenyl ligands between **6.17** and **4.10** was 1:10. Heating the reaction mixture at 323 K overnight, followed by subsequent investigation by *in situ* ^{1}H NMR spectroscopy (also at 323 K), revealed a change in the ratio of intensities to 1:20 (**6.17**:**4.10**). Further heating of the reaction mixture to 353 K resulted in the loss of the ^{1}H NMR resonances corresponding to the *meta*-substituted protons of the terphenyl ligand of **6.17**. Cooling the reaction mixture to ambient conditions afforded the same ratio of ligand intensities which was seen prior to the heating of the reaction mixture (1:10). These data suggest that the **4.10** and oct-4-yne are in equilibrium with **6.17**, and that the forward reaction is an exothermic process. The equilibrium can be shifted to **6.17** by the addition of *circa.* 40 equivalents of alkyne to the reaction mixture, as evidenced by the increased ratio of ligand resonance intensities between **6.17** and **4.10** (1:3.2 respectively). That the equilibrium lies so far to the reactants, at stoichiometric equivalents of alkyne, resulted in difficulties in performing the variable temperature NMR experiments necessary to establish the thermodynamic parameters of this reaction. Therefore, equilibria between **4.10** and other alkynes were sought.

6.2.2.2 Aryl(silyl)stannylene **4.10** and Hex-3-yne

Addition of hex-3-yne to a C_6D_6 solution of aryl(silyl)stannylene, **4.10**, leads to a colour change from teal to dark aquamarine over the course of 2 h. Investigation of the reaction by ^{1}H NMR spectroscopy shows the formation of new terphenyl ligand resonances (e.g. *meta*-protons of central phenyl ring: 7.08 ppm, *meta*-protons of flanking mesityl rings: 6.78 ppm). These signals integrate in an equimolar ratio with two new resonances (0.85 and 0.81 ppm), which are proposed to correspond to the methyl groups of the ethyl substituents bonded to the alkenyl moiety, formed by the insertion of hex-3-yne into the Sn–Si bond of **4.10** (Scheme 6-18). Whilst evidence could not be obtained to confirm the geometry of the product (**6.18**), it is proposed, based on previous results, that **6.18** is the Z-alkene isomer. Despite stirring for several days, the reaction did not reach completion. Therefore, as with **6.17** above (Scheme 6-17), investigations to determine whether the formation of **6.18** is reversible were undertaken.

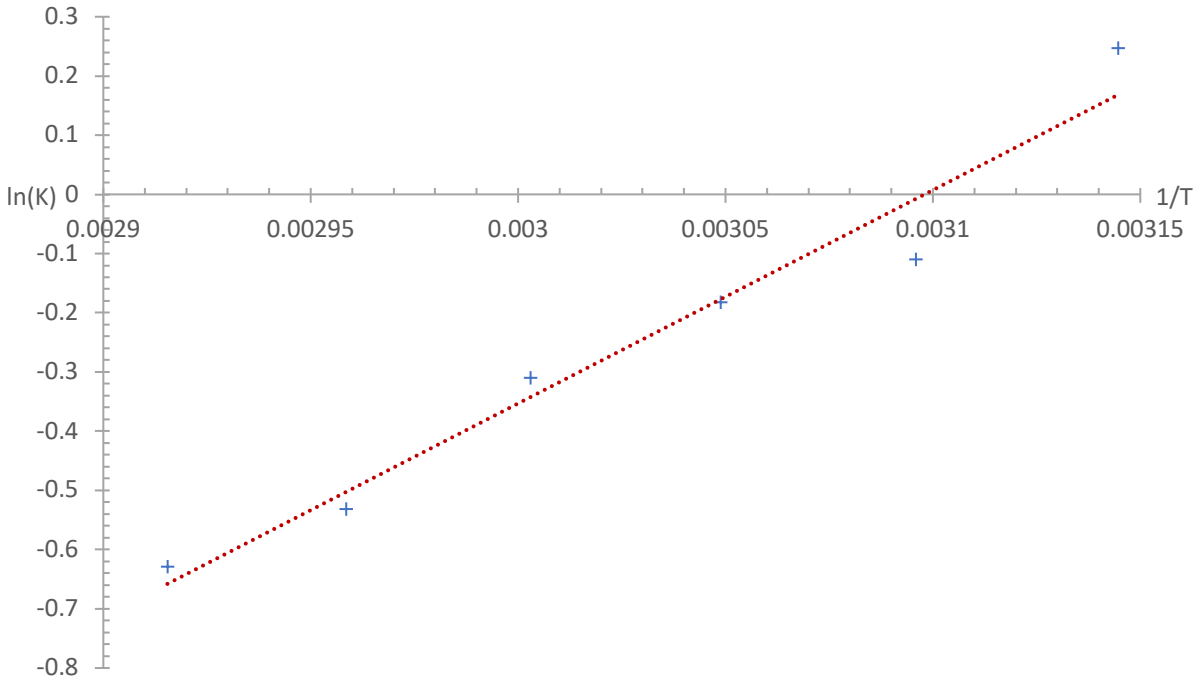


Scheme 6-18: Reversible insertion of hex-3-yne into the Sn–Si bond of aryl(silyl)stannylene, **4.10**.

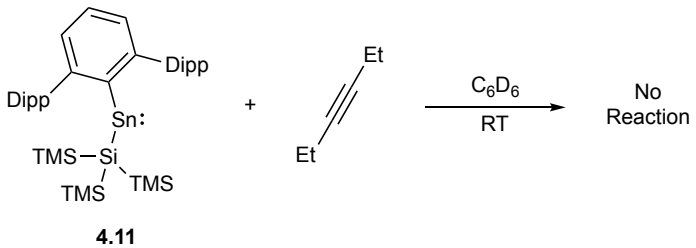
Confirmation of the reversibility of the reaction to form **6.18** was achieved by variable temperature ^{1}H NMR experiments. A C_6D_6 solution of the reaction mixture was warmed from 318 K to 348 K (in 5 K increments), and a ^{1}H NMR spectrum was obtained at each temperature. The ratio of intensities of the resonances assigned to the *meta*-protons of the central terphenyl ligand of **4.10** and **6.18** was thereby obtained at each temperature. The proportion

of **6.18** in solution decreased as the temperature of the reaction mixture was increased, implying not only the reversibility of the reaction but also the exothermic nature of the formation of **6.18**. In order to obtain the thermodynamic parameters for this reaction, a van't Hoff analysis was undertaken using variable temperature (45-75 K) ^{1}H NMR spectroscopy (Graph 6-1). From these data, the following values were obtained: ΔH_{Insert} = -30.0 ± 1.2 kJ mol^{-1} , ΔS_{Insert} = -92.8 ± 3.7 J K^{-1} mol^{-1}, and ΔG_{Insert}(298 K) = -2.3 ± 0.1 kJ mol^{-1}. The small negative value for ΔG_{Insert}(298 K) indicates that the reaction is favourable at ambient conditions, as evidenced by the reactivity observed in the initial NMR experiments. The negative enthalpy change determined for the forward reaction is consistent with the experimental observation of the reduced intensities of product resonances as the temperature was raised. Finally, the value obtained for the entropy of the reaction (-92.8 J K^{-1} mol^{-1}) is consistent with the increased molecular ordering for an insertion reaction.

Graph 6-1: van't Hoff plot relating to the reaction between aryl(silyl)stannylene, **4.10**, and hex-3-yne. Error estimated to be approximately 4%.



Once it had been observed that the equilibrium of alkyne insertion into the Sn–Si bond of aryl(silyl)stannylene, **4.10**, could be shifted towards the insertion product by decreasing the steric bulk of the alkyne used (oct-4-yne *vs.* hex-3-yne), investigations were carried out into the effect of the steric bulk of the stannylene on the reaction. When the bulkier aryl(silyl)stannylene ($SnAr^{Dipp}Si(TMS)_3$), **4.11**, was reacted with hex-3-yne, no reaction was seen, thereby offering further confirmation of the sensitivity to steric bulk of insertion reactions of alkynes into Sn–Si bonds.

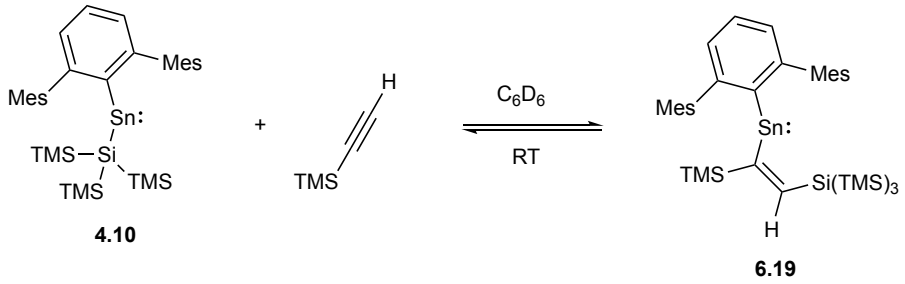


4.11

Scheme 6-19: Null of reaction between aryl(silyl)stannylene, **4.11**, and hex-3-yne.

6.2.2.3 Aryl(silyl)stannylene **4.10** and Trimethylsilylacetylene

The addition of trimethylsilylacetylene, Me_3SiCCH, to a C_6D_6 solution of aryl(silyl)stannylene, **4.10**, results in a change of colour from teal to deep blue over the course of 2 h. Analysis of the reaction mixture by *in situ* ^{1}H NMR spectroscopy shows the resonances of **4.10** as well as new signals. These correspond to a terphenyl ligand environment (e.g. *meta*-protons of central phenyl ring of terphenyl ligand: 7.10 ppm, *para*-proton of central phenyl ring of terphenyl ligand: 7.31 ppm) which integrate in an equimolar ratio with an alkenic resonance at 9.16 ppm. These data suggest that the product of the reaction, **6.19**, is formed *via* the insertion of a single equivalent of alkyne into the Sn–Si bond of **4.10**. While evidence to confirm the stereochemistry of **6.19** could not be obtained, it is proposed that **6.19** is the Z-isomer with the silyl ligand attached to the least hindered alkenic carbon (due to the reasons discussed above).[2–4]

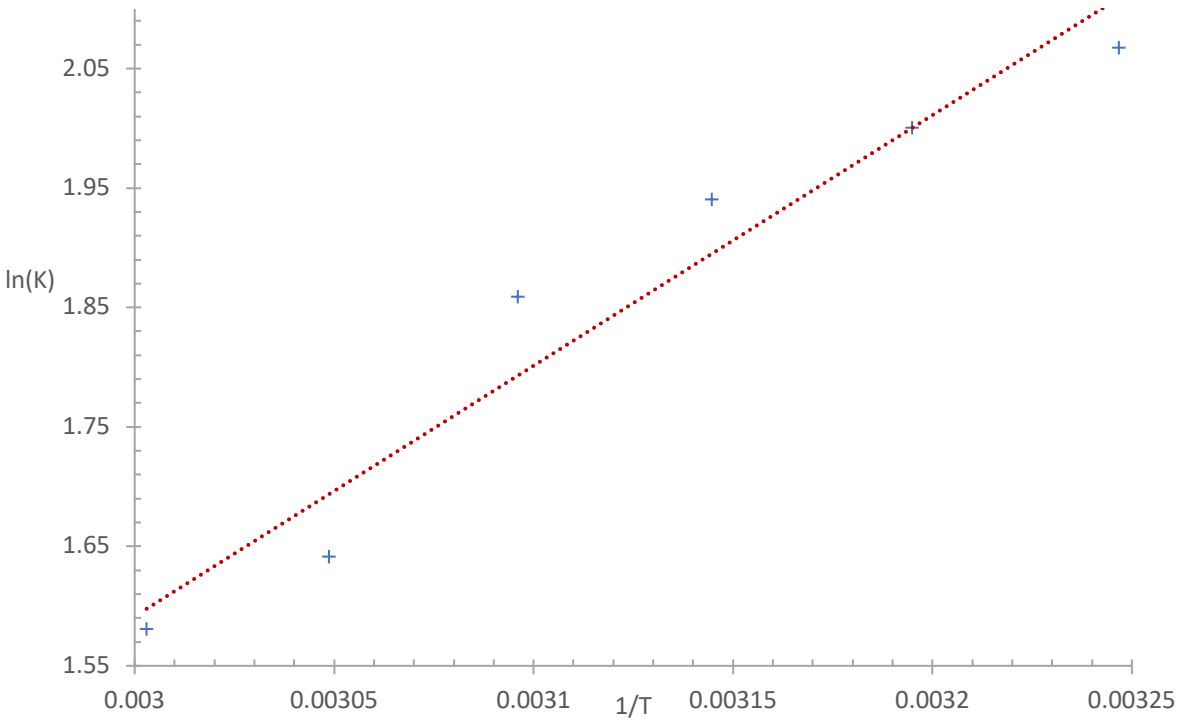


Scheme 6-20: Reversible insertion of trimethylsilylacetylene into the Sn–Si bond of aryl(silyl)stannylene, **4.10**.

As was seen with oct-4-yne and hex-3-yne above, the reaction between **4.10** and Me_3SiCCH to form **6.19** was found to be reversible, as shown by the temperature dependence of the resonances in the *in situ* ^{1}H NMR spectra. To understand the thermodynamics of the reaction, a van't Hoff analysis was performed using variable temperature (308-333 K) ^{1}H NMR spectroscopy. From these data, the following values were obtained: ΔH_{Insert} = -17.4 ± 1.1 kJ mol^{-1} , ΔS_{Insert} = -39.1 ± 2.4 J K^{-1} mol^{-1}, and ΔG_{Insert}(298 K) = -5.8 ± 0.4 kJ mol^{-1}. The

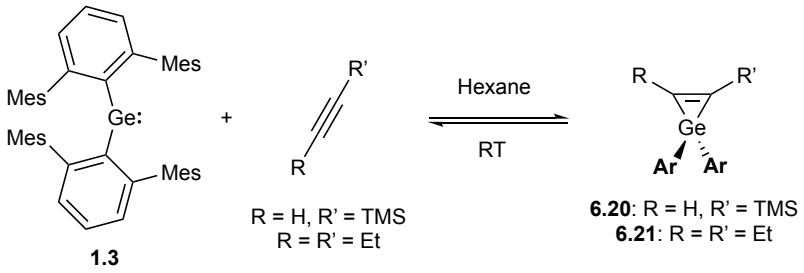
greater magnitude of ΔG_{Insert}(298 K) for the reaction between **4.10** and Me_3SiCCH, compared to its reaction with hex-3-yne (-5.8 *vs.* -2.3 kJ mol^{-1} respectively), shows it is a more favourable reaction at ambient conditions. The value of ΔS_{Insert} for the formation of **6.19** (-39.1 J K^{-1} mol^{-1}) is less than half the value for formation of **6.18** (-92.8 J K^{-1} mol^{-1}). This can be explained by the two ethyl groups of hex-3-yne being restricted in motion due to incorporation into **6.18**, whereas only the trimethylsilyl group is restricted in **6.19**, resulting in a smaller loss of degrees of freedom.

Graph 6-2: van't Hoff plot relating to the reaction between aryl(silyl)stannylene, **4.10**, and trimethylsilylacetylene. Error estimated to be approximately 7%.



Whilst no other examples of the reversible insertion of alkynes into E–X bonds have been reported, the results can be compared with the thermodynamic parameters determined by Lai *et al.* for the reversible cycloaddition reaction of Me_3SiCCH and hex-3-yne with bis(aryl)germylene, **1.3** (Scheme 6-21).[16] The values of ΔG_{assn}(298 K) for the formation of **6.20**

(from **1.3** + Me_3SiCCH) and **6.21** (from **1.3** + hex-3-yne) are +5.16 $kJmol^{-1}$ and -5.11 $kJmol^{-1}$ respectively.[16] These values are very similar to the values of ΔG_{Insert}(298 K) obtained for the formation of **6.19** (**4.10** + TMSCCH) and **6.18** (**4.10** + hex-3-yne) (-5.8 kJ mol^{-1} and -2.3 kJ mol^{-1} respectively), and the near zero values for ΔG_{Insert}(298 K) is of course what might be expected for reversible reactions.



Scheme 6-21: Reversible cycloaddition of trimethylsilylacetylene and hex-3-yne with bis(aryl)germylene, **1.3**.

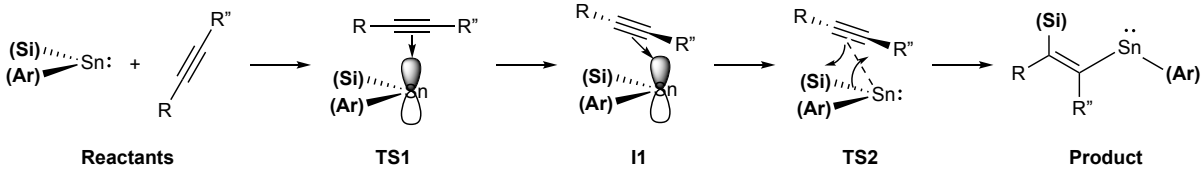
6.2.3 Mechanism of Insertion

Quantum chemical calculations were performed to investigate the mechanism that underpins the insertion chemistry demonstrated above. Aryl(silyl)stannylene, **4.10**, was used as the example of a generic silylstannylene for the calculations due to the wide range of alkynes with which it reacts. No simplifications were made to the ligands of **4.10** in the calculations to ensure that the representation of the mechanism obtained was as accurate as possible and that steric (as well as electronic) influences could be fully accounted for.

The first potential mechanism examined for feasibility was one in which the alkyne undergoes a [2+1]-cycloaddition at the tin centre, followed by subsequent migration of the silyl ligand leading to ring opening of the cyclopropene intermediate (Scheme 6-3). A similar mechanism has been proposed for the alkyne insertion chemistry observed with bis(silyl)germylenes (Schemes 1-19 and 1-20), and borylstannylenes (Schemes 1-22 and 6-2).[3,7,8] However, despite

repeated attempts, the geometries of the intermediates and transition states of the mechanism could not be optimised, suggesting that this mechanism might not be occurring between silylstannylenes and alkynes. As a result, other mechanistic pathways for this reaction were sought.

An alternative mechanistic postulate is depicted below (Scheme 6-22). The reaction occurs *via* the initial coordination of the alkyne to the formally vacant 5p-orbital of the stannylene, **TS1**. This coordination complex then distorts, and the R group of the alkyne shifts in the direction of the silyl ligand of the stannylene to form intermediate, **I1**. The R group then moves further towards the silyl ligand, meaning that the alkyne lies predominantly over the Sn–Si bond, in order that concerted activation of the alkyne across the Sn–Si bond can occur, *via* **TS2**, to yield the insertion product.



Scheme 6-22: General mechanism for the insertion of alkynes into the Sn–Si bond of aryl(silyl)stannylene, **4.10** (**(Ar)** is – C_6H_3-2,6-(C_6H_2-2,4,6-Me_3)$_2$ and **(Si)** is –$Si(SiMe_3)_3$).

From this proposed mechanism, both the regio- and stereospecificity of the reaction can potentially be understood. Firstly, since the activation of the alkyne across the Sn–Si bond occurs in concerted fashion, it naturally follows that the tin and silicon atoms would then be on the same side of the resulting alkene, therefore resulting in a Z-alkene product. Additionally, since the initial coordination of the alkyne occurs with one of the R groups of the alkyne directed at the ligand framework of the stannylene, it follows that the lowest energy reaction pathway will be the one with the smallest R group directed at the ligand framework,

to minimise steric repulsion. This is why the reaction typically results in the silyl ligand being attached to the least hindered carbon atom.

The free energy profile for the reaction between phenylacetylene and aryl(silyl)stannylene, **4.10**, is depicted below (Figure 6-6). The calculations show the reaction between **4.10** and PhCCH to be strongly exergonic (ΔG = -49.0 kJ mol^{-1}) and with low overall energy barrier to the reaction (52.8 kJ mol^{-1}) (Figure 6-6). This fits with the experimental results, in which insertion was found to occur immediately (and irreversibly) at room temperature. In addition, **TS2** which leads to formation of **6.10** (52.8 kJ mol^{-1}) was found to be significantly lower in energy than the transition state which would lead to the other regioisomer (92.0 kJ mol^{-1}), illustrating why **6.10** is the only product of the reaction.

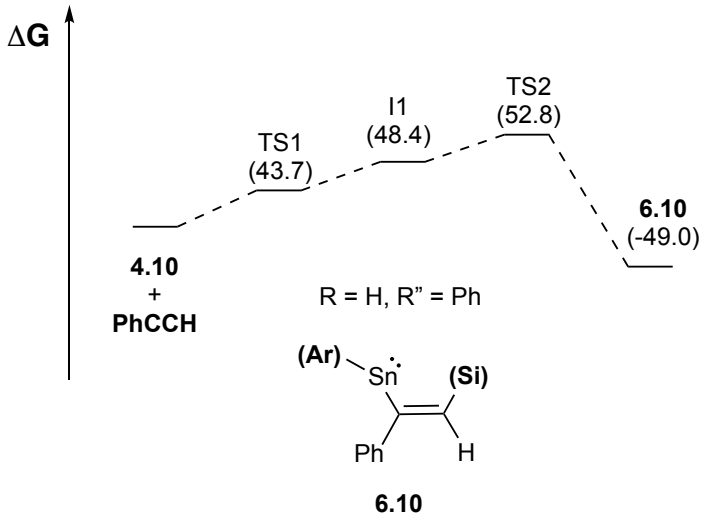


Figure 6-6: Free energy diagram for the reaction between phenylacetylene and aryl(silyl)stannylene, **4.10** (**(Ar)** is – C_6H_3-2,6-(C_6H_2-2,4,6-Me_3)$_2$ and **(Si)** is –$Si(SiMe_3)_3$). Energies in kJ mol^{-1}.

The free energy profiles for the reversible reactions of **4.10** with Me_3SiCCH and hex-3-yne were also calculated (Figure 6-7). For both the formation of **6.19** and **6.18**, the net energy change for the reactants to the products is close to zero (-3.0 and 1.4 kJ mol^{-1} respectively). This aligns closely with the reversibility displayed experimentally by both reactions.

Comparison of the two energies of the two transition states **TS1** for these reactions gives an insight into the impact of steric bulk on this reaction mechanism. **TS1** leading to the formation of **6.19** (52.4 kJ mol^{-1}) is half the size of the **TS1** for the formation of **6.18** (108.1 kJ mol^{-1}). This indicates the increased steric repulsion between the silyl substituent (-Si(TMS)$_3$) of **4.10** and an ethyl chain, compared to a proton, as the alkyne coordinates to the formally vacant 5p-orbtial.

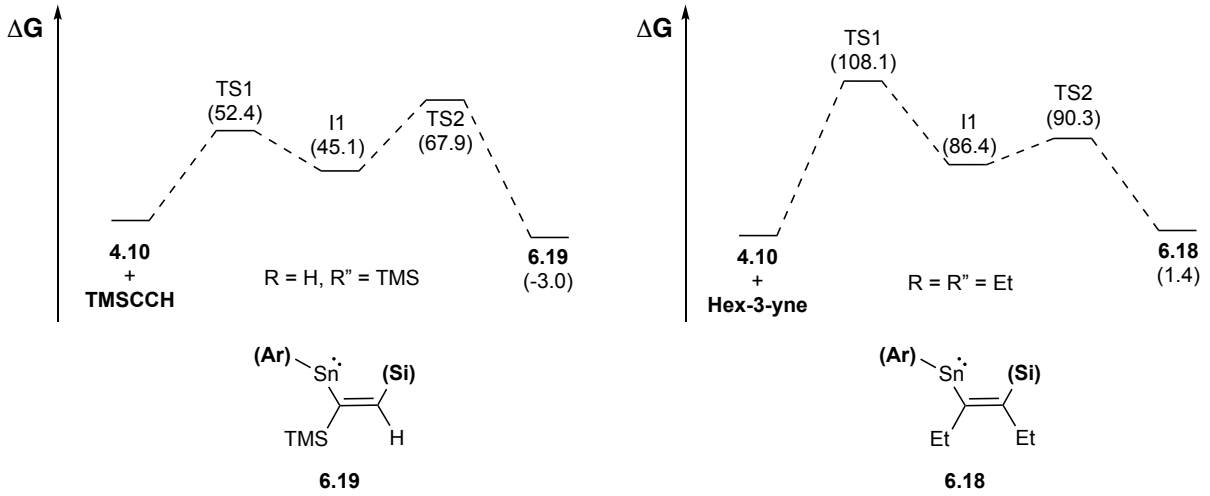


Figure 6-7: Left – Energy diagram for the reaction between trimethylsilylacetylene and aryl(silyl)stannylene, **4.10**. Right – Energy diagram for the reaction between hex-3-yne and aryl(silyl)stannylene, **4.10** (**(Ar)** is –C_6H_3-2,6-(C_6H_2-2,4,6-Me_3)$_2$ and **(Si)** is –Si($SiMe_3$)$_3$). Energies in kJ mol^{-1}.

The reaction between hex-1-yne and aryl(silyl)stannylene, **4.10**, is the only example in this thesis from which two regioisomers are proposed to form (Scheme 6-12 and Figure 6-3). The mechanism proposed in Scheme 6-22 can offer some explanation as to why this is the case whereas the cycloaddition/migration reaction mechanism (Scheme 6-3) cannot. If the alkyne insertion into the Sn–Si bond were *via* the cycloaddition/migration pathway, it would be expected that both hex-1-yne *and* 6-chlorohex-1-yne should produce two regioisomers. This is because the 6-position is very remote and therefore should not affect the migration of the silyl substituent (Figure 6-8). However, the reaction between 6-chlorohex-1-yne and **4.10** only

produces one stereoisomer (Scheme 6-13). In the intermediate of the reaction mechanism proposed in Scheme 6-22, the coordinating alkyne distorts so that it lies above (and near parallel with) the Sn–Si bond. In this intermediate one of the alkyne substituents will point at the silyl ligand ($Si(TMS)_3$) of **4.10** (Figure 6-8). Therefore, the 6-position of hex-1-yne will have a meaningful influence on the energy of the reaction intermediate, explaining why the reaction of 6-chlorohex-1-yne with **4.10** yields only one product.

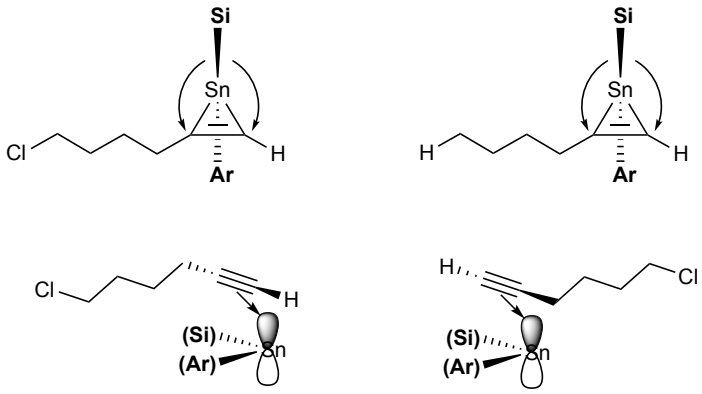


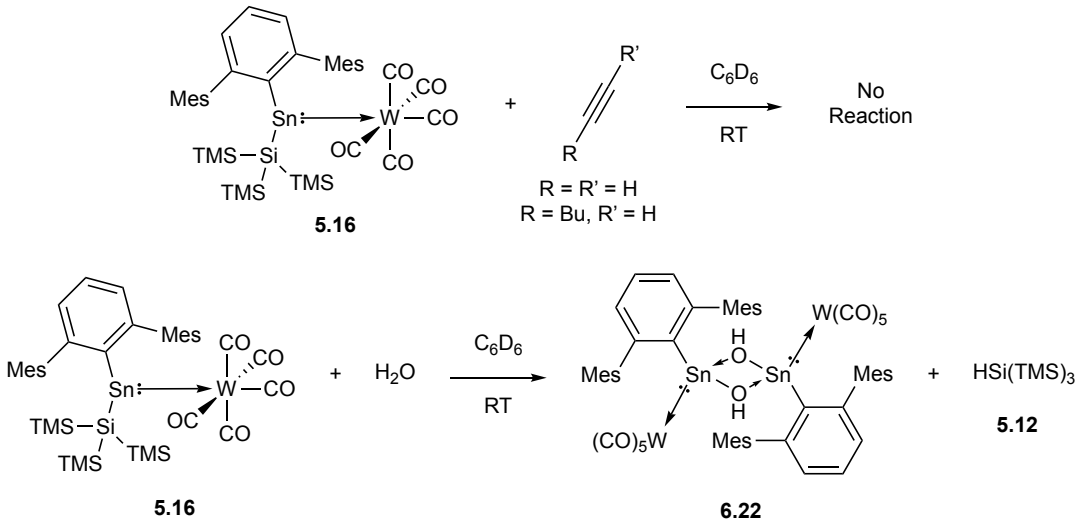
Figure 6-8: Top – Negligible effect of additional bulk of chlorine atom in 6-chlorohex-1-yne compared to hex-1-yne due to the large distance between the terminal carbon and where migration is occurring. Bottom – Two potential intermediates in the reaction between **4.10** and 6-chlorohex-1-yne, illustrating that one pathway will result in reduced steric clash with the silyl substituent.

6.2.3.1 Reactions Probing Mechanism

One major discrepancy between the mechanism proposed above and the cycloaddition/migration pathway proposed by Protchenko *et al.* is the role of the stannylene lone pair.[3] In the mechanism proposed in this thesis, the lone pair is not involved in the insertion process, whereas it is crucial in the formation of the cyclopropene intermediate in the alternate cycloaddition/migration pathway.[3] This is why, if insertion of an alkyne into the Sn–Si bond of a stannylene complex in which the lone pair was unavailable occurred, it would serve as strong evidence that a cycloaddition/migration pathway mechanism was not

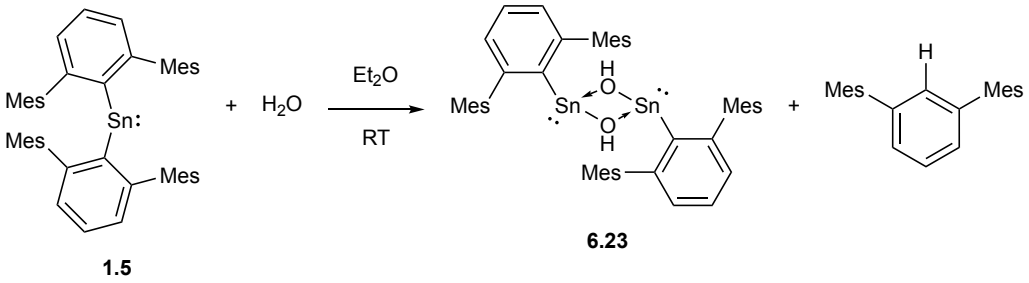
occurring. To this end, the reactivity of the tungsten pentacarbonyl stannylene complex, **5.3**, was investigated with alkynes.

When hex-1-yne was added to a solution of **5.3**, no immediate colour change was seen. Even after prolonged heating at 353 K, no reaction was observed. It was thought that due to the bulk of the tungsten pentacarbonyl fragment, the insertion chemistry would be even more sensitive to the bulk of the alkyne. Therefore, the reaction with acetylene was investigated. However, the exposure of a C_6D_6 solution of **5.3** to one atmosphere of ethyne does not yield an immediate colour change in the reaction mixture (Scheme 6-23). After 12 h, however, colourless crystals suitable for X-ray diffraction were obtained, allowing their identity as a bridging Sn(II) hydroxide species to be confirmed (Figure 6-9). This most likely results from the reaction of **5.3** with adventitious water in the acetylene used (Scheme 6-23). When the reaction was performed with pre-dried acetylene, no reaction was observed, implying that a cycloaddition/migration mechanism could be still be viable.



Scheme 6-23: Top – Absence of reactivity between tungsten pentacarbonyl stannylene complex, **5.16**, and hex-1-yne or acetylene. Bottom – Reaction of tungsten pentacarbonyl stannylene complex, **5.16**, with water.

The molecular structure of **6.22** is depicted below (Figure 6-9). It is a dimeric Sn(II) species featuring bridging hydroxide ligands, with the lone pairs of the stannylene units coordinated to the tungsten pentacarbonyl fragments. In a 2015 paper, Erickson *et al.* reported the reaction of bis(aryl)stannylene, **1.5**, with water to yield the bridging Sn(II) hydroxide species, **6.23** (Scheme 6-24).[17] The structural similarity between **6.22** and **6.23** is clear from their bond lengths (Sn–C: **6.22**, 2.180(5) Å; **6.23**, 2.208(3) Å, Sn–O: **6.22**, 2.129(3) and 2.138(3) Å ; **6.23**, 2.1345(14) Å) and confirms the assignment of **6.22** as a Sn(II) species. Interestingly, the mechanism of the formation of **6.23** is thought to proceed *via* coordination of the oxygen lone pair of the water to the formally vacant 5p-orbital of the stannylene, followed by the concerted addition of one of the O–H bonds across a Sn–C bond. This is not dissimilar to the mechanism of alkyne insertion into the Sn–Si bonds of silylstannylenes proposed in this thesis, and the difference in reactivity is due to the formation of a stronger complex between water and the formally vacant tin 5p-orbital, in comparison to acetylene.



Scheme 6-24: Reaction of bis(aryl)stannylene, **1.5**, with water.

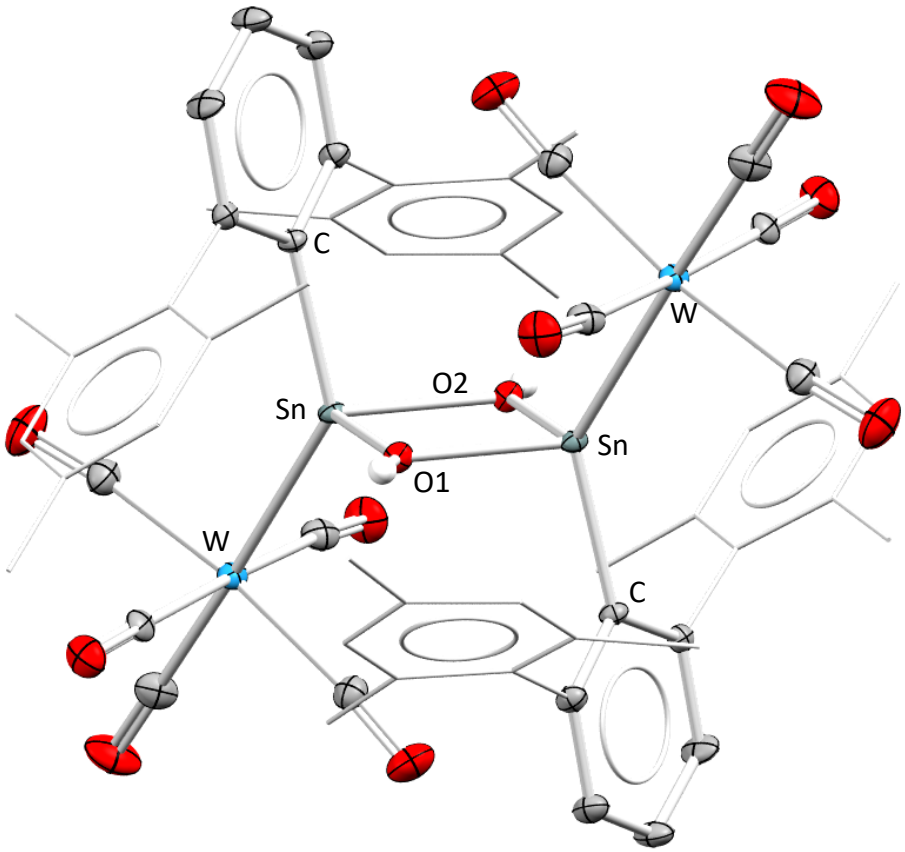


Figure 6-9: Molecular structure of **6.22** as determined by X-ray crystallography. Thermal ellipsoids are set at the 50% probability level. All hydrogen atoms, except those of the bridging hydroxides, are omitted for clarity. The flanking mesityl rings of the terphenyl ligand are depicted in wireframe for clarity. Key bond lengths (Å) and angles (°): Sn–W: 2.7741(6), Sn–O1: 2.129(3), Sn–O2: 2.138(3), Sn–C: 2.180(5), C–Sn–O1: 97.6(1), C–Sn–O2: 97.1, Sn–O1/O2–Sn: 110.3(1), O1–Sn–O2: 69.7, W–Sn–C: 134.78(9), W–Sn–O1: 118.34(8), W–Sn–O2: 119.70(8).

6.3 Conclusions

In this chapter, the reactivity of an array of silylstannylenes towards alkynes was explored. Acetylene was found to undergo an insertion reaction into the Sn–Si bond of aryl(silyl)stannylene, **4.10**, to yield **6.6** (Scheme 6-4). Similar reactivity was observed between but-2-yne and **4.10**, as well as with the bulkier aryl(silyl)stannylene, **4.11**, to yield **6.8** and **6.9** respectively (Schemes 6-6 and 6-7). Phenylacetylene was also found to insert regioselectively into the Sn–Si bond of **4.10** to yield **6.10** (Scheme 6-9). However, when reacted with

amido(silyl)stannylene, **4.19**, a protonolysis reaction occurred to yield aniline, **6.5**, and the (postulated) Sn(II) alkynyl bridged dimer, **6.11** (Scheme 6-10). The reaction between **4.10** and hex-1-yne (Scheme 6-12) generates two regioisomers from alkyne insertion into the Sn–Si bond, **6.12** and **6.13**, however by increasing the bulk of the alkyne to 6-chlorohex-1-yne (Scheme 6-13), the selectivity of the reaction was re-established and only one regioisomer was produced. Additionally, the reactions with two phenylprop-1-ynes (1-phenylprop-1-yne and $CF_3(C_6H_4)CCH$) with **4.10** were investigated (Schemes 6-14 and 6-15 respectively) and found to selectively produce alkenylstannylenes, **6.15** and **6.16**, both of which are Z-alkenes with the silyl group attached to the least hindered carbon atom. Additionally, reversible insertions of oct-4-yne, hex-3-yne, and Me_3SiCCH into the Sn–Si bond of **4.10** were disclosed (Schemes 6-17, 6-18, and 6-20 respectively). These serve as the first examples of reversible insertion into the Sn–X bonds of stannylenes and the thermodynamic parameters associated with the equilibria could be obtained for hex-3-yne and Me_3SiCCH. Additionally, a mechanism for the reaction between **4.10** and alkynes was proposed, based on quantum chemical calculations, and suggested that the reaction does not proceed *via* a [2+1]-cycloaddition intermediate. Instead, it is proposed that coordination of the alkyne to the formally vacant 5p-orbital occurs, followed by a concerted activation process across the Sn–Si bond (Scheme 6-22). The concerted nature of the bond activation explains why the reactions between **4.10** and alkynes yield the *syn*-addition products. Furthermore, as the intermediate of this mechanism involves one of the substituents of the alkyne pointing directly at the silyl ligand of **4.10**, it can be readily understood why the regioisomer in which the silyl ligand is bonded to the least bulky alkyne substituent, predominates.

6.4 Characterisation of Novel Materials

6.4.1 Synthesis of *Z*-Sn(Ar^{Mes})(C(H)=C(H)($Si(TMS)_3$), **6.6** (Scheme 6-4)

A solution of **4.10** (20 mg, 0.029 mmol) in C_6D_6 (0.40 mL) was degassed *via* 3 freeze-pump-thaw cycles before the atmosphere was charged with acetylene (*ca*. 1 bar). The colour of the reaction mixture immediately turned red upon vigorous shaking. *In situ* NMR data could be obtained from the reaction mixture. ^{1}H NMR (600 MHz, C_6D_6, 298 K) δ: 9.50 (d, Sn–C(*H)*=C, $^3J_{HH}$ = 16.7 Hz, 1H), 8.06 (d, Si–C(*H)*=C, $^3J_{HH}$ = 16.7 Hz, 1H), 7.33 (t, *p*-C*H* Ar^{Mes}, $^3J_{HH}$ = 7.5 Hz, 1H), 7.08 (d, *m*-C*H* Ar^{Mes}, $^3J_{HH}$ = 7.5 Hz, 2H), 6.77 (s, Mes-C*H*, 4H), 2.27 (s, *o*-CH_3 Mes, 12H), 2.16 (s, *p*-CH_3 Mes, 6H), 0.15 (s, Si(SiCH_3)$_3$, 27H) ppm. ^{13}C NMR (151 MHz, C_6D_6, 298 K) δ: 202.0, 177.5, 146.7, 146.2, 137.4, 136.2, 135.8, 129.0, 128.0, 128.4, 21.3, 21.2, 1.2 ppm. ^{29}Si NMR (79 MHz, C_6D_6, 298 K) δ: −14.1, −85.9 ppm. ^{119}Sn NMR (186 MHz, C_6D_6, 298 K) δ: -138.5 ppm.

6.4.2 Reaction of $SnAr^{Mes}Si(TMS)_3$ with But-2-yne (Scheme 6-6)

An excess of 2-butyne (0.050 mL, 0.64 mmol) was added to a solution of **4.10** (65 mg, 0.096 mmol) in toluene (5.0 mL), and the reaction mixture stirred at room temperature for 12 h. The solution was reduced in volume to incipient crystallisation, and storage at 243 K afforded the product, **6.8**, as purple crystals suitable for X-ray crystallography. The product could also be characterised by *in situ* ^{1}H NMR spectroscopy. Yield: 10 mg, 21 %. ^{1}H NMR (400 MHz, C_6D_6, 298 K) δ: 7.35 (t, *p*-C*H* Ar^{Mes}, $^3J_{HH}$ = 7.5 Hz, 1H), 7.11 (d, *m*-C*H* Ar^{Mes}, $^3J_{HH}$ = 7.5 Hz, 2H), 6.77 (s, Mes-C*H*, 4H), 2.53 (s, Sn–C(CH_3)=C, 3H), 2.48–2.23 (br. s, *o*-CH_3 Mes, 12H), 2.14 (s, *p*-CH_3 Mes, 6H), 1.87 (s, Si–C(CH_3)=C, 3H), 0.17 (s, Si(SiCH_3)$_3$, 27H) ppm.

6.4.3 Reaction of $SnAr^{Dipp}Si(TMS)_3$ with But-2-yne (Scheme 6-7)

To a solution of **4.11** (9.0 mg, 0.012 mmol) in C_6D_6 (0.40 mL) was added excess but-2-yne (2.9 μL, 0.037 mmol), with no immediate colour change observed. After 1 h at room temperature, a colour change from teal to purple occurred and the product, **6.9**, was characterised by *in situ* ^{1}H NMR spectroscopy. ^{1}H NMR (400 MHz, C_6D_6, 298 K) δ: 7.35–7.30 (m, Ar*H*, 1H), 7.26–7.17 (m, Ar*H*, 5H), 7.08 (d, *m*-Dipp-C*H*, $^3J_{HH}$ = 7.5 Hz, 4H), 3.32 (sept, ^{i}Pr-*H*, $^3J_{HH}$ = 6.8 Hz, 4H), 1.34 (d, ^{i}Pr-C*H*$_3$, $^3J_{HH}$ = 6.9 Hz, 12H), 1.08 (d, ^{i}Pr-C*H*$_3$, $^3J_{HH}$ = 6.8 Hz, 12H), 0.21 (s, SiC*H*$_3$, 27H) ppm.

6.4.4 Synthesis of *Z*-$Sn(Ar^{Mes})(C(Ph)=C(H)(Si(TMS)_3)$, **6.10** (Scheme 6-9)

Excess phenylacetylene (0.020 mL, 0.18 mmol) was added to a solution of **4.10** (100 mg, 0.15 mmol) in toluene (5.0 mL), resulting in an immediate colour change from teal to purple. The crude product, **6.11**, was isolated as a purple powder after removal of volatiles *in vacuo*. Extraction into pentane, concentration of the solution to incipient crystallisation, and storage at 280 K yielded the product as purple crystals suitable for X-ray crystallography. Yield: 30 mg, 26 %. ^{1}H NMR (600 MHz, Tol-d^8, 298 K) δ: 7.49 (s, Si–C(*H)*=C, 1H), 7.26 (t, *p*-C*H* Ar^{Mes}, $^3J_{HH}$ = 7.5 Hz, 1H), 7.04 (t, *m*-C*H* Ph, $^3J_{HH}$ = 7.5 Hz, 2H), 7.01 (d, *o*-C*H* Ph, $^3J_{HH}$ = 7.5 Hz, 2H), 6.91 (d, *m*-C*H* Ar^{Mes}, $^3J_{HH}$ = 7.5 Hz, 2H), 6.88 (t, *p*-C*H* Ph, $^3J_{HH}$ = 7.5 Hz, 1H), 6.76 (s, Mes-C*H*, 4H), 2.46 (s, Mes-C*H*$_3$, 6H), 2.17 (s, Mes-C*H*$_3$, 6H), 1.79 (s, Mes-C*H*$_3$, 6H), 0.17 (s, Si(SiC*H*$_3$)$_3$, 27H) ppm. ^{13}C NMR (151 MHz, Tol-d^8, 298 K) δ: 218.3 , 179.7, 153.1, 149.2, 146.1, 137.2, 136.8, 130.0 , 129.9, 129.5, 127.9, 127.7, 126.9, 126.0, 21.5, 21.2, 20.9 ppm. ^{29}Si NMR (79 MHz, Tol-d^8, 298 K) δ: −12.9, −86.9 ppm. ^{119}Sn NMR (149 MHz, Tol-d^8, 298 K) δ: 1689.6 ppm.

6.4.5 Reaction of $SnAr^{Mes}Si(TMS)_3$ with PhCCMe (Scheme 6-14)

Excess 1-phenylprop-1-yne (0.020 mL, 0.16 mmol) was added to a solution of **4.10** (100 mg, 0.15 mmol) in a mixture of hexane (5.0 mL) and toluene (2.0 mL). The reaction mixture was stirred at room temperature for 12 h and the crude product, **6.15**, isolated as a purple powder after removal of the volatiles *in vacuo*. Subsequent extraction into pentane, concentration to incipient crystallisation, and storage at 280 K yielded the product as purple crystals suitable for X-ray crystallography. Yield: 32 mg, 27 %. ^{1}H NMR (400 MHz, C_6D_6, 298K) δ: 7.22 (t, *p*-C*H* Ar^{Mes}, $^3J_{HH}$ = 7.5 Hz, 1H), 7.18–7.14 (m, Ph*H*, 1H), 6.95 (d, *m*-C*H* Ar^{Mes}, $^3J_{HH}$ = 7.5 Hz, 2H), 6.90–6.81 (m, Mes-C*H*, 4H), 6.77 (s, Ph*H*, 2H), 6.62–6.58 (m, Ph*H*, 2H), 2.46 (s, Mes-CH_3, 6H), 2.19 (s, Mes-CH_3, 6H), 1.85 (s, Mes-CH_3, 6H), 1.73 (s, Si–C(CH_3)=C, 3H), 0.21 (s, Si(SiCH_3)$_3$, 27H) ppm.

6.4.6 Reaction of $SnAr^{Mes}Si(TMS)_3$ with $CF_3(C_6H_4)CCMe$ (Scheme 6-15)

Excess of $CF_3(C_6H_4)CCMe$ (31 mg, 0.17 mmol) was added to a solution of **4.10** (100 mg, 0.15 mmol) in a mixture of hexane (5.0 mL) and toluene (2.0 mL). The reaction mixture was stirred at room temperature for 12 h and the crude product, **6.16**, isolated as a purple powder after removal of the volatiles *in vacuo*. Subsequent extraction into pentane, concentration to incipient crystallisation, and storage at 280 K yielded the product as purple crystals suitable for X-ray crystallography. Yield: 26 mg, 20 % ^{1}H NMR (400 MHz, C_6D_6, 298K) δ: 7.47 (d, *m*-C*H* Ph, $^3J_{HH}$ = 7.9 Hz, 2H), 7.18 (t, *p*-C*H* Ar^{Mes}, $^3J_{HH}$ = 7.5 Hz, 1H), 6.89 (d, *m*-C*H* Ar^{Mes}, $^3J_{HH}$ = 7.5 Hz, 2H), 6.79 (s, Mes-C*H*, 2H), 6.74 (s, Mes-C*H*, 2H), 6.53 (d, *o*-C*H* Ph, $^3J_{HH}$ = 7.9 Hz, 2H), 2.40 (s, Mes-CH_3, 6H), 2.18 (s, Mes-CH_3, 6H), 2.11 (s, Mes-CH_3, 3H), 1.72 (s, Mes-CH_3, 3H), 0.19 (s, Si(SiCH_3)$_3$, 27H) ppm. ^{19}F NMR (377 MHz, C_6D_6, 298K) δ: -61.4 ppm. ^{29}Si NMR (79 MHz, C_6D_6, 298 K) δ: -21.9 ppm.

6.4.7 Reaction of $SnAr^{Mes}Si(TMS)_3$ with TMSCCH (Scheme 6-20)

To a solution of **4.10** (15 mg, 0.022 mmol) in C_6D_6 (0.40 mL) was added TMSCCH (10 μL, 0.070 mmol) and an immediate colour change from teal to dark blue was seen. The reaction was allowed to equilibrate at room temperature for 1 h and the product, **6.19**, was characterised by *in situ* ^{1}NMR spectroscopy. ^{1}H NMR (500 MHz, C_6D_6, 298K) δ: 9.16 (s, C=C*H*, 1H), 7.31 (t, *p*-C*H* Ar^{Mes}, $^3J_{HH}$ = 7.5 Hz, 1H), 7.10 (d, *m*-C*H* Ar^{Mes}, $^3J_{HH}$ = 7.5 Hz, 2H), 6.79 (s, Mes-C*H*, 2H), 6.76 (s, Mes-C*H*, 2H), 2.43 (s, Mes-CH_3, 6H), 2.32 (s, Mes-CH_3, 6H), 2.12 (s, Mes-CH_3, 6H), 0.20 (s, N–SiCH_3, 9H), 0.11 (s, Si(SiCH_3)$_3$, 27H) ppm.

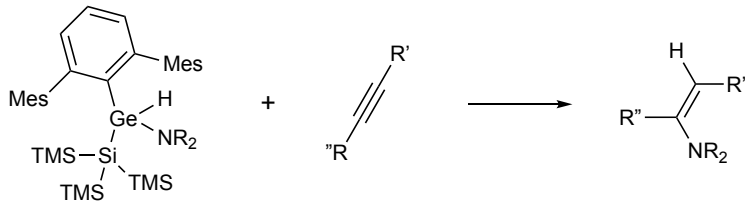
6.5 References

1 L. R. Sita and R. D. Bickerstaff, *J Am Chem Soc*, 1988, **110**, 5208–5209.
2 J. J. Maudrich, F. Diab, S. Weiß, M. Zweigart, K. Eichele, H. Schubert, R. Müller, M. Kaupp and L. Wesemann, *Chemistry – A European Journal*, 2021, **27**, 4691–4699.
3 A. V. Protchenko, M. P. Blake, A. D. Schwarz, C. Jones, P. Mountford and S. Aldridge, *Organometallics*, 2015, **34**, 2126–2129.
4 T. J. Hadlington, M. Hermann, G. Frenking and C. Jones, *Chem Sci*, 2015, **6**, 7249–7257.
5 H. C. Brown and J. B. Campbell, *Journal of Organic Chemistry*, 1980, **45**, 389–395.
6 L. A.-M. Harris, M. P. Coles and J. R. Fulton, *Inorganica Chim Acta*, 2011, **369**, 97–102.
7 M. Walewska, J. Baumgartner, C. Marschner, L. Albers and T. Müller, *Chemistry – A European Journal*, 2016, **22**, 18512–18521.
8 M. Walewska, J. Baumgartner and C. Marschner, *Chemical Communications*, 2014, **51**, 276–278.
9 F. Lips, A. Mansikkamäki, J. C. Fettinger, H. M. Tuononen and P. P. Power, *Organometallics*, 2014, **33**, 6253–6258.
10 D. Seyferth and S. C. Vick, *J Organomet Chem*, 1978, **144**, 1–12.
11 T. Soderberg, *Organic Chemistry with a Biological Emphasis Volume I*, University of Minnesota Morris, 2016.
12 M. Walewska, J. Baumgartner and C. Marschner, *Chemical Communications*, 2014, **51**, 276–278.
13 T. Sugahara, A. Espinosa Ferao, A. Rey Planells, J. D. Guo, S. Aoyama, K. Igawa, K. Tomooka, T. Sasamori, D. Hashizume, S. Nagase and N. Tokitoh, *Dalton Transactions*, 2020, **49**, 7189–7196.
14 T. Y. Lai, J. D. Guo, J. C. Fettinger, S. Nagase and P. P. Power, *Chemical Communications*, 2019, **55**, 405–407.
15 J. Zhu, Z. Lin and T. B. Marder, *Inorg Chem*, 2005, **44**, 9384–9390.
16 T. Y. Lai, K. L. Gullett, C. Y. Chen, J. C. Fettinger and P. P. Power, *Organometallics*, 2019, **38**, 1421–1424.
17 J. D. Erickson, P. Vasko, R. D. Riparetti, J. C. Fettinger, H. M. Tuononen and P. P. Power, *Organometallics*, 2015, **34**, 5785–5791.

7 Conclusions and Future Work

This thesis has explored the synthesis and small molecule reactivity of several silyl-substituted metallylenes.

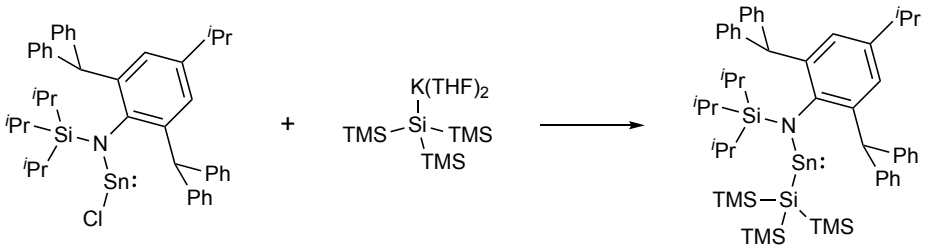
In Chapter 3, the small molecule reactivity of an aryl(silyl)germylene ($GeAr^{Mes}Si(TMS)_3$), **1.23**, was explored. Novel reactivity between **1.23** and PhCCH was displayed in which two equivalents of the alkyne were coupled together to yield a germole ($Ar^{Mes}Si(TMS)_3GeC(H)C(Ph)C(Ph)C(H)$). It was also found that **1.23** is capable of the oxidative addition of a range of N–H bonds of amines (e.g. $MeNH_2$, $^{s}BuNH_2$, $^{t}BuNH_2$, Et_2NH, and *p*-toluidine). Research should now focus on examining whether these Ge(IV) systems are capable of reacting with unsaturated substrates (e.g. alkenes, alkynes, and α-β-unsaturated ketones) to determine whether hydroamination with germylenes is possible.



Scheme 7-1: The proposed hydroamination of an alkyne by a Ge(IV) amido/hydride species. Where R, R', and R" are either hydrogen or small alkyl groups.

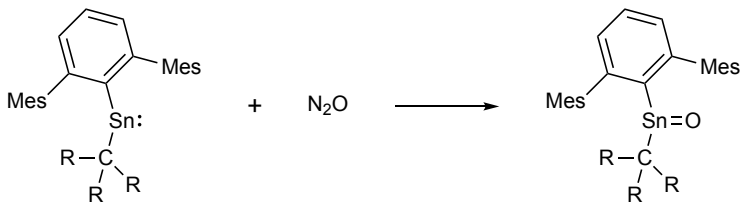
In Chapter 4, a variety of metallylenes were synthesised, featuring amido, aryl, and silyl ligands, and their structure and bonding properties compared. The first structurally characterised example of an amido(silyl)stannylene ($Sn(N(Dipp)(TMS))(Si(TMS)_3)$), **4.19**, was reported, a compound which displayed remarkable instability in solution (decaying at temperatures above 273 K). This behaviour is at odds with the aryl(silyl)stannylenes (($Sn(Ar^{Mes})(Si(TMS)_3)$), **4.10**; $Sn(Ar^{Dipp})(Si(TMS)_3)$, **4.11**) reported in the chapter (both are

stable to elevated temperatures in solution). This observation could reflect the reduced steric bulk of the amido substituent (-N(Dipp)(TMS)) compared to the terphenyl ligands (Ar^{Mes} and Ar^{Dipp}). As a result, the synthesis of a bulkier amido(silyl)stannylene should be attempted to ascertain if the instability is a result of insufficient steric bulk or the electronic structure of the stannylenes.



Scheme 7-2: The proposed synthesis of a bulky amido(silyl)stannylene.

In Chapter 5, the small molecule reactivity of two silylstannylenes, **4.10** and $Sn(Si(TMS)_2(Si^tBuPh_2))_2$, **4.13**, was explored. Reactions with azides ($TMSN_3$ and $DippN_3$) show that both stannylenes are capable of undergoing a 1,2-migration of the silyl-substituent from the Sn to N centres of a transient stanna-imine (Sn=N) intermediate. A similar phenomenon was also observed in the reaction between **4.10** and N_2O, in which multiple silyl-substituent migrations occur to yield a mixed Sn(II)/Sn(IV) complex, **5.34**. With a view to minimising these migrations and therefore synthesising a stannanone, replacing the silyl substituent ($-Si(TMS)_3$) with a bulky alkyl substituent might achieve this.



Scheme 7-3: The proposed formation of a stannanone (Sn=O) from the reaction of an aryl(alkyl)stannylene with N_2O. Where R is a generic alkyl group.

In Chapter 6, the reactivity of silyl-substituted stannylenes with alkynes was explored. The first examples of reversible alkyne insertion into the E–X bonds of metallylenes were reported with **4.10**, and with both TMSCCH and hex-3-yne. This is an exciting result and certainly warrants further research to determine whether the catalytic functionalisation of an alkyne at a tin centre could occur.

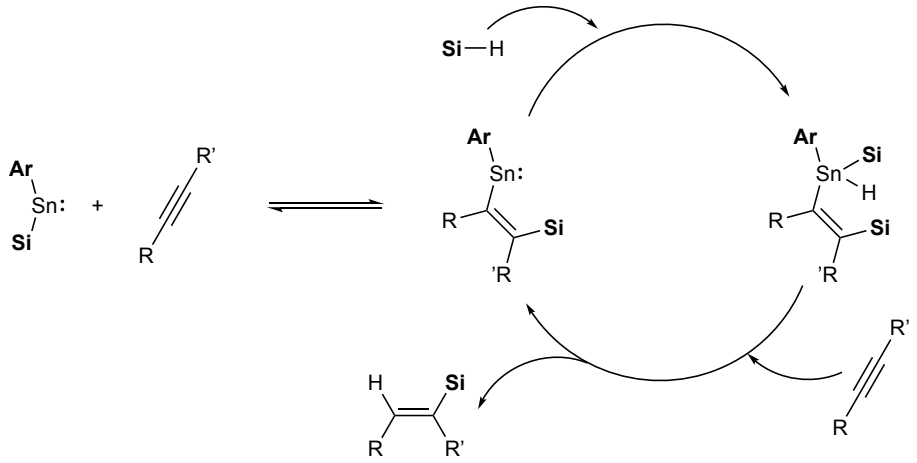


Figure 7-1: Proposed catalytic cycle for the formation of silyl alkenes, from a stannylene, an alkyne and a silane. Where **Ar** is a generic aryl ligand, **Si** is a generic silyl ligand, and R and R' are small alkyl groups or hydrogen.